INVESTIGATIONS INTO CAUSES OF FAILURE OF REGENERATIVE PERIPHERAL NERVE INTERFACES

by

R. COLLINS WATSON

Presented to the Faculty of the Graduate School of

The University of Texas at Arlington in Partial Fulfillment

of the Requirements

for the Degree of

DOCTOR OF PHILOSOPHY

THE UNIVERSITY OF TEXAS AT ARLINGTON

August 2012

ACKNOWLEDGEMENTS

I would like to formost acknowledge the support of my mentor, Dr. Mario Romero. His guidance and expertise have been invaluable throughout this journey. I would also like to thank my committee members, Dr. Young-Tae Kim, Dr. Samarendra Mohanty, Dr. Mauricio Delgado, and Dr. Khosrow Behbehani. I would like to acknowledge my fellow lab mates Dr. Jennifer Siefert, Jenny Stearns Bell, Dr. Swarup Dash, Eduardo Martinez, An Nguyen, Steve Kunkel, Rodrigo Lozano, and Vidhi Desai for their contributions to this research and for their friendship. I am grateful for the opportunity to have worked with such amazing people. I have learned and grown far more than I expected.

August 1, 2012

ABSTRACT

INVESTIGATIONS INTO CAUSES OF FAILURE OF REGENERATIVE PERIPHERAL NERVE INTERFACES

R. Collins Watson, PhD

The University of Texas at Arlington, 2012
Supervising Professor: Mario Ignacio Romero-Ortega

All highly selective methods of neural interfacing for mental control of a robotic prosthesis tested to date have exhibited high rates of failure over time. Regenerative peripheral nerve interfaces (RPNIs) may offer the greatest potential among the proposed technologies for providing the number of degrees of freedom necessary to control a robotic limb, but are unacceptable for clinical use due to several shortcomings of current technology: (1) all RPNIs tested to date have exhibited signal loss over time due to biological mechanisms of rejection of implanted electrodes; (2) all chronically tested interfaces have suffered from high rates of device failure of physical and mechanical origin; and (3) the technologies used to date have not yet proven capable of providing the selectivity and sensitivity of recordings that researchers hope they will obtain and that will be necessary for clinical use. Chapter 2 of this dissertation investigates the prominent causes of physical device failure inherent within current technologies. Complications regarding the transfer of internally recorded signals to the external environment via a wire represented the most common cause of device failure in a characteristic RPNI model (15% of animals over 15 days, 35% of animals over 30 days, 60% of animals over 60 days; n = 20 animals per group). While many researchers are investigating mechanisms of

biological rejection of cortically implanted electrodes, including the effects of micromotion and mechanical mismatch between electrodes and brain tissue, the complementary phenomenon of tissue movement related to nerve stretch during limb movement has not yet been investigated. Chapter 3 provides evidence that nerve stretch does not accelerate signal loss, does not decrease the number of regenerating axons, and does not increase the axon-depleted-area surrounding each electrode in a characteristic RPNI model. A proposed improvement to RPNI technology is microchannel encapsulation of regenerating axons. This has been shown through mathematical predictions to amplify extracellular recordings of action potentials from both myelinated axons and unmyelinated axons, potentially increasing the sensitivity and selectivity of an RPNI and possibly reducing the impact of biological mechanisms of rejection. *In vitro* and *in vivo* experiments have supported the mathematical predictions for myelinated axons. Chapter 4 provides direct experimental support for microchannel amplification of unmyelinated axons. Chapter 5 discusses the relevance of all of these findings toward the field of neural interfacing with attention toward the future state of this technology.

TABLE OF CONTENTS

ACKNOWLEDGEMENTS iii

ABSTRACT iv

LIST OF ILLUSTRATIONS vii

LIST OF TABLES viii

Chapter Page

1. INTRODUCTION 1

1.1 Overview 1

1.1.1 Medical Problem: Limb Loss 1

1.1.2 Robotic Prostheses 2

1.1.3 Proposed Mechanisms of Prosthesis Control 3

1.2 Cortical Interfacing 8

1.3 Peripheral Nerve Interfacing 12

1.3.1 Categories of Peripheral Nerve Interfaces Based on Invasiveness and Selectivity 12

1.3.2 History of Peripheral Nerve Interfacing 13

1.3.3 Cuff Electrode Interfaces 18

1.3.4 Intrafascicular Electrode Interfaces 19

1.3.5 Penetrating Electrode Interfaces 21

1.3.6 Regenerative Interfaces 22

1.4 Summary and Specific Aims 32

2. COMMON CAUSES OF PHYSICAL DEVICE FAILURE 35

2.1 Overview 35

2.1.1 Limitation of Current RPNI Technology 35

2.1.2 Specific Aim 35

2.1.3 Review of Published Recordings from Regenerative PNIs 36

2.1.4 Summary of Literature Review 42

2.1.5 Experimental Design 44

2.2 Materials and Methods 46

2.2.1 Regenerative Peripheral Nerve Interface 46

2.2.2 Surgical Implantation 46

2.2.3 Electrophysiological Recordings 47

2.2.4 Evaluation 48

2.3 Results 50

2.3.1 Routine Observations 50

2.3.2 Terminal Observations 52

2.3.3 Electrophysiological Results 54

2.3.4 Summary of Results 60

2.4 Discussion 62

2.4.1 Relevance of Experimental Setup 62

2.4.2 Common Causes of Failure 67

2.4.3 Relevance to the Field 75

2.4.4 Wireless 76

2.4.5 Conclusions 77

3. NERVE STRETCH 79

3.1 Overview 79

3.1.1 Limitation of Current Regnerative Peripheral Nerve Interfaceing 79

3.1.2 Specific Aim 79

3.1.3 Hypothesis 79

3.1.4 Background 80
3.1.5 Experimental Design 92
3.2 Methods 93
3.2.1 Peripheral Nerve Interface and Surgical Implantation 93
3.2.2 Limb Stretching 93
3.2.3 Quantification of Strain in the Nerve 94
3.2.4 Electrophysiological Recordings 95
3.2.5 Tissue Preparation 96
3.2.6 Histological Evaluation 98
3.3 Results 103
3.3.1 Characterization of the Experimental Model 103
3.3.2 Results of Electrophysiological Recordings 106
3.3.3 Axonal Regeneration 108
3.3.4 Axon-depleted Scar Areas 111
3.4 Discussion 114
4. MICROCHANNEL INDUCED AMPLIFICATION OF UNMYELINATED AXONS 122
4.1 Overview 122
4.1.1 Limitation of Current RPNI Technology 122
4.1.2 Hypothesis 122
4.1.3 Specific Aim 122
4.1.4 Background and Justification 123
4.2 Materials and Methods 125
4.2.1 Microfluidic Molds on Planar MEAs 125
4.2.2 Neuron Cell Culture 126
4.2.3 Electrophysiology 128
4.2.4 Experimental Setup 128

4.3 Results 130
4.4 Discussion 133
5. GENERAL DISCUSSION 135
5.1 Signal Drift 135
5.2 Characterization of the REMI 149
5.2.1 Development of the REMI 149
5.2.2 Causes of Device Failure Inherent in the REMI 150
5.2.3 Robustness of the REMI with respect to applied stress 153
5.2.4 Signal Stability and Presence Over Time 154
5.3 The Future of Regenerative Interfacing 156
5.4 Conclusions 159
APPENDIX
A. AXON COUNTS 161
B. AXON DEPLETED SCAR SIZES 167
REFERENCES 176
BIOGRAPHICAL INFORMATION 198

LIST OF ILLUSTRATIONS

Figure Page

1.1 Robotic prosthesis technology has advanced rapidly in the past decade. Scientists are hopeful that neural interfaces may be developed that will allow mental control over such devices. Image courtesy of DEKA Research and Development. 2

1.2 Proposed methods of brain-machine interfacing for robotic prosthesis control. Images adapted from Zhang et al., 2010; Bogue, 2010; Pistohl et al., 2008; Schalk et al., 2008 Donoghue et al., 2007; Hochberg, 2006. 4

1.3 Proposed methods of peripheral nerve interfacing for robotic prosthesis control. Aapted from Kim and Romero, 2012 5

1.4 Proposed Of the proposed strategies for peripheral nerve interfacing, regenerative electrode arrays are considered to be the most potentially selective as well as the most invasive. Adapted from Navarro et al., 2005 13

1.5 (A) A single human motorneuron action potential, transferred to a myofiber (top), results in a small, brief muscle contraction (bottom, measured by EMG). (B) The firing rate of a human motor neuron (top) linearly correlates with the total force of contraction (bottom) of distal myofibers within a motor unit. Highly selective PNIs aim to translate the firing rate of individually interfaced motor neurons into limb movements instead of muscle contraction. Adapted from Fruend et al., 1975 and Desmedt and Godaux, 1977, respectively. 14

1.6 An induced compound action potential of a mixed nerve appears as a traveling waveform with a single peak when measured near the point of stimulation (A). Due to heterogeneous conduction velocities of component axons, the traveling waveform devolves into a shape with multiple distinct peaks when measured farther from the point of stimulation (B). Time markers = 1 millisecond intervals. Adapted from Gasser, 1941. 16

1.7 Low-selectivity PNIs operate by translating the compound activity of many axons within a nerve or fascicle into desired whole-muscle contraction, as proposed by Stein *et al*. (1975) and de Luca (1978). The top plot shows the compound activity of a cat sciatic nerve, via a cuff electrode, as it takes three steps. The bottom plot shows the rectified and filtered waveform, clearly correlating with the three steps. Adapted from Stein *et al*., 1975. 17

1.8 Intrafascicular electrodes can provide greater sensitivity of recordings than cuff electrodes. In the example shown here, intentionally selected to highlight this difference, a rat leg was subjected to three rotations of the ankle joint. Corresponding nerve activity could be observed from a sciatic cuff electrode (left) and a tibial intrafascicular electrode (right). Adapted from Yoshida and Struijk, 2004. 19

1.9 (A) Schematic drawing of the first implemented regenerative PNI. (B) The first published electrophysiological recordings from a regenerative PNI, implanted into a frog sciatic nerve, showing a single-unit spike in response to a muscle stretch (top and middle) and a train of spikes (bottom) during swimming. Adapted from Mannard et al., 1974. 23

1.10 Micrograph (A) and schematic of implantation procedure (B) of a silicon-based sieve electrode interface. Adapted from Kovacs et al., 1994 and Kovacs, 1991, respectively. 23

1.11 Flexible polyimide sieve electrodes gained popularity among researchers, primarily based in Europe, in the mid-1990s. (A) An early flexible polyimide sieve electrode with integrated ribbon cable. Adapted from Lago et al., 2007. (B) Schematic of implantation of electrode with guidance tube into a peripheral nerve. Adapted from Navarro et al., 2005. 26

1.12 Schematic (A) and prototype (B) of a proposed architecture in which a flat array of microchannels with incorporated electrodes is “rolled” into a tube to serve as a nerve guide. Adapted from Suzuki et al., 2007. 29

1.13 Schematic of a regenerative device with SU8-based electrodes embedded within hollow axonal-guidance channels of a biodegradable medium within the lumen of a non-biodegradable nerve guide. Adapted from Cho et al., 2008. 29

1.14 The regenerative multielectrode interface (REMI) consists of a needle-electrode array embedded within a nerve guide tube. Scale bar = 1 mm. Adapted from Garde et al., 2009. 30

1.15 Example of a proposed method of generating microchannels (110 μm diameter) within a nerve guide conduit. Adapted from Lacour et al., 2009. 30

2.1 A REMI PNI is implanted into the hind left leg of the animal. Insulated wires connect the electrode array subcutaneously to a connector housed within a percutaneous titanium pedestal. Bone cement secures the pedestal to the pelvis bone. External wires allow for recording of electrophysiological signals by recording hardware. A typical recording session involves 5 minutes of continuous recording from an awake animal. 45

2.2 A connector cable was inserted into the titanium pedestal to allow electrophysiological recordings. 48

2.3 Explanted REMIs were cleaned and dissected to confirm successful regeneration of the nerve cable. 49

2.4 Single-unit spikes are often visibly detectable above the noise baseline on individual channels (top graph, time span = 1.5 seconds). Aggregates of individual single spikes, superimposed, are available in real time (bottom left, grids = 52 V, 100 s). 56

2.5 Failure of the mechanical integrity of the implanted REMI, as shown here in an explanted example in which the electrode array had become partially dislodged from the nerve guide tube, was observed in 2 of the 60 animals in this study. 68

2.6 Upon stereoscopic dissection of explanted interfaces, a majority displayed a regenerated nerve cable in which the electrode tips were positioned within the nerve cable (A). A minority of explanted interfaces (see Table 2.8) presented a nerve cable in which the electrode tips were all present outside of the regenerated nerve cable (B). 70

2.7 Noise baseline amplitudes recorded from 16 electrodes on each of six REMIs at 42 days post-implantation. No statistically significant difference was observed between REMIs from which action potentials had been recorded and those from which action potentials had not, as measured by a nested one-way analysis of variance ($p = 0.7735$). 72

2.8 Issues regarding the percutaneous interface, such as an internal wire being exposed and broken as shown here (arrow), represent a majority of all observed causes of failure over 60 days (see Table 2.1). 74

3.1 Nerve cables are capable of elastically accommodating a range of strain rates due to the internal structure of nerve components. (A) An example of the plexicular arrangement of nerve fiber bundles within an individual fascicle. Adapted from Raffe (1985). (B) Nerve fibers within fascicles tend to assume a wavy orientation when relaxed. Adapted from Sunderland (1991). (C) Local blood and lymph vessels supporting nerves typically form tortuous paths capable of lengthening during nerve stretch. Adapted from Lundborg and Rydevik, 1973. (D) Low magnification micrograph of a guinea pig sciatic nerve under relaxation (top) and tension (bottom). Scale bar = 0.5 mm. Adapted from Li and Shi (2006). 85

3.2 Stress-strain curve for rabbit tibial nerve. Adapted from Kwan et al. (1992). 86

3.3 Measurement of nerve strain under different experimental conditions is typically achieved by recording the change in distance between two marked locations on an exposed nerve. Adapted from Wall et al., 1991 (A) and Rickett et al., 2011 (B). 91

3.4 A computer-controlled mechanical stage was developed for cyclic stretching of the hind limb (left). Pelvic fixation allowed for cyclic stretching in the caudal direction of an anesthetized animal (right). 94

3.5 Images of a marked rat sciatic nerve at 0% limb stretch (A), 70% limb stretch (B), and 100% of maximum limb stretch (C). Red line between marked black dots added digitally to allow calculation of nerve strain. 95

3.6 Explanted REMIs with regenerated nerves (A) were cleaned (B), and the regenerated nerve cables were extracted (C) and marked for orientation (D). (image A taken at two weeks post-implantation; images B-D taken at 30 days post-implantation) 97

3.7 issue slices were stained for axons (NF200, green), myelin (P0, red), and macrophagic scar tissue (ED1, blue). The merged image (bottom right) shows clearly defined axon-depleted areas, filled with ED1+ scar tissue, surrounding each electrode. Orientation: proximal nerve, top; distal nerve, bottom. Scale bar = 200 μm. 99

3.8 Example of identification of axon-depleted areas. Original images (top left, bottom left) and ADA defined images (top right, bottom right). Scale bars = 100 μm (top images) and 200 μm (bottom images). (See Figure 3.7 for immunostaining identifications). 100

3.9 Example of line-crossing method used to characterize the number of axons and myelinated axons within a REMI nerve guide tube. Original image (left). Image highlighting windowed view used in Figure 3.10 (right). Scale bar = 200 μm. (See Figure 3.7 for immunostaining identifications). 101

3.10 Example of visual identification of axons crossing a characteristic center line within a regenerated nerve used for counting (top). Example for myelinated axons (middle). Merged (bottom). Scale bar = 200 μm. (See Figure 3.7 for immunostaining identifications). 102

3.11 Limb stretch lengths did not decrease over the length of the experiment. 105

3.12 The average number of detectable, distinct spiking units per animal over time by experimental stretch group. Difference in mean values were not statistically different (two-way ANOVA; with respect to stretch, $p = 0.387$; with respect to time, $p = 0.763$). 107

3.13 Percentage of animals displaying any single-unit spiking activity at a given time point. Limb stretch did not result in more rapid signal loss among the experimental stretch groups. 107

3.14 The averaged counts per animal of axons (A) and myelinated axons (B) at 30 days post-implantation compared across stretch groups. Differences in mean values are not statistically significant (nested one-way ANOVA; p = 0.391, total axons; p = 0.440, myelinated axons). 109

3.15 The averaged counts per animal of axons (A) and myelinated axons (B) at 60 days post-implantation compared across stretch groups. Differences in mean values are not statistically significant (nested one-way ANOVA; p = 0.490, total axons; p = 0.198, myelinated axons). 110

3.16 Averave ADA per slice by animal across all experimental groups. 112

3.17 Average ADA size per animal over experimental stretch groups. No statistical differences among stretch groups (nested one-way ANOVA; p = 0.092, A; p = 0.185, B). 113

3.18 Explanted REMI two weeks post implantation. A thick layer of fatty and fibrotic connective tissue forms around the implanted device within weeks (top). Removal of the connective tissue with microscissors and forceps allows for visual inspection of the nerve guide tube with regenerated nerve cable, external parts of the electrode array, and electrode array ribbon cable (bottom). Orientation: REMI positioned horizontally; proximal nerve to the left; distal nerve to the right; electrode ribbon cable to the top. Photograph field is approximately 1 cm in width. 116

3.19 Conceptualization of an elastic nerve cable (represented as a coiled spring) within a nerve guide tube with embedded electrodes. (Top) Unstretched. (Middle) Stretched assuming stationary confinement of elements within guide tube. (Bottom) Stretched assuming free mobility of elements within guide tube. 117

3.20 Count averages of regenerated axons across experimental stretch groups at 30 days (A) and 60 days (B). Error bars represent one SD. Alternative presentation of Figures 3.18 and 3.19. 119

3.21 Average axon-depleted scar sizes surrounding electrodes across experimental stretch groups at 30 days (left) and 60 days (right). Error bars represent one SD. Alternative presentation of Figure 3.23. 120

4.1 The UT Arlington microchannel scaffold design. (A,B) Mask layers used to produce a two-layer aligned microfabrication scheme. Layers correspond to microchannels and wells. (C) Fabricated mold; SU-8 atop silicon wafer. Scale bar = 4 mm. 125

4.2 PDMS-based compartmentalized culture system atop 64-channel MEA. (A) Schematic of two-chambered PDMS scaffold with microfabricated microchannels. (B) Micrograph of PDMS scaffold showing chambers (stars) and microchannels (arrow). (C,D) Diagram of MEA with dual 32-channel electrode arrays with and without PDMS scaffolds (arrows indicate PDMS scaffolds). 126

4.3 Cell culture within PDMS scaffold atop MEA allows recording of signals from within open wells and within microchannels. Cells are seeded into two wells within a molded PDMS scaffold atop a 64-channel planar MEA. Microfabricated channels within the PDMS scaffold are aligned atop substrate embedded electrodes. Recording hardware attaches to electrode contact pads and allows electrophysiological signals from cells and neurites within the wells and the channels to be recorded. 127

4.4 Cell culture design capable of recording from neurons within wells and within microchannels. (A) Neurites extending from well (right) into microchannels atop substrate-embedded electrodes (UT Arlington microchannel design). (B) Neuron cell bodies forming a neural network within a well. (C) PDMS microchannels aligned atop electrode array (Sandia microchannel design). Scale bars = 400 μm. 129

4.5 Strong statistical significance in support of signal amplification within microchannels. Recorded spike amplitudes measured 3.4 times higher within microchannels than in wells. Representative electrophysiological activity recorded from an open electrode (A,C) and from an electrode within a microchannel (B,D). (A) and (C) represent the superimposed waveshapes and spike raster plots, respectively, of 349 spikes recorded over 10 seconds with an average peak-to-peak amplitude of 189 μV. (B) and (D) represent the superimposed waveshapes and spike raster plots, respectively, of 65 spikes recorded over 10 seconds with an average amplitude of 786 μV. Individual spikes are labeled in different colors. 131

4.6 Action potential amplitudes recorded from within microchannels averaged 3.4 times higher than amplitudes recorded from within PDMS scaffold chambers or from open MEAs ($p \leq 0.001$, Kruskal-Wallis followed by Dunn's test). The mean action potential amplitudes recorded from open MEAs (n = 22) and open wells on MEAs containing PDMS scaffolds (n = 9) did not statistically differ. The mean action potential amplitudes recorded within 0.5 mm long microchannels (n = 39) and within 2.0 mm long microchannels (n = 82) did not statistically differ. 132

5.1 Examples of spiking unit continuity and waveshape fluctuations over time in cortically implanted electrode arrays. Adapted from Schmidt et al., 1976 (top left), Williams et al., 1999 (top right), Dickey et al., 2009 (bottom left), and Suner et al., 2005 (bottom right). 136

5.2 Example of signal stability within an individual spiking unit from a sieve electrode over 21 days. Image represents a composition of 21 waveshapes, each representing an averaged waveshape taken from multiple spikes on a given day. Adapted from Shimatani et al., 2003. 138

5.3 Six distinct spiking units were observed in one animal over the course of 23 hours at 21 days post-implantation. Images represent superimposed waveshapes recorded over a five minute interval at the beginning of each hour. Scales are given in Figures 5.4-5.9. 141

5.4 Averaged waveshape (of all spikes over a 5 minute interval) at each hour on Channel 12c (top). Amplitude of averaged waveshape at each hour (bottom). 142

5.5 Averaged waveshape (of all spikes over a 5 minute interval) at each hour on Channel 05b (top). Amplitude of averaged waveshape at each hour (bottom). 143

5.6 Averaged waveshape (of all spikes over a 5 minute interval) at each hour on Channel 05a (top). Amplitude of averaged waveshape at each hour (bottom). 144

5.7 Averaged waveshape (of all spikes over a 5 minute interval) at each hour on Channel 01 (top). Amplitude of averaged waveshape at each hour (bottom). 145

5.8 Averaged waveshape (of all spikes over a 5 minute interval) at each hour on Channel 12a (top). Amplitude of averaged waveshape at each hour (bottom). 146

5.9 Averaged waveshape (of all spikes over a 5 minute interval) at each hour on Channel 12b (top). Amplitude of averaged waveshape at each hour (bottom). 147

5.10 A summary of causes of physical device failure observed in the REMI. 150

5.11 A summary of reported causes of RPNI device failure present in the literature. Note: Lago et al., 2007, Cho et al., 2008, and Garde et al., 2009 reported failures associated with percutaneous signal transfer to account for "most" or a "majority" of animals. As such, they are represented here at 50%, though the actual value is implied to be higher. Many of these publications did identify one or more of these causes of failure as present but did not quantify them. See Table 2.10 for additional details. Publications present in this figure were selected from Table 2.1. 152

5.12 Percentage of animals that survived until scheduled termination at 30 days post-implantation without observable device failure relative to limb stretch intensity. Values represent the original 18 animals (n = 6 animals per group) within the limb stretching experiments presented in Chapter 3. 154

5.13 Examples of axonal expansion and bifurcation for the potential improvements of RPNIs. Adapted from Wieringa et al., 2010a; Wieringa et al., 2010b; Wieringa et al., 2010c. 158

LIST OF TABLES

Table Page

1.1 Overview of proposed and realized interfacing technologies 6

2.1 Summary of 16 published works to date reporting single-unit activity recorded from a regenerative PNIs. Note: Values listed in the “Duration of experiment” column reflect the length of time in which recordings from implanted arrays were attempted, not the duration over which single-units were observed. (“n/r” indicates not-reported) 43

2.2 Summary of results of routine observations. Numbers represent the number of animals that failed due to a given externally observable cause. 51

2.3 Summary of results of post-mortem observations. 53

2.4 Animals displaying single-unit spiking activity (30-day cohort). 57

2.5 Animals displaying single-unit spiking activity (60-day cohort). 58

2.6 Summary of electrophysiological results in relation to animal longevity and observed device failures 59

2.7 Failure rates among the three time points 60

2.8 Summary of observed causes of device failure from routine observations, terminal observations, and electrophysiological observations 61

2.9 Comparison of pertinent electrophysiological results reported by this work and by others. 64

2.10 Comparison of physical causes of failure reported by this work and by others. 66

3.1 Measured sciatic nerve strain at stretched positions relative to relaxed position 103

CHAPTER 1

INTRODUCTION

1.1 Overview

Developing technologies to provide mental control of a robotic prosthesis has been a goal of scientists for many decades. This Introduction will serve to briefly discuss the medical issue of limb loss, the state of current technology with regard to robotic prostheses, and the proposed methods of prosthesis control currently being investigated. Cortical and peripheral nerve interfacing are discussed in more detail. The history and state of technology of regenerative peripheral nerve interfacing are reviewed with specific interest in identifiable scientific and technical shortcomings. Three areas of research are identified based on these shortcomings, leading to the three Specific Aims of this dissertation.

1.1.1 Medical Problem: Limb Loss

As of the year 2005, there were an estimated 1.6 million people living in the USA with a missing limb. An estimated 185,000 more per year currently suffer from limb amputations, primarily due to disease and trauma (Ziegler-Graham *et al*., 2008). Recent efforts by the National Institutes of Health and by the Defense Advanced Research Projects Agency (DARPA) have spurred interest in development of robotic prostheses and mechanisms to provide both control and sensory feedback as a means of providing greater quality of life to individuals with amputated limbs or peripheral nerve pathologies (Ling *et al*., 2010). The U.S. military has expressed an interest in providing an improved quality of life for young veterans who have lost a limb.

1.1.2 Robotic Prostheses

Recent efforts have focused on producing an upper-limb robotic prosthesis and neural interface capable of providing 23 degrees of freedom, the number considered necessary for full, realistic control of a human arm (McLoughlin, 2009). Recent prototypes developed at DEKA Research and Development (Manchester, NH) and at the Applied Physics Laboratory at Johns Hopkins University have been constructed possessing 22 degrees of freedom, a weight of 9 pounds (similar to a human arm), and the demonstrated dexterity to pick up a grape or a glass of water without spilling it. Other researchers are working on improved sensory technology within robotic fingers (Dahiya *et al*., 2010; Loeb *et al*., 2011; Cipriani *et al*., 2012) and on MEMS-based "smart skin" (Gonenli *et al*., 2011). While robotics technology has developed fairly rapidly, providing prototypes comparable in size, strength, weight, and degrees of freedom to the human arm (Figure 1.1) along with rapidly developing surface sensors for pressure, texture, and temperature, the technology and methods used for control and feedback of the prosthesis lag far behind.

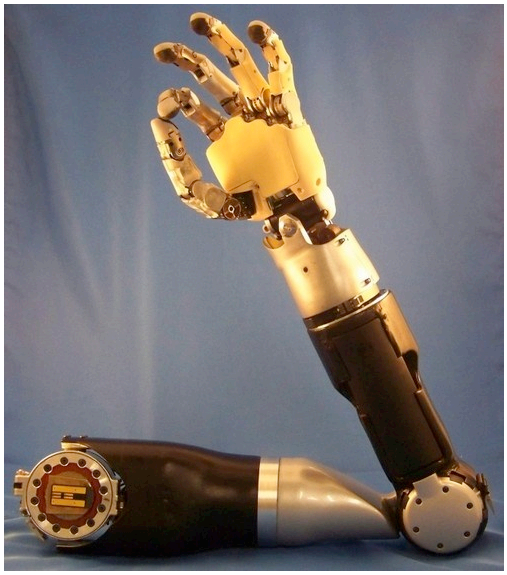

Figure 1.1 Robotic prosthesis technology has advanced rapidly in the past decade. Scientists are hopeful that neural interfaces may be developed that will allow mental control over such devices. Image courtesy of DEKA Research and Development.

1.1.3 Proposed Mechanisms of Prosthesis Control

Many technologies have been either proposed or demonstrated to be capable of providing volitional mental control over multiple degrees of freedom within a computer interface or robotic limb. These typically involve the interpretation of electrophysiological signals from the brain, from skeletal muscles, or from peripheral nerves (Table 1.1).

Interfacing technologies are often categorized based upon their invasiveness and their selectivity (see Navarro *et al*., 2005; Sanchez and Principe, 2007; Micera *et al*., 2008) as represented here in Figure 1.2. Typically, the more surgically invasive a technology, the more distinct, non-redundant signals it is capable of recording and interpreting into a desired outcome such as cursor motion or robotic limb movement. When interfacing with the brain, these signals can be brain waves, can be local field potentials due to the compound activity of groups of neurons, or can be the firing patterns of individual neurons (single-unit spikes). When interfacing with peripheral nerves, these signals can be the compound activity of entire nerve trunks, can be the compound activity of groups of axons within nerve fascicles, or can be the firing patterns of individual axons (single-unit spikes). When interfacing with skeletal muscles, skin-mounted electrodes detect compound electromyographic signals.

Techniques measuring compound brain activity, such as electroencephalography and electrocorticography, have been applied for clinical uses and may provide enhanced quality of life to para- and quadriplegics. However, they are generally considered insufficient for providing either the temporal resolution or the number of independent signals for realistic control of a prosthetic limb and as such will not be discussed in depth here. For in-depth reviews on such techniques with regard to device control and brain-machine interaction, see Schalk (2011) and Nicolas-Alonso and Gomez-Gil (2012).

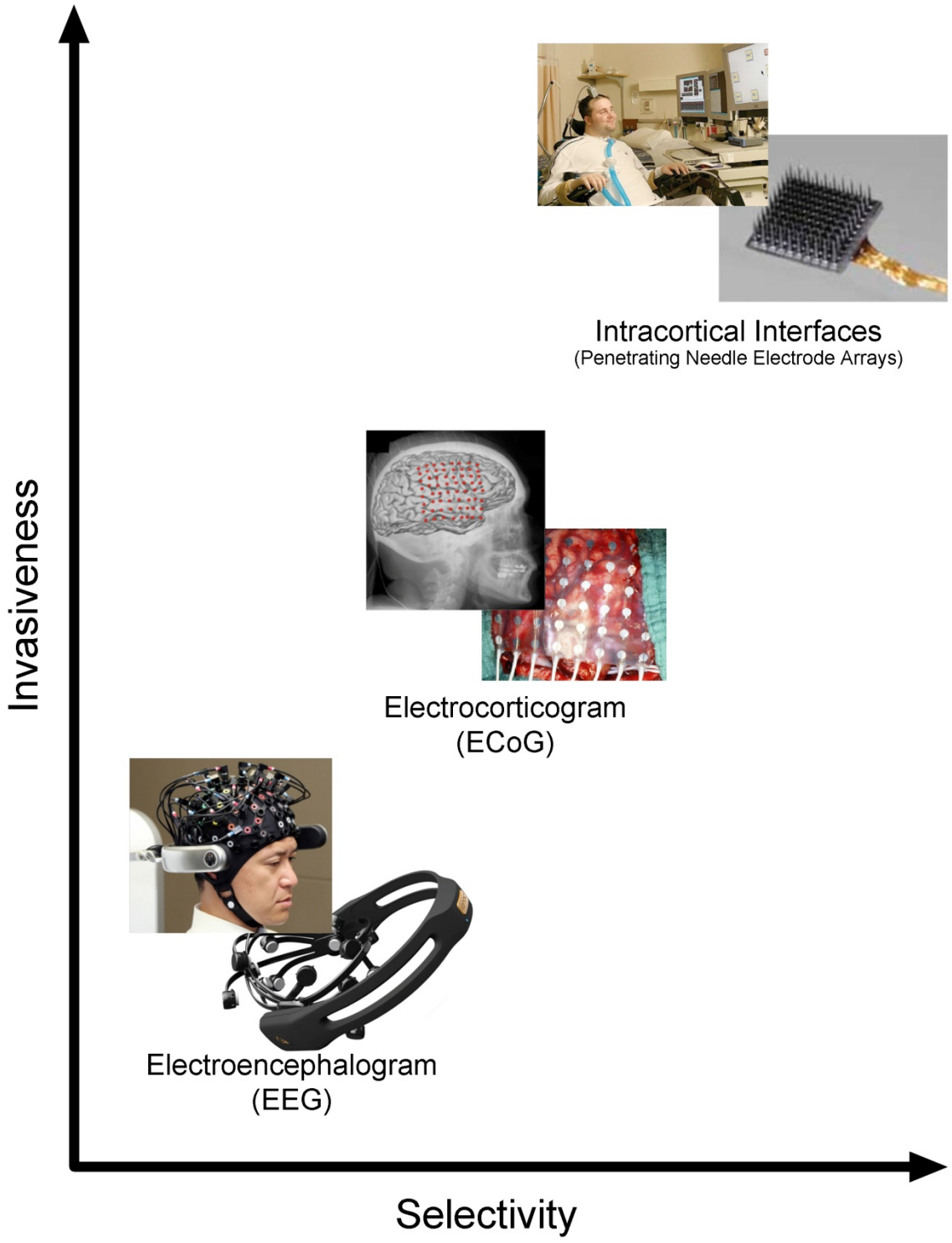

Figure 1.2 Proposed methods of brain-machine interfacing for robotic prosthesis control. Images adapted from Zhang *et al.*, 2010; Bogue, 2010; Pistohl *et al.*, 2008; Schalk *et al.*, 2008 Donoghue *et al.*, 2007; Hochberg, 2006.

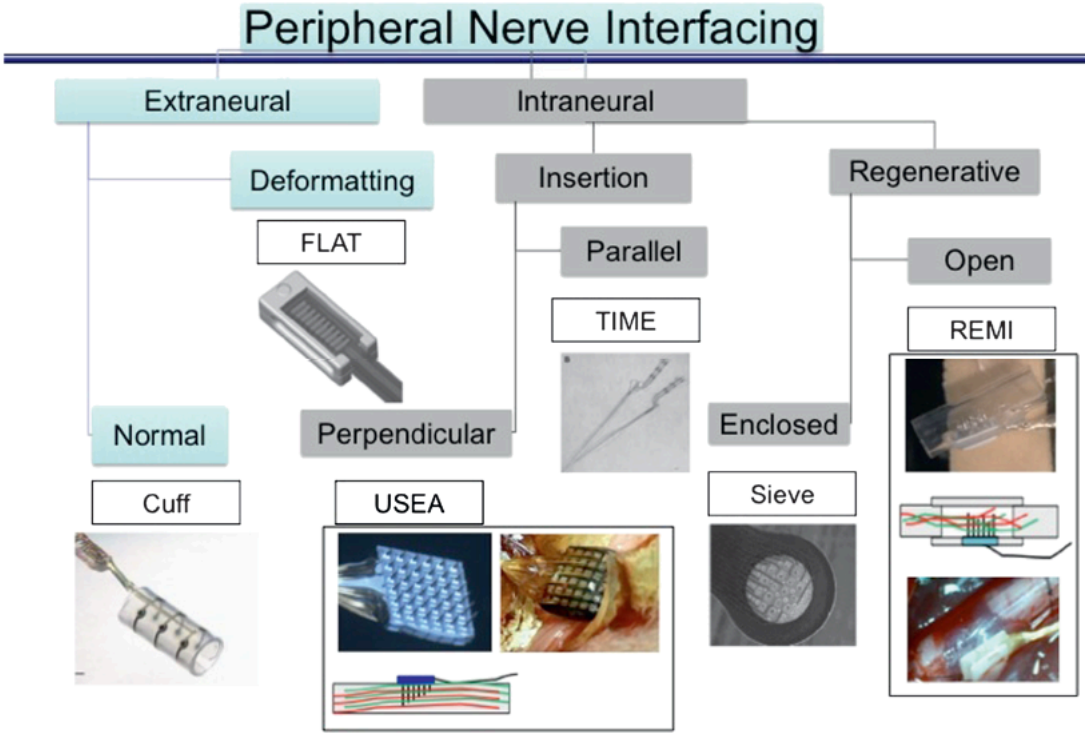

Figure 1.3 Proposed methods of peripheral nerve interfacing for robotic prosthesis control. Adapted from Kim and Romero, 2012.

Table 1.1 Overview of proposed and realized interfacing technologies.

Signal Source:	Interfacing Technology:	Current State of Technology:	Controllable Degrees of Freedom (Demonstrated):
Brain	EEG	Widely available for clinical, research, and entertainment purposes (Onose *et al*., 2012; Waters, 2008)	2, instant (Wolpaw and McFarland, 2004) 3,with training (McFarland *et al*., 2010)
	ECoG	Acute research on human subjects (for review, see Schalk and Leuthardt, 2011)	2, human, online (Schalk *et al*., 2008) 7, monkey, offline (Chao *et al*., 2010)
	Penetrative Needle Electrode Arrays	Clinical trials on humans	4, primates (Velliste *et al*., 2008) 3, humans (Simeral *et al*., 2011)
Skeletal Muscle	EMG with Targeted Muscle Reinnervation	Clinically used to treat humans	6, human (Miller *et al*., 2008)
Peripheral Nerves	Epineural Electrodes	Clinical use in humans for stimulation (Navarro *et al*., 2005)	Typically used for stimulation
	Intrafascicular Electrodes	Acute research on humans (Horch *et al*., 2011)	1, human (Dhillon and Horch, 2005)
	Penetrative Needle Electrode Arrays	Chronic research on cats (Clark *et al*., 2011) One chronic implantation into a human (Gasson *et al*., 2003)	1, cat (Clark *et al*., 2011) 1 human (Gasson *et al*., 2003)
	Regenerative Interfaces	Limited to acute and chronic research on rodent models (see Section 1.3.6)	Not yet attempted.

The technique with the greatest clinical success to date is a combination of surface electromyography with targeted muscle reinnervation (Kuiken *et al*., 2004; Ohnishi *et al*., 2007; Kuiken *et al*., 2007; Huang *et al*., 2008; Miller *et al*., 2008; Kuiken *et al*., 2009). Developed within the last decade mostly by researchers at Northwestern University, targeted muscle reinnervation involves denervating one or more large muscles (such as the pectoralis major or the deltoids) of an amputee and reinnervating small segments of those large muscles with nerves originally innervating targets within the missing limb. Employing a large number of surface myoelectrodes following targeted muscle reinnervation has been demonstrated to provide up to six degrees of freedom toward the use of a robotic prosthetic arm (Miller *et al*., 2008). A complementary technique of targeted sensory reinnervation is also being explored to provide sensory feedback (Kuiken *et al*., 2007). The benefits of targeted muscle reinnervation include a singular surgery with no implanted devices or materials, the use of large muscles as transducers to amplify signals delivered by peripheral nerves, the proven capacity to provide up to six degrees of freedom, and the capacity to record from signals that are presumed not to fade with time.

The fields of cortical interfacing and peripheral nerve interfacing, in which use of highly selective implantable electrode arrays into either the cerebral cortex of the brain or into peripheral nerves for the sake of recording the activity of individual neurons or axons, have been in development for over fourty years. Researchers aim to be able to interpret intended limb movements (cortical interfaces) or desired muscle contractions (peripheral nerve interfaces) with enough independent signals to provide on the order of twenty or more controllable degrees of freedom. It is hoped that one or both of these interfacing paradigms will eventually be able to provide intuitive mental control of a robotic prosthesis to restore function to amputees.

Due to their complimentary nature, much of what we have learned about peripheral nerve interfacing (and much of its associated technology) has been and will continue to be

derived from experiments focusing on cortical interfaces. As such, knowledge of the status and history of cortical interfacing is necessary for investigations into improvements of peripheral interfaces. Several bottlenecks and inadequacies in current knowledge and technology will need to be overcome before either interfacing paradigm is capable of clinical use in humans.

1.2 Cortical Interfacing

Experiments using simple metal wires as electrodes to stimulate areas of the brain and record from individual and groups of neurons in the central nervous system have been reported as far back as the 1930s (see Dalgleish, 2004; Coates, 2008). In the 1950s and 1960s, Dr. José M. R. Delgado gained a degree of public notoriety for a series of experiments upon awake animals using implanted wire electrodes both to study and to influence behavior (Delgado, 1969). In the late 1960s, it was discovered that the firing rates of individual neurons and groups of neurons within regions of the cerebral cortex were associated with specific muscle contractions and with intended movements (Evarts, 1966; Evarts, 1968). This led to development of the concept of the motor homunculus and laid the theoretical foundation for a cortical interface that could interpret intended limb movements, even of a missing limb.

Improvements in silicon microfabrication technology in the 1970s and 1980s allowed for the creation of electrode arrays with large numbers of needle-shaped electrodes that could be implanted into the cerebral cortex. Since that time, many multi-electrode array (MEA) architectures have been built (for reviews, see Schmitd, 1999 and DiLorenzo, 2008).

Advances during the 1990s in both computer processing power and methods to interpret signals from collections of individual cortical neurons (Nicolelis *et al*., 1995; Nicolelis *et al*., 1997) helped lead to the first example of successful control of a robotic device in real time using a cortical interface (Chapin *et al*., 1999). Four out of six rats were capable of controlling

the position of a one-degree-of-freedom lever solely with signals recorded from ensembles of 21-46 individual neurons (mean of 33.2) through the cortical interface.

In subsequent experiments within the last decade, cortical interfaces have been shown capable of providing up to four degrees of freedom within a robotic arm (x, y, and z motion plus grip) within a primate model (Serruya *et al*., 2002; Taylor *et al*., 2002; Carmena *et al*., 2003; Velliste *et al*., 2008). They have also demonstrated the capacity to provide multiple, controllable degrees of freedom upon interfaced electronics and devices in a human subject with quadriplegia (Hochberg *et al*., 2006). Recent works have begun investigating the capacity of stimulatory cortical electrode arrays within the somatosensory cortex to provide adequate sensation and feedback from a prosthetic device (O'Doherty *et al*., 2009; O'Doherty *et al*., 2011).

Other works have investigated the capacity of animals to learn to control the firing rates of both individual neurons and collections of neurons in hopes that such a capacity could allow for control of multiple degrees of freedom based upon a much smaller number of cortical neurons as opposed to correlating pre-learned activity from motor and pre-motor cortex neurons in the appropriate locations within the motor homunculus. This concept has its theoretical roots in a series of works by Eberhard Fetz and Dom Finocchio in the 1970s. Using metal wire electrodes, they showed that awake monkeys could be conditioned to consciously modify the firing rates of individual cortical neurons (for example, to earn a food pellet) (Fetz, 1969; Fetz and Finocchio, 1971; Fetz and Baker, 1973; Fetz and Finocchio, 1975). Edward Schmidt is credited with proposing that this phenomenon could be used to provide volitional control of a robotic device (Schmitd, 1980). This capacity was confirmed in 2008 (Moritz *et al*.) when a monkey with a peripheral nerve block was able to control the level of contraction of a forearm muscle (and therefore wrist movement, one degree of freedom) via a closed-loop connection with a cortical interface solely based on the firing rate of a single cortical neuron, which the monkey had learned to influence volitionally within ten minutes of practice.

In a 2006 review, Lebedev and Nicolelis identified several key bottlenecks limiting the capacity of cortical interfacing technology toward clinical use. Two of these bottlenecks involved the development of technology not directly related to the biological interface, namely the construction of more realistic powered robotic prostheses and the advancement of computational power and efficient software algorithms capable of real-time interpretation of signals form a large number of neurons (this computational power can be assumed to progress in the near future in concert with Moore's law). An additional bottleneck (and likely the most difficult to overcome of these three) is the development of implant technology capable of obtaining stable, long-term recordings over many years from a large number (hundreds to thousands) of distinct neurons.

Lebedev and Nicolelis summarize the state of cortical microelectrode array technology as capable of providing stable, chronic recordings typically for several months. Specific examples have shown small numbers of individual recorded signals lasting for several years. Quality of signal recording is considered to deteriorate over time due to several biologically related causes and mechanisms which ultimately lead to either fibrous encapsulation and scar tissue buildup around the implanted electrode, physically distancing it from nearby neurons, or inflammatory mechanisms resulting in the deaths of nearby neurons. Numerous researchers are engaged in investigating the underlying mechanisms behind this inflammation and scar tissue buildup (for reviews, see Polikov *et al*., 2005; Grill *et al*., 2008; Marin and Fernandez, 2010). Contributing factors are considered to include acute trauma due to electrode insertion, foreign body response to implanted materials, and friction or micromotion due to mechanical mismatch between brain tissue and electrode materials. Whereas brain tissue is mechanically soft and elastic (modulus of elasticity in the kPa range), silicon electrodes tend to be hard and relatively inflexible (modulus of elasticity in the 100s of GPa range). Proposed engineering solutions to these issues have included the use of surface coatings and modifications (Kotov *et*

al., 2009) and of elastic electrode materials that more closely resemble the mechanical properties of the brain (Mercanzini *et al*., 2008; Wester *et al*., 2008).

Several research groups at Stanford University, the University of Utah, and the Fraunhofer Institute are currently investigating wireless electronics that would be capable of transmitting both sufficient power to run an isolated, implanted device and a continuous signal with sufficient bandwidth to include information from 100 or more electrodes (Harrison *et al*., 2007; Wise *et al*., 2008; Kim *et al*., 2009). Such technology will be necessary for clinical use in humans to prevent injury and infection at the site of percutaneous wire crossings.

Cortical interfacing technologies have many realized and promised benefits. They have been shown capable of providing multiple degrees of freedom toward computer interfaces in both primate and human models. They have shown the potential to provide multiple degrees of freedom from a smaller number of neurons through learned control over the firing rates of those neurons.

Cortical interfacing also has many deficits and drawbacks. Over the long run, the loss of recordable signals over time due to biological rejection of the electrodes makes them, as yet, inappropriate for human clinical use. Signals from neuronal ensembles within the motor cortex require a high degree of processing for decoding of desired outcomes. Of primary concern with regards to the use of cortical interfaces in amputees is the invasiveness of the implantation procedure. While quadriplegics may gain very large improvements to their quality of life by the additional control of even simple devices, such as motorized wheel chair movement or a computer mouse pointer position, a patient suffering from an upper-limb amputation might not risk open brain surgery and implantation of foreign devices into the central nervous system simply to gain control of an additional arm. Implantation of interfaces into peripheral nerves may have the potential to provide equal or even superior control of a robotic prosthesis with much less risk and inconvenience to the patient.

1.3 Peripheral Nerve Interfacing

1.3.1 Categories of Peripheral Nerve Interfaces based on invasiveness and selectivity

Peripheral nerve interfaces may be classified based upon their inherent degree of external-to-internal invasiveness (Figure 1.4). Epineurial electrodes, such as the cuff electrode, are capable of recording the compound activity of an entire nerve, weighted toward large axons and fascicles near the periphery of the nerve. They cannot record the activity of individual axons or from individual, distinct fascicles within the nerve, but are minimally invasive and are considered safe for clinical use in humans. Intrafascicular electrodes are inserted into the nerve, breaking the integrity of the epineurium and of fascicular perineuria. More invasive than cuff electrodes, they are capable of recording the compound activity of individual fascicles. Intraneural or penetrative electrode arrays are inserted within the nerve, penetrating even the endoneuria. They are capable of recording single-unit action potentials of nearby axons. Regenerative electrode arrays are considered to be the most selective and most invasive of the interfacing strategies currently being developed for use in peripheral nerve interfacing. Considered more appropriate for interfacing with the nerves of amputees than with the nerves of otherwise healthy individuals, they require transection of the entire nerve to allow growth of regenerating axons through a tube with embedded electrodes.

Whereas the theoretical foundations for controlling a device based upon the firing patterns of cortical neurons were laid in the 1960s (Evarts, 1966), the theoretical foundations for peripheral nerve interfacing were laid in the 1920s (see following section). Both fields required the development of microfabrication technologies during the 1970s and 1980s for the construction of appropriate electrodes to begin investigating actual interfaces.

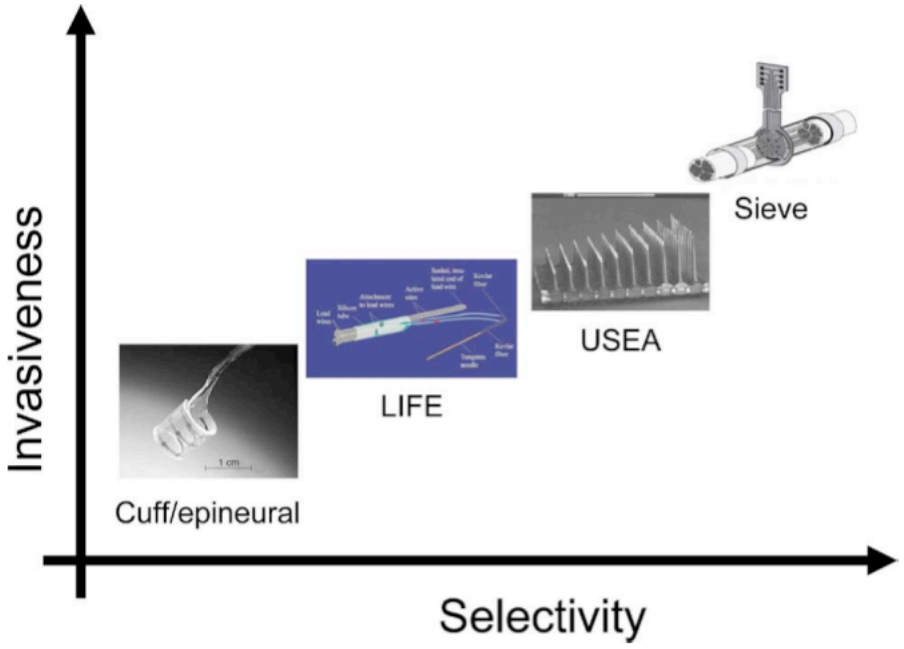

Figure 1.4 Of the proposed strategies for peripheral nerve interfacing, regenerative electrode arrays are considered to be the most potentially selective as well as the most invasive. Adapted from Navarro *et al*., 2005.

1.3.2 History of Peripheral Nerve Interfacing

Luigi Galvani and Alesandro Volta, pioneers in the fields of physics and physiology, demonstrated in the late 1700s that peripheral nerves are capable of carrying electrical signals and that electrical stimulation of a peripheral nerve can cause the contraction of distal muscle groups (for a historical review, see Piccolino, 1998). Emil du Bois-Reymond, a German physician and philosopher is credited with the discovery of the nerve action potential in the mid-1800s, with the first drawings of observed action potentials published by his student, Julius Bernstein (see Schuetze, 1983). Almost 100 more years passed before Hodgkin and Huxley's

giant squid axon experiments provided the modern electrophysiological model of action potential propagation (Hodgkin and Huxley, 1952).

With the invention of the cathode ray oscilloscope and its incorporation into neuroscience research in the 1920s, it was learned that a series of electrical impulses (action potentials) carried by individual nerve fibers (axons) correlated directly with the contractile force of a distally innervated muscle (see Adrian and Bonk, 1928). The firing rates of individual motor neuron fibers were transferred to multiple muscle fibers to form distinct motor units that displayed a graded contraction up to a point of saturation (see Cooper and Eccles, 1930; Clark, 1931). Current models of highly selective interfaces, such as regenerative and penetrative PNIs, aim to correlate the firing rates of individual interfaced motor neuron axons with the movement of a robotic hinge instead of the contractile force of a (now missing) distal muscle (Figure 1.5).

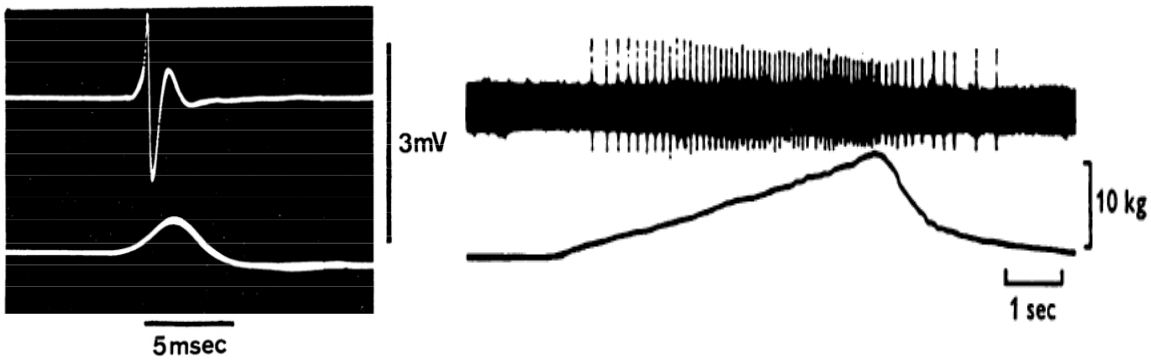

Figure 1.5 (A) A single human motorneuron action potential, transferred to a myofiber (top), results in a small, brief muscle contraction (bottom, measured by EMG). (B) The firing rate of a human motor neuron (top) linearly correlates with the total force of contraction (bottom) of distal myofibers within a motor unit. Highly selective PNIs aim to translate the firing rate of individually interfaced motor neurons into limb movements instead of muscle contraction. Adapted from Fruend *et al.*, 1975 and Desmedt and Godaux, 1977, respectively.

Low-selectivity peripheral nerve interfaces work on a somewhat different principle, whose theoretical roots also lie in the 1920s. Erlanger and Gasser (1924) showed that the "action current" of a whole nerve was comprised of the summed potentials of all of the individual axons within it. They did this by electrically stimulating a dog phrenic nerve at a specific location, causing the coordinated depolarization of many axons at that location, and then observing that the action current changed shapes as it traveled away from the point of stimulation. Noting that the shape devolved from a wave with a single peak to one with multiple peaks, they hypothesized that in the case of the phrenic nerve (and we now hold it true for all mixed nerves) that the action current of the whole nerve was the summed action potentials of multiple distinct axon types that travel at different velocities. These axon types were characterized as $A\alpha$, $A\beta$, $A\gamma$, or $A\delta$ based upon their conduction velocities (Figure 1.6). It was later determined that the $A\gamma$ distinction was not unique (Erlanger and Gasser, 1930) and for that reason has been mostly discontinued. C fibers were characterized several years afterwards (Erlanger and Gasser, 1930). Their contribution to the compound action potential went unnoticed initially because (1) they require a higher excitation voltage than A fibers, (2) they possess a conduction velocity typically one sixth that of A fibers, resulting in their contributory peak often falling outside of the viewed range on an oscilloscope, and (3) they typically contribute a much lower amplitude peak than the resultant peaks from A fibers. It was initially obvious through morphological analysis of nerves with varying myelination content and differing A and C wave contributions that the C fiber waveform was the resultant contribution of unmyelinated fibers and the A fiber waveforms were the resultant contributions of myelinated fibers. It was speculated initially, and later confirmed (Gasser and Grundfest, 1939), that axon diameter size directly contributed to the conduction velocity of an individual fiber.

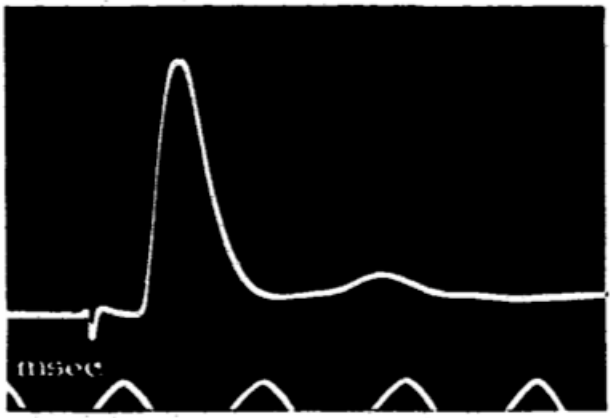

(A)

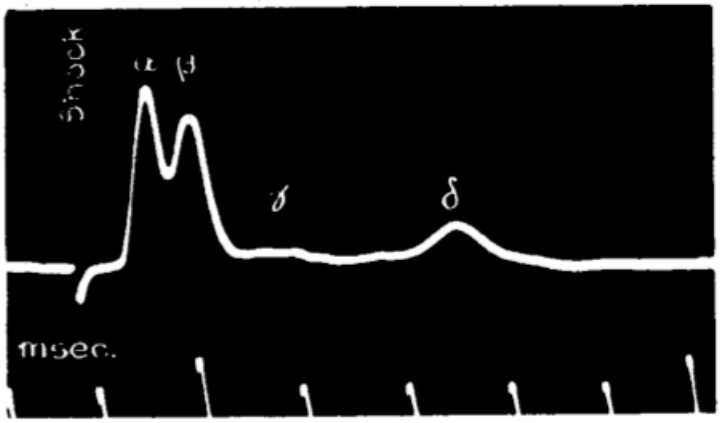

(B)

Figure 1.6 An induced compound action potential of a mixed nerve appears as a traveling waveform with a single peak when measured near the point of stimulation (A). Due to heterogeneous conduction velocities of component axons, the traveling waveform devolves into a shape with multiple distinct peaks when measured farther from the point of stimulation (B). Time markers = 1 millisecond intervals. Adapted from Gasser, 1941.

As a result of this summed contribution of many axons, information relating to the overall activity of a nerve, a fascicle, or a large group of coordinated axons cannot be interpreted as a series of repetitive waveshapes as it can with individual axons. It can instead be interpreted as an increase in indistinct, shapeless spikes represented visually as a swelling of the “noise” baseline. Figure 1.7 shows an example of the overall activity of a cat sciatic nerve during three steps on a treadmill. Such a signal may be rectified and enveloped to allow for continuous monitoring of the activity of the interfaced nerve. See also Figure 1.8.

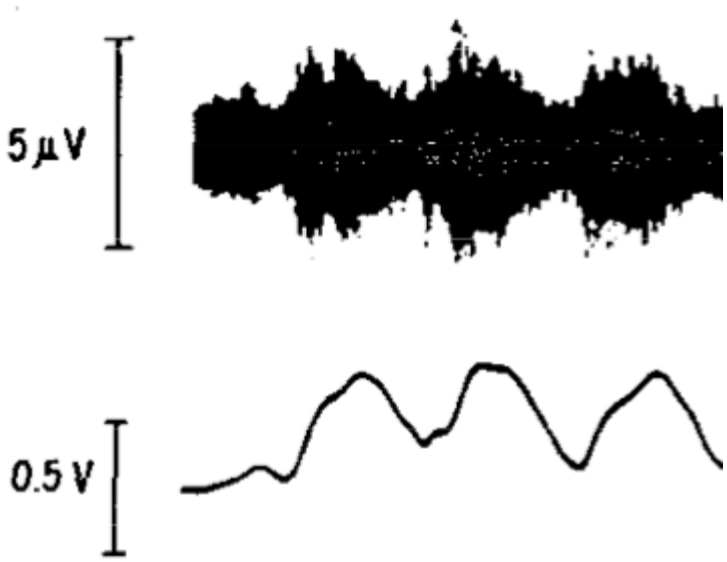

Figure 1.7 Low-selectivity PNIs operate by translating the compound activity of many axons within a nerve or fascicle into desired whole-muscle contraction, as proposed by Stein *et al*. (1975) and de Luca (1978). The top plot shows the compound activity of a cat sciatic nerve, via a cuff electrode, as it takes three steps. The bottom plot shows the rectified and filtered waveform, clearly correlating with the three steps. Adapted from Stein *et al*., 1975.

Electrophysiological recordings of nerves throughout the mid-1900s was primarily conducted in terminal experiments in laboratory settings where nerves could be isolated and insulated or in non-mammalian animal models. Epineural electrodes and various needle

electrodes found clinical use in humans but only for stimulatory and therapeutic purposes. The development of microfabrication techniques during the 1970s allowed for construction of the first devices used with the express intention of developing interfaces between computers or machines and the peripheral nervous system.

1.3.3 Cuff Electrode Interfaces

In the mid-1970s, it was shown that wrapping a length of nerve in an insulating material, such as silicone, with an electrode inside could effectively lower ambient noise to the point where nerve activity from awake, moving mammals could be monitored (Stein and Pearson, 1971; Stein *et al*., 1975; de Luca and Gilmore, 1976; Stein *et al*., 1977). The resulting electrode model quickly came to be known as a cuff electrode and has since found continued use in both basic research and clinical medicine (for reviews see Struijk *et al*., 1999 and Navarro *et al*., 2005). While cuff electrodes may have complementary uses, such as whole-nerve stimulation, they are not considered candidates for providing volitional control over multiple degrees of freedom.

Over the last decade, several researchers at Case Western University have attempted to improve upon the basic cuff electrode with architectures that slowly flatten an entrapped nerve with the goal of increasing selectivity by physically broadening the nerve and separating internal fascicles. Multiple epineural electrode contacts allow for more selective recording and stimulation of those fascicles (Perez-Orive and Durand, 2000; Tyler and Durand, 2002; Leventhal and Durand, 2004; Schiefer *et al*., 2005; Gustafson *et al*., 2009; Tyler *et al*., 2011). They have also investigated the potential of cuff-like shape-changing devices that slowly insert electrode tips into a nerve *in situ*, penetrating the epineurium but not the perineuria, referring to these as interfascicular electrodes (Tyler and Durand, 1997a; Tyler and Durand, 1997b).

1.3.4 Intrafascicular Electrode Interfaces

The class of interfacing devices known as intrafascicular electrodes aims to measure compound nerve activity from bundles of axons within a nerve by inserting one or more low-selectivity electrode contacts within the epineurium of a nerve. This is often done by threading a wire with embedded electrode contacts through a nerve longitudinally. Intrafascicular interfaces were first introduced in 1989 and developed in the early 1990s with the goal of providing greater selectivity than cuff electrodes as well as improved signal quality (Malagodi *et al*., 1989; Lefurge *et al*., 1991; Goodall *et al*., 1991; Goodall and Horch, 1992; McNaughton and Horch, 1994; McNaughton and Horch 1996; Yoshida and Horch, 1996). The capacity of intrafascicular electrodes to record signals with better signal-to-noise ratio than is typically seen in a cuff electrode is well documented (see Figure 1.8).

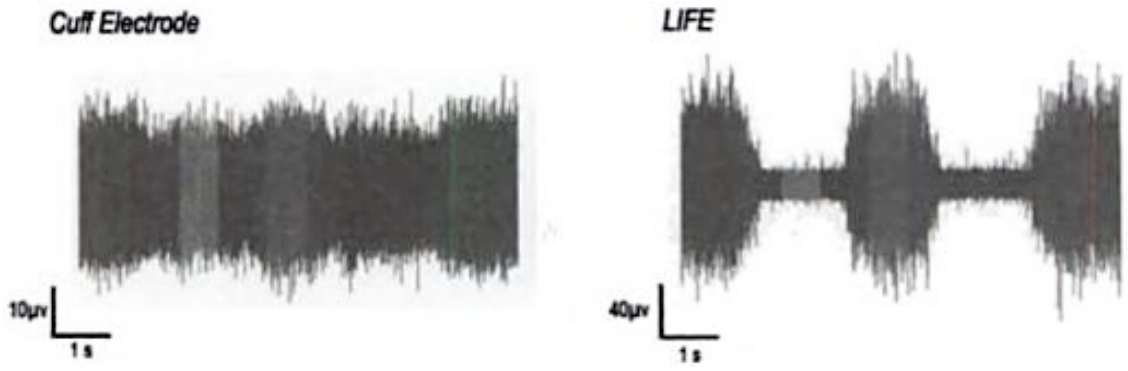

Figure 1.8 Intrafascicular electrodes can provide greater sensitivity of recordings than cuff electrodes. In the example shown here, intentionally selected to highlight this difference, a rat leg was subjected to three rotations of the ankle joint. Corresponding nerve activity could be observed from a sciatic cuff electrode (left) and a tibial intrafascicular electrode (right). Adapted from Yoshida and Struijk, 2004.

It should be noted that there is no clear, definitive distinction between what is called an intrafascicular electrode and what is called a penetrative electrode. Intrafascicular electrodes do penetrate the nerve and microfabricated arrays of penetrating needle electrodes have been referred to as 'intrafascicular,' especially if intended for stimulating multiple axons within a

fascicle. If designed with fine dimensions, longitudinally inserted intrafascicular electrodes begin to resemble fine needle or wire electrodes and have been shown capable of detecting and discriminating between multiple single-unit action potentials within a fascicle (Lefurge *et al*., 1991; Goodall and Horch, 1992; McNaughton and Horch, 1996). In general, and for the devices reviewed in the following paragraph, 'intrafascicular electrode' is used to refer to a device used for the detection of compound activity only.

In a series of articles investigating the use of intrafascicular electrodes implanted into peripheral nerves of human amputees, researchers at the University of Utah showed that peripheral nerves remain viable carriers and receivers of information even years after initial amputation (Dhillon *et al*., 2004) and that humans can control a one-degree-of-freedom device while receiving feedback information that can be interpreted to encode for limb position (Dhillon and Horch, 2005; Horch and Dhillon 2006). In the last several years, research on human subjects has continued. A group of researchers associated with Shanghai Jiao Tong University and Johns Hopkins University have investigated the simultaneous implantation of intrafascicular electrodes into multiple nerves of a single human patient (Jia *et al*., 2007). Another collaborative group of researchers, centered around Rome, Italy, has investigated new electrode designs and advanced signal processing techniques on intrafascicular array recordings from human patients (Citi *et al*., 2008; Micera *et al*., 2008; Micera *et al*., 2010a; Micera *et al*., 2010b; Rossini *et al*., 2010; Rossini *et al*., 2011). Additional recent research involving intrafascicular arrays has included investigations into new device architectures (Boretius *et al*., 2010) and neural plasticity in human amputees (Dhillon *et al*., 2005; Di Pino *et al*., 2009). Intrafascicular electrodes will likely have a future clinical role in some capacity with regards to electrical stimulation, neuromodulation, or limited interfacing. They have been very valuable in showing that it is possible for humans with amputated limbs to control a device with information from peripheral nerves and receive feedback information. Due to their lack of selectivity, they will likely not be capable of providing control of up to 23 degrees of freedom.

1.3.5 Penetrating Electrode Interfaces

Much of what has been learned about the physiology of peripheral nerves in the last century has been from the laboratory use of simple penetrating microneedle electrodes, capable of recording the activity of individual axons (for historical and methodological reviews, see Thomas, 1961; Gandevia and Hales, 1997; Vallbo *et al*., 2004). Simple microneedle electrodes can also be used to stimulate single axons (Ochoa and Torebjork, 1983). The incorporation of microneedles into packaged arrays for the simultaneous recording of multiple individual neurons as well as the microfabrication of penetrative electrodes with multiple electrode contacts per shaft occurred during the 1980s and 1990s, primarily for the purpose of cortical investigations (see Najafi, 1994; Schmidt, 1999; Schwartz 2004). In the late 1990s, researchers began implanting some of these electrode array devices into peripheral nerves for both stimulation (Smit *et al*., 1999; Rutten *et al*., 1999) and recording (Branner and Normann, 2000).

One of the most popular manufactured multielectrode arrays for use in electrophysiological investigations is the Utah Electrode Array (Blackrock Microsystems, Salt Lake City, Utah) (see Figure 1.4, USEA). Variations of this array have been used to investigate, stimulate, or interface with the motor cortex (Hochberg *et al*., 2006), the sensory cortex, (Rouche and Normann, 1998), the visual cortex (Torab *et al*., 2011), dorsal root ganglia (Aoyagi *et al*., 2003), and peripheral nerves. Researchers at the University of Utah have conducted a series of experiments over the last decade in which this array was implanted into peripheral nerves of cats. They have demonstrated that penetrative electrode arrays in peripheral nerves are capable of selective and graded muscle stimulation (Branner *et al*., 2001; McDonnall *et al*., 2004; Branner *et al*., 2004; Dowden *et al*., 2009; Frankel *et al*., 2011), capable of selectively inducing a local nerve block using alternating currents (Dowden *et al*., 2010), capable of recording distinct single-unit action potentials from multiple axons in response to sensory stimulation (Branner and Normann, 2000; Branner *et al*., 2004), and capable of wirelessly controlling a one degree of freedom robotic limb (Clark *et al*., 2011).

In a 2002 experiment that was highly publicized in the popular media as creating the first “human cyborg,” investigators implanted a 100-electrode penetrative array into an isolated fascicle of the median nerve of a healthy recipient who was able to use it for several months to control one degree of freedom (grip) of a robotic limb and detect a feedback signal through electrical stimulation (Warwick *et al*., 2003; Gasson *et al*., 2005). The experiment had to be terminated due to complications with interconnect wires.

Penetrating electrode arrays will likely play a major role in future investigations into peripheral nerve interfaces and will likely find clinical use in a stimulatory capacity. While more invasive than epineural arrays and intrafascicular arrays (the human trial did require isolation of an individual fascicle and dissection of the covering perineurium), they are much less invasive than regenerative arrays. They have been shown capable of recording high quality signals, but researchers have commented that rapid signal loss (within months) is currently an issue.

1.3.6 Regenerative Interfaces

1.3.6.1 Early works (mid 1960s to early 1980s)

The concept of creating an electrode architecture through which regenerating axons of a cleanly transected peripheral nerve could grow is considered to have initially developed as early as the 1960s with several unpublished communications showing construction of prototypes as early as 1965 (see Kovacs, 1991). The first published work investigating the feasibility of a regenerative PNI was done by A. F. Marks (Marks, 1969). Her experiments showed that transected peripheral axons would indeed grow through a porous polytetrafluoroethylene implant in an amphibian model. The first micromachined silicon design for an implantable regenerative electrode was presented in 1973 (Llinás *et al*), followed quickly by the first published electrophysiological recordings from a regenerative electrode (Figure 1.9) (Mannard *et al*., 1974). Loeb *et al*. (1977), Matsuo *et al*. (1978) and Edell (1986) helped advance electrode device design by incorporating microfabrication and wet etching techniques

to device construction. Until the mid-1970s, all *in vivo* experiments had been performed on amphibians with acute recording sessions, meaning electrode contacts were surgically exposed several weeks post-implantation (to allow time for nerve regeneration) during a terminal recording session followed by sacrifice.

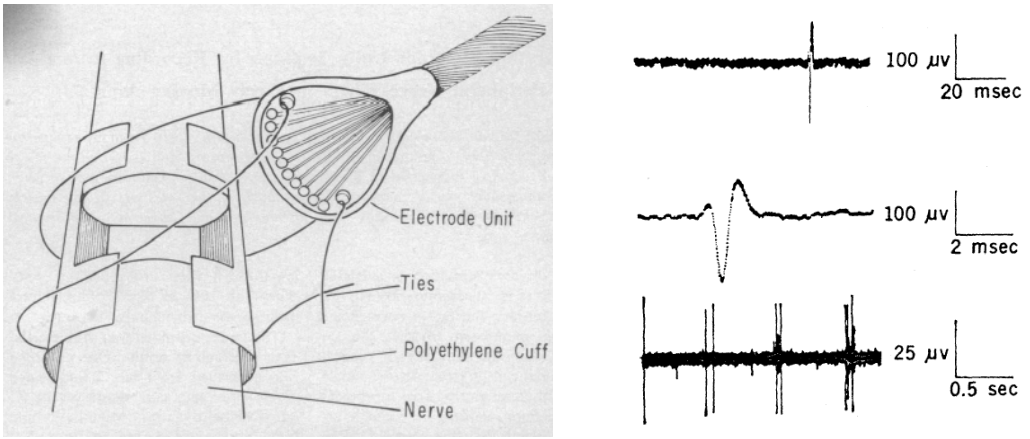

(A) (B)

Figure 1.9 (A) Schematic drawing of the first implemented regenerative PNI. (B) The first published electrophysiological recordings from a regenerative PNI, implanted into a frog sciatic nerve, showing a single-unit spike in response to a muscle stretch (top and middle) and a train of spikes (bottom) during swimming. Adapted from Mannard *et al*., 1974.

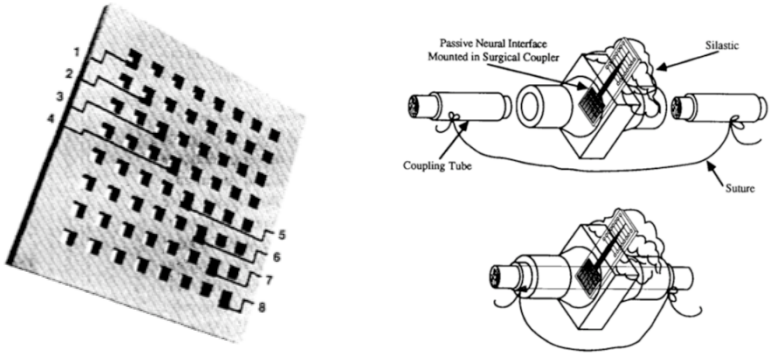

(A) (B)

Figure 1.10 Micrograph (A) and schematic of implantation procedure (B) of a silicon-based sieve electrode interface. Adapted from Kovacs *et al*., 1994 and Kovacs, 1991, respectively.

1.3.6.2 Microfabricated Silicon Sieve Electrodes (mid 1980s to late 1990s)

Chronic recordings from peripheral nerves in a mammal, in which electrode contacts were more permanently exposed outside of the skin to allow for repeated recording sessions at varying time intervals without sacrifice of the animal, were first proposed and developed using cuff electrodes (de Luca and Gilmore, 1976; Stein *et al*., 1977). These techniques were expanded toward regenerative interfaces starting in the late 1980s.

Edell investigated the biocompatibility of silicon-based electrodes (Edell *et al*., 1982) and obtained the first chronic recordings using a regenerative-style electrode in a mammal (rabbit) (Edell, 1986). Researchers at Stanford University developed a silicon-based sieve-style electrode array and conducted several experiments involving peroneal nerves of rats and cranial nerves of frogs (Rosen *et al*., 1990; Wan and Kovacs, 1990; Kovacs, 1991; Kovacs *et al*., 1992; Kovacs *et al*., 1994; Della Santina *et al*., 1997). The authors showed that single-unit neural activity could be successfully recorded from an implantable silicon-based device compatible with CMOS technology. They speculate that such technology will be beneficial in the future to allow integrated circuitry and multiplexing on a wireless implantable device.

Researchers from the University of Michigan conducted a series of experiments involving a custom-made silicon sieve electrode implanted into the rat glossopharyngeal nerve (Bradley *et al*., 1992; Akin *et al*., 1994; Najafi, 1994; Bradley *et al*., 1997; Akin *et al*., 1998;). The experiments culminated in the development of a system for chronic recordings using a percutaneous headcap and a proposal for a wireless transmission system. Of note in these experiments is that the glossopharyngeal nerve is comprised mostly of smaller, unmyelinated sensory axons (see Bradley *et al*., 1992; Jang and Davis, 1987; Oakley, 1985). They later obtained recordings from the VIIIth cranial nerve in a fish model (Mensinger *et al*., 2000).

A group of researchers from Sweden published a series of papers investigating differences in sieve electrode pore size and geometry using custom-fabricated silicon chips (Zhao *et al*., 1997; Wallman *et al*., 1999; Wallman *et al*., 2001). In 2004, a group from Japan

presented a conference paper (Kawada *et al*.) in which they describe the microfabrication and *in vivo* testing of a silicon-based sieve electrode device. It was implanted into the vagal nerve of rats and into the renal sympathetic nerve of rabbits, from which spontaneous action potentials were observed. The work was not published in a peer reviewed journal.

1.3.6.3 Microfabricated polyimide sieve electrodes (mid-1990s to present)

Starting in the mid-1990s, a number of researchers with loose collaborations between several universities and institutes in Germany, Spain, and Italy began experimenting using flexible polyimide-based regenerative sieve electrodes instead of silicon-based ones. First presented in publication in 1997 (Stieglitz *et al*), the flexible polyimide design offered several proposed improvements to previous electrode designs, including a monolithic structure in which the electrodes, conducting cable or ribbon, and external contact pads were all of one microfabricated device without need of interconnects (which sometimes required soldering and housing and were considered a common source of device failure (Stieglitz *et al*., 1997; Dario *et al*., 1998)). Initially, a custom-made silicon-based electrode array was built (Navarro *et al*., 1996; Blau *et al*., 1997) and bonded to a flat, flexible polyimide interconnect cable (Dario *et al*., 1998). Functional regeneration was confirmed during acute testing in an unspecified number of rabbits, but no active devices were used, and this paradigm appears to have been dropped in favor of a fully polyimide-based device.

Four studies to date have involved using the polyimide sieve electrode for recording single-unit action potentials from peripheral nerves (Navarro *et al*., 1998; Shimatani *et al*., 2003; Ramachandran *et al*, 2006; Lago *et al*., 2007). Several publications investigated the capacity for functional nerve regeneration and axonal growth patterns through the fully polyimide-based device in both the rat sciatic nerve (Klinge *et al*., 2001; Ceballos *et al*., 2002) and the rat optic nerve (Heiduschka *et al*., 2001). A later study involved a custom-made 4-channel electrode implanted into the chorda tympani nerve within a rat skull to investigate receptor cell turnover in

taste buds (Shimatani *et al*., 2003). A group of researchers from Yonsei University in Korea implanted polyimide sieve electrodes into rat sciatic nerves to develop methods to analyze functional recovery of regenerating nerves (Lee *et al*., 2006; Kim *et al*., 2007a; Kim *et al*., 2007b; Kim *et al*.,2009). Compound whole-nerve potentials were recorded from an exposed nerve during acute experiments using additional stimulating and recording electrodes. More recent studies involving polyimide electrodes have tended to focus more on understanding patterns of axonal regeneration and have not involved electrophysiological recordings (Negredo *et al*., 2004; Lago *et al*., 2005; Castro *et al*., 2008). One study investigates the long-term effects of an implant in the peripheral nerve upon the central nervous system of cats (Panetsos *et al*., 2008).

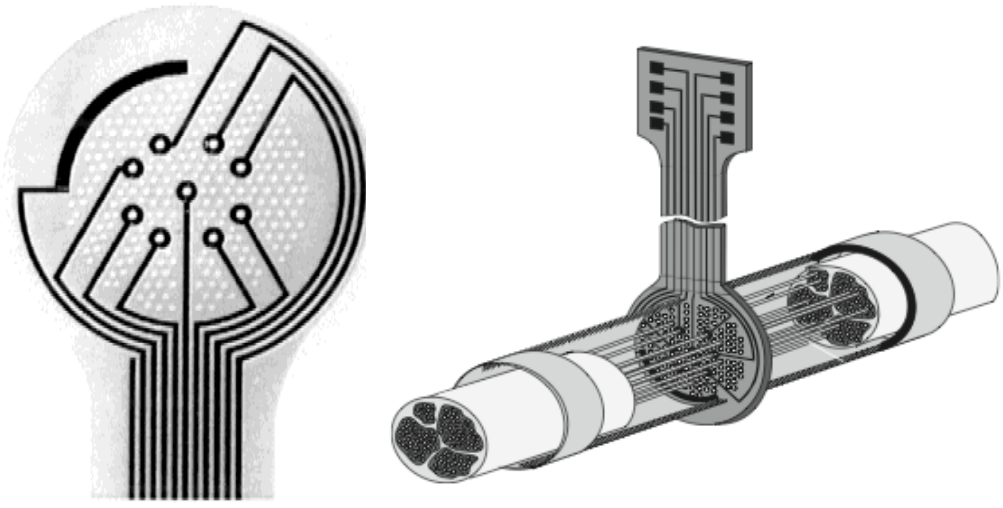

(A) (B)

Figure 1.11 Flexible polyimide sieve electrodes gained popularity among researchers, primarily based in Europe, in the mid-1990s. (A) An early flexible polyimide sieve electrode with integrated ribbon cable. Adapted from Lago *et al*., 2007. (B) Schematic of implantation of electrode with guidance tube into a peripheral nerve. Adapted from Navarro *et al*., 2005.

1.3.6.4 Recent Designs and Developments (2007 to present)

Up until 2007, published work involving regenerative peripheral nerve interfaces had focused almost exclusively on sieve-style electrodes as the interfacing platform. Research and advancement focused mostly on materials, geometry, interconnects, and regeneration potential of axons through the sieve. Difficulties in early designs involving electrodes falling out of poorly confined nerves appear to have diminished in later designs using plastic nerve guide tubes anchored to either side of the sieve. Only ten peer-reviewed papers between 1974 and 2007 contain evidence of single-unit action potentials recorded from regenerative PNIs. Of these, only three involved chronic recordings. Perceived weaknesses included an inability to incorporate a large number of electrodes onto a single device and potential constrictive axonopathy due to small pore size and rigid materials. In the last few years, several new strategies involving novel electrode designs have emerged to address some of these challenges.

Researchers at the University of Texas Dallas and the University of Texas Southwestern Medical Center have presented two regenerative electrode designs not based on a sieve device. The first design (Cho *et al*., 2008) aimed to avoid the effects of constrictive axonopathy by using a non-biodegradable plastic nerve guide tube filled with a biodegradable agarose gel containing 250 μm diameter hollow channels. The hollow channels were intended to guide regenerating axons into distinct bundles resembling natural nerve fascicles. After initial migration of regenerating axons, as axonal diameter and myelination increase, degradation and resorption of the agarose gel would prevent undesirable constrictive effects upon the nerve tissue. Such a design had been shown to facilitate nerve regeneration superiorly to a hollow (collagen-filled) tube (Tansey *et al*., 2011). Small (50 μm x 120 μm cross sectional area) bipolar electrodes fabricated out of SU8 epoxy and gold were inserted into the hollow channels (Figure 1.13). A single *in vivo* experiment has been reported in which chronic recordings were made

from devices implanted into the rat sciatic nerve. Additional work by this group has focused on integrating wireless electronics onto the SU8 platform (Cho *et al*., 2010).

The second design consisted of a hollow collagen-filled tube into which a needle electrode array (the type typically used as a penetrative electrode array within the central nervous system in rodent and primate experiments) was inserted (Figure 1.14) (Garde *et al*., 2009). This design was intended to negate the concern of restrictive axonopathy and to provide a relatively clear path for nerve regeneration through the guide tube (compared to a sieve design) while still providing a comparable number of recording electrodes. This interface design is used extensively throughout the experiments that comprise this dissertation.

Researchers from the University of Tokyo introduced, first in a conference proceedings (Suzuki *et al*., 2006) and subsequently in a published paper (Suzuki *et al*. 2007a) the idea of incorporating a series of microchannels into the architecture of the nerve guidance tube as a means of allowing for the presence of more electrodes within the design. They proposed a "rolled" device architecture that has since inspired several other designs (Figure 1.12). They have also proposed the incorporation of fluidic channels into the device architecture that would allow for *in situ* drug delivery. In addition to this work, this group has explored the use of flexible polymers within a sieve architecture (Suzuki *et al*., 1997; Gojo *et al*., 2009; Gojo *et al.,* 2010).

A group of researchers from Cambridge University have claimed that encapsulation of axons within microfluidic channels effectively amplifies extracellular recordings by encapsulated electrodes. This has been supported by a mathematical model for both myelinated and unmyelinated axons (Fitzgerald *et al*., 2008) and by *in vitro* and *in vivo* evidence for myelinated axons (Fitzgerald *et al*., 2009; Minev *et al*., 2012). These researchers have published several works investigating microchannel amplification and flexible materials for interface and electrode design (Lacour *et al*., 2008; Lacour *et al*., 2009; Lacour *et al*., 2010; Benmerah *et al*., 2009). They have recently begun investigating new device architectures based on microchannel designs in animal studies (Fitzgerald *et al*., 2012).

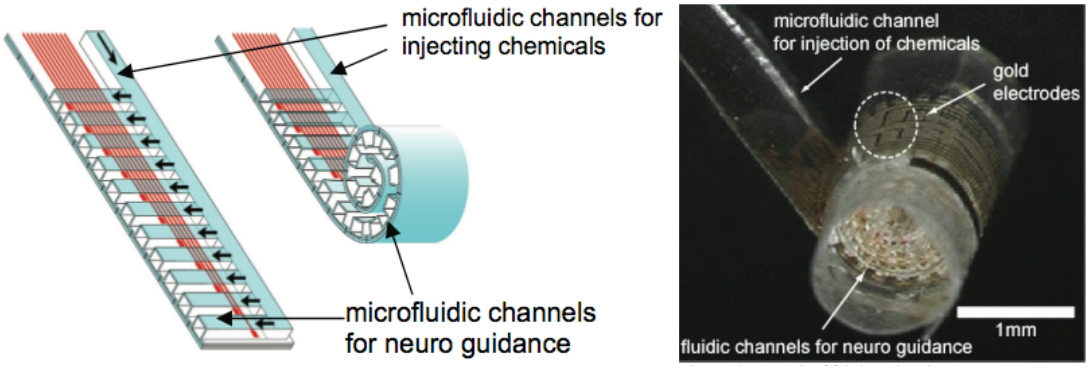

(A) (B)

Figure 1.12 Schematic (A) and prototype (B) of a proposed architecture in which a flat array of microchannels with incorporated electrodes is "rolled" into a tube to serve as a nerve guide. Adapted from Suzuki *et al*., 2007.

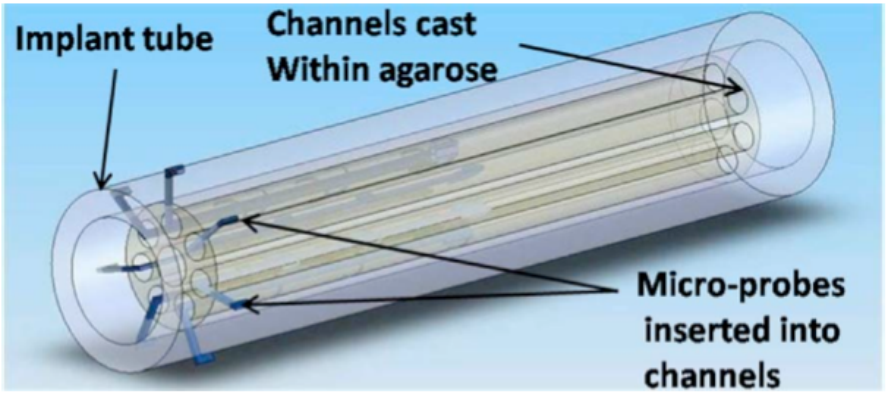

Figure 1.13 Schematic of a regenerative device with SU8-based electrodes embedded within hollow axonal-guidance channels of a biodegradable medium within the lumen of a non-biodegradable nerve guide. Adapted from Cho *et al*., 2008.

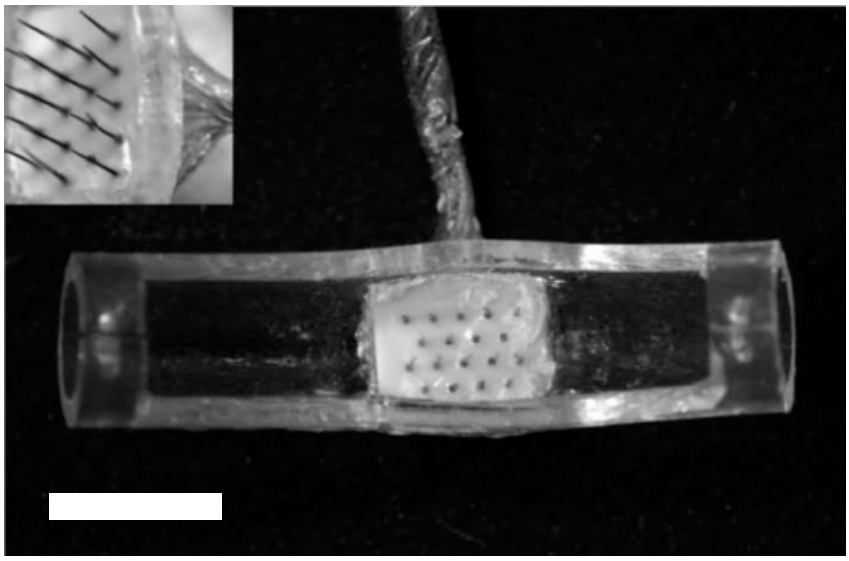

Figure 1.14 The regenerative multielectrode interface (REMI) consists of a needle-electrode array embedded within a nerve guide tube. Scale bar = 1 mm. Adapted from Garde *et al*., 2009.

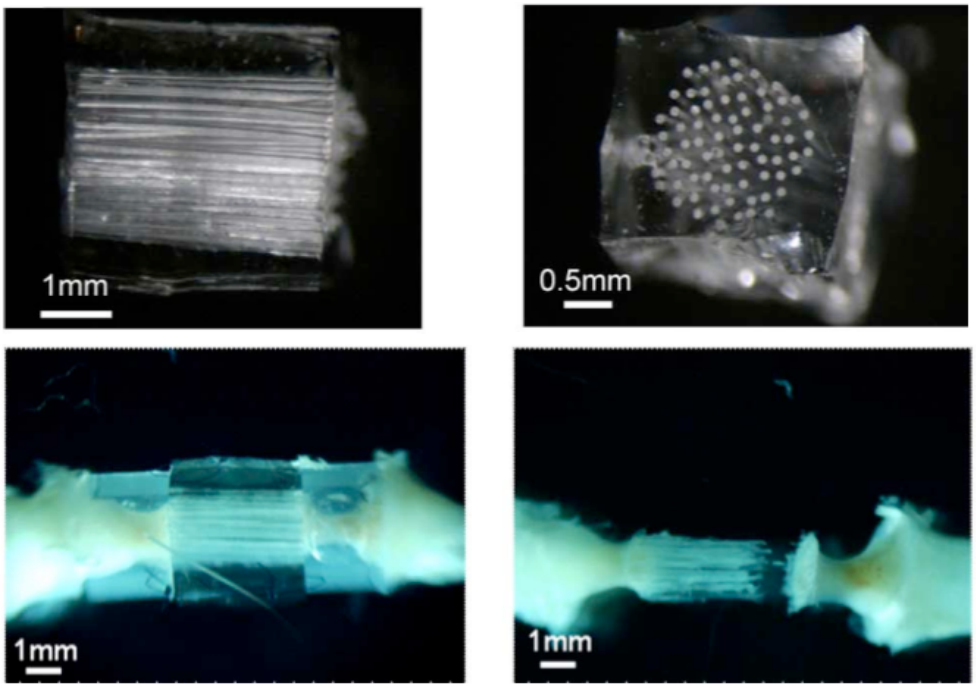

Figure 1.15 Example of a proposed method of generating microchannels (110 μm diameter) within a nerve guide conduit. Adapted from Lacour *et al*., 2009.

Researchers at the Georgia Institute of Technology have developed a prototype platform resembling the 'rolled' electrode design of Suzuki *et al*. (2007) into which they aim to incorporate integrated electronics for amplification and signal processing (Guo *et al*., 2010; Srinivasan *et al*., 2011). A group of researchers primarily associated with Johns Hopkins University has introduced a separate 'rolled' device architecture consisting of multiple, longitudinal guidance channels containing embedded electrodes within a bulk polymer that is biodegradable (Lewitus *et al*., 2011). This design aims to guide initial nerve regeneration to position axons close to electrode tips while allowing axonal and tissue growth to proceed without constriction as the bulk scaffold degrades. Electrodes would remain physically entrapped by nerve tissue.

A group of researchers consisting mostly of physicians from the University of Michigan Medical School has introduced the idea of interfacing with a severed peripheral nerve by allowing groups of axons within the nerve to grow into and innervate encapsulated bundles of transplanted myoblasts. Electrophysiological signals may then be recorded from the resultant innervated myofibers. These proposed procedures take advantage of some of the benefits of targeted muscle reinnervation, in which muscle fibers act as signal transducers (electrophysiological signals are much more easily recorded from muscle fibers than from peripheral axons due to the greatly increased cellular surface area) and improve upon it by potentially allowing for an increased number of available recording channels. It also does not require denervation of large muscles in the host. Much of their published work to date involves the development and characterization of implantable electrode materials, specifically the electrically conductive polymer poly(3,4-ethylenedioxythiophene) (PEDOT) (Egeland *et al*., 2010a; Urbanchek *et al*., 2011a; Frost *et al*., 2012).

1.4 Summary and Specific Aims

Of the currently proposed strategies for providing realistic volitional control of a robotic prosthesis, regenerative peripheral nerve interfacing is considered to be the most selective. While regenerative interfacing has been in development for over 40 years, the field is far from able to produce a device sufficient for clinical use.

Three specific limitations of the current state of the field are here identified, based upon review of the literature. Analysis of these three limitations led to the three specific aims of this dissertation.

1.4.1 Limitation #1:

All *in vivo* experiments to date have suffered from a high degree of physical and mechanical failure of implanted devices. This represents an engineering problem, not a biological one. From a research perspective, premature failure of implanted devices precludes the ability to test biological hypotheses. From a practical perspective, high rates of device failure add significant cost to an already expensive field of research. From a medical perspective, a high rate of mechanical failure of devices is unacceptable for clinical use in humans.

To date, only 16 published experiments have demonstrated single-unit action potentials recorded from implanted regenerative PNIs. Physical device failure has been described as a large impediment to research, but details are rarely given. No large-cohort animal experiments have been conducted.

1.4.2 Limitation #2:

Most *in vivo* experiments to date which have recorded single-unit activity have suffered from signal loss over time. This usually occurs within months. A practical device capable of clinical use would be required to function for many decades.

As with highly selective cortical interfacing paradigms, this signal loss is considered to be due to complex biological causes. Causes related to electrode rejection, scar formation, inflammation, and micromotion are sources of intense research by scientists investigating cortical implants. This research is expected to yield benefits to the field of peripheral interfacing as well. A factor relevant only to peripheral interfaces, potential acceleration of biological rejection due to physical stretching of the nerve during limb movement, has not yet been investigated.

1.4.3 Limitation #3:

No device architecture proposed to date has demonstrated sufficient sensitivity and selectivity of recordings necessary to control a prosthetic device with many degrees of freedom. Microchannel encapsulation has been proposed as a means to amplify recorded signals, increasing sensitivity, and possibly thus decrease signal loss over time. This phenomenon has been predicted for both myelinated and unmyelinated axons. *In vitro* evidence exists in support of the predictions for myelinated axons.

1.4.4 Specific Aims

Specific Aim I: Identify the common causes of physical device failure inherent within regenerative peripheral nerve interfaces.

Specific Aim II: Determine if nerve stretch due to limb extension contributes to accelerated signal loss in regenerative nerve interfaces.

Specific Aim III: Validate the capacity for microfluidic channels to amplify extracellular recordings of unmyelinated axons.

Two large-cohort *in vivo* experiments and one *in vitro* experiment have been conducted addressing these specific aims. The experiments and their results are presented in the following three chapters. Chapter 5 includes a discussion of the relevance of the findings to the future of the field of regenerative interfacing.

CHAPTER 2

COMMON CAUSES OF PHYSICAL DEVICE FAILURE

2.1 Overview

2.1.1 Limitation of current RPNI technology

All *in vivo* experiments to date have suffered from a high degree of physical and mechanical failure of implanted devices. As mentioned in the introductory chapter, this represents an engineering problem, not a biological one. Engineering solutions will likely be found, and the field could benefit from a more thorough quantification of common causes of device failure inherent within the current regenerative interfacing paradigm. The published literature to date is generally vague about specific causes of device failure, but reports them to be a significant impediment to research. To quantify what is currently known in the field, the 16 identified articles that have been published to date which include reports of single-unit spikes recorded from a RPNI, along with a few other relevant works, are reviewed in Section 2.1.3 and summarized in Section 2.1.4.

2.1.2 Specific Aim

The specific aim of this chapter is to identify the common causes of physical device failure inherent within current regenerative peripheral nerve interfacing technology. In addition to reviewing the relevant literature, which tends to report on small-cohort experiments, this chapter presents the results of a large-cohort experiment (n = 60 animals) conducted in our laboratory.

2.1.3 Review of Published Recordings from Regenerative PNIs

The first published recording of action potentials from a regenerative PNI was in 1974 (Mannard *et al*.). The authors used a custom-made device in which 17 electrode holes were mechanically drilled into an epoxy wafer substrate. The interface was implanted into the hind sciatic nerves of 6 frogs. Acute experiments were conducted 12-25 weeks post implantation in which implanted electrode contacts were surgically exposed to allow for recording. Single-unit bursting activity was observed in a total of 6 channels within 3 frogs. The authors speculate that inadequate regeneration, damage to nerves, and lead wire breakage might be possible causes for lack of signal acquisition in half of their implanted animals.

The first published attempts at recording from mammalian nerves using regenerative PNIs were made by Loeb *et al*. (1977). Silicon-based microfabricated electrodes were designed and fabricated with impedances reported at 800 kΩ to 1.5 MΩ. According to the authors, *in vivo* attempts at recording were unsuccessful due to technical difficulties surrounding connectors and anchoring of the electrode to transected nerves.

Edell (1986) published the first action potentials recorded from a mammal (rabbit) using a regeneration-style electrode. Few details on the experimental setup, number of animals involved, and challenges faced were given. Implanted wires connected the implant in the tibial nerve to a percutaneous connector in the sacral area. The report mentioned that myoelectric signals and motion artifacts were a concern during recordings.

The regenerative sieve electrode used in the Stanford University experiments in the 1990s was a custom-made silicon-based device (Kovacs, 1991). During an acute experiment in which electrodes were implanted into rat peroneal nerves, the author reports evidence of recorded single-unit action potentials and the ability to stimulate muscle activity. A subsequent experiment involved the same electrode implanted into the peroneal nerve of 9 rats (Kovacs *et al*., 1992). The authors report that acute recording sessions were attempted on 8 rats with the majority proving unsuccessful due to shifting of the implanted electrode array out of the nerve.

Single-unit action potentials were reported in an undisclosed number of electrode channels and animals. In another publication (Kovacs *et al*., 1994), the authors used both rats and frogs. Three rats were implanted with sieve electrodes into the peroneal nerve. All three displayed single-unit spiking activity during acute recording sessions. Four frogs were implanted with similar arrays into the eighth cranial nerve to investigate the use of sieve electrodes in a cranial nerve model. Two frogs displayed single-spike activity during acute recording sessions. Dissection of the other two frogs revealed that the nerves regenerated around the electrode device and not through it. Additional similar work with frogs (Della Santina *et al*., 1997) included 11 implanted animals, of which 2 displayed recordable action potentials. Low yield was attributed to difficulties with implant surgeries leading to post-operative mortality and brain damage.

The first use of the sieve electrode architecture that was developed in the 1990s at the University of Michigan was to investigate regeneration of sensory fibers in the rat glossopharyngeal nerve (supplies the tongue) (Bradley *et al*., 1992). Twenty-eight rats were implanted with sieve electrodes, of which 21 displayed successful nerve regeneration upon histological examination at 91 to 118 days. Electrophysiological activity of the whole nerve showed successful functional regeneration through the electrode device, but electrophysiological activity was not recorded from the device itself. The authors comment that in the 7 unsuccessful animals, the electrode array had often been pulled out of the guide tube. A follow-up analysis of the electrical properties of the electrode (Akin *et al*., 1994) characterizes the electrodes as having an impedance less than 100 kΩ and introduces the authors' intentions to develop an electrode capable of chronic recordings. The authors mention that the mechanical strength and possibility of breakage of an attached ribbon cable connecting the electrode array to the outside world is a concern. In 1997, these researchers presented chronic recordings of single-unit action potentials from a polyimide electrode array connected to the external environment by an integrated ribbon cable and a percutaneous headcap (Bradley *et al*.,

1997). Thirty-two rats were implanted (sciatic nerve). Of these, 24 were reported terminated due to loss of the headcap or broken connector cable. An unspecified number of animals did not show action potentials and were reported to have suffered from the nerve leaving the guide tube post-implantation. Successful recordings from an evoked sensory response were reported in three rats. In addition, the authors report difficulty distinguishing axonal action potentials from muscle potentials and other biopotentials during unanesthetized recordings.

Navarro *et al*. (1998) report the first recordings from a polyimide-based sieve electrode. Interfaces were implanted into the sciatic nerves of 10 rats. Acute recording sessions were conducted at various times ranging from 10 to 28 weeks. Evoked compound muscle and compound nerve action potentials confirmed functional regeneration in all 10 rats. Single-unit action potentials from both motor and sensory fibers were observed in an unreported number of rats.

Wallman *et al*. (1999) report detection of compound action potentials from a silicon-based sieve electrode implanted in the sciatic nerve of one of three rats upon electrical stimulation of the nerve during an acute recording session. The two remaining rats suffered from either displacement of the electrode from the nerve or corrosion and disconnection of the contact wires internally.

Mensinger *et al*. (2000) implanted 9-channel silicon-based sieve electrodes fabricated at the University of Michigan into the VIIIth cranial nerves of toadfish. Spontaneous action potentials were observed in seven out of an unreported number of fish during chronic recordings lasting up to 42 days.

In Ceballos *et al*. (2002), polyimide sieve electrodes were implanted into the sciatic nerves of 13 rats, with 12 showing successful nerve regeneration. During acute experiments, the electrodes were used to stimulate the nerve and induce muscle contractions. No attempts were to record signals from the electrodes were reported.

Shimatani *et al*. (2003) implanted a custom-designed 4-channel polyimide based electrode into the chorda tympani nerve of 18 rats, routing the connector ribbon to a percutaneous head cap. Recordings of action potentials were reported in 7 rats on a minority of channels. Two rats suffered electrode failures and 9 displayed no action potentials despite no obvious signs of failure over the 3 month testing interval. It is reported that for most animals, observed neural activity typically remained stable for between one and two weeks, however one animal remained active for a total of nine weeks. In two animals, an active signal was observed to disappear after eight days and reappear a few days later on a different electrode channel. The authors speculate that signals may be short lived due to possible shifts of axon location and Nodes of Ranvier in the regenerating nerves.

In a conference paper from 2004, Kawada *et al*. report the construction of a 5-channel silicon-based sieve electrode to investigate the autonomic nervous system. Two experiments were conducted. Sieve electrodes were implanted into the vagal nerve of 5 rats and into the renal nerve of three rabbits. Acute recording sessions were conducted at 40 days. Functional regeneration of all 8 nerves was confirmed using cuff electrodes and the recording of compound action potentials. No single-unit spikes were observed in the five rats. Spontaneous single-unit spikes, correlated with sympathetic nerve activity, were recorded in an unreported number of rabbits.

In Ramachandran *et al*. (2006), a polyimide-based sieve electrode into which multiplexing electronics were incorporated was implanted into fifteen rats (sciatic nerve). A transcutaneous head connector allowed for chronic recordings. The authors report that nine of the fifteen rats displayed functional regeneration with three rats providing recordable action potentials from a minority of electrodes. A broken connector ribbon was observed in six rats upon dissection.

Lago *et al*. (2007) implanted polyimide regenerative sieve electrodes into the sciatic nerves of 19 rats for acute recordings at 2 to 6 months. The authors report that nerve

regeneration failed in several animals. Of an unspecified number of animals upon which electrophysiological recordings were attempted, short bursts of action potentials could be observed on a minority of electrodes within 50% of the animals. Upon dissection of the remaining 50%, it was observed that the polyimide ribbon had been severed internally.

Kim *et al*. (2007a; 2007b; 2009) and Lee *et al*. (2006) recorded compound action potentials from whole nerves (rat, sciatic) implanted with polyimide sieve electrodes during acute recording sessions involving whole-nerve stimulation. The authors' aim was to compare methods used to estimate functional regeneration and they did not attempt to record single-unit action potentials through the sieve electrodes.

In Cho *et al*. (2008), a custom-made device consisting of multiple SU8 epoxy-based bipolar electrodes (microprobes) embedded within hollow channels of an agarose-filled nerve guide tube were implanted into the sciatic nerves of 13 rats. Conductive wires interfaced with a percutaneous headcap to allow for chronic recordings. Each rat was implanted with three to five individual microprobes. The authors report observed recordings of neural spike signals in 39 out of 50 implanted microprobes. In all cases, signals were recorded up until device failure (between 4 and 51 weeks) due to breakage of the connector wire, usually near the headcap.

Panetsos *et al*. (2008) implanted polyimide-based sieve electrodes into the median nerves of three of cats to study effects of interfaces upon the central nervous system. Acute recording sessions were conducted at either 15 or 30 months. The authors claim that recordings were made from the implanted sieve electrodes during stimulation of the limb yet provide no evidence or details. This is understandable given the context of the paper toward studying the CNS and not the interface itself.

Garde *et al*. (2009) report observed neural activity recorded from electrodes in 7 out of 10 rats implanted with a REMI device (sciatic nerve). Chronic recordings were made via a connecting cable routed to a percutaneous headcap. Spontaneous neural activity was observed from between eight days and three months. Internal breakage of the connector cable

and issues surrounding the headcap were described as common sources of device failure over time. All animals experienced device failure within 223 days.

Goji *et al*. (2009, 2010) presented a modified sieve design that was implanted into the sciatic nerve of rats for sacrifice at two months to investigate regeneration. They report that "signals were recorded," but provide no information on the nature of the signals.

Researchers at the University of Michigan Medical School have published a series of papers and abstracts focusing on the potential use of PEDOT as an electrode material capable of interfacing with nerves and muscles. In one abstract (Frost *et al*., 2009), they report successful recording of spontaneous EMG potentials from implanted, innervated myofibers in response to sensory stimulation. Few details were given, and this work has yet to be presented in its entirety or in a peer-review publication.

Fitzgerald *et al*. (2012) implanted two different types of regenerative devices into the sciatic nerves of rats and recorded from them during acute sessions at three months. The first device consisted of a monolithic piece of silicone with 20 hollow microchannels of 130 um diameter (similar to that of Figure 1.12) inserted into a larger silicone nerve guide tube implanted into 8 rats. To record single-unit action potentials, the device was surgically exposed and a window area was cut into the guide tube. A tungsten needle microelectrode was inserted into different microchannels using a micromanipulator. The authors report the presence of myelinated axons within 85% of microchannels across the eight rats. Behavioral and physiological tests demonstrated functional regeneration of the nerves. Evoked single unit action potentials were observed both during proximal electrical stimulation and movement of the distal limb. Causes of failure of this device could not be reported given that nerve regeneration was robust and an extraneous electrode (not an implanted one) was used to record from within the microchannels. A second device was a prototype 'rolled' design microfabricated out of polyimide and gold consisting of 180 microchannels, 20 of which contained exposed electrodes, implanted into six rats. An integrated connector ribbon led to contact pads which remained

implanted until exposure during the recording session. The electrodes within the device were capable of eliciting twitching of muscles distal to the nerve upon electrical stimulation of the electrodes, and compound action potentials could be recorded from the electrodes following distal electrical stimulation of the nerve, but single-unit action potentials, whether evoked or spontaneous, were not observed with this device.

Lewitus *et al*. (2011) implanted a biodegradable, 'rolled,' multiluminal interface device into the sciatic nerve of three rabbits. The authors describe a recording methodology in which the implanted connector interface is surgically exposed to allow for 30-minute recording sessions under anesthesia and then re-implanted under the skin in a non-terminal experiment. While this may technically be considered a chronic recording methodology, for the purposes of comparing with other reported experiments, this will be considered as a series of acute recordings since no semi-permanent (non-surgical) means of signal access was incorporated. The authors report acquisition of action potentials at 4 weeks and at 8 weeks. As this was a proof-of-concept paper which focused more on device construction and *in vitro* testing, few details were given of the electrophysiological results. No information was included on any complications with recordings or with the device or on the reasons for termination of the experiment at 8 weeks.

2.1.4 Summary of Literature Review

It is believed that the preceding review accounts for all published experiments to date in which single-unit activity was recorded from a regenerative PNI. The review highlights the lack of specific information regarding the nature and frequency of physical device failure inherent in current regenerative PNI methodologies while noting that it is often mentioned as a cause for termination of an experiment or for the lack of successful signal acquisition in a large number of animals. A summary of this review is presented in Table 2.1. has.

Table 2.1 Summary of 16 published works to date reporting single-unit activity recorded from a regenerative PNIs. Note: Values listed in the "Duration of experiment" column reflect the length of time in which recordings from implanted arrays were attempted, not the duration over which single-units were observed. ("n/r" indicates not-reported)

Year	Authors:	Electrode:	Animal model:	Nerve:	Number of animals implanted:	Number of animals from which single units were detected:	Experiment design:	Duration of experiment:
1974	Mannard *et al*	Machined sieve	frog	sciatic	6	3	acute	12-25 weeks
1986	Edell	Silicon sieve	rabbit	sciatic	n/r	n/r	chronic	up to 32 weeks
1991	Kovacs *et al*	Silicon sieve	rat	peroneal	n/r	n/r	acute	up to 377 days
1992	Kovacs *et al*	Silicon sieve	rat	peroneal	9	n/r	acute	137-397 days
1994	Kovacs *et al*	Silicon sieve	rat	peroneal	3	3	acute	3 months
"	"	Silicon sieve	frog	auditory	4	2	acute	7-24 weeks
1997	Della Santina *et al*	Silicon sieve	frog	8th cranial	11	2	acute	> 7 weeks
1997	Bradley *et al*	Silicon sieve	rat	glosso-pharyngeal	32	n/r	chronic	5-26 weeks
1998	Navarro *et al*	Polyimide sieve	rat	sciatic	10	n/r	acute	10-28 weeks
2000	Mensinger *et al*	Silicon sieve	fish	8th cranial	n/r	7	chronic	up to 42 days
2003	Shimatani *et al*	Polyimide sieve	rat	chorda tympani	18	7	chronic	over 3 months
2004	Kawada *et al*	Silicon sieve	rabbit	renal nerve	3	n/r	acute	40 days
2006	Ramachandran *et al*	Polyimide sieve	rat	sciatic	15	3	chronic	2-7 months
2007	Lago *et al*	Polyimide sieve	rat	sciatic	19	n/r	acute	2-7 months
2008	Cho *et al*	SU8-based	rat	sciatic	13	13	chronic	up to 51 weeks
2009	Garde *et al*	REMI	rat	sciatic	10	7	chronic	up to 233 days
2011	Lewitus *et al*	"Rolled"	rabbit	sciatic	7	n/r	acute	4 and 8 weeks

2.1.5 Experimental Design

To determine the common physical causes of device failure inherent in typical regenerative PNI methodologies, a large-cohort (n = 60 animals) experiment was conducted in which a REMI interface was implanted into the sciatic nerve of a rat. A subcutaneous wire connected the 16-channel electrode array to a percutaneous pedestal that was secured to the animal's pelvis using bone cement (see Figure 2.1 for experimental setup). Animals were inspected daily for externally observable signs of device failure. Electrophysiological recordings from the implanted electrodes were conducted once per week to provide insight into any potential internal problems and to confirm the capacity of this experimental setup to serve as a representative model of the field. The animals were separated into three cohorts and sacrificed at 15 days (n = 20 animals), 30 days (n = 20 animals) and 60 days (n = 20 animals). Upon sacrifice, each animal was perfused with paraformaldehyde and dissected for a post-mortem inspection of the implant. All observed causes of device failure were recorded and compared across the three experimental groups as well as to what has been reported in the literature. In this context, all implanted materials were considered to constitute "the device."

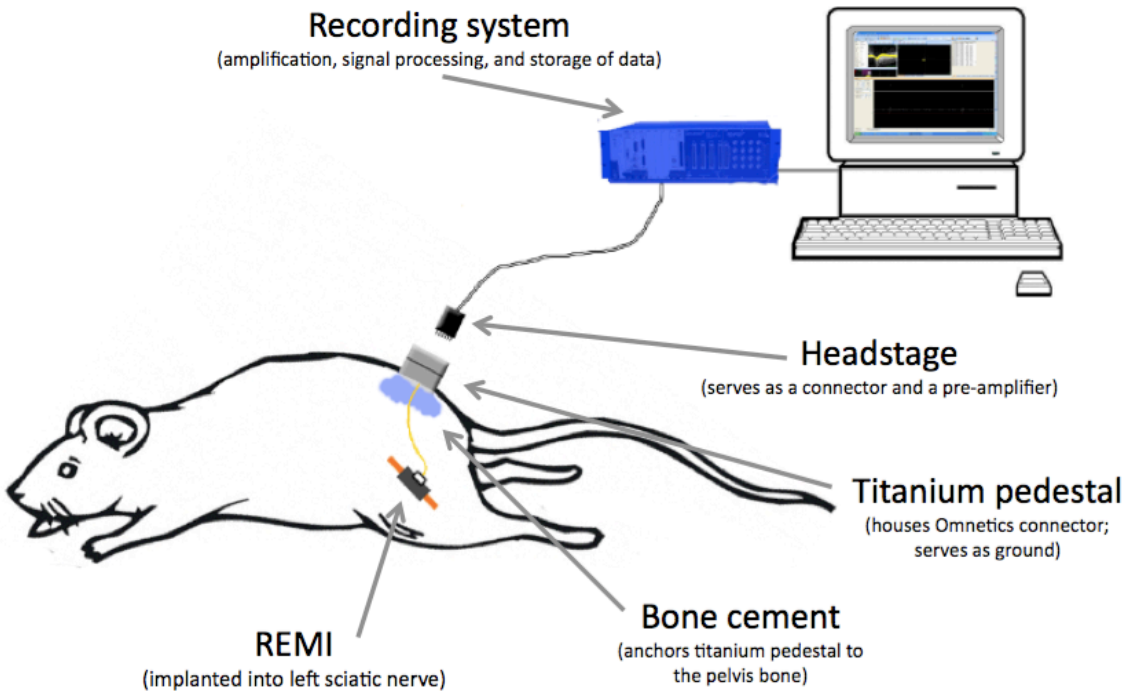

Figure 2.1 A REMI PNI is implanted into the hind left leg of the animal. Insulated wires connect the electrode array subcutaneously to a connector housed within a percutaneous titanium pedestal. Bone cement secures the pedestal to the pelvis bone. External wires allow for recording of electrophysiological signals by recording hardware. A typical recording session involves 5 minutes of continuous recording from an awake animal.

2.2 Materials and Methods

2.2.1 Regenerative Peripheral Nerve Interface

Regenerative multielectrode interface (REMI) PNIs (see Figure 1.11) were constructed using 18-pin platinum/iridium needle electrode arrays (Microprobes Inc., Gaithersburg, MD) with impedances between 150 and 300 kΩ. Electrodes were arranged in a 5-4-5-4 pattern with a uniform inter-electrode spacing of 400 μm. Electrode shafts tapered from a sharp point to a 50 μm diameter at the base and varied between 0.7 and 1.0 mm in length. A 4.5 cm cable of wound gold wires coated in Parylene-C connected the electrode array to a connector (Omnetics, Minneapolis, MN). The connector was housed within a custom-machined titanium pedestal containing two base flanges to facilitate adhesion to the pelvic bone and a removable lid attached with two screws. The electrode array was inserted into a small window cut within the side of a 5 mm long polyurethane guide tube (Braintree Scientific Inc., Braintree MA). The guide tube measured 3 mm in diameter with a 1.75 mm diameter lumen. Prior to implantation, the device was sterilized with ethanol and overnight exposure to UV light and filled with a cold liquid collagen that polymerizes at 37ºC (Chemicon, Temecula, CA).

2.2.2 Surgical Implantation

Interfaces were implanted into the left sciatic nerve of 60 female Lewis rats (215-275 g). Animals were anesthetized with inhaled isoflurane in oxygen (5% for induction and 2-2.5% for maintenance. The dorsal pelvic and leg area was shaved and cleaned with povidone-iodine and isopropyl alcohol. An incision was made longitudinally along the sacral spine. Muscle and fascia were removed from the spine, dorsal processes were removed, and an exposed area of pelvic bone was cleaned and dried. The percutaneous titanium pedestal housing the connector was attached to the pelvic bone using bone cement (Biomet, Warsaw, IN). A second incision on the leg exposed the semitendinosus and biceps muscles which were separated to expose the sciatic nerve for transaction. The connecting wire from the implanted PNI was routed under

the skin from the pelvic area to the leg. The distal and proximal nerve stumps were inserted into opposing ends of the PNI nerve guide tube and sutured in place. The muscles and skin of the leg were sutured closed. The skin around the percutaneous pedestal was closed using surgical staples. Antibiotics (cephazolin; 5 mg/kg, IM) and analgesics (buprenorphine; 0.05-0.1 mg/kg, SC) were administered post-surgery. Procedures were performed in accordance with the guidelines of the Institutional Animal Care and Use Committee of the University of Texas Arlington.

2.2.3 Electrophysiological Recordings

Electrophysiological recordings from each animal were obtained weekly (starting at post-operative day 7) until termination. During a typical recording session, the animal was briefly anesthetized (3% inhaled isoflurane in oxygen) to allow removal of the pedestal lid and insertion of a connector cable with attached 20x headstage amplifier to the Omnetics connector (Figure 2.2). The cable, headstage, and associated recording hardware and software were purchased from Plexon Inc. (Dallas, TX). A grounding wire was connected to a screw attached to the titanium pedestal. Five minutes after the animal regained consciousness, continuous electrophysiological recordings were obtained from 16 electrode channels (41 kHz sampling rate, 3 Hz high-pass filter) from a freely-moving animal within a faraday cage. The animal was again anesthetized for removal of the connector and returned to its cage. Single-unit spikes were subsequently identified from the recorded data by template sorting using Offline Sorter (Plexon Inc.) and analyzed using NeuroExplorer (Nex Technologies, Westford, MA) and MATLAB (MathWorks, Natick, MA).

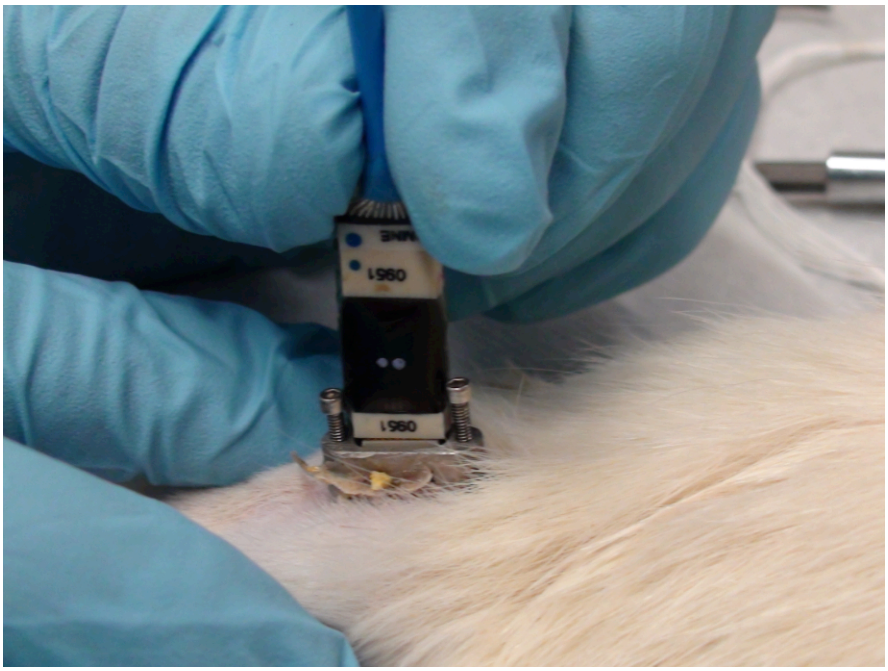

Figure 2.2 A connector cable was inserted into the titanium pedestal to allow electrophysiological recordings.

2.2.4 Evaluation

Animals were inspected daily for obvious signs of device failure. Weekly electrophysiological recording sessions served to confirm the capacity of the experimental setup to serve as a representative model of a typical regenerative PNI and to provide insight into internal device complications; for example, an excessively high or nearly absent noise baseline often indicated a broken internal cable. Upon scheduled termination, animals were sacrificed by intraperitoneal injection of sodium pentobarbitol (100 mg/kg) and perfused transcardially with saline (0.9%, 5 minutes) and paraformaldehyde (4%, 15 minutes). The sciatic nerve was exposed and transected several millimeters from each side of the REMI nerve guide tube. Connective tissue was carefully removed and the nerve guide tube was dissected beneath a stereomicroscope to allow confirmation of successful nerve cable regeneration (Figure 2.3) and confirm the presence or absence of needle electrode tips within the regenerated nerve cable.

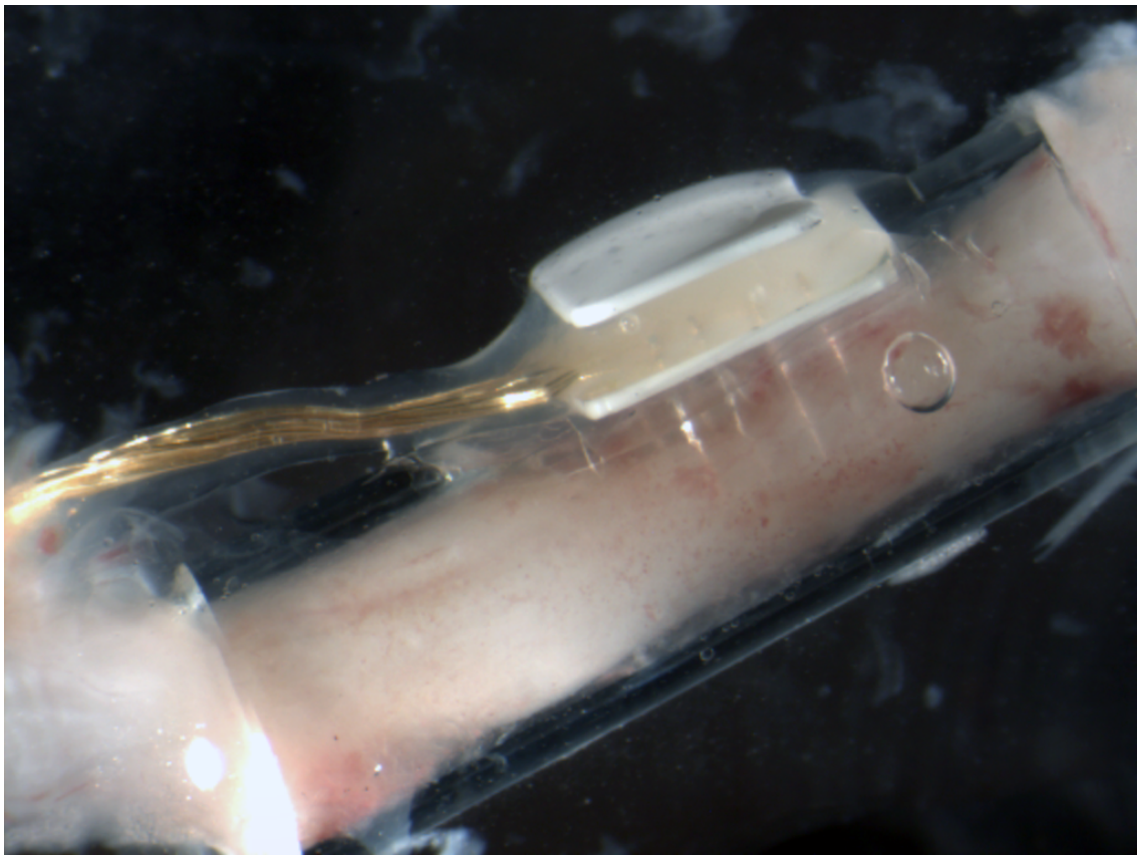

Figure 2.3 Explanted REMIs were cleaned and dissected to confirm successful regeneration of the nerve cable.

2.3 RESULTS

Sixty animals were implanted with REMIs for this study and sacrificed after 15 days (n = 20), 30 days (n = 20), and 60 days (n = 20). Implanted animals were observed daily for obvious signs of device failure. Electrophysiological recordings from the implanted electrodes were taken weekly for insight into the internal integrity of the interface. Animals were dissected post-sacrifice to observe the state of nerve regeneration.

2.3.1 Routine Observations

Among the animals scheduled for sacrificed at 15 days, 16 out of 20 survived to scheduled termination without external signs of device failure. Three animals are considered failed due to a broken internal cable that had been exposed at the base of the percutaneous pedestal. One rat could not be used for electrophysiological recordings due to a defect in the connector/pedestal complex. This could be considered device failure due to poor manufacturing.

Among the animals scheduled for sacrifice at 30 days, 11 out of 20 survived to scheduled termination without an overt observable device failure. Five were terminated early due the percutaneous pedestal dislodging and leaving the animal. One termination occurred during the second week post-implantation, one occurred during the third week, and three occurred near the four week mark. Two animals failed during the first week due to a broken exposed wire at the base of the percutaneous pedestal. Two were considered failed due to poor manufacture of the connector/pedestal complex.

Among the animals scheduled for sacrifice at 60 days, 7 out of 20 survived to scheduled termination without an overt observable device failure. Twelve were terminated early due to the percutaneous pedestal dislodging and leaving the animal. These terminations occurred during weeks 3 (one animal), 4 (one animal), 5 (three animals), 6 (two animals), 7 (two

animals), and 9 (two animals). One animal was considered failed due to poor manufacture of the connector/pedestal complex.

Table 2.2 Summary of results of routine observations. Numbers represent the number of animals that failed due to a given externally observable cause.

	15 Day Cohort: (n = 20)	**30 Day Cohort:** (n = 20)	**60 Day Cohort:** (n = 20)
Failed as a result of component manufacturing:	1	2	1
Failed due to a broken percutaneous wire:	3	2	0
Failed due to expulsion of percutaneous pedestal:	0	5	12
No externally observable signs of device failure at scheduled termination:	16	11	7

2.3.2 Terminal Observations

Among the 20 animals sacrificed at day 15, the implanted devices of all 20 were observed post-sacrifice. It was observed that the electrode array of one animal was completely dislodged from the nerve guide tube. In a second animal, the electrode array was partially dislodged, with a majority of needle electrodes present outside of the nerve guide tube. Six of 20 animals were chosen randomly for use in a separate experiment in which the nerve cables were removed from the implants immediately post-sacrifice; all 6 possessed successfully regenerated nerve cables. Of the remaining 12 animals, the explanted interfaces of all 12 were dissected and observed microscopically. Regeneration of the nerve cable was observed in all 12. The electrode tip positions in one animal could not be observed due to the presence of opaque blood within the nerve guide tube; upon further dissection, nerve cable regeneration was confirmed. In two animals, the regenerated nerve cable had grown in a position within the guide tube near the base of the electrode array such that all of the needle electrode shafts extended through the nerve cable and the electrode tips were positioned outside of the nerve cable (see Figure 2.5).

Among the animals intended to be sacrificed at day 30, the implants of 17 out of 20 animals were observed post-sacrifice. Three animals required pre-scheduled termination due to dislodgement and expulsion of the percutaneous pedestal. A mechanically intact interface was observed in 17 out of 17 animals at day 30. Two of the 17 animals were used in a separate experiment in which the nerve cables were removed from the implants immediately post-sacrifice; regeneration of the nerve cable through the guide tube was macroscopically observed in both. The implants of the remaining 15 animals were observed microscopically post-sacrifice. In one implant, the regenerated nerve cable had grown such that all electrode tips were positioned outside of the nerve cable.

Among the animals intended to be sacrificed at day 60, 8 of the 20 animals survived until their scheduled termination. An additional two animals were sacrificed at day 56 after

expulsion of the percutaneous pedestal; both were perfused and are included here for terminal observations. Ten animals out of the 20 were terminated at or prior to 42 days post-implantation due to expulsion of the percutaneous pedestal and are not included here for terminal observations. Of the 10 animals posthumously observed at 56 or 60 days post-implantation, all 10 possessed an intact interface with a successfully regenerated nerve cable within the guide tube and were observed microscopically. In two animals out of the 10, the regenerated nerve cable had grown such that all electrode tips were positioned outside of the nerve cable. The results of this section are summarized in Table 2.1.

Table 2.3 Summary of results of post-mortem observations.

	15 Day Cohort:	**30 Day Cohort:**	**60 Day Cohort:**
Animals observed at scheduled termination date:	20 out of 20	17 out of 20	10 out of 20
Animals possessing a mechanically intact interface at termination:	18 out of 20	17 out of 17	10 out of 10
Implants possessing a regenerated nerve cable:	20 out of 20	17 out of 17	10 out of 10
Implants with electrode tips present inside regenerated nerve cable:	9 out of 11	14 out of 15	8 out of 10

2.3.3 Electrophysiological Recordings

Among the group of animals sacrificed at 15 days, apparent single-unit action potentials with odd qualities were observed on one animal at day 14. It was later determined that our electronic recording equipment was incorrectly configured, greatly decreasing the likelihood that otherwise recordable action potentials would be detected. It was also later observed during dissection that the electrode array of the one animal in question had dislodged from the nerve guide tube at an unknown time post-implantation with the needle electrodes firmly lodged into a nearby muscle. It may be possible that the apparent action potentials were myoelectric and not axonal in origin. The electrophysiological results from this group will not be included in further analysis.

Among the group of animals sacrificed at 30 days, electrophysiological recording sessions were conducted at 7, 14, 21, and 28 days post-implantation. Two of the 20 animals could not be electrophysiologically monitored due to poorly manufactured connectors. One additional animal was later discovered to have no electrode tips within the regenerated nerve cable. Five animals suffered from percutaneous pedestal or wire failures throughout the course of the 30 days. At 7 days post-implantation, 5 out of the 17 eligible animals displayed single-unit spiking. At 14 days, 5 out of the 16 eligible animals displayed single-unit spiking. At 21 days, 4 out of the 15 eligible animals displayed single-unit spiking. At 28 days, 3 out of the 13 eligible animals displayed single-unit spiking. Over the course of the four recording sessions, a total of 9 out of the eligible 17 animals had displayed single-unit spiking activity at one time. During a given recording session in which spiking activity was detected in an animal, a range of 1 to 10 (average 3.29) distinct spiking waveforms were observed in that animal. These results are summarized in Table 2.4.

Among the group of animals sacrificed at 60 days, electrophysiological recordings were attempted on 19 animals. Upon post-mortem evaluation, it was discovered that one implanted

device was damaged with unsuccessful nerve cable regeneration and two devices possessed no electrode tips within the regenerated nerve cable; no spiking activity was observed from these three and they are not included in this analysis. Among the remaining 16 animals, electrophysiological recordings were attempted every 7 days starting at 14 days post-implantation for 4 animals, starting at 21 days post-implantation for an additional 5 animals, and starting at 35 days post-implantation for the remaining 7 animals. These results are presented in Table 2.1. Over the course of the four recording sessions, a total of 9 out of the eligible 17 animals displayed single-unit spiking activity at one time. During a given recording session in which spiking activity was detected in an animal, a range of 1 to 12 (average 3.28) distinct spiking waveforms were observed in that animal. These results are summarized in Table 2.5.

Overall, 53% of eligible animals within the 30 day cohort and 76% of the eligible animals within the 60 day cohort displayed single-unit spikes during the course of the experiment. Of the 17 animals considered eligible for recordings within the 30 day cohort, 10 survived to the time of scheduled termination without an observable cause of device failure. Of these 10 animals, 8 had displayed single-unit recordings during at least one recording session, and 2 had not. Of the 16 animals considered eligible for recordings in the 60 day cohort, 5 survived to time of scheduled termination without an observable cause of device failure. Of these 5 animals, 3 had displayed single-unit recordings during at least one recording session, and 2 had not. These results are summarized in Table 2.6.

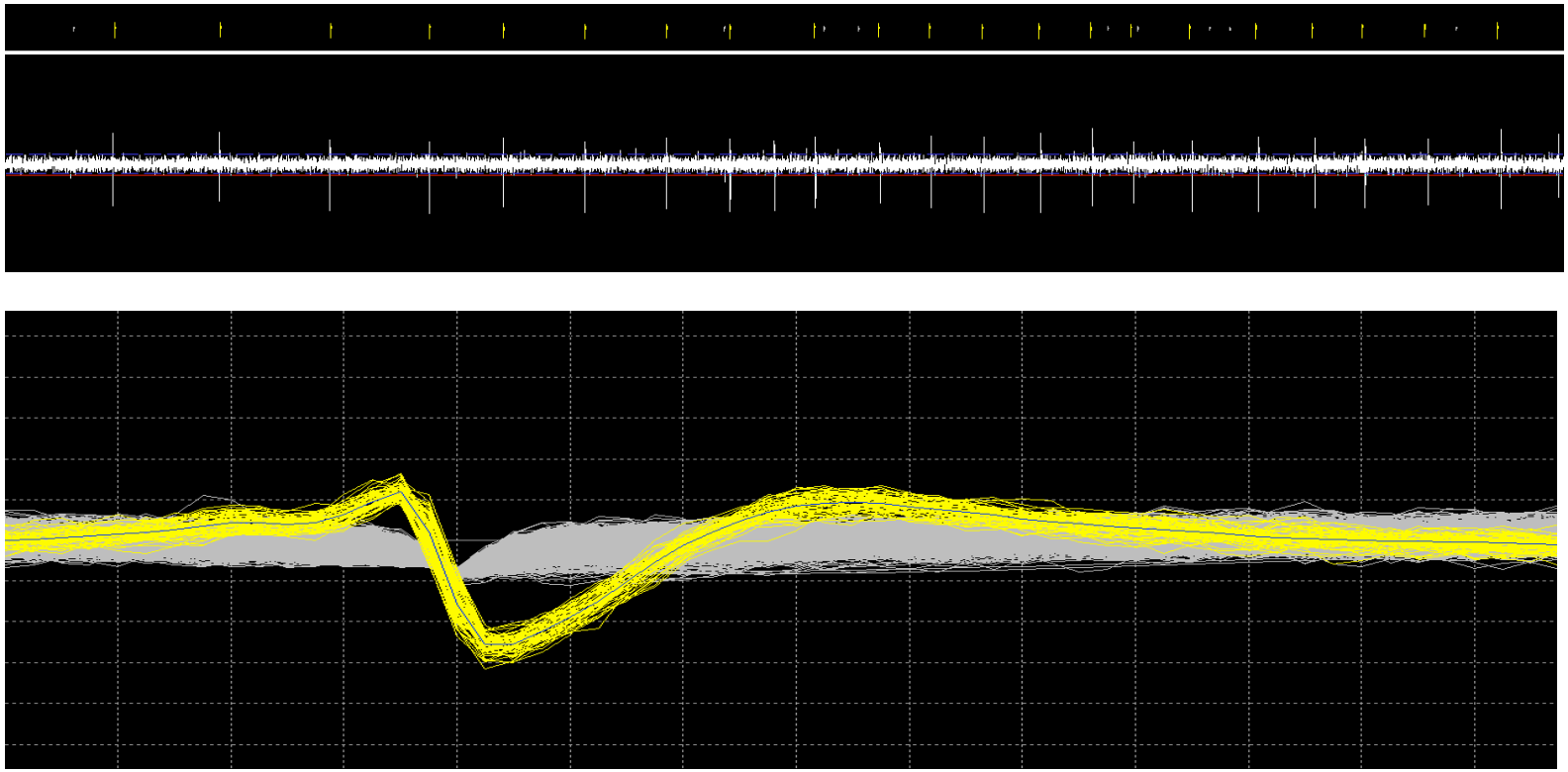

Figure 2.4 Single-unit spikes are often visibly detectable above the noise baseline on individual channels (top graph, time span = 1.5 seconds). Aggregates of individual single spikes, superimposed, are available in real time (bottom left, grids = 52 μV, 100 μs).

Table 2.4 Animals displaying single-unit spiking activity (30-day cohort).

	7 days post implantation:	14 days post implantation:	21 days post implantation:	28 days post implantation:	**Over all four recording sessions:**
Number of eligible animals:	17	16	15	13	**17**
Number of animals displaying single-unit spiking activity:	5	5	4	3	**9**
Percentage of eligible animals showing single-unit spiking activity:	29%	31%	27%	23%	**53%**

Table 2.5 Animals displaying single-unit spiking activity (60-day cohort).

	14 days post implant-ation:	21 days post implant-ation:	28 days post implant-ation:	35 days post implant-ation:	42 days post implant-ation:	49 days post implant-ation:	56 days post implant-ation:	**Over all seven recording sessions:**
Number of eligible animals:	4	8	5	10	8	7	7	**17**
Number of animals displaying single-unit spiking activity:	3	7	4	2	3	0	1	**13**
Percentage of animals showing single-unit spiking activity:	75%	88%	80%	20%	38%	0%	14%	**76%**

Table 2.6 Summary of electrophysiological results in relation to animal longevity and observed device failures.

Cohort:	Failure status:	Presence or absence of observed single-unit activity:
30 Day Cohort (17 eligible animals)	10 animals survived to scheduled termination without device failure.	8 with recorded activity.
		2 without recorded activity.
	7 animals suffered device failure prior to scheduled termination.	1 with recorded activity.
		6 without recorded activity.
60 Day Cohort (17 eligible animals)	6 animals survived to scheduled termination without device failure.	3 with recorded activity.
		3 without recorded activity.
	11 animals suffered device failure prior to scheduled termination.	8 with recorded activity.
		3 without recorded activity.

2.3.4 Summary of Results

A summary of rates of failure at different time intervals, as observed among the three cohorts at 15 days, 30 days, and 60 days, is presented in Table 2.7. Failure in this context is considered any undesired impediment that prevents the capacity to record electrophysiological signals from electrodes embedded within a successfully regenerated nerve. This would not include animals (of which there were 5, see Table 2.1) in which no physical cause of failure was observed yet single-unit action potentials were not observed.

An overall summary of all identified causes of failure along with relative contribution at each time point is presented in Table 2.8.

Table 2.7 Failure rates among the three time points.

	15 Day Cohort	30 Day Cohort	60 Day Cohort
Suffered an observable cause of device failure prior to scheduled termination:	8 animals **(40%)**	10 animals **(50%)**	14 animals **(70%)**
Survived to scheduled termination without an observed device failure:	12 animals (60%)	10 animals (50%)	6 animals (30%)

Table 2.8 Summary of observed causes of device failure from routine observations, terminal observations, and electrophysiological observations.

	15 Day Cohort:	30 Day Cohort:	60 Day Cohort:
Poor Connector Manufacturing:	1 of 20 (5%)	2 of 20 (10%)	1 of 20 (5%)
Failures related to percutaneous pedestal and internal wires:	3 of 20 (15%)	7 of 20 (35%)	12 of 20 (60%)
Failure due to loss of integrity of implanted interface:	2 of 20 (10%)	0 of 17 (0%)	0 of 10 (0%)
Failed regeneration of nerve cable through implant:	0 of 20 (0%)	0 of 17 (0%)	0 of 10 (0%)
Lack of electrodes within nerve cable:	2 of 11 (18%)	1 of 15 (7%)	2 of 10 (20%)
Did not display recordable single-unit spike activity over course of experiment despite no observable cause of failure:	n/a	2 animals	4 animals

2.4 Discussion

2.4.1 Relevance of Experimental Setup

The goal of this chapter is to identify, through a large-cohort animal model experiment, the common causes of device failure inherent in current regenerative peripheral nerve interfacing methodologies. For these results to be relevant, it must be shown that our experiment conducted here is representative of typical methodologies.

Of the sixteen papers summarized in Table 2.1, thirteen discuss experiments performed on a mammalian model. Pertinent aspects of these thirteen are summarized in Table 2.1, along with results from our own experiment.

Eleven of the thirteen reports utilized a rat model with the remaining two utilizing a rabbit model. Our experiments utilized a rat model. Eleven of thirteen reports utilized the sciatic nerve or a distal branch of it. Our experiments utilized the sciatic nerve. The number of electrode channels per device was reported in twelve of the thirteen publications and has varied from 4 to 27 with an average of approximately 10. Our device utilizes 16 electrode channels. Of the thirteen, ten reported upon measured electrode impedances with seven of those ten reporting an impedance between 100 and 600 kΩ. Our experiments utilize electrodes with impedances of 150-300 kΩ.

While most of the thirteen reports include a figure depicting recordings of single-unit action potentials, only six of those reports comment directly on the amplitudes of action potentials typically recorded. Five of those six studies report typical amplitudes ranging from 100 to 600 μV. The sixth reported a range of 40 to 120 μV. In our experiment, 117 distinct single-unit spiking waveforms were observed in 22 rats over 66 recording sessions with typical peak-to-peak amplitudes ranging from 50 to 300 μV.

Only six of the thirteen report on the percentage of animals from which single-unit spikes were recorded. Kovacs *et al*. (1994) report observation of action potentials in 3 out of 3

implanted animals in acute experiments over many months using a silicon-based sieve; Shimatini *et al*. (2003) report 7 out of 18 (39%) over three months using a polyimide-based sieve; Ramachandran *et al*. (2006) report 3 out of 15 (20%) over 2-7 months using a polyimide-based sieve; Lago *et al*. (2007) report 50% out of an unspecified number (less than 19) over 2-7 months using a polyimide-based sieve; Cho *et al*. (2008) imply 13 out of 13 (100%) over 3 months using a BNI/SU8 design; Garde *et al*. (2009) report 7 out of 10 (70%) over several months using a REMI. In our experiment, we observed single units on 9 out of 20 (45%) implanted animals within the 30 day cohort and on 13 out of 20 (65%) implanted animals within the 60 day cohort.

All of the results of this experiment lie within the range of what has been reported by others in regenerative PNI experiments using a mammalian model. The electrophysiological results of this experiment support the contention that the experimental setup used here is typical and representative of the field.

Table 2.9 Comparison of pertinent electrophysiological results reported by this work and by others.

	Edell, 1986	Kovacs, 1991	Kovacs *et al.*, 1992	Kovacs *et al.*, 1994	Bradley *et al.*, 1997	Navarro *et al.*, 1998	Shima-tani *et al.*, 2003
Acute or chronic experiment:	Chronic	Acute	Acute	Acute	Chronic	Acute	Chronic
Animal model:	Rabbit	Rat	Rat	Rat	Rat	Rat	Rat
Nerve:	Tibial	Peroneal	Peroneal	Peroneal	Glosso-pharyn-geal	Sciatic	Chorda tympani
Interface architecture:	Sieve, silicon	Sieve, silicon	Sieve, silicon	Sieve, silicon	Sieve, silicon	Sieve, poly-imide	Sieve, poly-imide
Number of electrode contacts per interface:	10	n/r	16	8	4	7	4
Electrode impedance (at 1 kHz):	n/r	600 kΩ	~600 kΩ	~61 kΩ or ~1.1MΩ	~100 kΩ	200 kΩ	n/r
Action potential amplitudes:	up to 600 μV	~100μV (one example shown)	~100μV	~100μV	n/r	n/r	n/r
Number of animals with single-unit spikes:	n/r	n/r	n/r	100% (3 of 3 at ~3 months)	n/r	n/r	39% (7 of 18)
Number of single-unit spikes per active animal:	n/r	n/r	n/r	n/r	n/r	n/r	n/r
Max number of distinct spiking units per animal:	n/r	n/r	n/r	n/r	n/r	n/r	n/r

Table 2.9 – *Continued*

	Kawa-da, 2004	Rama-chan-dran *et al*., 2006	Lago *et al*., 2007	Cho *et al*., 2008	Garde *et al*., 2009	Lewitus *et al*., 2011	Our experi-ment:
Acute or chronic experiment:	Acute	Chronic	Acute	Chronic	Chronic	Acute	Chronic
Animal model:	Rabbit	Rat	Rat	Rat	Rat	Rabbit	Rat
Nerve:	Renal nerve	Sciatic	Sciatic	Sciatic	Sciatic	Sciatic	Sciatic
Interface architecture:	Sieve, silicon	Sieve, poly-imide	Sieve, poly-imide	BNI/ SU8	REMI	Rolled	REMI
Number of electrode contacts per interface:	6	27	9	3 to 5	16	10	16
Electrode impedance (at 1 kHz):	n/r	~6 kΩ	~6 kΩ	~100 kΩ	150-250 kΩ	<10 kΩ	150-300 kΩ
Action potential amplitudes:	n/r	n/r	n/r	100-500 μV	≥300 μV	40-120 μV	100-300 μV (typical)
Number of animals with single-unit spikes:	n/r	20% (3 of 15)	<50%	100% (13 of 13)	70% (7 of 10)	n/r	53% (30 days) 81% (60 days)
Number of single-unit spikes per active animal:	n/r	n/r	n/r	n/r	n/r	n/r	1-11 (mean = 3.3)
Max number of distinct spiking units per animal:	n/r	n/r	n/r	n/r	5	n/r	11

Table 2.10 Comparison of physical causes of failure reported by this work and by others.

Reported Cause of Failure:	Investigators:	Year:	Number of Animals:
Complications regarding percutaneous interface:	Mannard *et al*.	1974	n/r
	Loeb *et al*.	1977	n/r
	Bradley *et al*.	1997	66% (24 of 32 animals)
	Ramachandran *et al*.	2006	40% (6 of 15 animals)
	Lago *et al*.	2007	≥50%
	Cho *et al*.	2008	majority
	Garde *et al*.	2009	"most"
	This Work	2011	Up to 60% (12 of 20 animals at 60 days)
Failed regeneration of nerve through the implant or failure of implant integrity:	Mannard *et al*.	1974	n/r
	Loeb *et al*.	1977	n/r
	Kovacs *et al*.	1992	"most"
	Bradley *et al*.	1997	25% (7 of 28 animals)
	Wallman *et al*.	1999	2 of 3 animals
	Shimatani *et al*.	2003	11% (2 of 18 animals)
	Lago *et al*.	2007	n/r
	This Work	2011	0-10%
Unexplained absence of spiking activity despite no identifiable cause:	Bradley *et al*.	1997	n/r
	Shimatani *et al*.	2003	9 of 18 animals
	This Work	2011	6 of 40 animals
Poor component manufacturing:	This Work	2011	5-10%
Observed lack of electrode contacts within regenerated nerve:	This Work	2011	~10-20%

2.4.2 Common Causes of Failure

2.4.2.1 Implant Integrity and Regeneration of Nerve Cable.

Successful regeneration of the nerve cable from the proximal to the distal stump through the nerve guide tube was observed in 60 of the 60 animals used in this study. In two of the 60 animals, the nerve cable regenerated through the tube, but the electrode array became mechanically separated and partially or fully dislodged from the guide tube. The REMI interface was specifically designed to allow relatively unimpeded nerve growth through the guide tube compared to sieve electrode designs. Assuming a well-implemented surgical implantation of the device and maintenance of mechanical integrity once implanted, a high yield (of nerve cable regeneration) was expected given the relatively unimpeded lumen of the nerve guide tube. Such successful regeneration might not be expected in other device architectures, both those used traditionally and those being currently proposed.

The earliest, machined sieve designs (Mannard *et al*., 1974; Loeb *et al*., 1977) and the silicon-based sieve designs of the 1990s (Kovacs *et al*., 1992, Bradley *et al*., 1997, Wallman *et al*., 1999) reported that failed nerve regeneration, often due to mechanical failure of the interface post-implantation resulting in dissociation of the electrode array and two halves of the guide tube, was often a cause of device failure, sometimes accounting for more than 50% of implanted animals (see Table 2.1). These problems seem to have significantly subsided in the last 15 years with the flexible polyimide sieve designs, possibly due to improved adhesion between the components. Such issues have not yet been reported upon in the newest, non-sieve based designs. Regenerative PNI failure due to mechanical dissociation of parts within the implant without associated failure of nerve cable regeneration was observed in 3% of animals (2 of 60) tested in this study. Reports of similar failures have lessened over the past decade. Shimatani *et al*. (2003) report such failure in 11% of animals (2 of 18). Implant integrity within the near proximity of the nerve does not currently appear to be a large impediment to research in the sense that it does not greatly increase costs or hamper the ability to test hypotheses. In a clinical capacity, such issues would, of course, need to be resolved.

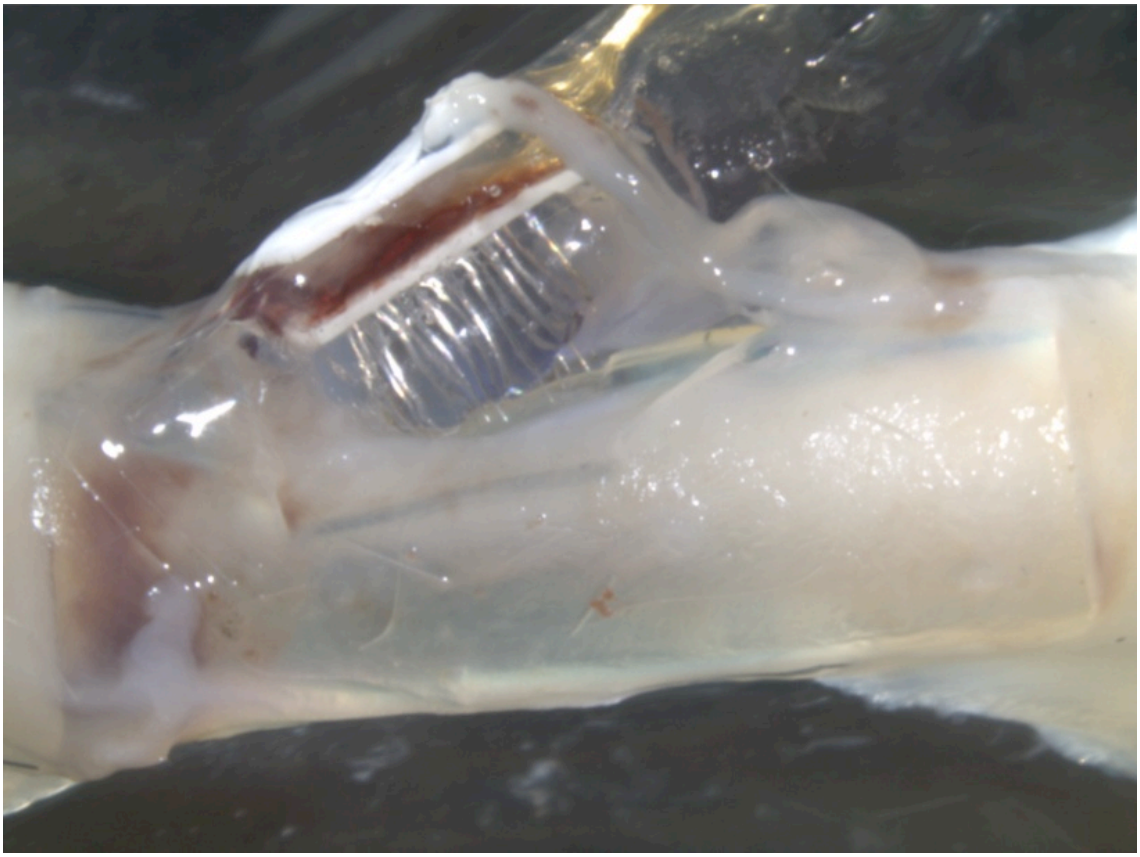

Figure 2.5 Failure of the mechanical integrity of the implanted REMI, as shown here in an explanted example in which the electrode array had become partially dislodged from the nerve guide tube, was observed in 2 of the 60 animals in this study.

2.4.2.2 Component Manufacture

Among the 60 animals implanted in this study, 4 animals (6.7%) were considered failed due to poor manufacturing of components that resulted in an inability to connect the electrophysiological recording equipment to the animal. Similar occurrences have not been (and would likely not be) specifically mentioned in the literature. While this cause of failure should be noted for completeness of this study, it is unlikely that it would represent a long-term problem for any laboratory. Once noted, it was quickly resolved in our laboratory and is not expected to occur in future experiments.

2.4.2.3 Electrode-Nerve Contact

Thirty-six interface devices were examined microscopically after explantation. It was observed that in 5 of the 36 devices (14%), the tips of the electrode shafts within the guide tube of the interface were not in contact with the regenerated nerve cable (Figure 2.6, B).

It is possible that this failure in a minority of devices represents a statistically likely outcome of nerve regeneration through this specific device architecture. If this is the case, analogies could be made with the percentage of via holes through which axons regenerate in a sieve electrode or the percentage of channels through which axons regenerate in a BNI-based or microchannel-based design. Such issues reflect upon the biological interactions inherent within specific interface designs and not upon unintended physical failings.

It is also possible, and more likely given that many explanted guide tubes possessed robustly regenerated nerve cables filling the guide tube, that this represents a failure of nerve regeneration to its typical extent due to inconsistencies within device construction and surgical implantation.

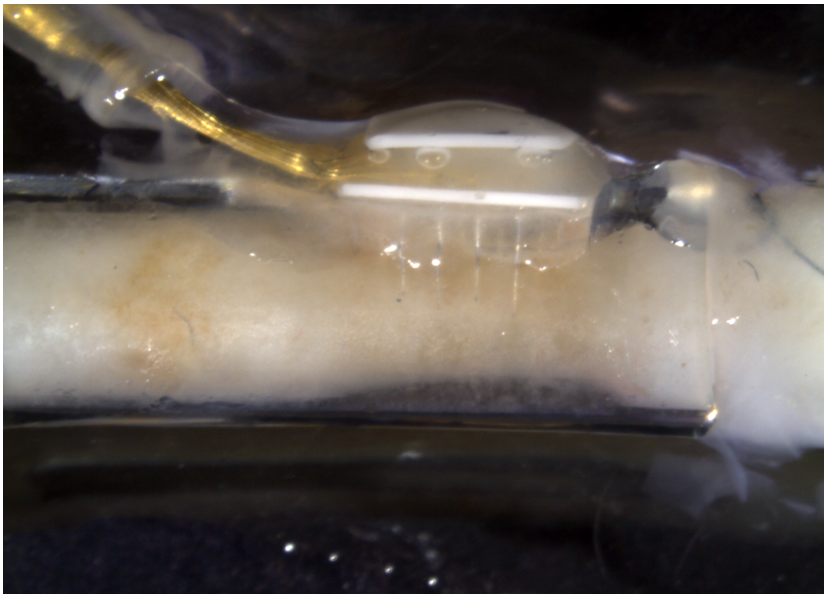

(A)

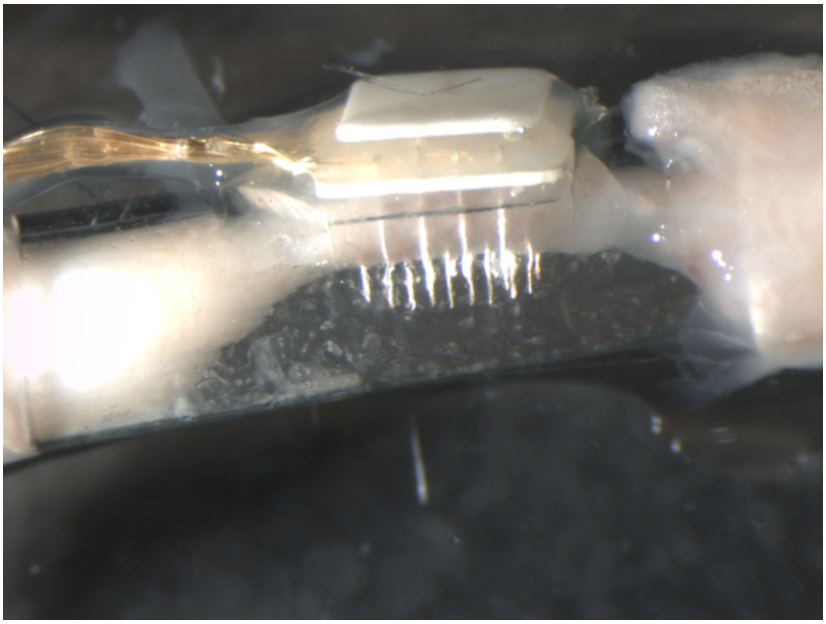

(B)

Figure 2.6 Upon stereoscopic dissection of explanted interfaces, a majority displayed a regenerated nerve cable in which the electrode tips were positioned within the nerve cable (A). A minority of explanted interfaces (see Table 2.8) presented a nerve cable in which the electrode tips were all present outside of the regenerated nerve cable (B).

2.4.2.4 Unexplained lack of single-unit recordings

Out of the 60 animals used in this study, 6 animals out of 40 (15%) displayed no recordable single-unit spiking activity despite the lack of any observable causes. This situation has been implied in many publications and directly mentioned in a few (Bradley *et al*., 1997; Shimatani *et al*., 2003).

The likely assumption is that, by chance, no unmyelinated axons or nodes of Ranvier were positioned physically within recording distance of an electrode. While this issue is of paramount importance in the capacity of a regenerative PNI to successfully function, and it is appropriate that it be reviewed and quantified here, it is considered here to be a consequence of a biological interaction and of interface design and not a consequence of undesired mechanical failure of the PNI.

In this study, no difference was observed in the amplitudes of the noise baselines between devices from which action potentials had been recorded and devices from which no action potentials had been recorded. This is exemplified in Figure 2.7.

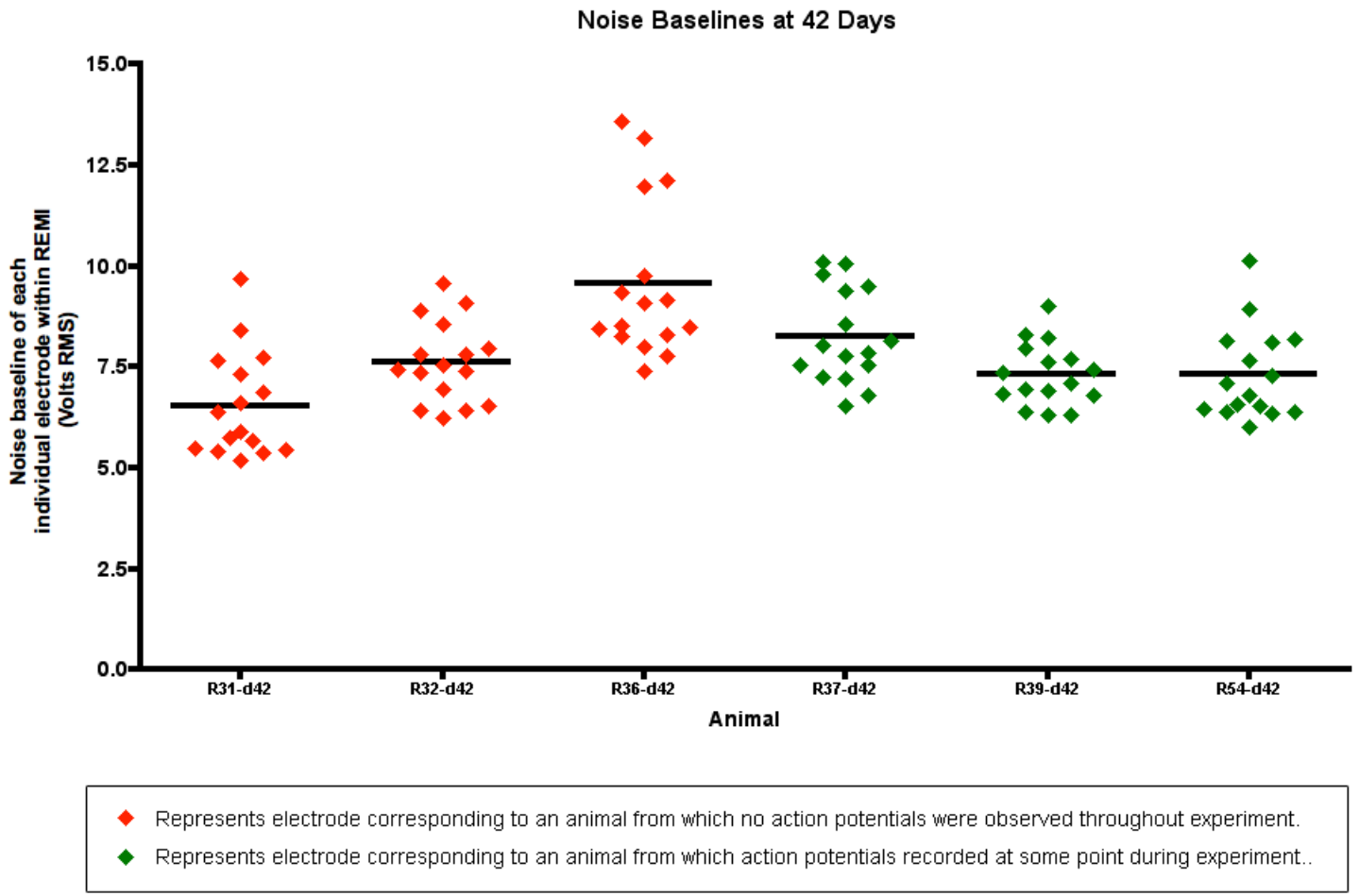

Figure 2.7 Noise baseline amplitudes recorded from 16 electrodes on each of six REMIs at 42 days post-implantation. No statistically significant difference was observed between REMIs from which action potentials had been recorded and those from which action potentials had not, as measured by a nested one-way analysis of variance ($p = 0.7735$). Solid black lines represent group means.

2.4.2.5 Percutaneous Transfer of Signal

A majority of failures over time observed in this study were due to issues surrounding the percutaneous transfer of the signal detected by the implanted electrodes to the external environment of the animal. A broken wire resulting from motion of the percutaneous pedestal or expulsion of the pedestal from the animals resulted in failed ability to acquire a signal in 3 animals (15%), 7 animals (35%), and 12 animals (60%) of the 15 day, 30 day, and 60 day cohorts, respectively. This issue, instead of stabilizing, has shown to become progressively worse with time, resulting in an almost complete inability to record past 60 days in this experimental setup. While infection was not observed in any of the 60 animals, skin irritation, detachment of skin from the pedestal, detachment of the pedestal from the bone, and exposed internal wires all contributed to this mode of failure. This issue is not unique to the experimental setup used here but appears to be representative of the field as a whole.

Six experiments involving chronic recordings from a mammalian model have been reported to date. Three of these six, Bradley *et al*. (1997), Cho *et al*. (2008), Garde *et al*. (2009), report that issues surrounding a percutaneous cap/pedestal or a broken wire near that pedestal resulted in an eventual failure of more than half of their implanted animals. A fourth, Ramachandran *et al*. (2006) reports that 6 of 9 animals dissected (out of a total of 15 animals) displayed a broken internal connector wire at one of several possible sites of tension within the animal. Shimatani *et al*. (2003) do not report any problems with internal wires or a transcutaneous pedestal; their experiment used a skull-mounted pedestal with a short connector wire to a 4-channel sieve electrode implanted within a cranial nerve for 3 months. The sixth, Edell (1986) reports use of a pelvic-mounted transcutaneous pedestal (similar to that used in this study) in rabbits. No details regarding survival rates, failures, or complications are given. An additional recent report involving acute experiments (Lago *et al*., 2007) report a broken internal wire in 50% of an unspecified number of animals.

A majority of investigations into regenerative PNIs involving chronic recordings, including this one, have reported a failure of over half of implanted animals over time (typically 2 to 5 months) due to complications arising from a broken wire or a percutaneous pedestal.

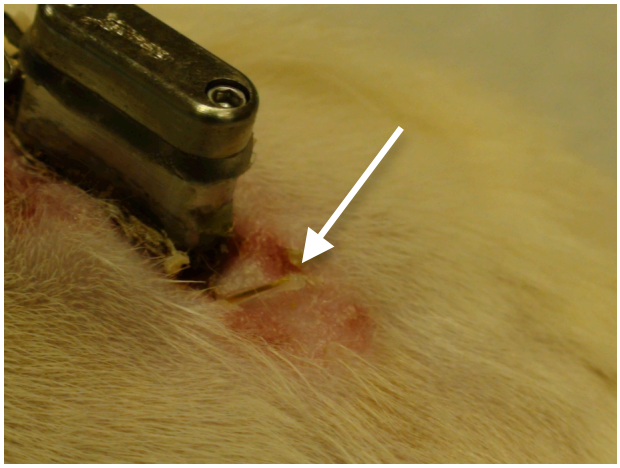

Figure 2.8 Issues regarding the percutaneous interface, such as an internal wire being exposed and broken as shown here (arrow), represent a majority of all observed causes of failure over 60 days (see Table 2.1).

2.4.2.6 Additional Observations

It should be noted that an additional complication, though not necessarily a cause of failure, was the presence of large amplitude (~1 mV and higher) noise artifacts, which can appear similar in shape to action potentials. This was occasionally observed in our recordings of awake, moving animals and has been reported and commented on by others as a concern (Edell, 1986; Kovacs *et al*., 1992). These artifacts may be attributable to myoelectric interference as they are more commonly reported in awake animals than in anesthetized animals. While the presence of such artifacts may preclude the ability of simple "thresholding" methods to determine action potential firing rates, modern signal processing typically takes advantage of templating or other more advance spike identification methods that would not be significantly hindered by the presence of such artifacts, assuming the action potential waveforms themselves are still recordable.

An additional cause of failure within experiments that has been noted in the literature is premature animal death. This is usually reported along with a specific and pertinent cause, such as morbidity due to brain damage or infection following an open-skull surgery to expose a cranial nerve (della Santina., 1997). As such, this is not considered here to be a common cause of failure inherent within current regenerative PNI methodologies.

2.4.3 Relevance to the Field

It is hoped and predicted by many researchers that regenerative peripheral nerve interfacing techniques will eventually allow for voluntary mental control of a robotic prosthesis. Current technology suffers from several limitations rendering it far from capable of achieving this goal. Current methods of investigating regenerative interfacing in animal models suffer from high failure rates due to physical causes as well as signal loss over time due to biological causes.

While it can be assumed that most, if not all, of these physical causes of failure would be addressed through engineering and manufacturing means prior to clinical use of a device in

humans, high failure rates during research experiments not only add great cost to an already expensive field of study, they can potentially limit the ability of researchers to test hypotheses and further the advancement of the field.

An example of this is the ability to test the longevity of recordings in newly proposed devices. For over three decades, the only style of architecture investigated in regenerative PNIs was that of a sieve electrode within a nerve guidance tube. In the last five years, many new styles of device architecture including microchannel-based devices, biodegradable devices, and rolled devices have been proposed as means of improving signal strength, improving regenerative capacity, improving the number of independent signals detected by the device, and reducing the loss of signal strength over time. All of these proposed architectures and others (see Chapter 5) will need to be investigated for their potential to provide not only quality neural signals, but to be able to provide them on the order of years to decades. A high rate of device failure over weeks to months precludes even the ability to test the benefits of these new proposed architectures in laboratory animals.

2.4.4 Wireless Signal Transmission

A future interface capable of clinical use would undoubtedly rely on wireless technology for both signal and power transfer. A percutaneous wire would be unacceptable for human use due to propensity for infection and damage.

Among all chronic experiments reported to date, an experimental setup is used involving a subcutaneous wire or cable connected to a percutaneous pedestal mounted either to the skull or to the pelvis. Such an experimental setup may or may not be simpler and more cost effective for long-term evaluation of implanted interfaces. Failure of the integrity of either the wire or the percutaneous pedestal is reported to result in the effective premature loss of over 50% of implanted test animals within several months in a majority of studies (60% loss over 60 days in this study).

Wireless transmission devices for use in chronic recording of implanted cortical electrode arrays are currently available on the market. While not designed to be implanted, they show that wireless transmission over many meters from a small device with the necessary bandwidth and battery power for continuous transmission of signals from 16 electrode channels for several hours is currently available for a cost similar to that of a REMI electrode array. Any wireless technology that doubled the cost per animal but also doubled the number of animals that functionally survived the course of an experiment would be cost effective. Several research laboratories are currently working on developing implantable wireless technology for both signal and power transfer that would allow for the discontinued use of a long internal transfer wire and percutaneous connector (Harrison *et al*., 2007; Wise *et al*, 2008; Kim *et al*., 2009c; Cho *et al*., 2010). One laboratory has already reported successful *in vivo* use of a prototype to acquire signals in real time from an implanted penetrative array (Clark *et al*., 2011).

2.4.5 Conclusions

As the field of peripheral nerve interfacing continues to advance, researchers and technologists will desire to investigate more stable methodologies than the ones currently employed. This dissertation provides the first quantitative analysis of prominent physical causes of failure inherent in the current methodologies that will need to be overcome.

Causes of failure related to mechanical integrity of implanted electrodes or of the interface guiding tube with or without consequential failure of nerve regeneration currently account for failure in a minority of implanted animals (7% in this study). As such, this may be considered a lesser impediment to research.

Failure of an interface due to issues related to the percutaneous transfer of signals through the skin via a wire or cable and a percutaneous pedestal generally results in a premature loss of over 50% of all test animals (60% in this study, over 60 days). Such an experimental setup is universal among chronic investigations reported to date.

Many new regenerative PNI architectures have been proposed in the last several years with hopes of overcoming current limitations such as long-term signal loss. The results presented here suggest that physical device failure inherent within current experimental methodologies will serve as a major impediment to the ability to investigate these newly proposed architectures. More stable methodologies, such as incorporation of wireless signal and power transmission, would improve the capacity to investigate these new technologies.

CHAPTER 3

NERVE STRETCH

3.1 Overview

3.1.1 Limitation of Current Regenerative Peripheral Nerve Interfacing

Most *in vivo* experiments to date which have recorded single-unit activity have suffered from signal loss over time. This usually occurs within months. A practical device capable of clinical use would be required to function for many decades. The biological mechanisms resulting in signal loss inherent within cortically implanted interfaces are under active investigation by many researchers. Inflammation due to micromotion and mechanical mismatch between tissue and electrode is considered to be a contributing factor in cortical implants. A complimentary phenomenon in peripheral nerve interfaces would be inflammation due to tissue motion around the electrodes resultant from nerve stretch during limb movement. Such a phenomenon has not yet been investigated as a potential contributor to signal loss in peripheral interfaces.

3.1.2 Specific Aim

Determine if nerve stretch due to limb extension contributes to accelerated signal loss in regenerative nerve interfaces.

3.1.3 Hypothesis

We hypothesize that chronically stretching an interfaced nerve to a length commensurate with either full or moderate limb extension will accelerate the rate of signal loss over time. We further hypothesize that such stretching will increase the average size of the

axon-depleted-area surrounding each electrode shaft and reduce the number of regenerating axons through the interface.

3.1.4 Background

The current understanding of biological mechanisms of rejection of cortical implants, with particular focus on micromotion, is reviewed here and compared to potential complementary mechanisms of rejection for RPNIs. The mechanical properties of peripheral nerves are reviewed with attention to functional and structural impairments that can occur under stretch.

3.1.4.1 Biological Mechanisms of Signal Loss in Cortical Electrodes

The current understanding of the biological interactions between electrodes and brain tissue that result in signal loss or signal attenuation over time involves both an acute response to electrode insertion and a chronic response to the presence of a foreign body. This response can be due to encapsulation of the electrode within a fibrous and insulating scar or displacement or death of nearby neurons (for reviews see Polikov *et al*., 2005; Marin and Fernandez, 2010; Leach *et al*., 2010). Acutely, insertion of a needle electrode into the brain causes tissue damage and broken microvasculature allowing serum and cerebrospinal fluid proteins to cross the blood brain barrier, resulting in activation of nearby astrocytes and microglia. These two cell types mitigate a healing response and migrate to the surface of the electrode forming a glial scar (Figure 3.1). This response is generally complete within 6-8 days. The chronic response to the foreign tissue typically involves a progressive buildup of the glial scar as well as persistence of a local inflammatory state. This inflammatory state is associated with progressive cell death and neurodegeneration (McConnell *et al*., 2009; see also Whitney *et al*., 2009).

Any factors which increase the local inflammation around the electrode can result in loss of acquirable signals by that electrode from nearby neurons by increasing the size of the

glial scar or death of nearby neurons due to inflammation-associated degeneration. Current bioengineering attempts to mediate this inflammatory response include the local administration of anti-inflammatory compounds (Spataro *et al*., 2005), incorporation of anti-inflammatory surface molecules onto the electrode shaft (He *et al*. 2007), electrode surface coatings to mitigate the foreign body response (Higgins *et al*., 2011), surface topology modifications at the nanoscale (for a review see Kotov *et al*., 2009), the use of *in vivo* imaging during implantation to avoid initial microvascular damage (Kozai *et al*., 2010), covalent attachment of neural adhesion molecules (Azemi *et al*., 2011), the use of RNA interference to silence gene expression of degenerative proteins (Smith *et al*., 2012), modified electrode geometries (Seymour and Kipke, 2007), incorporation of MEMS technology to move electrodes out of the glial scar several weeks post-implantation (Stice and Muthuswamy, 2009), and incorporation of neural stem cells (Purcell *et al*., 2009) as well a host of strategies to mediate damage associated with mismatch of mechanical properties (see below). Many of these strategies may eventually find use in peripheral nerve interfaces as well.

Brain tissue is relatively soft, with a modulus of elasticity on the order of 10 kPa (Ommaya 1968). Silicon-based needle electrodes, however, possess a modulus of elasticity on the order of 150 GPa (see Hopcroft *et al*., 2010), a greater than ten million fold increase in stiffness. This has been referred to as the "fork in the jello problem." Given that the brain is subjected to deformations during behavioral movements and due to cyclic cardiac pulse pressures (see Britt and Rossi, 1982; Gilletti and Muthuswamy, 2006), there is potential for shear stress at the tissue surface interface.

Edell *et al*. (1992) and Hoogerwerf and Wise (1994) speculated that electrode movement could exacerbate local damage. In 2001, Rousche *et al*. introduced a flexible (~3 GPa) polyimide based needle electrode array hypothesizing that it could provide relief against the forces of "micromotion" at the device-tissue interface. Kim *et al*. (2004) showed that a plastic needle-like device implanted into brain tissue elicits a greater foreign body response when anchored to the skull than when left floating in isolation, providing evidence that motion of

an implanted hard object with respect to the surrounding tissue increases inflammation at the interface. Subbaroyan *et al*. (2005) and Lee *et al*. (2005) modeled the mechanics of electrode-tissue interaction using finite element analysis and supported the contention that mechanical mismatch produces shear stress at the electrode-tissue interface sufficient to cause delamination of the tissue. In a follow-up to Kim *et al*. (2004), Biran *et al*. (2007) confirmed the tendency for small, silicon based needle electrodes to induce a greater astroglial scar and surrounding neuronal cell death when anchored to the skull as opposed to being untethered, providing additional support to the propensity for motion of stiff electrodes to contribute to local inflammation. Since then, many engineering solutions have been proposed to minimize the effects of micromotion due to mechanical mismatch including flexible electrode shafts (Mercanzini *et al*., 2008; Wester *et al*., 2008), electrode shafts that alter their mechanical properties post-implantation (Capadona *et al*., 2008; Lind *et al*., 2010; Hassler *et al*., 2011a; Harris *et al*., 2011), insertion shuttles or biodegradable insertion scaffolds to deliver flexible electrodes (Kozai *et al*., 2009; Foley *et al*., 2009), and magnetically driven insertion of flexible electrodes (Jaroch *et al*., 2009). For a review of flexible polymers used and proposed for neural implants, see Hassler *et al*. (2011b).

3.1.4.2 Comparisons with Peripheral Nerve Interfaces

The biological mechanisms that result in signal loss over time from electrodes implanted into peripheral nerves, whether of a penetrative or a regenerative design, are likely to differ somewhat from those of electrodes implanted into the cerebral cortex. The most obvious difference, from a signal source point of view, is that peripheral nerve interfaces record signals from individual axons instead of individual neuronal cell bodies.

The cell types that mediate the foreign body response also differ. The central nervous system possesses both astrocytes and microglia, both of which contribute to scar formation at the electrode surface, with the astroglial scar suspected of producing an observed neurodegenerative effect. Peripheral nerves do not possess astrocytes. Microglia and

activated microglia are considered to be central nervous system counterparts to the immune cells monocytes and macrophages (activated monocytes), respectively. Both cell types are characterized by increased ED1 expression in the rat (analogous to human CD68) upon activation (Damoiseaux *et al*., 1994; Dijkstra *et al*., 1994). An ED1+ scar is observed covering electrode shafts in both the CNS and the PNS, but the astrocytic contribution is absent in the PNS.

The mechanical properties of peripheral nerves differ from those of the brain. As such the nature of "motion" or "micromotion" of an imbedded electrode within the nerve will differ as will its potential to contribute to local damage and inflammation. Peripheral nerves possess a longitudinal modulus of elasticity that varies somewhat with tension in the range of 20-35 MPa (Rickets *et al*. 2009).

3.1.4.3 Mechanical Properties of Peripheral Nerves

A brief analysis of the literature reveals that the strains at which a nerve exhibits functional or structural deficits will depend greatly upon the nature of the nerve with respect to size, connective tissue composition, and host species. For the purpose of investigating whether nerve stretch due to moderate and exaggerated limb movement would contribute to signal loss of a regenerative PNI in a rat sciatic nerve model, this review focuses on rodent models of nerve stretch.

A nerve can exist either in a relaxed state, such as a loose rope capable of coiling, or it can exist under tension. From the point of initial tension (straight nerve) up to a point of stress that varies greatly depending upon animal species and nerve structure/size, a stretched nerve exhibits an almost completely elastic stress-strain relationship. This is considered to be due to the structural nature of the nerve in which components such as capillaries and nerve fibers typically do not run in straight lines in the longitudinal direction of the nerve. Elastic proteins within the connective tissue and the plexicular arrangement of nerve fiber bundles, as depicted in Figure 3.1 (A and B), allow a range of stretch over which elements of the nerve cable

compensate for stretch by “straightening” in the longitudinal direction until such elements become taught. Lundborg and Rydevik (1973) describe a relationship of supporting blood vessels to a nerve that allows for straightening of tortuous vessels to accommodate nerve stretch (Figure 3.1, C). Visual inspection of a peripheral nerve under low microscopy typically reveals a wavy pattern with vertical elements known as bands of Fontana (Figure 3.1; D, top) produced by undulating elements within a completely relaxed nerve. These bands typically disappear when the nerve is placed under tension (Figure 3.1; D, bottom) and the internal elements straighten. A strain can be reached beyond which the nerve no longer exhibits elastic behavior. Stretch beyond this point can be modeled as having a complex viscoelastic response with functional and structural deficits occurring at varying degrees of strain.

Kwan *et al*. (1992) measured the stress-strain relationship within the rabbit tibial nerve (extended at a rate of 1 cm/min) revealing the elastic portion of nerve stretch to exist with very low stress over strains varying from 0% to approximately 11% (Figure 3.2). The stress-strain relationship exhibits a nonlinear relationship between approximately 11% and 22% strain. The relationship becomes linear again at strains above approximately 22%. It should be noted, however, that nerves held at such strains exhibit viscoelastic properties and creep. Kwan *et al*. report structural failure of the nerve at strains of 38.5% ± 2.0% (n=9), with failure defined by rupture of the perineurium surrounding nerve fascicles.

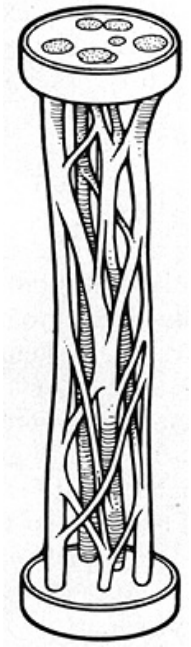

(A)

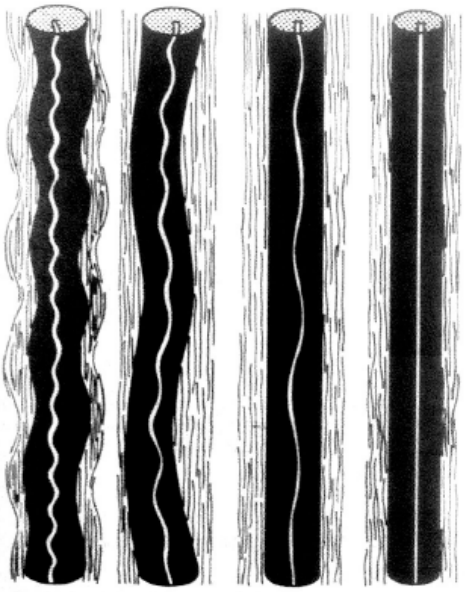

(B)

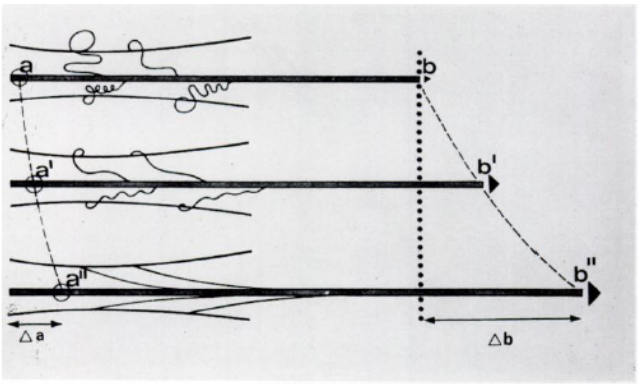

(C)

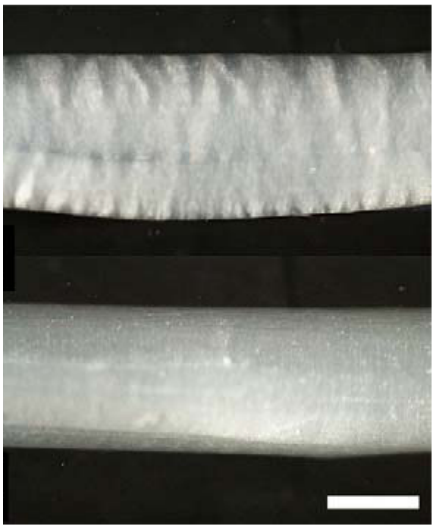

(D)

Figure 3.1 Nerve cables are capable of elastically accommodating a range of strain rates due to the internal structure of nerve components. (A) An example of the plexicular arrangement of nerve fiber bundles within an individual fascicle. Adapted from Raffe (1985). (B) Nerve fibers within fascicles tend to assume a wavy orientation when relaxed. Adapted from Sunderland (1991). (C) Local blood and lymph vessels supporting nerves typically form tortuous paths capable of lengthening during nerve stretch. Adapted from Lundborg and Rydevik, 1973. (D) Low magnification micrograph of a guinea pig sciatic nerve under relaxation (top) and tension (bottom). Scale bar = 0.5 mm. Adapted from Li and Shi (2006).

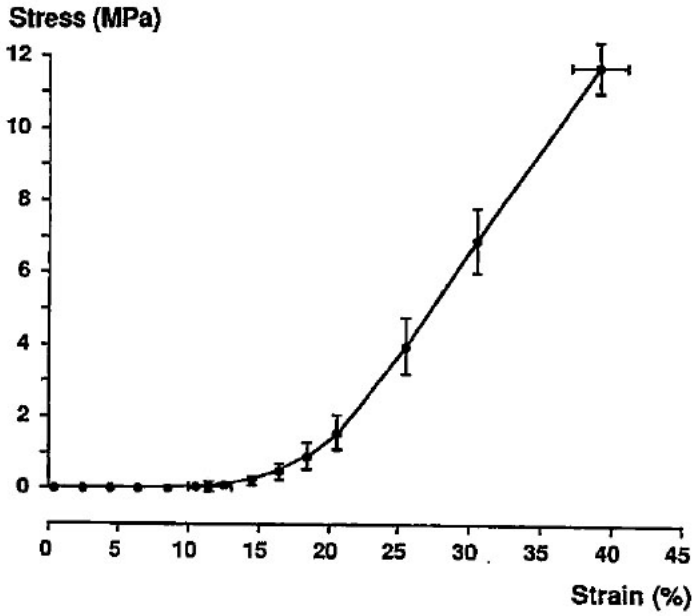

Figure 3.2 Stress-strain curve for rabbit tibial nerve. Adapted from Kwan *et al*. (1992).

3.1.4.4 Nerve Stretch and Structural Damage

The effects of stretching on the integrity of peripheral nerves have been investigated in many animal models. In 1951, Turner demonstrated that the pedal nerve of the invertebrate yellow slug could be stretched to more than twice its original length without any change in conduction velocity of the fastest fibers. Denny-Brown and Doherty (1945) report (according to Sunderland and Bradley, 1961) that transient stretching (5-10 seconds using a gloved finger) of a cat peripheral nerve of up to 100% increase in original length could be achieved without visible damage to the nerve and with functional motor deficits that recovered within two weeks. Stress beyond 100% resulted in partial rupture of the nerve. They also report that upon release, the nerve retains much of its new length, demonstrating a plastic quality to nerves stretched past a certain length. In 1961, Sunderland and Bradley presented an analysis of the stress-strain relationship of peripheral nerves in humans. In human median, ulnar, and popliteal nerves, they report an upper limit of elastic elongation in the range of 20-22% beyond which stretched nerves exhibit plastic deformation. They report an upper limit of maximum

loading in the range of 26-32% elongation, beyond which structural damage and mechanical failure is observed.

It was still unknown during the 1960s the order in which damage to different parts of a nerve under stretch would occur (for reference on classification of nerve injuries see Sunderland, 1968). Haftek *et al*. (1970) investigated this using gradual stretching in a rabbit tibial nerve model. It was observed that elongations of near 30% would result in compressive expulsion of blood from the nerve vasculature with one observed case of a ruptured blood vessel. Six nerves were stretched to a point just prior to the loss of epineurial integrity with elongations to between 39% and 72% (mean of 51%). Histological evaluations of nerves stretched to near this limit revealed intact epineuria, perineuria, and endoneuria but morphologically abnormal capillaries and nerve fibers arrangements as well as disruptions of myelin sheaths. Seven nerves were stretched to the point of partial rupture of the epineurium, with elongations between 42% and 91% (mean of 69%). At points of rupture, internal funiculi (fascicles) were visible. Histological evaluations revealed intact endoneuria, intact but abnormal perineuria, and damaged myelin in most fibers. Eleven nerves were stretched to the point of rupture with elongations of 53% to 122% (mean of 73%). For the rabbit tibial nerve, these results imply a progressive order (in response to progressive nerve stretch) of blood vessel constriction, neurapraxia (damage to nerve fibers resulting in conduction loss but without loss of axonal integrity), rupture of endoneurium, and finally rupture of perineuria and endoneuria. Axonotmesis (damage to axons resulting in distal wallerian degeneration) in the presence of a structurally intact nerve does not appear to occur due to gradual stretching as it can with other types of nerve trauma (see Feinberg and Speilholtz, 2003 (book)).

3.1.4.5 Nerve Stretch and Axonal Regeneration

Concerned with the capacity of axons within a sectioned nerve to regenerate if sutured under tension, Lundborg and Rydevik (1973) hypothesized that stretching of a nerve could lead to dysfunction of the capacity of the perineurium to act as a diffusive barrier to external proteins

and other molecules and that the resultant leakage could potentially interfere with successful axonal regeneration. They showed that a progressive stretch of a healthy rabbit tibial nerve starting at approximately 8% and concluding at approximately 15% elongation resulted in the progression from partial to complete obstruction of capillary blood flow through the nerve. If elongation was held just at the point of capillary blood flow occlusion for 30 minutes, no signs of perineurial diffusion of a tracer protein were observed. These results imply that transient stretch less than approximately 15% would not negatively affect regeneration of a rodent nerve.

Using a transected rat sciatic nerve model, Terzis *et al*. (1975) showed that evoked compound action potential conduction velocities and amplitudes measured across a sutured gap repair after 6-10 weeks diminished if the nerve was sutured under tension. Without quantifying the tension or stretch of the nerve, they report a progressive decrease in conduction velocity and amplitude from zero to mild to moderate to severe tension. Speculating that this could be the result of fibroblast infiltration into the gap or constrictive effects on axonal regeneration due to scar effects that increase with tension, the authors provide evidence that constant tension within a regenerating nerve could deleteriously impact axonal regeneration.

Ogata and Naito (1986) discuss the propensity for lack of blood flow in a nerve under constant tension to result in ischemic damage and reduced generation capacity. They report complete occlusion of blood flow in a nerve stretched at greater than 15.7% elongation in a rabbit sciatic nerve model.

3.1.4.6 Nerve stretch and signal conduction

It has been known since Sunderland (1968) that transient functional deficits in nerve conduction can manifest at small strains at which no apparent structural damage occurs. The causes of these deficits are not fully understood and, while transient ischemia due to capillary constriction is generally considered to be the primary cause of conduction block due to static nerve stretch, several groups consider it likely that transient mechanical responses may contribute as well (see Ochs *et al*., 2000; Li and Shi, 2006).

Riyi Shi and associates have released a series of papers investigating the functional deficits within the sciatic nerve branches of a guinea pig in response to increased nerve stretch. In Li and Shi (2006), they report the onset of diminished compound action potential amplitude at sustained strains of near 8% with a 50% loss in amplitude at strains near 17%. Full recovery occurred within minutes. Bands of Fontana disappeared near 9% strain. In Li and Shi (2007), they investigated deficits resulting from sustained nerve stretches of 2.5 minutes in duration followed by several minutes of continual electrophysiological observation. At 5% strain, they observed a minor (approximately 7%) decrease in amplitude that recovered immediately. At 10% strain, they observed a near 50% decrease in amplitude that recovered over about three minutes. At 20% strain, they observed a rapid decrease in amplitude to nearly 0% which did not recover over the course of the experiment. In a similar experiment (Rickett, 2011), they observed no functional deficits at 5% strain, a near 15% loss in compound action potential amplitude at 10% strain, a near 50% loss in amplitude at 15% strain, and a near 85% loss in amplitude at 20% strain.

Using a rabbit tibial nerve model, Kwan *et al*. (1992) demonstrated a gradual loss of compound action potential amplitude to near 50% amplitude within 45 minutes under a 6% nerve strain. A nearly complete loss of conduction (near 10% amplitude) was observed within 45 minutes for a sustained strain of 12%. The 6% strain recovered fully within thirty minutes. The 12% strain recovered only to about 50% amplitude. Also in a rabbit tibial nerve model, Driscoll *et al*. (2002) describe minor detectable deficits in nerve conduction velocity at 8% strain and gradually increasing deficits at sustained 16% strain that show signs of irreversibility. In a rabbit brachial plexus model, Takai *et al*. (2002) observed a complete conduction block measuring compound muscle action potentials in the triceps muscle after elongation of the lower trunk of the brachial plexus to a strain of near 8%.

Methods of determining nerve strain vary among researchers, but typically involve the placement of two dots, using dye or ink, upon an exposed nerve (Figure 3.3). Measurement of

changes in the distance between the dots allows for the calculation of strain under different conditions.

While the strain values at which onset of transient functional deficits may be observed and the values at which those deficits become lasting appear to vary significantly by report and author, a trend can be observed in which smaller nerves, as well as nerves within small animal models, appear to be capable of accommodating greater amounts of strain than can larger nerves in larger animal models.

3.1.4.7 Summary of Effects of Peripheral Nerve Stretch

While there is understandably a large variability of reported biological consequences of nerve stretch within the literature (dependent upon animal model, nerve of interest, measurement techniques, quantitative methodologies, etc.), several conclusions can be drawn with respect to the rat sciatic nerve model. Functional deficits likely occur at a sustained nerve strain of greater than 4-6%. The limit of low-stress elastic deformation is likely between 9-15% nerve strain. Complete occlusion of capillary blood flow likely occurs near 15% nerve strain. Temporary (hours to days) functional deficits would likely occur from sustained stretch of greater than 15% nerve strain; the effects of transient stretches in this range have not been investigated. Lasting deficits (weeks or more) would likely occur due to damage to internal components (myelin sheath damage or perineurial tears) at nerve strains greater than approximately 38%. Sustained tension within a nerve, but not transient tension, has been shown to limit the regenerative capacity of axons.

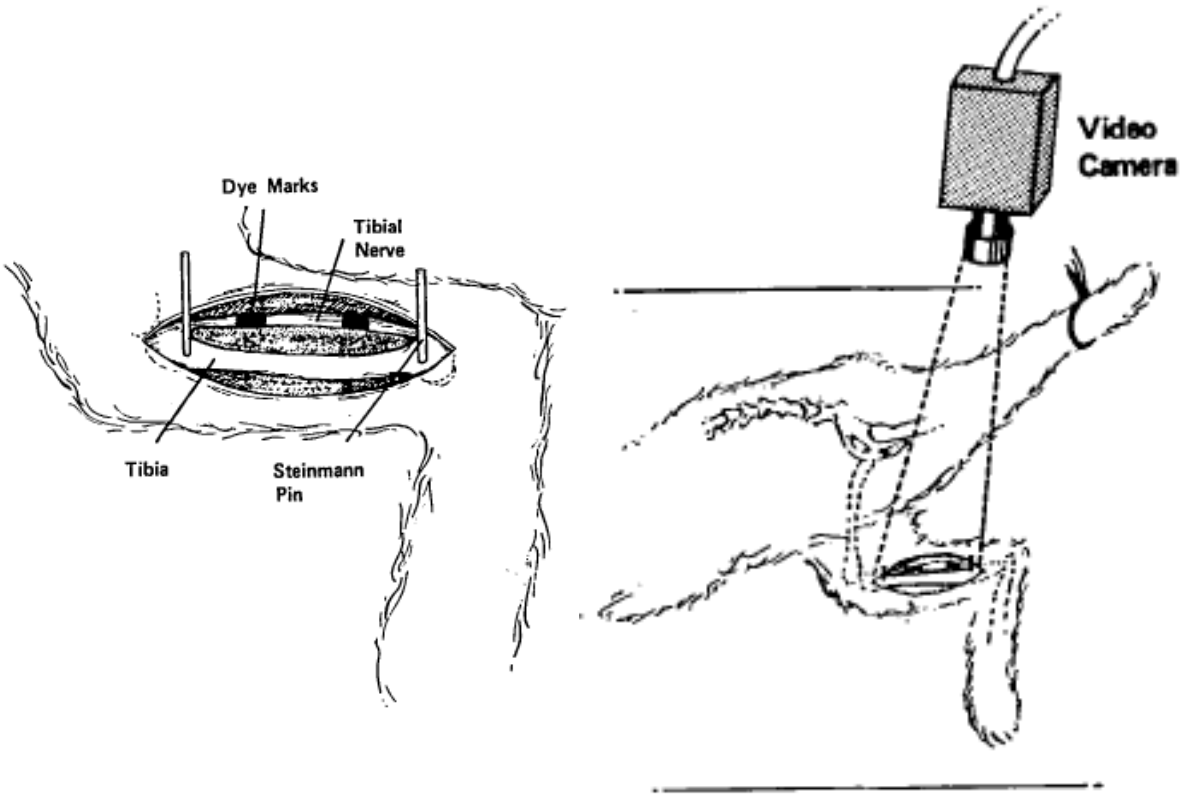

(A)

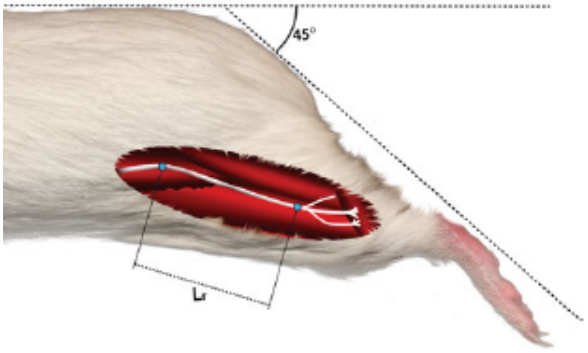

(B)

Figure 3.3 Measurement of nerve strain under different experimental conditions is typically achieved by recording the change in distance between two marked locations on an exposed nerve. Adapted from Wall *et al*., 1991 (A) and Rickett *et al*., 2011 (B).

3.1.5 Experimental Design

To test the hypothesis that periodic limb stretching contributes to signal loss over time, a custom device was built that allows for cyclic stretching of the hind limb of a rat model. A total of 36 rats were implanted with REMIs in the left sciatic nerve. One third of the animals were subjected to cyclic limb stretching once per week at full limb extension (to represent exagerated limb extension); one third of the animals were subjected to cyclic limb stretching once per week at 70% of full limb extension (to represent moderate limb extension); one third of the animals were not subjected to cyclic limb stretching (control group). The animals were equally divided into two cohorts; one half of the animals were sacrificed at 30 days post-implantation and one half of the animals were sacrificed at 60 days post-implantation. Electrophysiological recordings through the REMI were performed weekly upon the 30-day cohort. Histological analysis was performed upon the explanted regenerated nerves of both cohorts to quantify the average size of the scar surrounding each electrode shaft and the number of regenerating axons through the implant. Overall there were six experimental groups (n=6 animals per group) representing three stretching treatments (0%, 70%, and 100% limb stretch) and two sacrificial time points (30 days and 60 days).

3.2 Methods

3.2.1 Peripheral Nerve Interface and Surgical Implantation.

The REMI interface was selected as a representative model of a regenerative peripheral nerve interface. For a description of the REMI and the methods of surgical implantation, see Sections 2.2.1 and 2.2.2.

3.2.2 Limb Stretching

Cyclic limb stretching was achieved using a custom-built device in which a computer controlled linear actuator propels a clamp along two stationary rails (Figure 3.4). The clamp attaches to the foot of a rat anesthetized via continuous inhalation of 2% isoflurane. The device cyclically stretches the limb from a relaxed position to either 70% or 100% of full limb extension. The animal's body is immobilized by two rods clamping the sides of the pelvis. The device was controlled via custom designed LabVIEW script.

Animals within the treatment groups were subjected to once weekly stretching sessions, beginning at 7 days post implantation and lasting until scheduled sacrifice, in which the hind limb was stretched cyclically for a total of ten minutes. A typical stretching session involved approximately 130 stretch cycles.

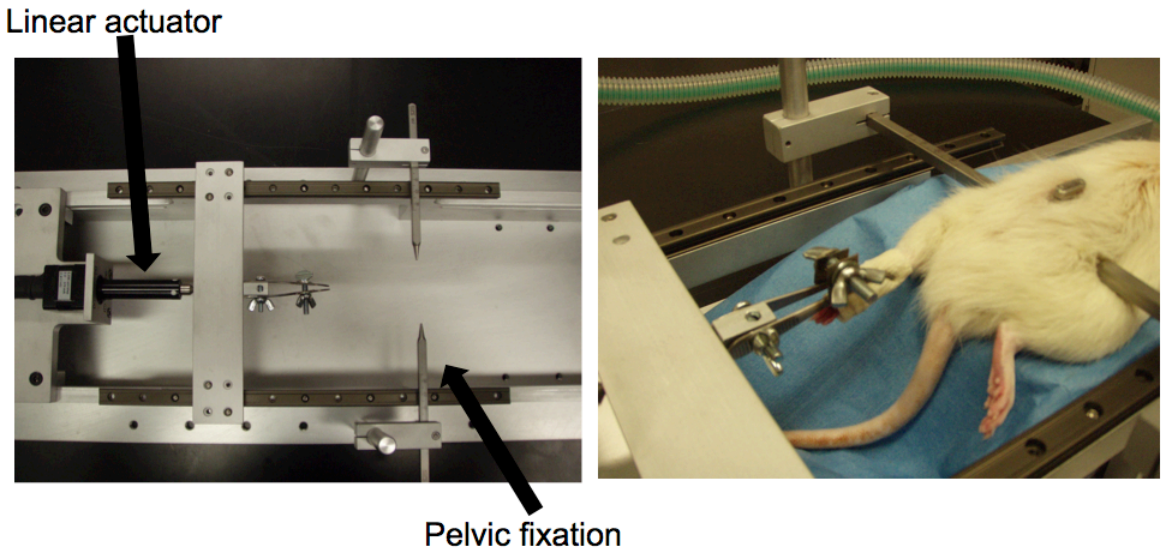

Figure 3.4 A computer-controlled mechanical stage was developed for cyclic stretching of the hind limb (left). Pelvic fixation allowed for cyclic stretching in the caudal direction of an anesthetized animal (right).

3.2.3 Quantification of Strain in the Nerve

To quantify the degree to which extension of the limb stretches and deforms the sciatic nerve in this experimental model, we employed a technique similar to that used by Rickett *et al*. (2011) and Wall *et al*. (1991) to visually inspect a marked nerve under different stretching conditions (see Figure 3.3). Four rats total were used for this quantification. Each animal was euthanized via intraperitoneal injection of sodium pentobarbitol (100 mg/kg). After loss of consciousness and immediately upon cardiac arrest, but before the onset of rigor mortis, one of the hind limbs was cleaned and shaved, and the sciatic nerve surgically exposed. Two locations on the nerve, approximately one centimeter apart, were marked with permanent ink. The animal was placed into the stretching apparatus described in Section 3.2.2 and adjusted to first a neutral position (0% stretch), then a position of full limb extension (100% stretch), then to a position of moderate limb extension (70% stretch). Using a near-focus digital camera placed in a perpendicular line of sight, images of the nerve, with the two marking dots visible, were

taken at each stretch position. Digital quantification of the changes in distance between the two dots allowed for calculation of strain induced in the nerve at the three different limb stretch positions. The time necessary for acquisition of measurements for each animal, including time for the surgical exposure and marking of the nerve, took approximately 4 minutes from the time of cardiac arrest. Partial resistance to limb stretch due to the onset of rigor mortis could be felt manually starting at about 10 minutes.

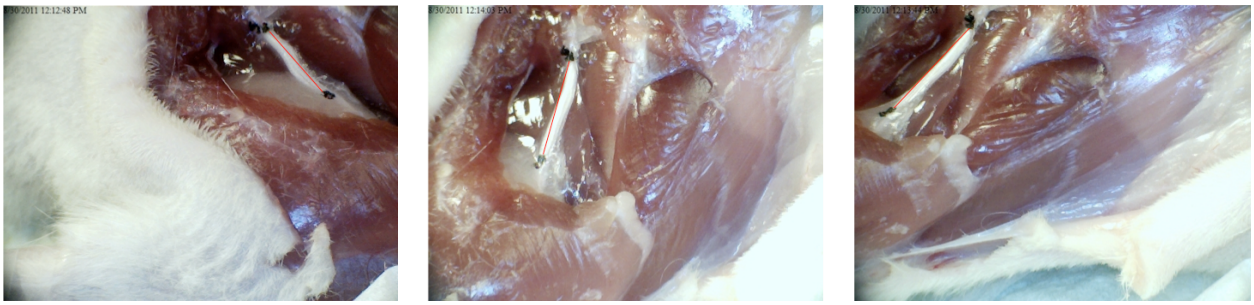

(A) (B) (C)

Figure 3.5 Images of a marked rat sciatic nerve at 0% limb stretch (A), 70% limb stretch (B), and 100% of maximum limb stretch (C). Red line between marked black dots added digitally to allow calculation of nerve strain.

3.2.4 Electrophysiological Recordings

Electrophysiological recordings were performed weekly upon the 18 animals within the 30 day cohort, starting at 7 days post-implantation. Among the control animals (0% limb stretch), the weekly recording session involved anesthetization of the animal to allow for connection of the recording equipment, approximately 5 minutes to allow the animal to recover, and a five minute recording session in which the animal was allowed to move freely within a small cage. The animal was re-anesthetized to allow for disconnection of the recording equipment. For animals within the treatment groups (70% and 100% limb stretch), the weekly recording session involved anesthetization of the animal to allow for connection of the recording

equipment, approximately 5 minutes to allow the animal to recover, a five minute recording session in which the animal was allowed to move freely within a small cage, re-anesthetization to allow for limb stretching session, an additional 5 minutes to allow for recovery, and a second 5 minute long recording session. The animal was then re-anesthetized to allow for disconnection of the recording equipment. The total time in between the pre-stretch recording session and the post-stretch recording session was typically about 30 minutes. For details on the procedural methodology and processing of electrophysiological recordings, see Section 2.2.3.

3.2.5 Tissue Preparation

Upon scheduled termination, animals were sacrificed by intraperitoneal injection of sodium pentobarbitol (100 mg/kg) and transcardially perfused with saline (0.9%, 5 minutes) and paraformaldehyde (4%, 15 minutes). The REMI was surgically exposed and extracted including several centimeters of ribbon cable and several millimeters of sciatic nerve both proximal and distal to the nerve guide tube (Figure 3.6, A) and placed in 4% paraformaldehyde overnight. Connective tissue was carefully removed and the nerve guide tube was dissected beneath a stereomicroscope (Figure 3.6, B-C). The regenerated nerve cable was marked with tissue marking dye to preserve orientation with respect to the electrode array (Figure 3.6, D). The marked nerve was processed for paraffin embedding and sliced longitudinally in a horizontal perspective relative to vertically positioned electrodes. Slices were approximately 6 μm thick. Typically 5-6 slices per nerve were obtained.

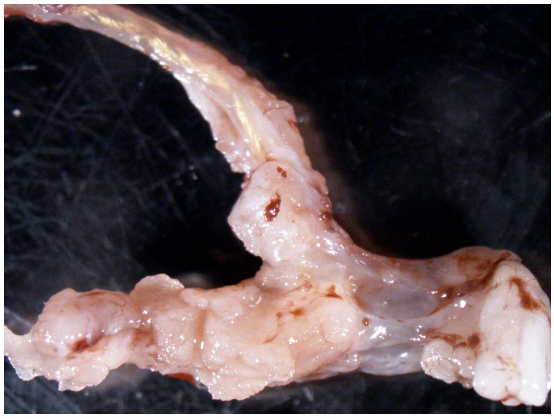

(A)

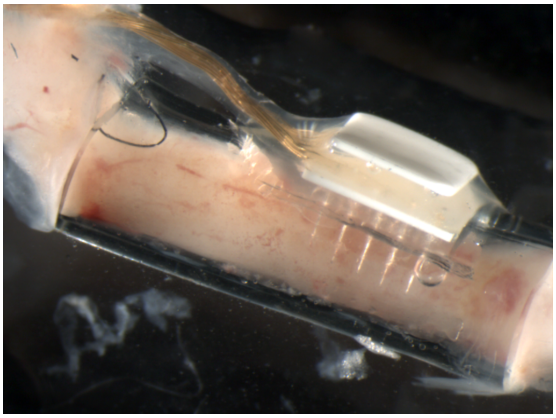

(B)

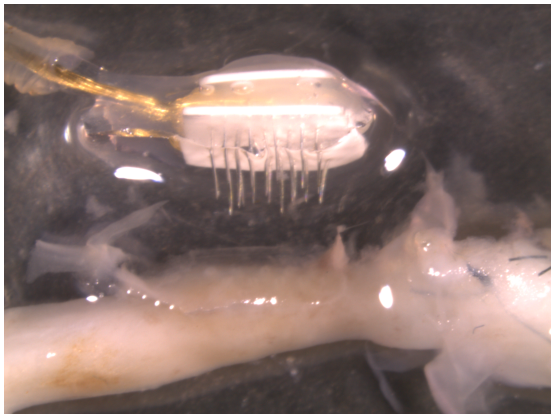

(C)

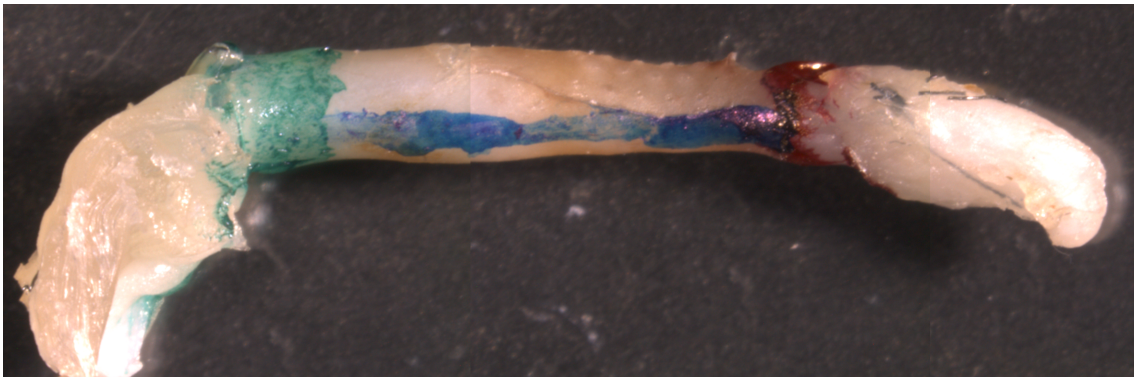

(D)

Figure 3.6 Explanted REMIs with regenerated nerves (A) were cleaned (B), and the regenerated nerve cables were extracted (C) and marked for orientation (D). (image A taken at two weeks post-implantation; images B-D taken at 30 days post-implantation)

3.2.6 Histological Evaluation

3.2.6.1 Immunostaining

The slices of explanted nerve tissue were immunostained for regenerating axons (primary antibody: NF200, Rabbit IgG, 1:200, Sigma; secondary antibody: goat anti-rabbit IgG Dylight 488, 1:220, Jackson Immunoresearch), for myelin (primary antibody: Protein zero, Chicken IgY, 1:200, Millipore; secondary antibody: goat anti-Chicken IgY Dylight 594, 1:220, Jackson Immunoresearch), and for activated macrophages (primary antibody: ED-1, Mouse IgG1, 1:500, AbD Serotec; secondary antibody: goat anti-mouse IgG1 Alexa 350, 1:220, Invitrogen). Immunostained slices typically revealed an array of holes, corresponding to explanted electrode shafts, surrounded by $ED1^+$ scars. $NF200^+$ axons, most of which were surrounded by Protein Zero-positive myelin, typically extended from the proximal to the distal end of the slice while circumventing the electrode holes (Figure 3.7).

3.2.6.2 Electrode Scar Sizes

Axons and myelin were not present within the scar tissue but were generally present within the immediate area of the $ED1^+$ scar allowing for simple visual determination of the axon-depleted scar area surrounding each electrode hole. To compare the average size of the axon-depleted scars between the different limb stretch groups, the axon-depleted area surrounding each electrode and the area of the hole left by each electrode were visually identified and highlighted (Photoshop, Adobe Systems Incorporated, San Jose, California). The total area of each axon-depleted scar was determined using scaled, automated pixel counting of the defined area (scar area minus hole area). The average axon-depleted area (ADA) was calculated for each slice, and the slice averages were averaged to provide an average value for each explanted nerve. The average nerve ADA values were compared across groups using a doubly nested one-way analysis of variance with $p \leq 0.05$ considered statistically significant.

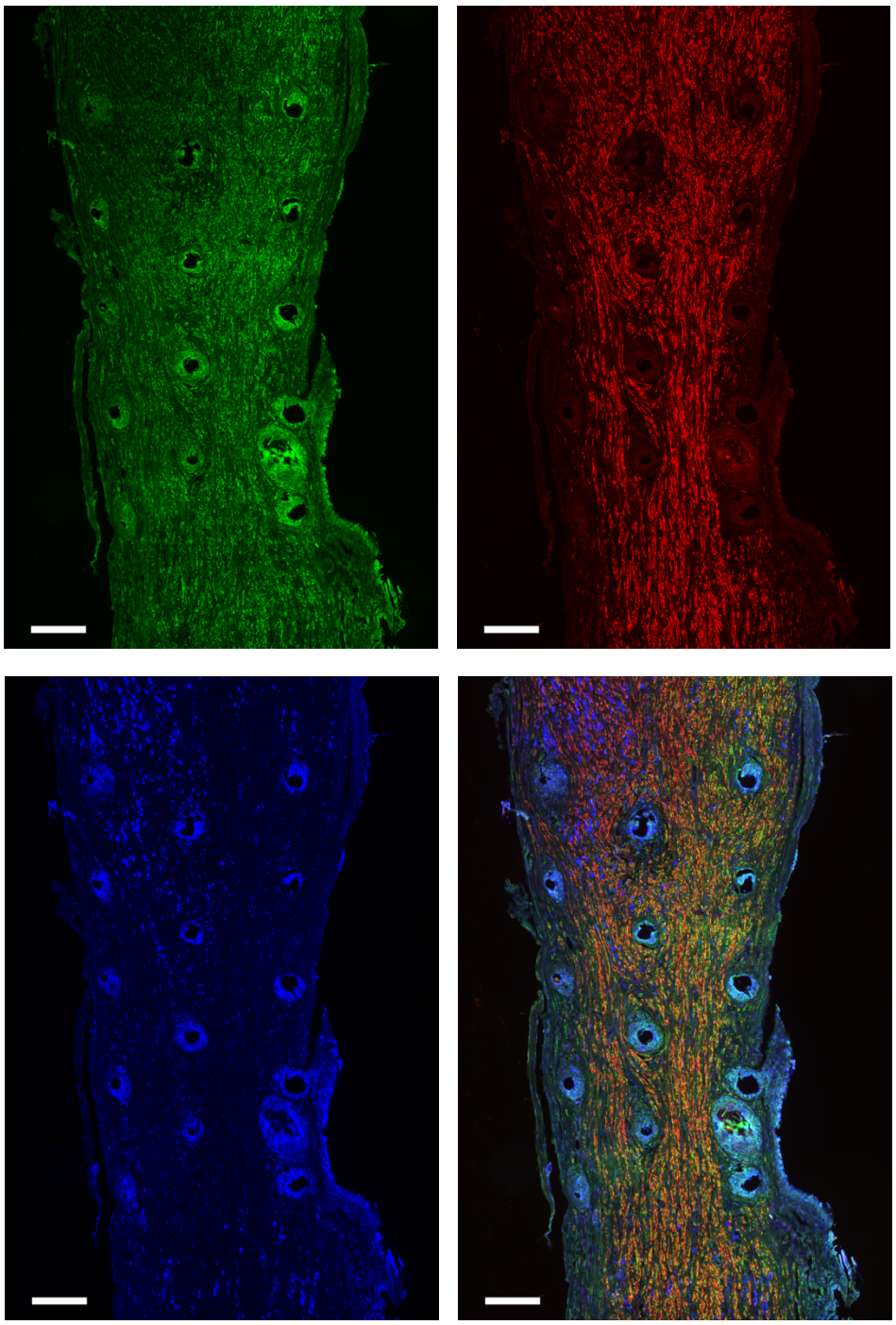

Figure 3.7 Tissue slices were stained for axons (NF200, green), myelin (P0, red), and macrophagic scar tissue (ED1, blue). The merged image (bottom right) shows clearly defined axon-depleted areas, filled with $ED1^{+}$ scar tissue, surrounding each electrode. Orientation: proximal nerve, top; distal nerve, bottom. Scale bar = 200 μm.

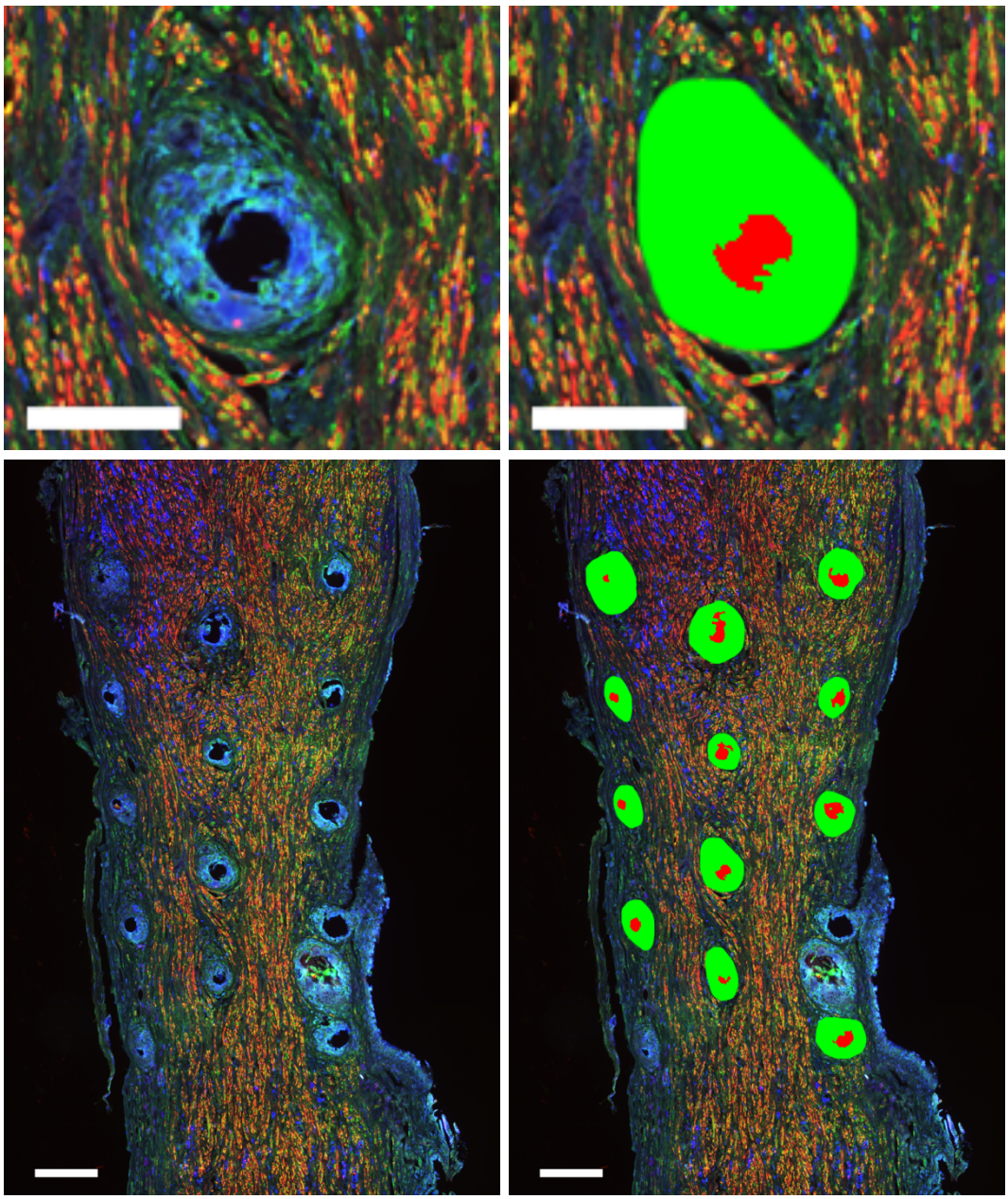

Figure 3.8 Example of identification of axon-depleted areas. Original images (top left, bottom left) and ADA defined images (top right, bottom right). Scale bars = 100 μm (top images) and 200 μm (bottom images). (See Figure 3.7 for immunostaining identifications).

3.2.6.3 Axon Counts

To compare the quality of axonal regeneration through the REMI nerve guide tube across different limb stretch groups, the number of both axons and myelinated axons which crossed a horizontal (from the perspective of the histological image) line set roughly near the middle of the electrode array holes but without crossing any electrode shaft scars were identified and counted (Figures 3.9 and 3.10) for each slice. The average number of axons and myelinated axons for each explanted nerve was computed. The average number of axons per nerve and the average number of myelinated axons per nerve, as determined using the line crossing method, were compared across experimental groups using a nested one way analysis of variance with $p \leq 0.05$ considered statistically significant.

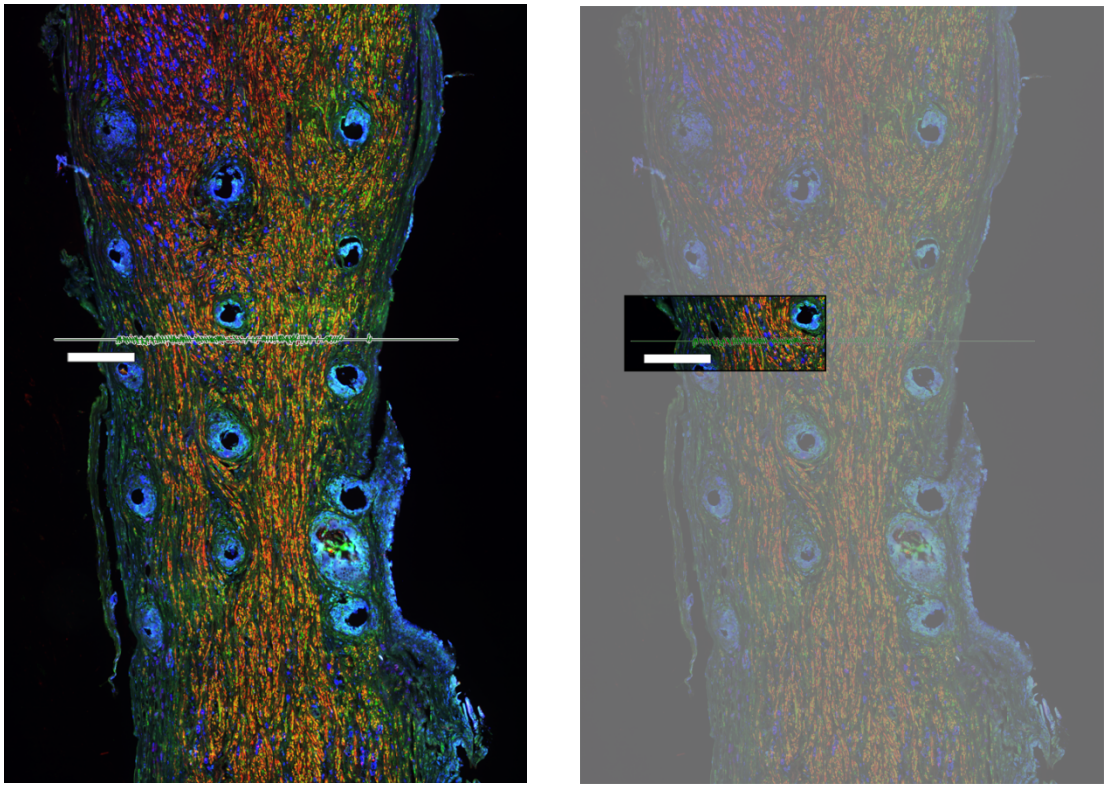

Figure 3.9 Example of line-crossing method used to characterize the number of axons and myelinated axons within a REMI nerve guide tube. Original image (left). Image highlighting windowed view used in Figure 3.10 (right). Scale bar = 200 μm. (See Figure 3.7 for immunostaining identifications).

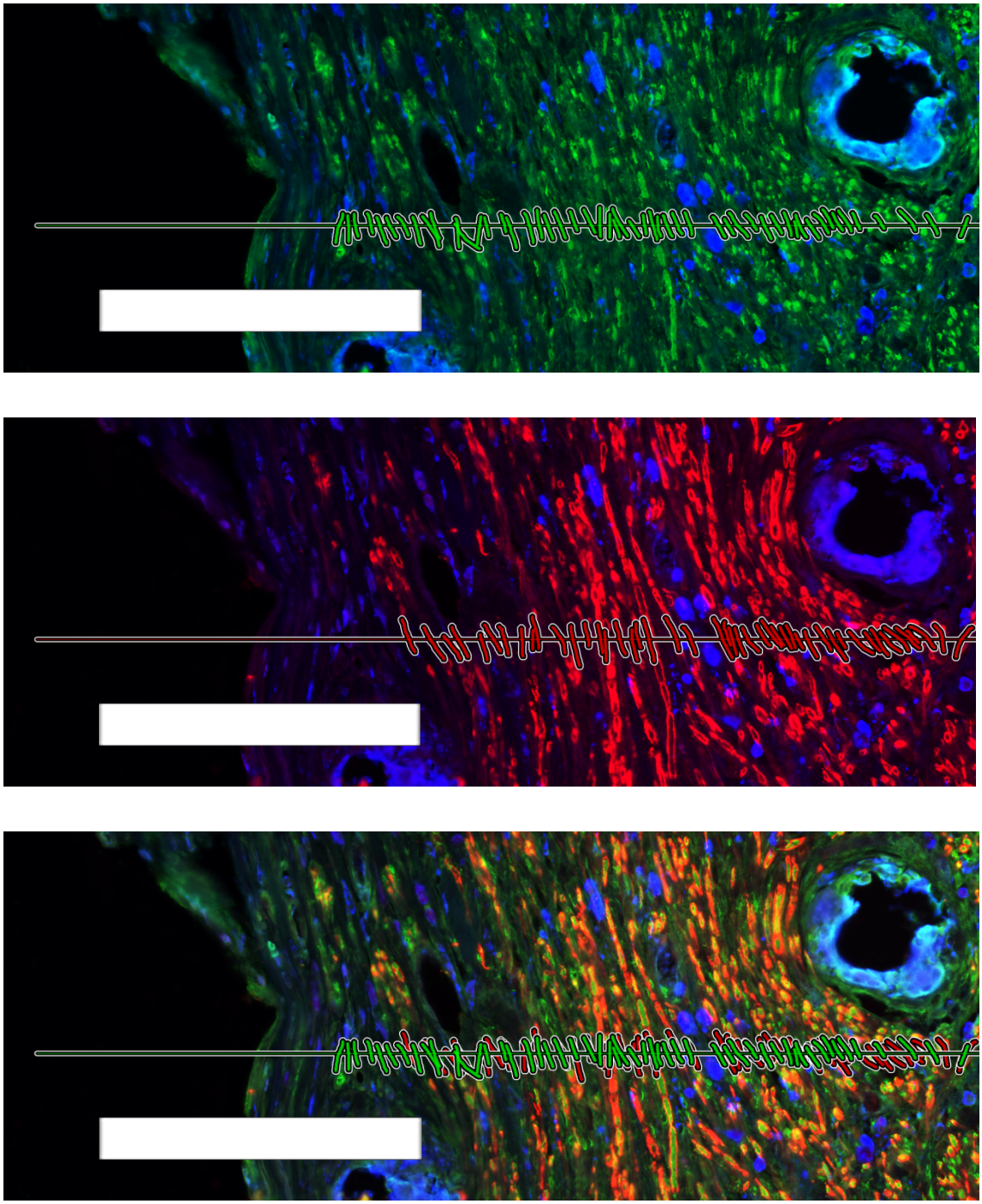

Figure 3.10 Example of visual identification of axons crossing a characteristic center line within a regenerated nerve used for counting (top). Example for myelinated axons (middle). Merged (bottom). Scale bar = 200 μm. (See Figure 3.7 for immunostaining identifications).

3.3 Results

3.3.1 Characterization of Experimental Model

3.3.1.1 Quantification of Nerve Strain

The strain in the nerve corresponding to limb extension at 70% and 100% stretch was measured in four separate trials (Table 3.1). Limb stretch of 70% of maximum limb extension resulted in a strain in the nerve of 18.3% ± 1.0(%). Limb stretch of 100% of maximum limb extension resulted in a strain in the nerve of 34.7% ± 1.3(%). Values given as the mean ± one standard deviation.

Table 3.1 Measured sciatic nerve strain at stretched positions relative to relaxed position.

	0% Limb Stretch:	70% Limb Stretch:	100% Limb Stretch:
Trail 1:	1	1.1947	1.3618
Trial 2:	1	1.1882	1.3392
Trail 3:	1	1.1742	1.3519
Trial 4:	1	1.1743	1.3339

3.3.1.2 Limb Stretch Lengths Over Time

Any contractures within the limb that were to develop following surgical implantation of the interface could possibly shorten the stretchable length of the limb, resulting in slack within the nerve during limb stretching and invalidating the results of this experiment. A contracture is an abnormal shortening of a tissue within a limb, typically a muscle, tendon, or ligament, that results in stiffening of a joint or increased resistance to passive stretch.

Volkmann's contracture, or ischemic contracture, is the result of necrotic muscle tissue following a traumatic injury (see Seddon, 1964; Stevanovic and Sharpe, 2006). Scar contractures may result from the activity of fibroblasts and myofibroblasts in wound healing near a joint (Grinnell, 1994; Ehrlich *et al*., 1994). Prolonged immobilization of a joint can result in contracture due to collagenous hardening and buildup of connective tissue (for review, see Farmer and James, 2001). Atrophy of muscles due to immobilization or denervation can result in contracture of a muscle, or of a joint if the atrophy is asymmetric (Farmer and James, 2001). Other types of contractures, such as congenital contractures, burn scar contractures, or contractures resultant from muscle spasticity due to cerebral palsy or central nervous system trauma, are not of concern here.

To ensure that the passive stretch capacity of the limb did not diminish over time following surgical implantation of the PNI, the length of stretch during our stretching sessions was measured by the software controlling our stretching apparatus. In a sampling of stretch lengths recorded from several rats in both the 70% stretch and 100% stretch cohorts over the course of many weeks (Figure 3.11), it can be seen that stretch length remained fairly constant over time, indicating that contractures were not adversely affecting the ability of this experiment to test the hypothesis.

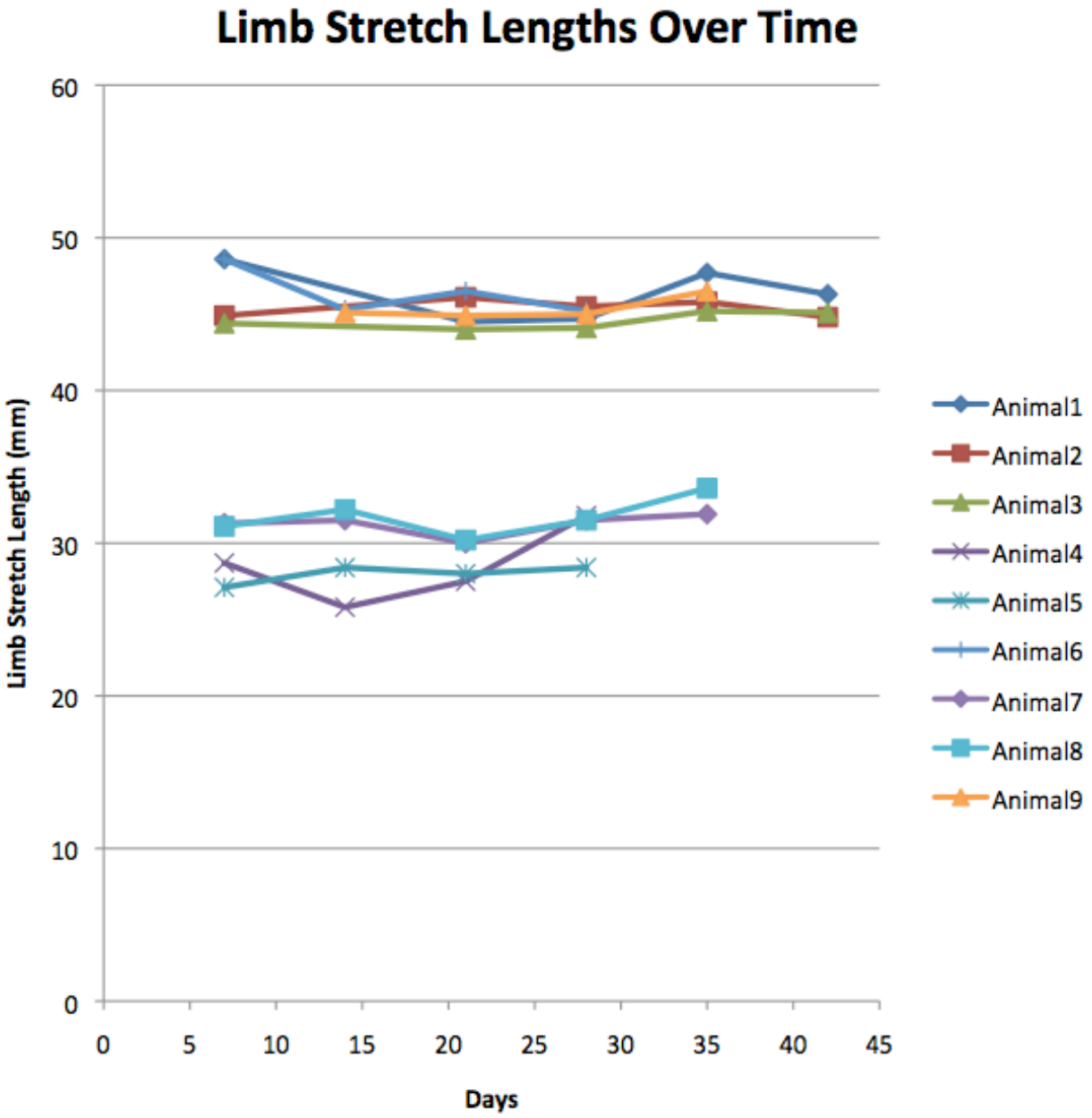

Figure 3.11 Limb stretch lengths did not decrease over the length of the experiment.

3.3.2 Results of Electrophysiological Recordings

Recordings of the electrophysiological activity, through the implanted PNI, of 18 animals were attempted weekly over the course of 28 days. Two of the six original animals of the 0% stretch group suffered premature device failure and were replaced. One of these two had suffered expulsion of the percutaneous pedestal after day 14; the other lacked electrodes within the nerve cable upon terminal inspection. All six of the original animals within the 70% stretch group survived to scheduled termination without observable device failures. Two of the six animals of the 100% stretch group suffered premature device failure between 21 and 28 days and were not replaced. Both suffered from breakage of the connector wire at the base of the percutaneous pedestal followed by expulsion of the pedestal.

Three of the six animals within the 0% stretch group displayed single unit spiking activity at some point during the experiment. All six of the animals within the 70% stretch group displayed single unit activity at some point during the experiment. Two of the six animals within the 100% stretch group displayed single unit activity at some point during the experiment.

While spiking activity is typically not observed at 7 days post-implantation (presumably due to the time necessary for regenerating axons to reach the electrode tips from the proximal nerve stump), one animal within the 100% stretch group and 4 animals within the 70% stretch group displayed spiking activity at day seven. Starting at day 14, the 0% stretch group displayed a progressive loss of spiking activity from 10 units over three animals at day 14 to 6 units over two animals at day 21 to 1 unit on one animal at day 28. The 70% stretch group, from recordings taken after limb stretching sessions, displayed 2 units on one animal at day 14, 2 units on one animal at day 21, and 5 units over two animals at day 28. The 100% stretch group, from recordings taken after limb stretching sessions, displayed 4 units over two animals at day 14, 1 unit on one animal at day 21, and 1 unit on one animal (out of four remaining animals) at day 28. These results are summarized in Figure 3.12. The percentage of animals displaying single-unit spiking activity at specific time points is summarized in Figure 3.13.

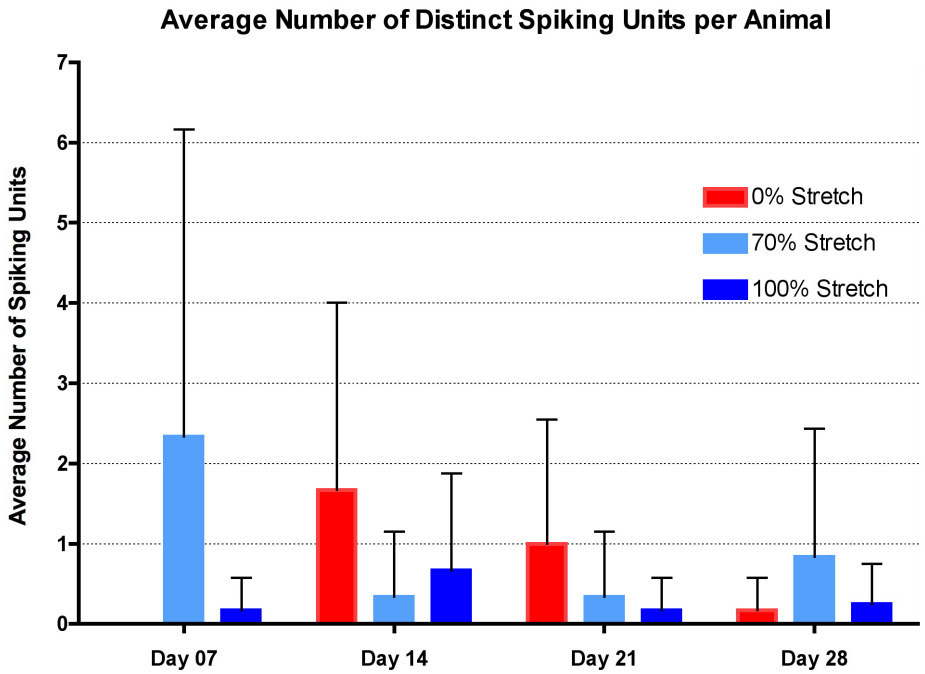

Figure 3.12 The average number of detectable, distinct spiking units per animal over time by experimental stretch group. Difference in mean values were not statistically different (two-way ANOVA; with respect to stretch, p = 0.387; with respect to time, p = 0.763).

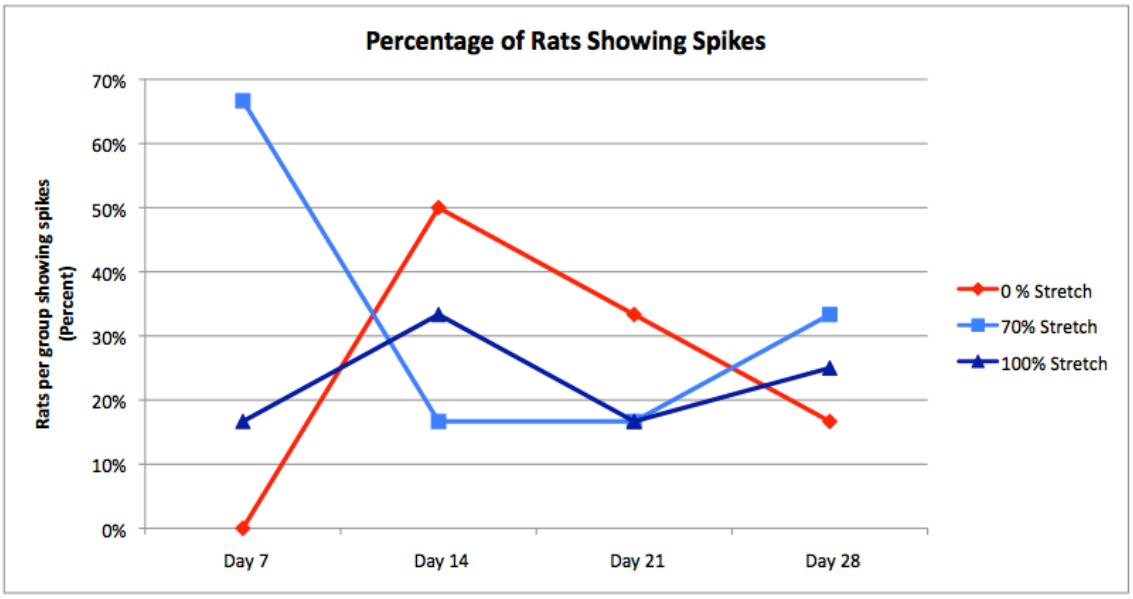

Figure 3.13 Percentage of animals displaying any single-unit spiking activity at a given time point. Limb stretch did not result in more rapid signal loss among the experimental stretch groups.

The electrophysiological results show no increase in the rate of signal loss among either of the stretching groups compared to the control group. While the trend lines appear to reject the hypothesis, the sample size is small and dependent upon an apparently random probability (see Table 2.4 and Section 2.4.2.3) of near 50% for an intact interface to successfully detect single-unit activity over a 30 day period. Statistically, there was no difference between the average number of spiking units (two-way analysis of variance) with respect to limb stretch ($p = 0.387$) or time ($p = 0.763$).

3.3.3 Axonal Regeneration

Among the 30 day cohort of animals, the number of axons and myelinated axons per histological slice were counted over 57 slices representing 13 animals. Among the 60 day cohort of animals, the number of axons and myelinated axons per histological slice were counted over 50 slices representing 13 animals. This data is presented graphically in Appendix A.

Contrary to what would be predicted by the hypothesis, the means of the counted numbers of axons and myelinated axons tended to increase as a result of limb stretch (Figures 3.14, 3.15). The relationships were not statistically significant as measured by nested one-way analysis of variance with averaged slice count per animal as the primary grouping and average count per slice as the nested grouping ($p = 0.391$, total axons, 30 days; $p = 0.440$, myelinated axons, 30 days; $p = 0.490$, total axons, 60 days; $p = 0.198$, myelinated axons, 60 days).

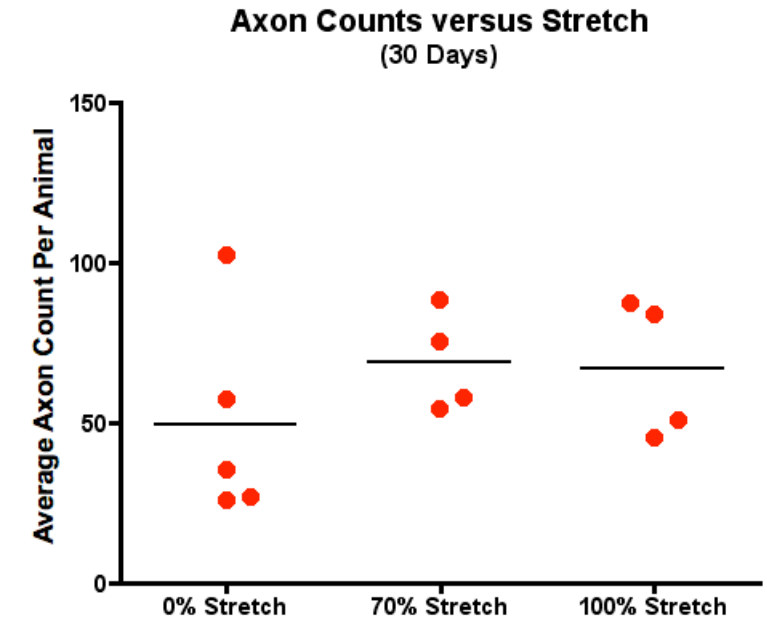

(A)

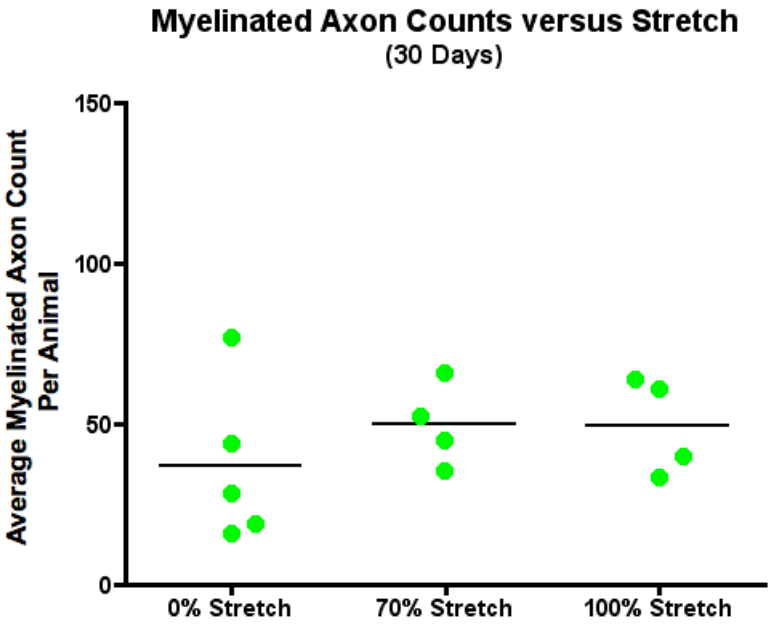

(B)

Figure 3.14 The averaged counts per animal of axons (A) and myelinated axons (B) at 30 days post-implantation compared across stretch groups. Differences in mean values are not statistically significant (nested one-way ANOVA; $p = 0.391$, total axons; $p = 0.440$, myelinated axons). Solid black lines represent group means.

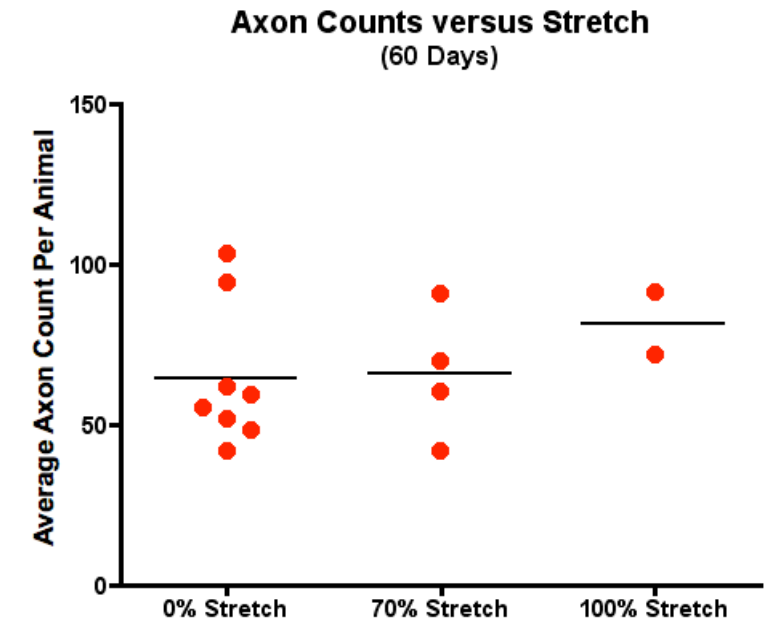

(A)

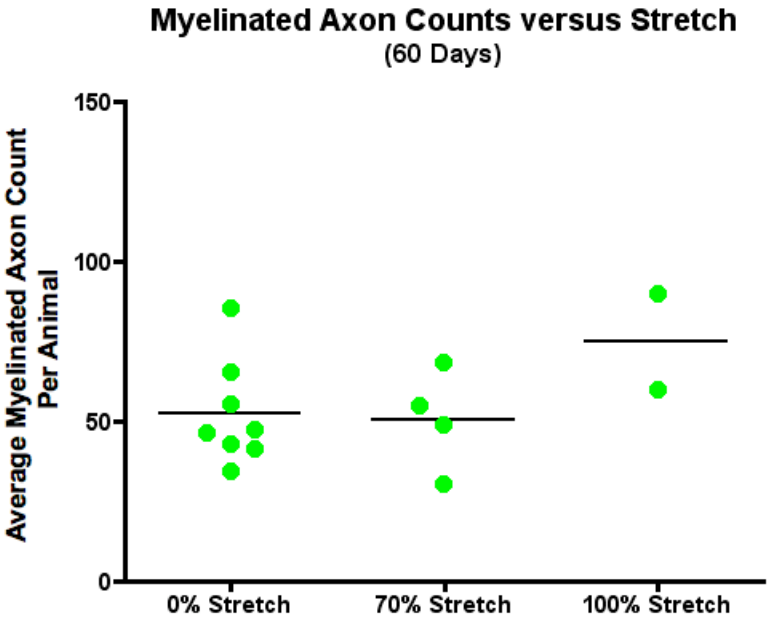

(B)

Figure 3.15 The averaged counts per animal of axons (A) and myelinated axons (B) at 60 days post-implantation compared across stretch groups. Differences in mean values are not statistically significant (nested one-way ANOVA; $p = 0.490$, total axons; $p = 0.198$, myelinated axons). Solid black lines represent group means.

3.3.4 Axon-Depleted Scar Areas

Among the 30 day cohort of animals which were not stretched, the size of the axon-depleted areas surrounding 230 electrode holes over 28 nerve slices representing 5 animals were calculated. Among the 30 day cohort of animals which were stretched at 70% of maximum limb extension, the size of the axon-depleted areas surrounding 160 electrode holes over 21 nerve slices representing 4 animals were calculated. Among the 30 day cohort of animals which were stretched at 100% of maximum limb extension, the size of the axon-depleted areas surrounding 229 electrode holes over 27 nerve slices representing 5 animals were calculated. Among the 60 day cohort of animals which were not stretched, the size of the axon-depleted areas surrounding 411 electrode holes over 49 nerve slices representing 9 animals were calculated. Among the 60 day cohort of animals which were stretched at 70% of maximum limb extension, the size of the axon-depleted areas surrounding 73 electrode holes over 15 nerve slices representing 3 animals were calculated. Among the 60 day cohort of animals which were stretched at 100% of maximum limb extension, the size of the axon-depleted areas surrounding 122 electrode holes over 12 nerve slices representing 2 animals were calculated. This data is presented graphically in Appendix B.

The average ADA per slice was calculated and plotted with respect to the individual animal over all experimental groups within both cohorts. The results are plotted in Figure 3.16 to demonstrate the variance within each animal average.

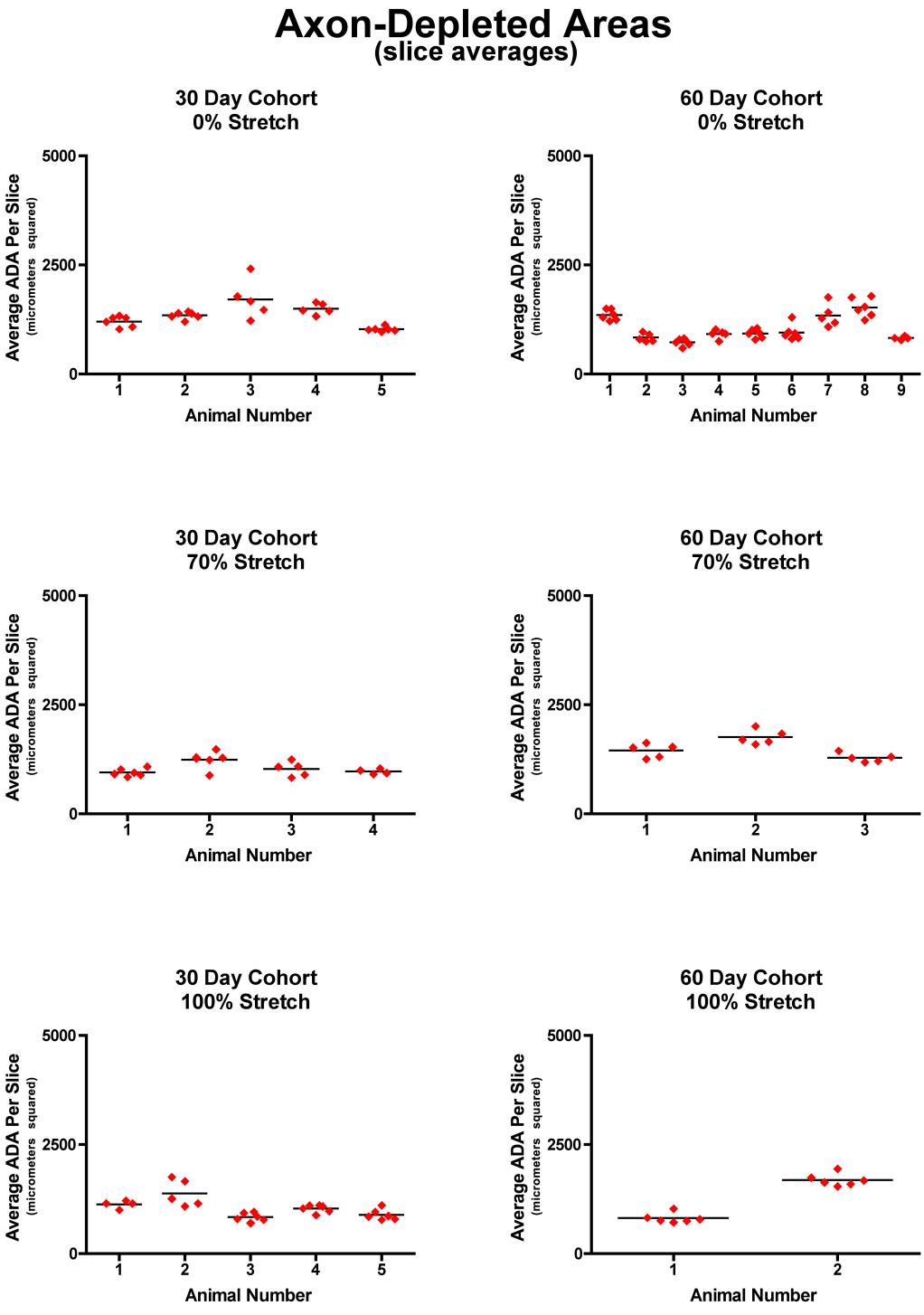

Figure 3.16 Average ADA per slice by animal across all experimental groups.

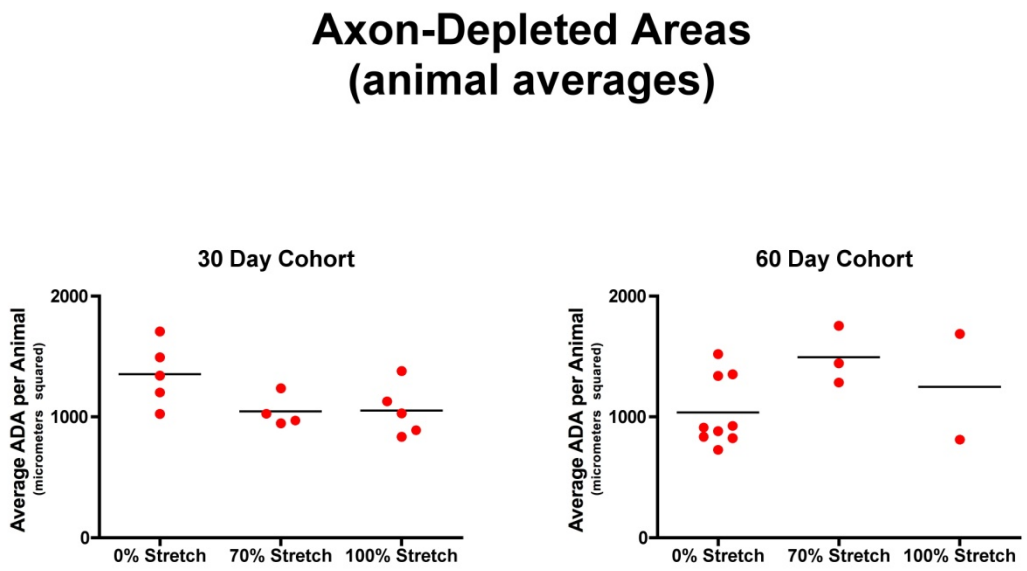

Figure 3.17 Average ADA size per animal over experimental stretch groups. No statistical differences among stretch groups (nested one-way ANOVA; p = 0.092, A; p = 0.185, B). Solid black lines represent group means.

Among the 30 day cohort animals, stretching did not result in an increase in the axon-depleted scar sizes surrounding each electrode. The mean scar size for both of the stretched groups was actually less than that of the unstretched group (Figure 3.17, A). The differences between group means were not statistically significant (nested one-way analysis of variance with average scar size per animal as the primary grouping and average scar size per slice as the nested grouping; p = 0.092).

Among the 60 day cohort of animals (Figure 3.17, B), differences in axon-depleted scar size between stretch groups were not statistically significant (nested one-way analysis of variance with average scar size per animal as the primary grouping and average scar size per slice as the nested grouping; p = 0.185).

3.4 Discussion

Whereas cortical implants are subject to the “fork in the jello” problem in which waves, vibrations and compressive/expansive movements of brain tissue can be conceptualized as resulting in compression and shear against an inflexible electrode, such a conceptualized model would be inappropriate for understanding the mechanical interaction of stiff electrodes imbedded within peripheral nerve tissue, which resembles a woven rope more so than a piece of jello. Internal nerve components, such as individual fascicles, are capable of sliding with respect to each other. Even the myelin sheath surrounding an individual axon is capable of sliding longitudinally with respect to that axon (see Abe *et al.* 2004).

A simplistic conceptualization of two possible scenarios of the mechanical interaction between stiff electrodes and nerve tissue components within a typical RPNI is illustrated in Figure 3.19. At one possible extreme, the connective tissue growth around the nerve guide tube (see Figure 3.18) helps form a monolithic structure in which the guide tube, proximal and distal nerve cables, electrode array, electrode shafts, and regenerated nerve components are effectively “locked in.” In this scenario, the internal motion or “wiggle” of elements with respect to each other is minimized and does not result in increased inflammation nor promote progressive signal loss. At the other possible extreme, limb movements cause internal components of the regenerated nerve cable to shift and slide with respect to each other, producing shear at the electrode shaft interface, increasing the inflammatory response, and increasing the size of the foreign-body scar surrounding each electrode shaft. Increased scar size would result in fewer nearby (detectable) axons, and increased inflammation could result in poorer health and viability of nearby axons and supportive Schwann cells. It is also conceivable that nerve stretch due to limb movement could inhibit or suppress axonal regeneration through the guide tube.

Of these two conceptualized cases, the former would be ideal for the successful adaptation of this technology to the clinic. If the second conceptualized case is more

representative of the true mechanical relationship within a RPNI, bioengineers will likely need to take steps in the design of future regenerative interfaces (such as possibly including longer guide tubes, incorporating internal stabilizing elements, using smaller guiding lumens or channels for individual fascicles and/or pseudo-fascicles, or developing entirely new architecture/interfacing concepts) to compensate for it. The results of the experiments presented in this chapter reject the hypothesis and support the conclusion that the first conceptualized case is a closer representative of the actual nerve-interface relationship than the latter case.

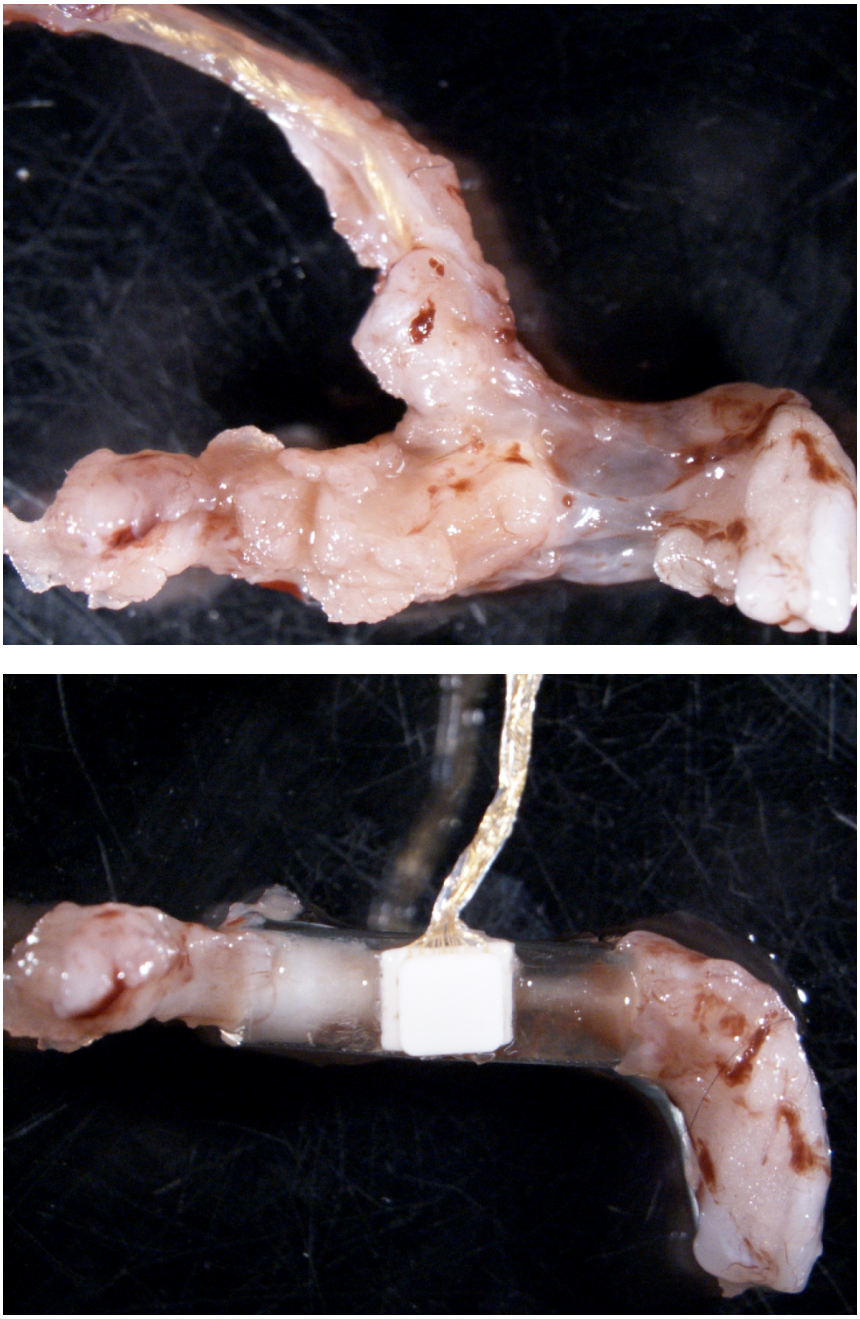

Figure 3.18 Explanted REMI two weeks post implantation. A thick layer of fatty and fibrotic connective tissue forms around the implanted device within weeks (top). Removal of the connective tissue with microscissors and forceps allows for visual inspection of the nerve guide tube with regenerated nerve cable, external parts of the electrode array, and electrode array ribbon cable (bottom). Orientation: REMI positioned horizontally; proximal nerve to the left; distal nerve to the right; electrode ribbon cable to the top. Photograph field is approximately 1 cm in width.

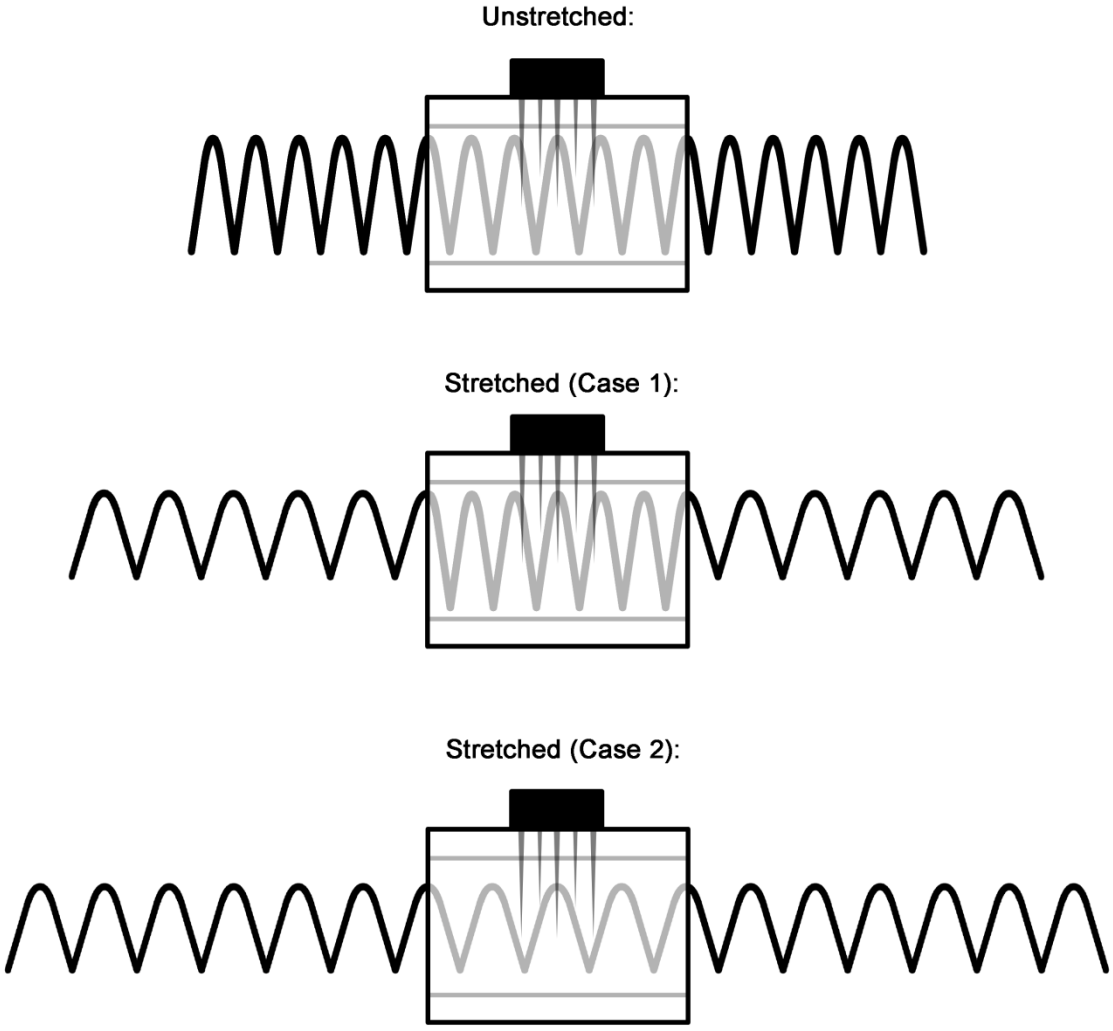

Figure 3.19 Conceptualization of an elastic nerve cable (represented as a coiled spring) within a nerve guide tube with embedded electrodes. (Top) Unstretched. (Middle) Stretched assuming stationary confinement of elements within guide tube. (Bottom) Stretched assuming free mobility of elements within guide tube.

The limb stretch model used here was shown to produce a near 35% strain in the sciatic nerve at full (100%) limb extension and a near 18% strain at moderate (70%) limb extension (Table 3.1). Both of these strains (18% and 35%) are greater than the reported strain necessary to produce temporary conduction block in a nerve. The 35% strain is slightly less than the reported ranges at which such a nerve might be expected to receive structure damage (see Section 3.1.4.7). These results support the use of this model as sufficient for testing the effects of nerve stretch near the limits of naturally occurring strains due to normal (both moderate and exaggerated) limb movement. Transient limb movement should not be expected to produce nerve strains capable of damaging nerves and nerve components. It should be noted that a potential improvement to our experimental setup would be the inclusion of a force transducer within the linear actuator applying the stretching force to the hind limb. Such a setup would allow for measurement of the force applied to the limb during stretch and could allow for greater consistency of applied limb stretch force across stretching sessions.

If natural limb motion, as simulated in this experiment, were to produce detrimental levels of nerve strain and shearing effects of nerve components with respect to the electrode shafts inside the nerve guide tube of the interface, we would expect to observe either a decrease in the number of regenerating axons or an increase in the axon-depleted scar size surrounding each electrode shaft. As illustrated in Figures 3.20 and 3.21, we observed neither of these at either 30 days or 60 days post-implantation. Overall, the trends, while statistically insignificant, actually imply improved axonal regeneration due to stretching.

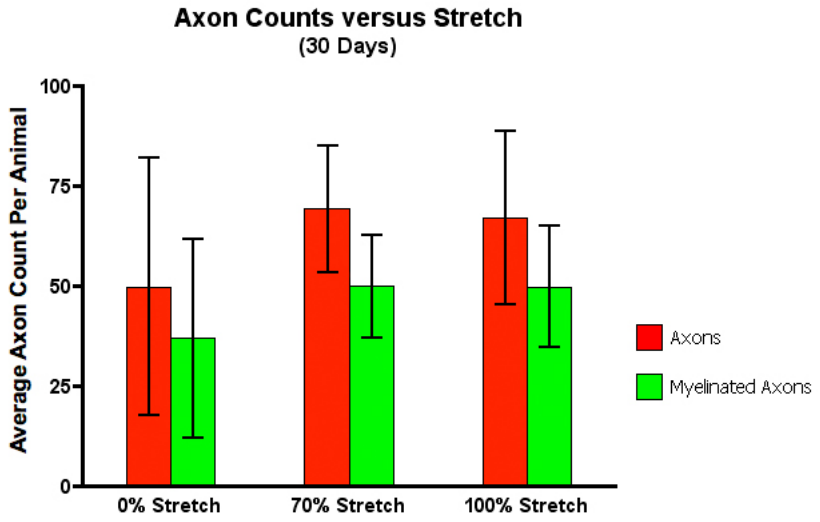

(A)

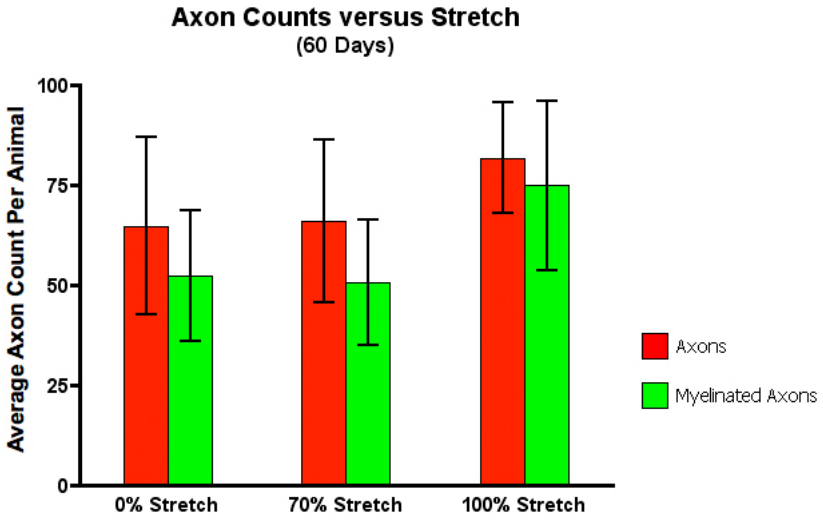

(B)

Figure 3.20 Count averages of regenerated axons across experimental stretch groups at 30 days (A) and 60 days (B). Error bars represent one standard deviation.Alternative presentation of Figures 3.14 and 3.15.

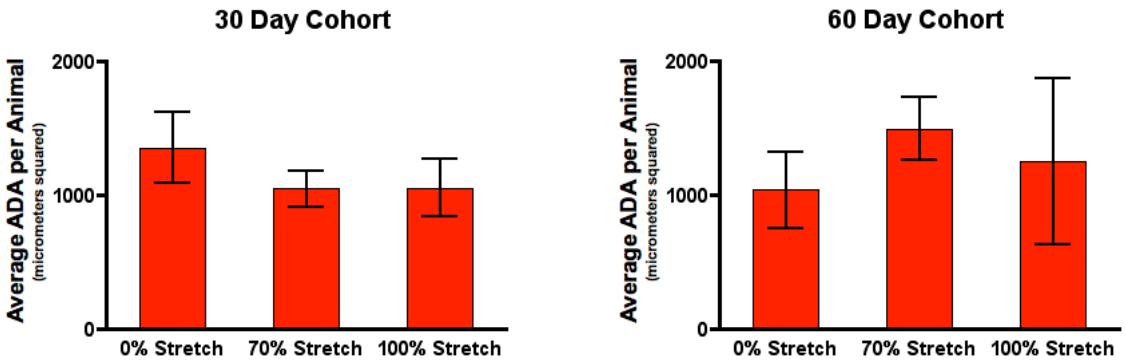

Figure 3.21 Average axon-depleted scar sizes surrounding electrodes across experimental stretch groups at 30 days (left) and 60 days (right). Error bars represent one standard deviation. Alternative presentation of Figure 3.17.

The electrophysiological data, while not as conclusive as the histological data, also rejects the hypothesis. Acquisition of signals was no less likely among stretched animals than among unstretched animals as measured up to 28 days post-implantation.

The limitations of these findings should be noted. These results should be taken in the context of a regenerating nerve of approximately 1 mm in diameter with 2-4 fascicles in a rodent model. A human median nerve is approximately 5 mm in diameter with three to greater than thirty fascicles depending upon location; the architecture of any device used for human clinical treatment would likely be of different size and dimensions. Recently proposed RPNI architectures, such as rolled architectures, multiluminal architectures, microchannel-based architectures, and biodegradable-component architectures may result in superior or inferior stability of nerve components. Also, the nerve cable within the nerve guide tube is still undergoing regeneration, myelination, axonal growth, and cellular remodeling during the first 60 days. A fully regenerated, more stable nerve might exhibit different mechanical properties and respond in a different way to stretch.

Taken as a whole, these results support the likelihood that peripheral nerve interfaces based upon regenerative guide tubes are robust with respect to nerve stretch due to limb movement. While micromotion of electrodes within cortical tissue is of concern in the development of cortical interfaces, negative effects of nerve stretch upon continued signal acquisition are likely not of concern in a typical regenerative PNI.

CHAPTER 4

MICROCHANNEL INDUCED AMPLIFICATION OF UNMYELINATED AXONS

4.1 Overview

4.1.1 Limitation of Current Regenerative Peripheral Nerve Interfacing

No device architecture proposed to date has demonstrated sufficient sensitivity and selectivity of recordings necessary to control a prosthetic device with many degrees of freedom. Microchannel encapsulation has been proposed as a means to amplify recorded signals, increasing sensitivity, and possibly thus decreasing signal loss over time. This phenomenon has been predicted for both myelinated and unmyelinated axons. *In vitro* and *in vivo* evidence exists in support of the predictions for myelinated axons.

4.1.2 Hypothesis

We hypothesize that encapsulation of an unmyelinated axon within a microfluidic channel of dimensions on the order of a few micrometers will effectively amplify the extracellular recordings as observed by an electrode within the microchannel.

4.1.3 Specific Aim

The Specific Aim of this chapter is to validate the capacity for microfluidic channels to amplify extracellular recordings of unmyelinated axons. An *in vitro* experiment has been conducted and is presented here in which primary murine neurons are cultured upon a planar microelectrode array. A polymer scaffold guides extending axons into non-porous microchannels under which surface electrodes record extracellular potentials.

4.1.4 Background and Justification

Mathematical and physical modeling of phenomena predicted to pose a benefit to human health or an advancement to technology are typically followed up, if possible, by experimental evidence validating or rejecting the model. From the 1920s to the 1970s, whole nerve electrophysiology was typically performed using hook electrodes upon a semi-exposed nerve suspended within air or an insulating liquid medium to provide electrical isolation from the surrounding tissue of an anesthetized animal. Richard B. Stein and colleagues predicted that encapsulation of a whole nerve within a plastic "cuff" of sufficient length, with metal electrodes suspended within the cuff lumen, would provide sufficient electrical isolation of the compound action currents of the nerve to allow for whole nerve recordings of awake animals (Stein and Pearson, 1971; Stein *et al.,* 1975). Their predictions were subsequently verified (de Luca and Gilmore, 1976; Stein *et al*., 1977). The cuff electrode is currently a common and useful tool in laboratory research and has found limited clinical application.

Recently, researchers associated with James Fawcett at Cambridge University have predicted that encapsulation of a myelinated or unmyelinated axon within a nonporous channel of micrometer dimensions would limit ion diffusion away from the axon or a node of Ranvier, effectively increasing the electrical resistance of the extracellular space and amplifying the extracellular potential upon membrane depolarization. This results in an amplified action potential signal as viewed by a recording electrode within the channel (Fitzgerald *et al*., 2008). Amplification increases with increased channel length and decreased cross sectional area.

This predictive model has been validated for myelinated axons using *in vitro* experiments (Fitzgerald *et al*., 2009). Since all motor axons, all proprioceptive axons, and most non-nociceptive sensory axons in the mammalian model are myelinated, it is appropriate for researchers interested in current strategies for peripheral nerve interfacing to focus primarily on interfacing with signals from myelinated axons.

While cortical arrays of 100 electrodes have been demonstrated capable of recording over 100 distinct signals from relatively large neuronal cell bodies, with many signals lasting for

several years (Hochberg *et al.,* 2006; Simeral *et al*., 2011), peripheral nerve interfaces attempt to record from relatively small axons and have not been demonstrated capable of recording a large number of signals or recording chronically for over a year (signals are typically lost within two to three months). It is hoped that incorporation of microchannels into a device to amplify signals from myelinated axons could greatly improve the capacity of RPNIs to detect a large number of independent signals over time.

There are many potential benefits, however, to interfacing with unmyelinated axons. Unmyelinated axons tend to have superior regenerative capacity through small pores than do larger, myelinated axons (Castro *et al*., 2008). Future generations of peripheral nerve interfaces may be able to take advantage of tissue engineering and molecular mechanisms to produce stable demylination of otherwise myelinated fibers. Unmyelinated axons are not dependent upon node of Ranvier positioning for either recording or stimulation. This chapter aims to provide conclusive evidence of the capacity for microchannel amplification of unmyelinated axons.

4.2 Materials and Methods

4.2.1 Microfluidic Molds on Planar MEAs

Microchannel scaffolds were fabricated by pouring liquid polymer atop a microfabricated mold and allowing it to cure. Imprints from the mold provide two open wells connected by microchannels. The mold of patterned SU8 epoxy (MicroChem, Newton, MA, USA) was fabricated by spinning a layer of SU8-5 polymer on a 100 mm silicon wafer and exposed using UV light. Unexposed polymer was removed using a developer. The resultant strips measured 4.6 μm tall and 80 μm wide with an inter-strip spacing of 120 μm (Figure 4.1).

The PDMS scaffolds were cut into 2 cm square pieces, UV sterilized, and O_2 plasma-treated to achieve non-permanent binding to the planar multielectrode arrays prior to placing the PDMS scaffold atop the 64-electrode multielectrode array (Figure 4.2). The MEAs (Center for Network Neuroscience, Denton, TX, USA) were designed with two sets of thirty-two 25 μm square electrodes spaced 200 μm apart over an area of 1 mm^2. PDMS scaffolds with two specific microchannel lengths (0.5 mm and 2.0 mm) were tested.

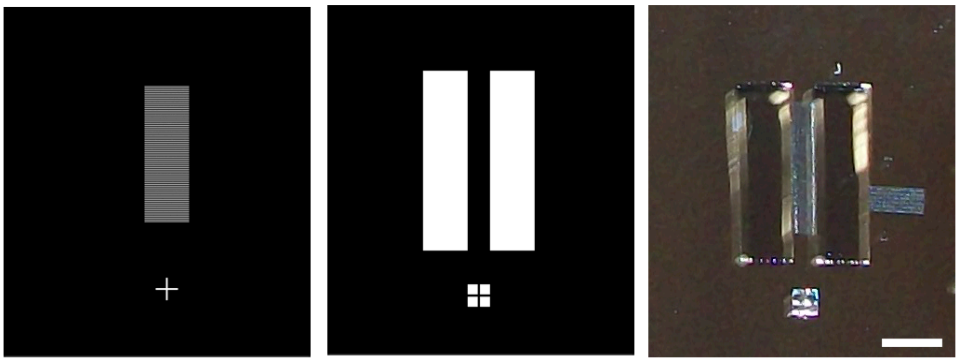

(A) (B) (C)

Figure 4.1 The UT Arlington microchannel scaffold design. (A,B) Mask layers used to produce a two-layer aligned microfabrication scheme. Layers correspond to microchannels and wells. (C) Fabricated mold; SU-8 atop silicon wafer. Scale bar = 4 mm.

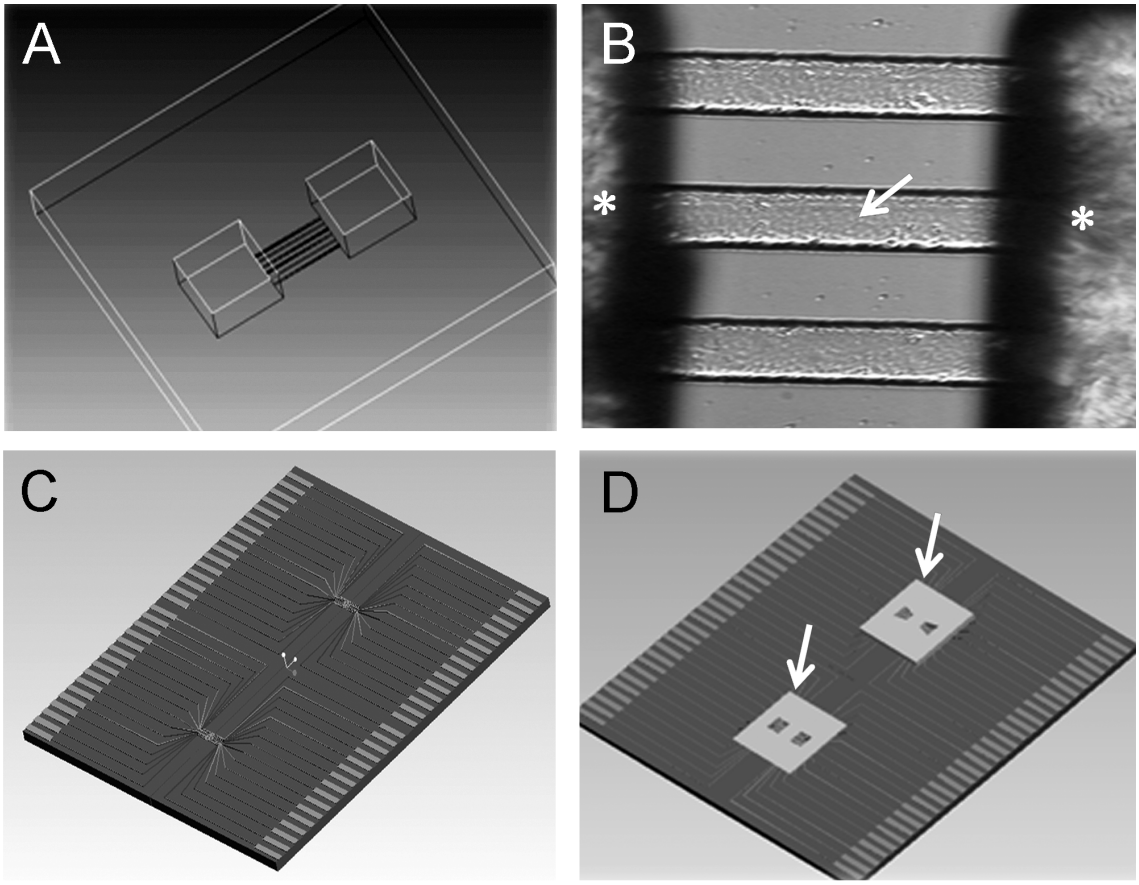

Figure 4.2 PDMS-based compartmentalized culture system atop 64-channel MEA. (A) Schematic of two-chambered PDMS scaffold with microfabricated microchannels. (B) Micrograph of PDMS scaffold showing chambers (stars) and microchannels (arrow). (C,D) Diagram of MEA with dual 32-channel electrode arrays with and without PDMS scaffolds (arrows indicate PDMS scaffolds).

4.2.2 Neuron Cell Culture

Neurons were cultured atop MEAs within microchannel constructs (Figure 4.3). A silicon rubber gasket attached to the MEA provided a container for culture media (Gross *et al*., 1982). The device was autoclave sterilized, coated with poly-D-lysine (25 mg/mL) overnight followed by laminin (0.02 mg/mL), and seeded with murine embryonic day 18 cortical or spinal cord neurons. Timed-pregnant mice were euthanized, embryos removed by c-section, and

spinal cords were surgically removed and pooled in D1SGH hibernation media as described in Ransom *et al*. (1977). Spinal cords were digested in papain for 15 minutes at 37˚C and manually triturated to dissociate cells. Spinal cord cells were seeded at 80,000 cells per 6 mm diameter chamber.

Cells were cultured in Minimum Essential Medium supplemented with 10% fetal bovine serum, 10% horse serum, 1% l-glutamine, 1% B-27 supplement, 0.2% ascorbic acid, and 1% penicillin-streptomycin. After 72 hours, the media was replaced with media lacking fetal bovine serum. Thereafter, media was half-changed every three days and used for recordings over 1 – 3 months. During this time, neurons grew processes through microchannels into the distal culture chamber.

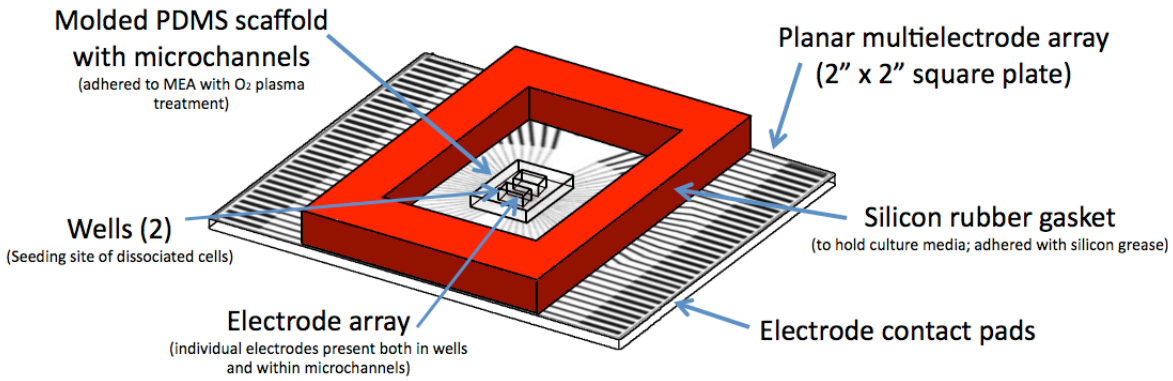

Figure 4.3 Cell culture within PDMS scaffold atop MEA allows recording of signals from within open wells and within microchannels. Cells are seeded into two wells within a molded PDMS scaffold atop a 64-channel planar MEA. Microfabricated channels within the PDMS scaffold are aligned atop substrate embedded electrodes. Recording hardware attaches to electrode contact pads and allows electrophysiological signals from cells and neurites within the wells and the channels to be recorded.

Traditional compartmentalization techniques involving Campenot chambers were incompatible with this study due to the need to scratch grooves into the substrate surface, a process that would damage the embedded electrodes (Campenot, 1997; MacInnis and

Campenot, 2002; Campenot *et al*., 2009). Molded PDMS was chosen as a scaffolding material because it is optically transparent (allowing for visual microscopic inspection of cells within microchannels). Similar techniques have been presented several times in the literature over the last seven years, however the design presented here is the first compartmentalized culture design that allows for simultaneous monitoring of electrophysiological signals from components both within microchannels and outside of microchannels (Rhee *et al*., 2005; Taylor *et al*., 2005; Ravula *et al*., 2006; Ravula *et al*., 2007; Dworak and Wheeler, 2009).

4.2.3 Electrophysiology

Recordings of neuronal activity from cultures were obtained at 37˚C and 5% CO_2 in an incubated microscope chamber. The osmolarity of the culture media was measured at 380 mOsm. Signals from the MEAs were detected and amplified using a 64-channel MEA recorder system (Plexon Inc., Dallas, TX). Action potential waveforms were identified using MEA Sort Client (Plexon Inc). For this analysis, only the first 200 recorded waveshapes of each selected channel were used. Active channels deemed to be indistinguishable from noise were omitted; quantitatively, this resulted in the omission of all channels with average peak-to-peak spike amplitudes less than 100 μV. Comparison between groups was performed using Kruskal-Wallis one-way analysis of variance followed by Dunn's multiple comparison test using Prism 4.0 software (Graphpad, Inc, San Diego, CA, USA). Values are presented as the mean and the standard deviation of the mean. p-Values ≤ 0.05 were considered significant.

4.2.4 Experimental Setup

PDMS microchannel scaffolds were aligned over planar multielectrodes (Figure 4.4, C) and adhered to the substrate. Cultured neurons formed spontaneously active networks within open wells (Figure 4.4, B) and grew neurites into the microchannels (Figure 4.4, A). Electrophysiological signals were recorded from electrodes within the wells and within the microchannels.

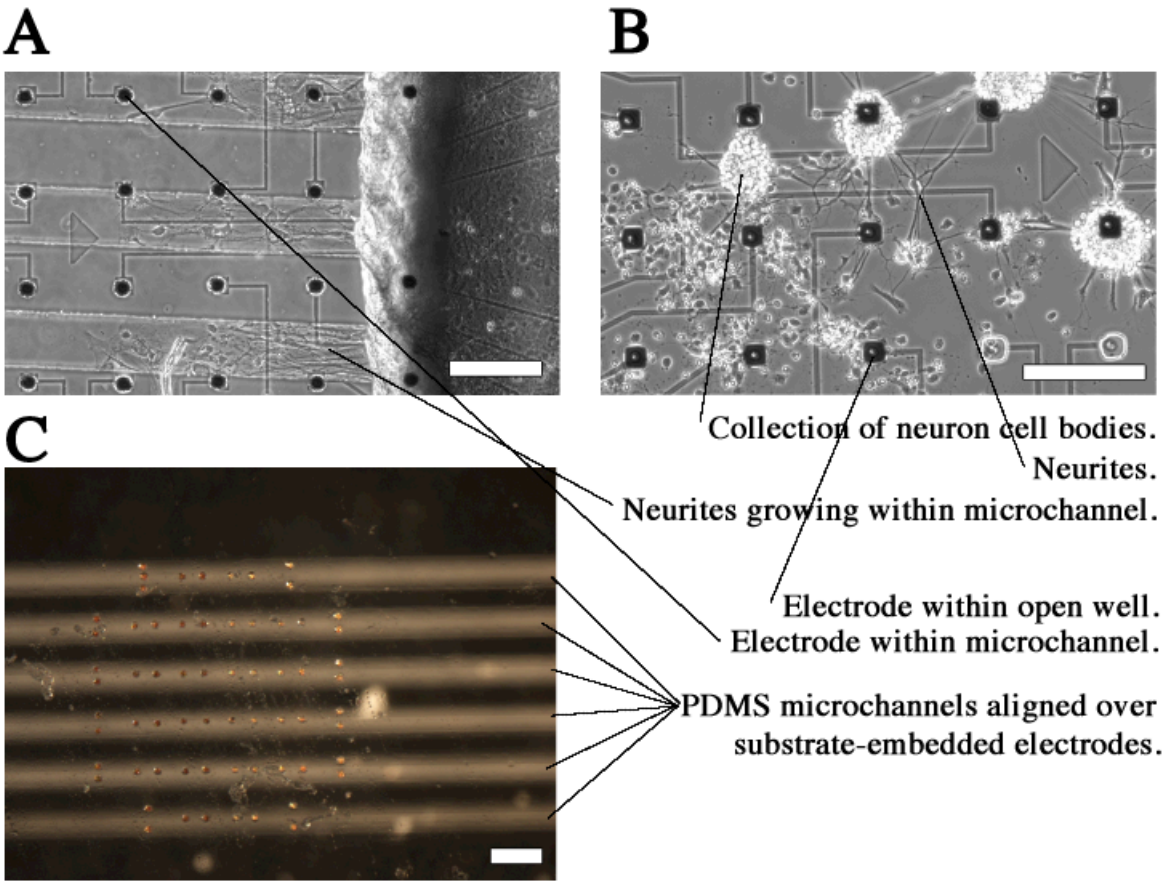

Figure 4.4 Cell culture design capable of recording from neurons within wells and within microchannels. (A) Neurites extending from well (right) into microchannels atop substrate-embedded electrodes (UT Arlington microchannel design). (B) Neuron cell bodies forming a neural network within a well. (C) PDMS microchannels aligned atop electrode array (Sandia microchannel design). Scale bars = 400 μm.

4.3 Results

A total of 152 distinct spiking units were recorded over nine cultures. Recorded action potential spike amplitudes were observed to be 3.4 times higher from electrodes within microchannels than electrodes in open wells or on open MEAs (qualitative example in Figure 4.5). The amplitudes within the four groups were compared across groups using a Kruskal-Wallis ANOVA followed by Dunn's multiple comparison test. p-Values ≤ 0.05 were considered significant.

The mean amplitudes of spikes recorded from within 2.0 mm long microchannels and 0.5 mm long microchannels measured 504 ± 220 μV and 636 ± 352 μV, respectively. The mean amplitudes of spikes recorded from open MEAs and from uncovered electrodes within scaffolded MEAs measured 165 ± 46 μV and 154 ± 16 μV, respectively. Overall, the mean amplitude of spikes recorded within microchannels measured 3.4 times higher than those measured outside of microchannels (Kruskal-Wallis analysis of variance followed by Dunn's test, $p<0.001$) (Figure 4.6).

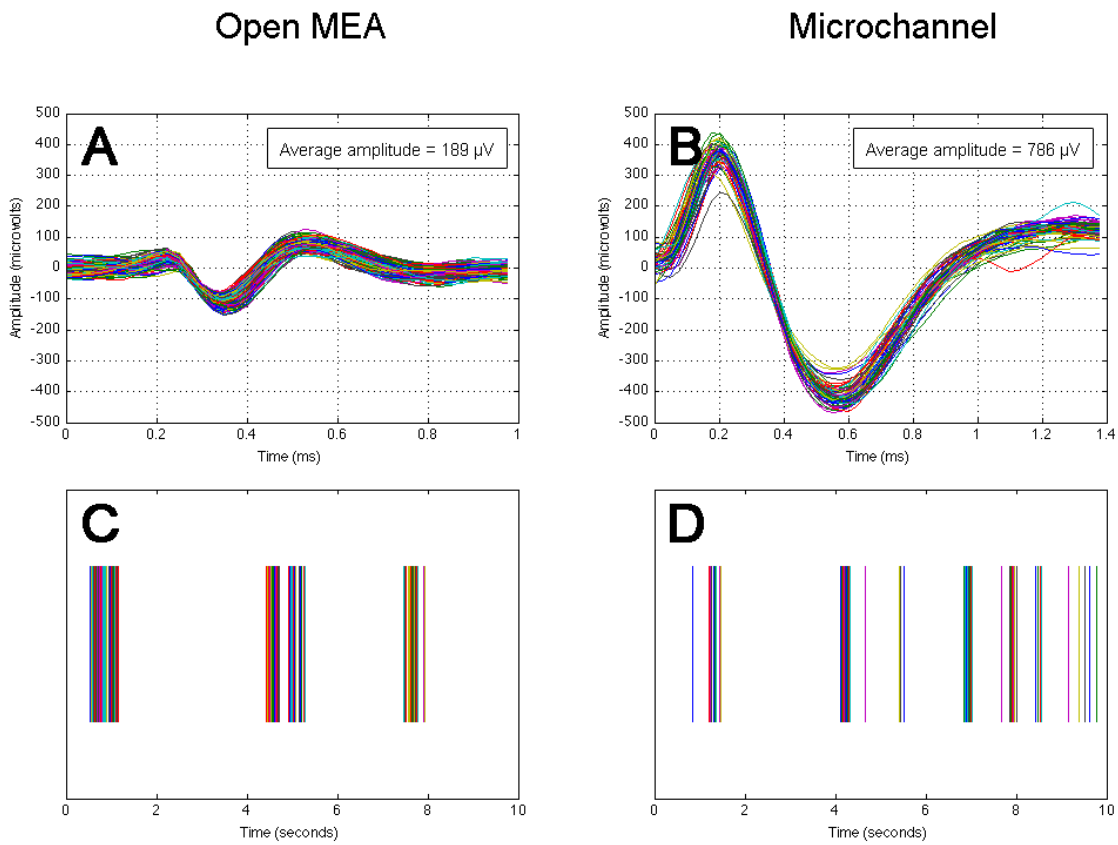

Figure 4.5 Strong statistical significance in support of signal amplification within microchannels. Recorded spike amplitudes measured 3.4 times higher within microchannels than in wells. Representative electrophysiological activity recorded from an open electrode (A,C) and from an electrode within a microchannel (B,D). (A) and (C) represent the superimposed waveshapes and spike raster plots, respectively, of 349 spikes recorded over 10 seconds with an average peak-to-peak amplitude of 189 µV. (B) and (D) represent the superimposed waveshapes and spike raster plots, respectively, of 65 spikes recorded over 10 seconds with an average amplitude of 786 µV. Individual spikes are labeled in different colors.

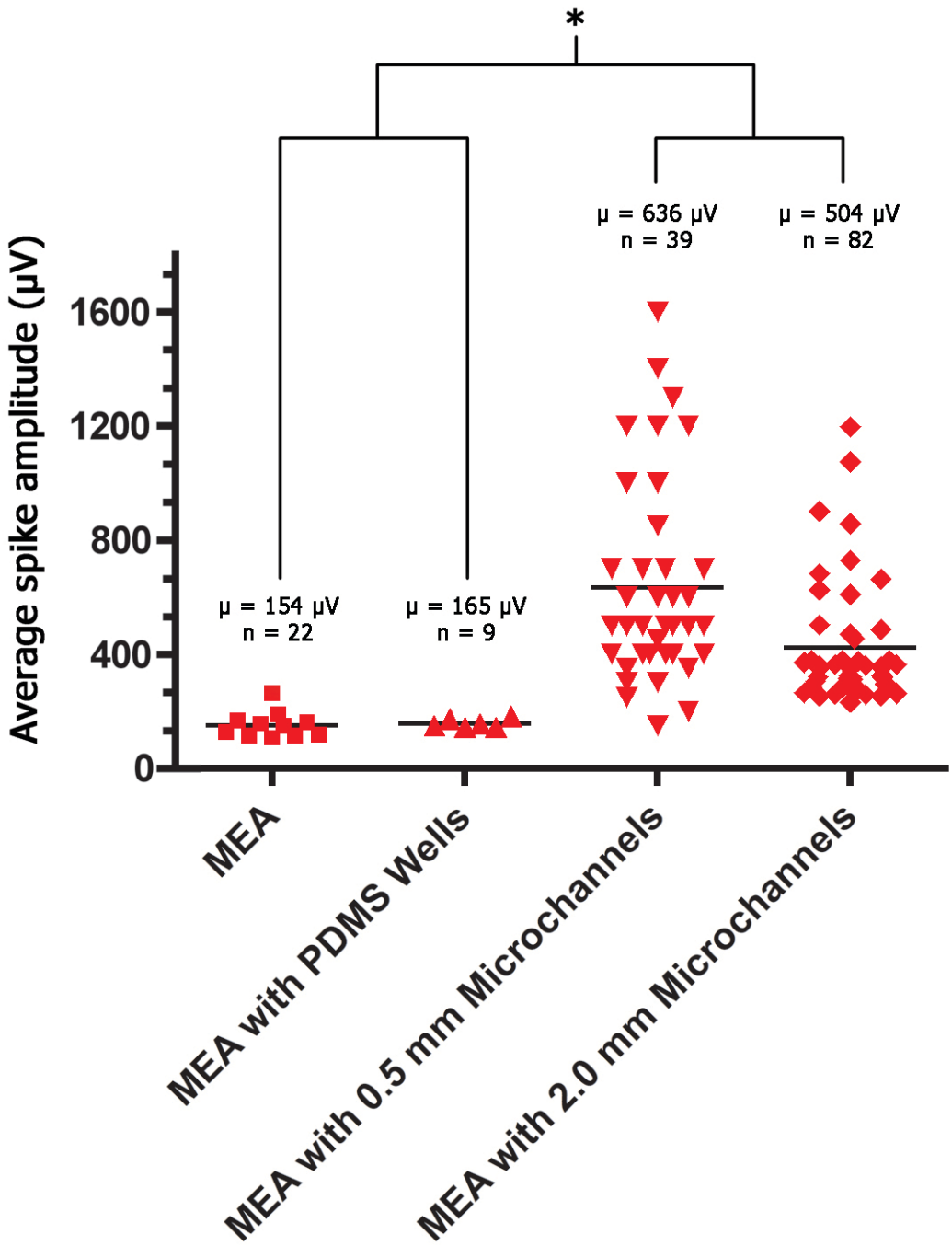

Figure 4.6 Action potential amplitudes recorded from within microchannels averaged 3.4 times higher than amplitudes recorded from within PDMS scaffold chambers or from open MEAs ($p \leq 0.001$, Kruskal-Wallis followed by Dunn's test). The mean action potential amplitudes recorded from open MEAs (n = 22) and open wells on MEAs containing PDMS scaffolds (n = 9) did not statistically differ. The mean action potential amplitudes recorded within 0.5 mm long microchannels (n = 39) and within 2.0 mm long microchannels (n = 82) did not statistically differ. Solid black lines represent group means.

4.4 Discussion

In 2008, Fitzgerald *et al.* predicted an amplification of extracellular action potentials of myelinated and unmyelinated axons growing through non-porous microchannels due to limited ion diffusion following depolarization. The model predicts recorded action potentials of 1000 μV for a 2 μm diameter unmyelinated axon growing within a 1 cm long microchannel of 400 μm^2 cross-sectional area. In our study, we recorded action potentials of 504 ± 200 μV and 636 ± 352 μV from axons growing through 400 μm^2 microchannels with channel lengths of 0.5 mm and 2.0 mm, respectively. The recorded action potential amplitudes averaged 3.4 times higher than those recorded from neurons and other axons within open wells or atop open MEAs. This effect is highly significant and confirms the phenomenon of microchannel-induced amplification of signals from unmyelinated axons in microchannels as short as 0.5 mm in length. These results are consistent with the mathematical model proposed by Fitzgerald *et al*. Recently, a report by Wieringa *et al.* (2010a) also confirmed the amplification of extracellular action potentials recorded from axons within microchannels *in vitro*, but it is difficult to compare their results to our own as they did not report on the statistically significance of their data.

No RPNI device architecture proposed to date has been demonstrated to be capable of long term recordings with the sensitivity and selectivity necessary to provide multiple degrees of freedom for control of a robotic prosthesis. Recently, several groups have proposed RPNI architectures that attempt to take advantage of microchannel amplification (Lacour *et al.,* 2009; Fitzgerald *et al*., 2012). *In vivo* experiments using surgically teased nerve strands from rat dorsal root ganglia into “micro-cuff” electrodes with channel cross-sectional areas of 700 μm^2 have produced action potential recordings of approximately 100 μV (Minev *et al*., 2012). Furthermore, these electrodes have been used to record successfully to distinguish two types of afferent nerve activity related to bladder filling and contraction (Delivopoulos *et al*., 2012). While these reports support the feasibility of action potential detection through microchannel electrodes, it remains unknown whether microchannel amplification, which has been observed

in vitro, including in the present work, would be translated into increased sensitivity of action potential detection from an RPNI *in vivo*.

CHAPTER 5

GENERAL DISCUSSION

5.1 Signal Drift

The concept of signal drift, defined here as the tendency of a given single-unit spike detected by a recording electrode to appear, disappear, or change shape over time, is critical to the functioning of a nervous-system interface that operates based upon the firing rates of individual spikes. This phenomenon has been well characterized and is routinely discussed in publications regarding cortical interfaces but is rarely mentioned and poorly characterized for regenerative peripheral nerve interfaces.

With regards to cortically implanted arrays of recording needle electrodes, Schmidt *et al.* (1976) show minimal change in the shape of a given action potential over the course of 100 days; Williams *et al.* (1999) show a high degree of signal stability in single-unit waveshapes in an array of 32 electrodes between 105 and 226 days; Liu *et al.* (1999) show a strong degree of signal stability with moderate fluctuations in action potential shape among three distinct units recorded on a single electrode over the course of three months; Suner *et al.* (2005) characterize the change in action potentials waveshapes of four distinct units from days 1-5 to day 83; Liu *et al.* (2006) show a back-and-forth fluctuation in the amplitude of a distinct unit over the range of approximately 400 μV to 500 μV over 80 days to 140 days post-implantation; Dickey *et al*. (2009) characterize the near daily fluctuations in action potential waveshape of a single spiking unit over the course of 15 days; members of the Shenoy laboratory have characterized the fluctuations in recorded action potential waveshapes and amplitudes over the timespans of hours, days, and months (Gilja *et al*., 2010; Gilja *et al*., 2011; Chestek *et al*., 2011) (Figure 5.1). It can be seen that, over the course of weeks and months, it is not uncommon for given spiking

units to disappear or for new units to occasionally appear. It is not uncommon for individual spiking units to maintain their presence for many months with moderate fluctuations in waveshape and peak-to-peak amplitude occurring over hours to days.

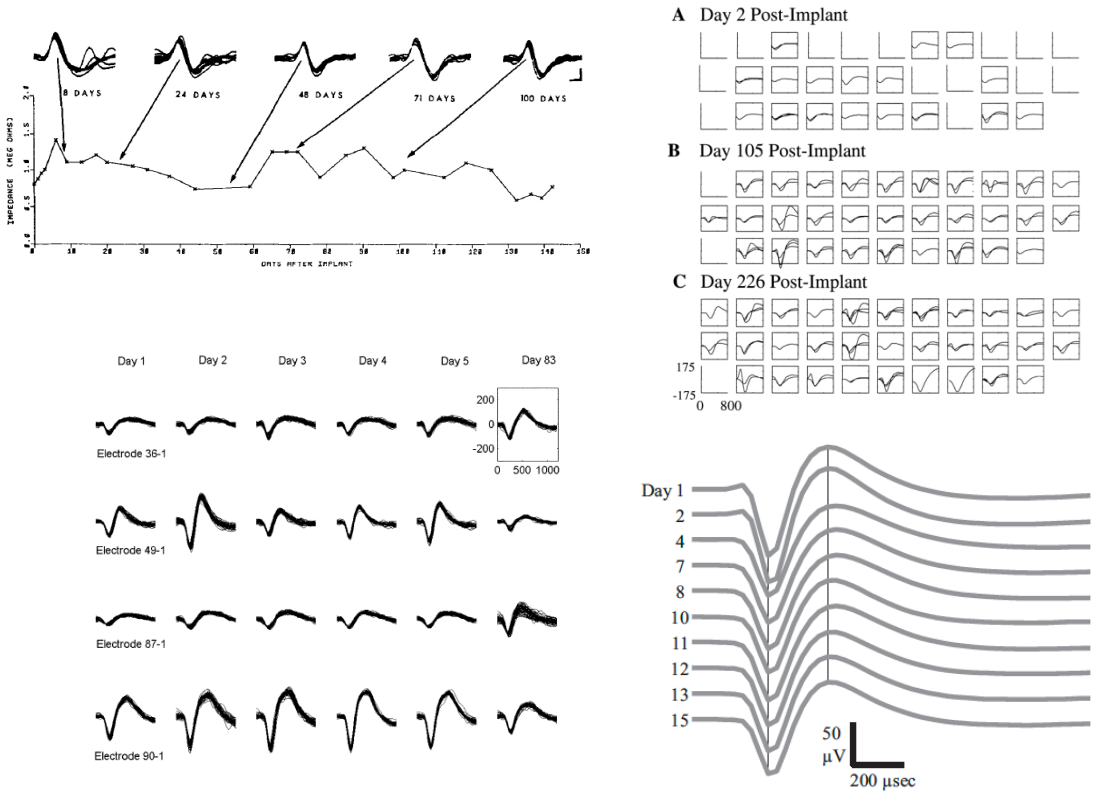

Figure 5.1 Examples of spiking unit continuity and waveshape fluctuations over time in cortically implanted electrode arrays. Adapted from Schmidt *et al*., 1976 (top left), Williams *et al*., 1999 (top right), Dickey *et al*., 2009 (bottom left), and Suner *et al.,* 2005 (bottom right).

For penetrative electrode arrays inserted into intact peripheral nerves in a cat model, Branner and Normann (2000) show slight fluctuations in a given single unit waveshape over the course of 5 to 36 hours post-implantation and report the gradual loss of nearly all observable waveshapes within either 30 hours or 60 hours post-implantation (n = 2 cats). Improved electrode-nerve isolation and immobilization techniques (see Branner *et al.,* 2004) have recently allowed for penetrative array recordings of units for up to four months (terminal point of the

experiment) (Clark *et al.* 2011); details regarding signal drift and stability from this experiment are expected in upcoming publications. The ability to mechanically secure the nerve with respect to inserted needle electrodes appears to have a very strong bearing on the capacity to maintain signals over days to months. Whether those signals can maintain individual unit continuity and waveshape stability over months to years has yet to be seen.

Since the first implanted RPNI in 1974, there have been sixteen publications reporting single-unit activity recorded from a RPNI (see Section 1.3.6, Section 2.1.3, Table 2.1). Among these sixteen, eight can be classified as acute, meaning that the recordings were all obtained during a single, terminal recording session. The other 8 can be classified as chronic, meaning that the recordings were obtained periodically over the course of several weeks or months. While the term "chronic" is routinely used to describe this recording methodology, the term "periodic" may be more appropriate given that the recordings are generally taken weeks to months apart. While in Chapters 1 and 2, the results of Lewitus *et al.* (2011) were considered "acute" due to the fact that no implanted hardware allowed for non-surgical access to recording contacts, in this chapter, these results will be reclassified as "chronic" given that recordings were attempted at both 4 weeks post-implantation and again at 8 weeks post-implantation. Of these eight publications that are here classified as chronic, seven only attempted recordings at periodic intervals of one week or greater. No attempt was made to characterize the continuity of distinct, individual spiking units from one recording session to the next. In one of these eight publications, Shimatani *et al*. (2003) used a silicon-based sieve interface with 9 via holes (4 of which possessed recording electrodes) implanted into the chorda tympani nerve (part of the VIIth cranial nerve) and routed to a percutaneous pedestal mounted to the skull in a rat model. Their goal was not to characterize the interface but was to investigate turnover within taste buds. They report that evoked (through chemical stimulation of the tongue) potentials typically remained stable for between one to two weeks. Few details were given on the continuity or stability of spontaneous single units except that their number and signal-to-noise ratios "varied

from recording to recording" (Shimatani *et al.*, 2003). They present recordings of one evoked single-unit that remained relatively stable for the course of 21 days (from days 77 to 97 post-implantation) (Figure 5.2). The authors' discussion implies this unit to be atypical, but this example shows that a high degree of signal stability within a single interfaced sensory axon from a cranial nerve is possible for up to three weeks within a silicon-based sieve electrode architecture.

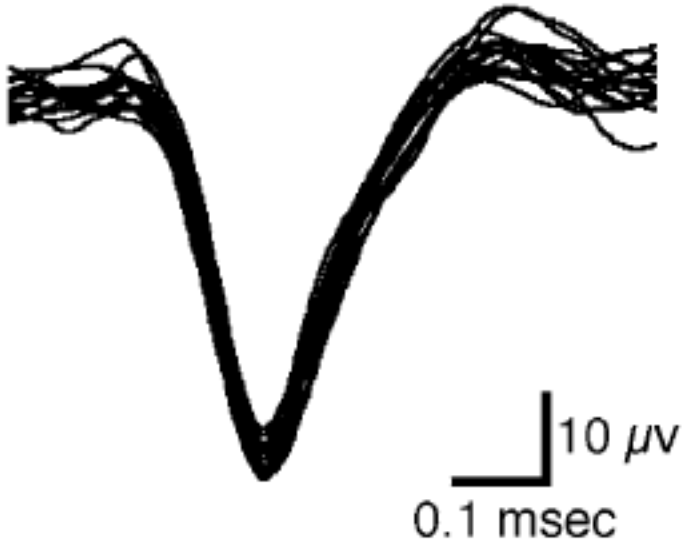

Figure 5.2 Example of signal stability within an individual spiking unit from a sieve electrode over 21 days. Image represents a composition of 21 waveshapes, each representing an averaged waveshape taken from multiple spikes on a given day. Adapted from Shimatani *et al.*, 2003.

One of the most touted presumed benefits of peripheral nerve interfaces over cortical interfaces is the greatly diminished need for signal processing to decode limb movement intentions. Cortical interfaces, as currently designed for use in human and non-human primates, typically rely on real-time recordings from ensembles of directionally tuned neurons (typically several dozen individual spiking units per ensemble) to provide goal-oriented movement to control 2-4 dimensions of movement of either a robotic device or a computer

cursor (see Simeral *et al*., 2011). This requires computer hardware capable of recording and sorting spikes from nearly 100 continuous channels and processing the firing rates of those spikes into intended goals or movements in real time. This author recently heard a prominent researcher in the cortical interfaces field state that for our current real-time processing needs, our signal processing equipment can be currently be shrunk to the size of a laptop; it will need to be shrunk to the size of an iPhone before it can be considered portable or implantable. In contrast, the processing required for decoding intended movements from signals acquired from a peripheral nerve interface is presumed to be much simpler in that the firing rates of individual, interfaced motor neurons directly correlate to intended contractions of distal muscles. This is of course complicated by the need to identify individual motor unit fibers as well as their distal muscular targets, but, once identified, assuming a high degree of signal stability, decoding from a PNI should require much less processing power and, possibly, many fewer acquired spiking units to provide a large number of mentally controllable degrees of freedom. This will likely be a prominent area of investigation as soon as biomedical scientists are able to design a device capable of interfacing with a large number of distinct (motor) spiking units that maintain signal stability over time.

This signal stability over time is likely to vary, possibly greatly, between different proposed device architectures such as sieve architectures, rolled architectures, multi-luminal biodegradable architectures, microchannel-based architectures, and upcoming as-yet-unconsidered device architectures. The potential clinical success of any proposed architecture will be dependent both upon the longevity of signal acquisition and upon the stability of acquired signals over time. Previous publications have tended to focus almost solely on proof-of-concept and have not (with the partial exception of Shimatani *et al.,* 2003) attempted to characterize the modalities of acquired single units or characterize the stability or drift of those units over time. The capacity of any proposed device architecture to maintain a stable signal over time should be included in any proof-of-concept. We demonstrate here a characterization of signal stability

within a REMI PNI over the course of 23 hours at 21 days post-implantation into a rat sciatic nerve model.

Over the course of 23 hours, a total of six distinct, individual spiking units were observed on three of 16 implanted electrodes (Figure 5.3). These will be described in order from least stable to most stable. A relatively large spiking unit of approximately 200 μV appeared briefly on electrode #12 (Channel 012c) near hour 9 of the experiment (Figure 5.4). It fired infrequently and was not observed since. A single spiking unit of approximately 150 μV appeared briefly on electrode #05 (Channel 05b) near hour 18 of the experiment (Figure 5.5). It was not observed since. A single spiking unit appeared on electrode #05 (Channel 05a) near hour 11 and was observed intermittently throughout the course of the experiment (Figure 5.6). It maintained a fairly constant waveshape (when present) with the exception of recordings near hour 18 when the unit amplitude temporarily jumps from near 100 μV to near 160 μV. Incidentally, this coincided temporally with the presence of the observed unit of Channel 05b on the same electrode. A single spiking unit appeared on electrode #01 (Channel 01) near hour 6 (Figure 5.7). With two brief absences at hours 8 and 10, this signal was present until the end of the experiment and steadily grew in amplitude from near 90 μV to near 160 μV. Two distinct spiking units were present on electrode #12 (Channels 12a and 12b) at the beginning of the experiment. The unit of Channel 12a disappeared briefly at hours 4 and 8 but maintained a fairly uniform waveshape, ranging in amplitude from near 145 μV to near 175 μV over the 23 hours (Figure 5.8). The unit of Channel 12b was present consistently over the course of the experiment with an amplitude ranging from near 75 μV to near 105 μV over the 23 hours (Figure 5.9).

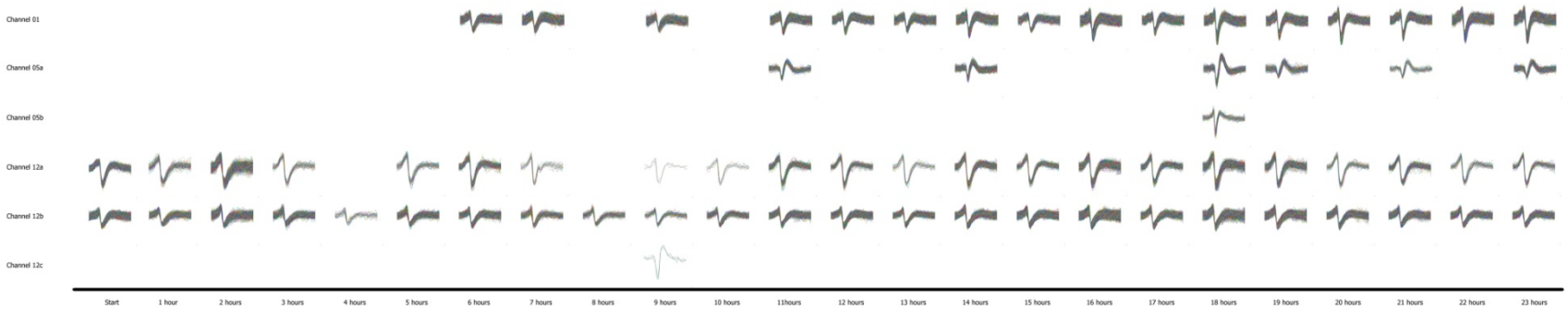

Figure 5.3 Six distinct spiking units were observed in one animal over the course of 23 hours at 21 days post-implantation. Images represent superimposed waveshapes recorded over a five minute interval at the beginning of each hour. Scales are given in Figures 5.4 through 5.9.

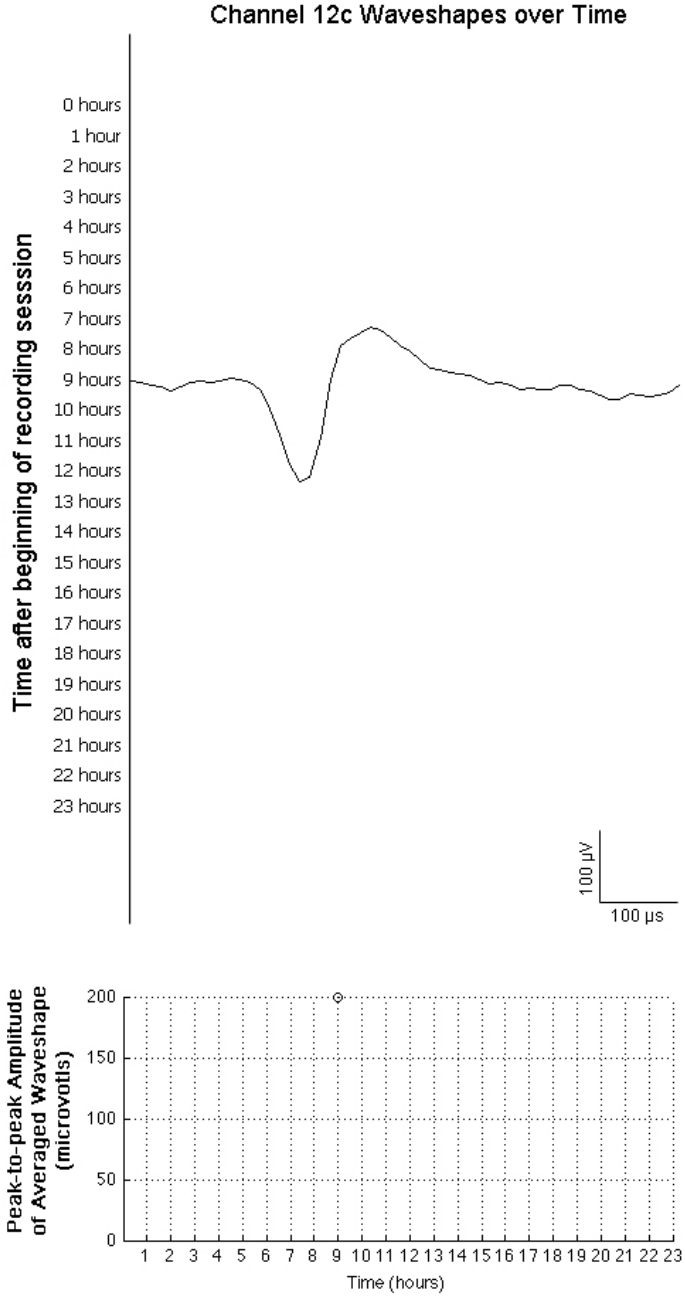

Figure 5.4 Averaged waveshape (of all spikes over a 5 minute interval) at each hour on Channel 12c (top). Amplitude of averaged waveshape at each hour (bottom).

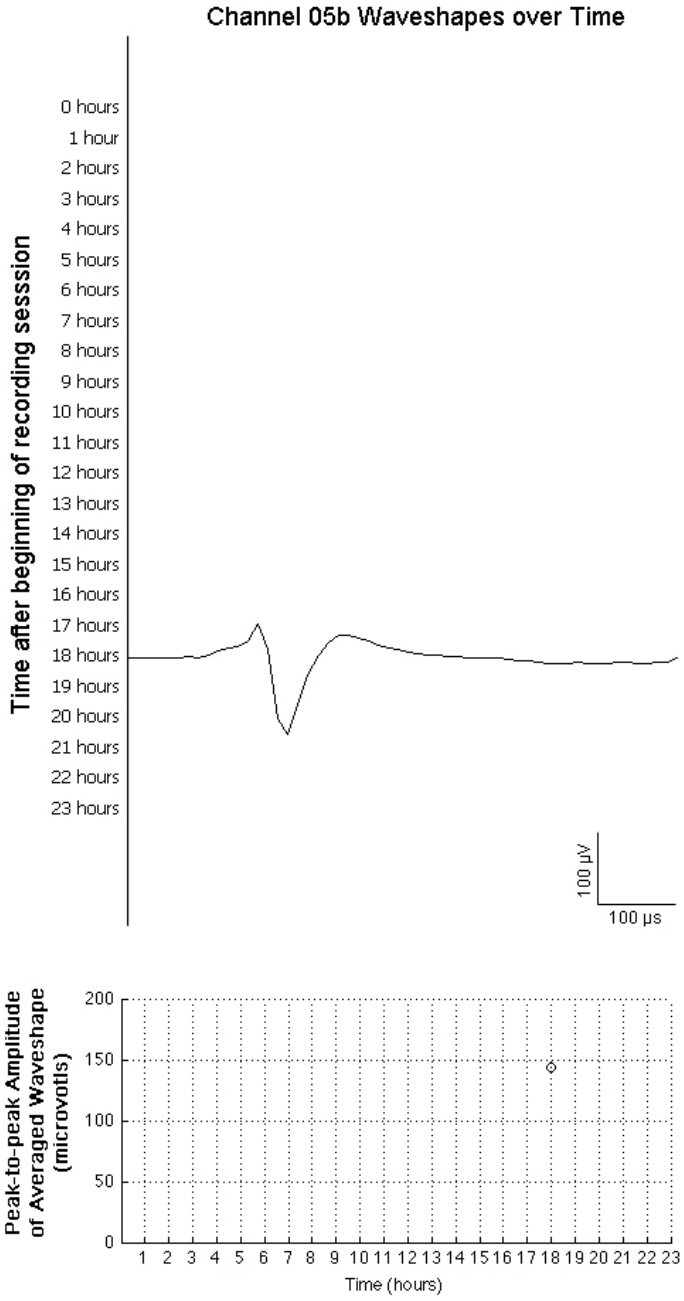

Figure 5.5 Averaged waveshape (of all spikes over a 5 minute interval) at each hour on Channel 05b (top). Amplitude of averaged waveshape at each hour (bottom).

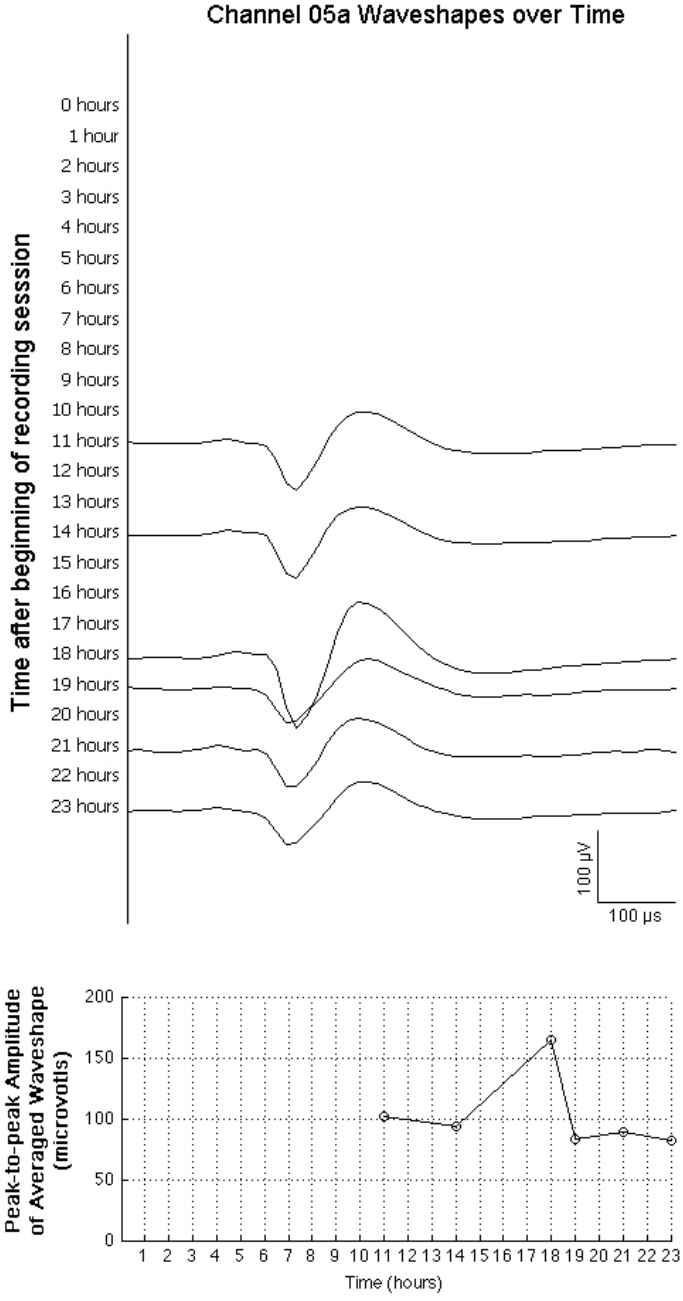

Figure 5.6 Averaged waveshape (of all spikes over a 5 minute interval) at each hour on Channel 05a (top). Amplitude of averaged waveshape at each hour (bottom).

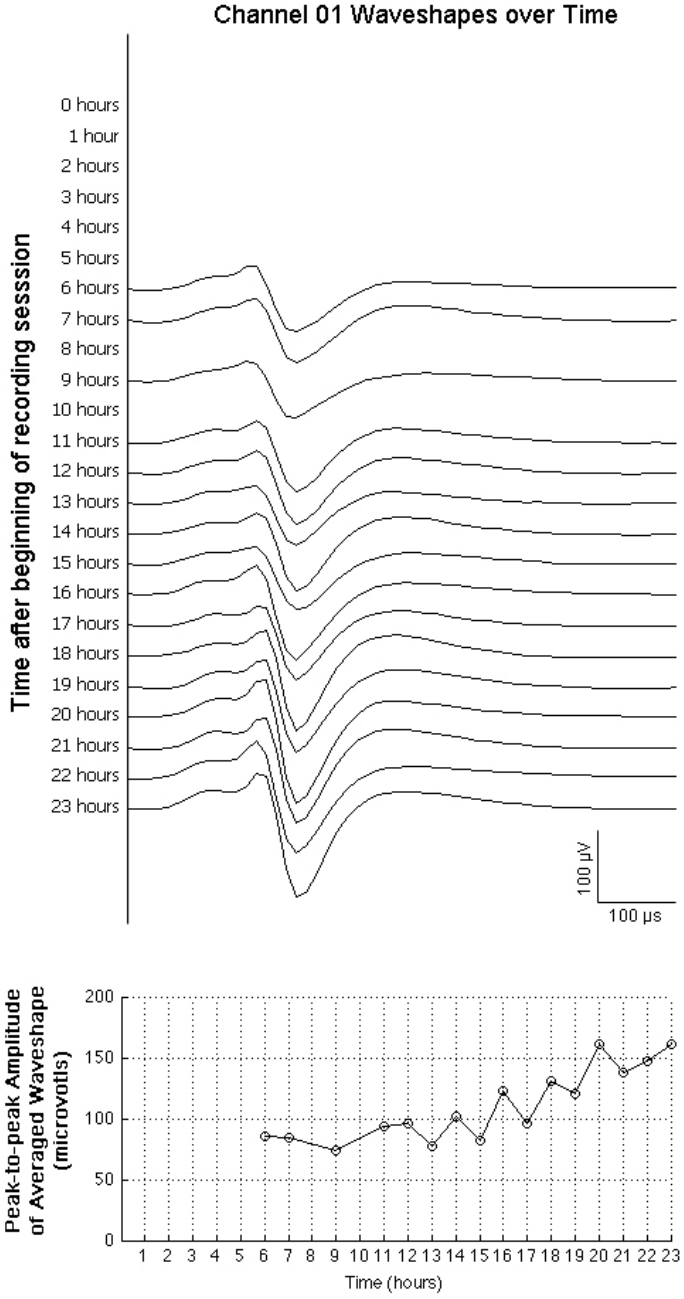

Figure 5.7 Averaged waveshape (of all spikes over a 5 minute interval) at each hour on Channel 01 (top). Amplitude of averaged waveshape at each hour (bottom).

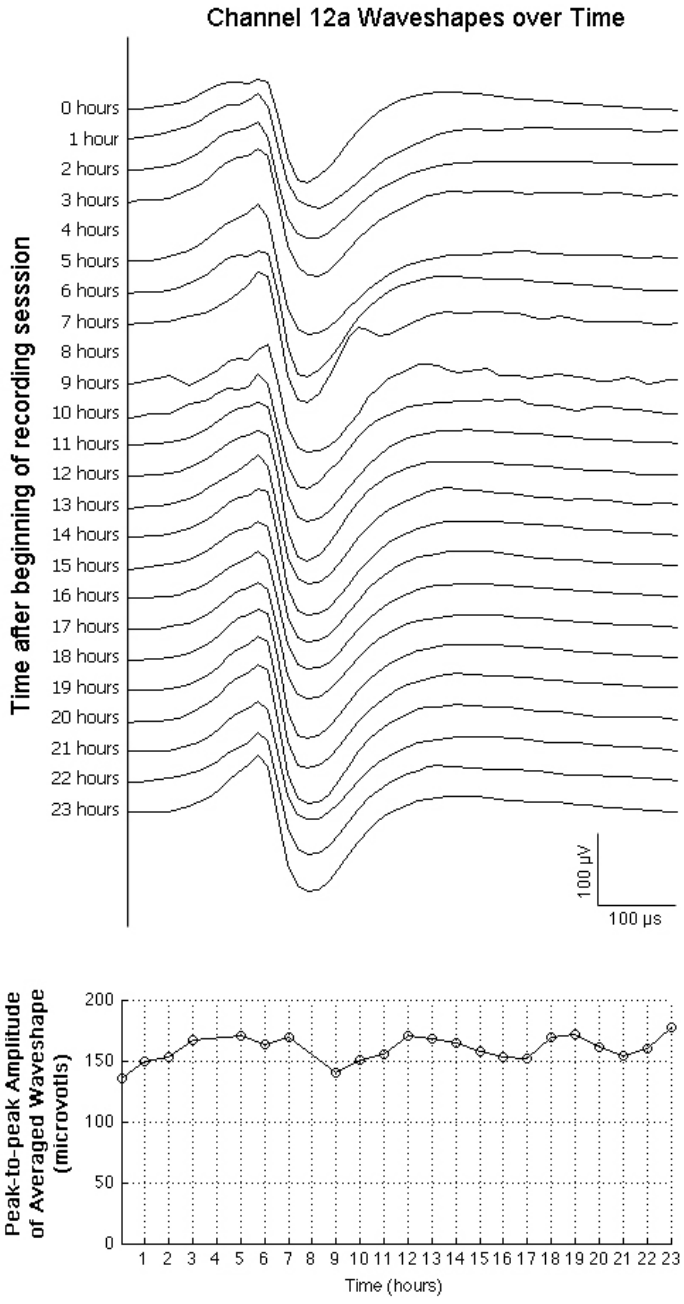

Figure 5.8 Averaged waveshape (of all spikes over a 5 minute interval) at each hour on Channel 12a (top). Amplitude of averaged waveshape at each hour (bottom).

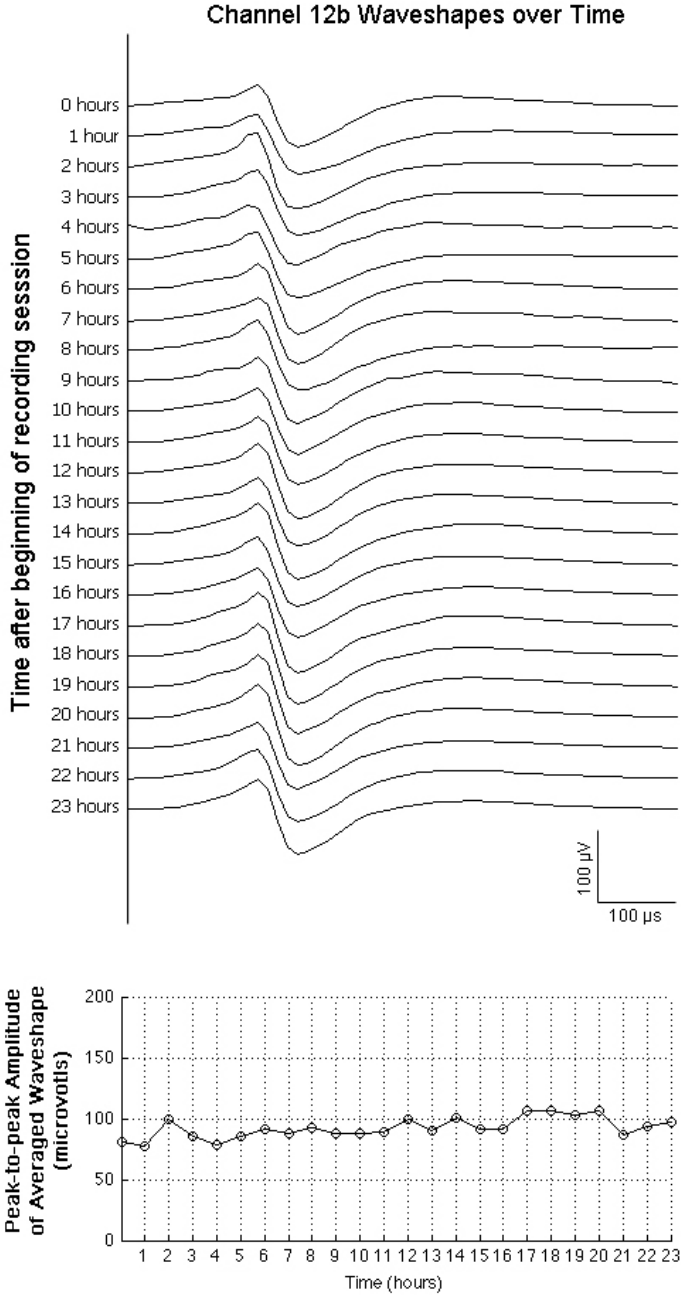

Figure 5.9 Averaged waveshape (of all spikes over a 5 minute interval) at each hour on Channel 12b (top). Amplitude of averaged waveshape at each hour (bottom).

Among these six identified spiking units, two appeared briefly and did not return (Channels 12c and 05b). One appeared during the course of the experiment and was present intermittently through to the end (Channel 05a). It maintained a fairly uniform waveshape with the exception of a brief period during which a second unit was present on the same electrode. One spiking unit appeared during the experiment and progressively grew in amplitude over the course of 17 hours (Channel 01). Two units were present throughout the 23 hours (one displayed two intermittent absences) with a relatively high degree of waveshape stability. Among the four waveshapes that were present over multiple hours, three of these possessed a nearly tonic firing rate that did not appear to alter based upon animal movement or behavior but did fluctuate from hour to hour (Channels 01, 12a, 12b). It may be possible that these represent tonically firing sensory afferents. One spiking unit possessed a bursting pattern that correlated directly with attempts by the animal to stand on its hind legs (Channel 05a) implying that this channel represents a motor neuron.

It should be noted that these recordings represent signals from axons that are likely regenerating and have not yet found distal targets. Regenerating axons through a nerve guidance tube are still undergoing morphological changes such as growth and myelination at 21 days. It is likely that these early morphological changes result in increased signal instability that may not be present at a later time point in a more matured nerve cable.

The REMI architecture was designed specifically to allow a more robust regeneration of axons through the nerve guidance tube than other architectures, such as sieve and multiluminal architectures which may obstruct axonal regeneration and constrict regenerating axons. There may be a trade-off regarding the use of internal structures which may limit regeneration capacity but may also more effectively “entrap” axonal components within a proximity of a recording electrode thus increasing signal stability over time.

5.2 Characterization of the REMI

5.2.1 Development of the REMI

As of 2006, the only highly selective methods proposed for interfacing with peripheral nerves that had been tested within animal models were the regenerative sieve electrode (see Section 1.3.6) and the penetrative electrode array (see Section 1.3.5). It was becoming known that the sieve electrode architecture tended to suffer from differential regeneration potential based upon fiber size, to the detriment of large, myelinated motor fibers, as well as progressive restrictive axonopathy within the first several months (see Lago et al., 2007; Castro et al., 2008). Penetrative electrode arrays, while capable of recording a relatively large number of distinct signals immediately upon implantation, tended to lose all recorded signals within a matter of days to weeks, presumably due to lack of sufficient mechanical stability and integrity with respect to the nerve (Branner and Normann, 2000; Branner et al., 2004). The regenerative multielectrode array (REMI; see Section 2.2.1) was proposed with the intention of alleviating the deficits of these two designs. By incorporating an array of needle electrodes within a hollow (collagen filled) guide tube, axons would be allowed a relatively unimpeded regeneration path compared to a sieve electrode, and regenerated axons would be capable of growth without constrictive consequences. Compared to the electrode shafts of a penetrative electrode array, the electrode shafts within a REMI would be mechanically stabilized with respect to the host nerve as fibrotic tissue growth would encapsulate and stabilize the nerve, nerve guide tube, and electrode array (Figure 3.6).

The REMI was first introduced in 2008 in a preliminary study using 8 animals to verify its capacity to record single units from regenerated axons (Garde et al.). To further investigate the potential of the REMI to serve as an interface, investigators from DARPA and our own laboratory were interested in more fully characterizing the REMI. We were interested in answering several questions: How reliable is the REMI over time? What are the most

prominent causes of physical device failure inherent within the REMI? How do these causes of failure compare to reports from other device architectures?

5.2.2 Causes of Device Failure Inherent in the REMI

Using a large cohort animal study (n = 60 rats), we observed the prominent causes of device failure inherent within the REMI over time. The results are presented in Figure 5.10. For additional details, see Table 2.8.

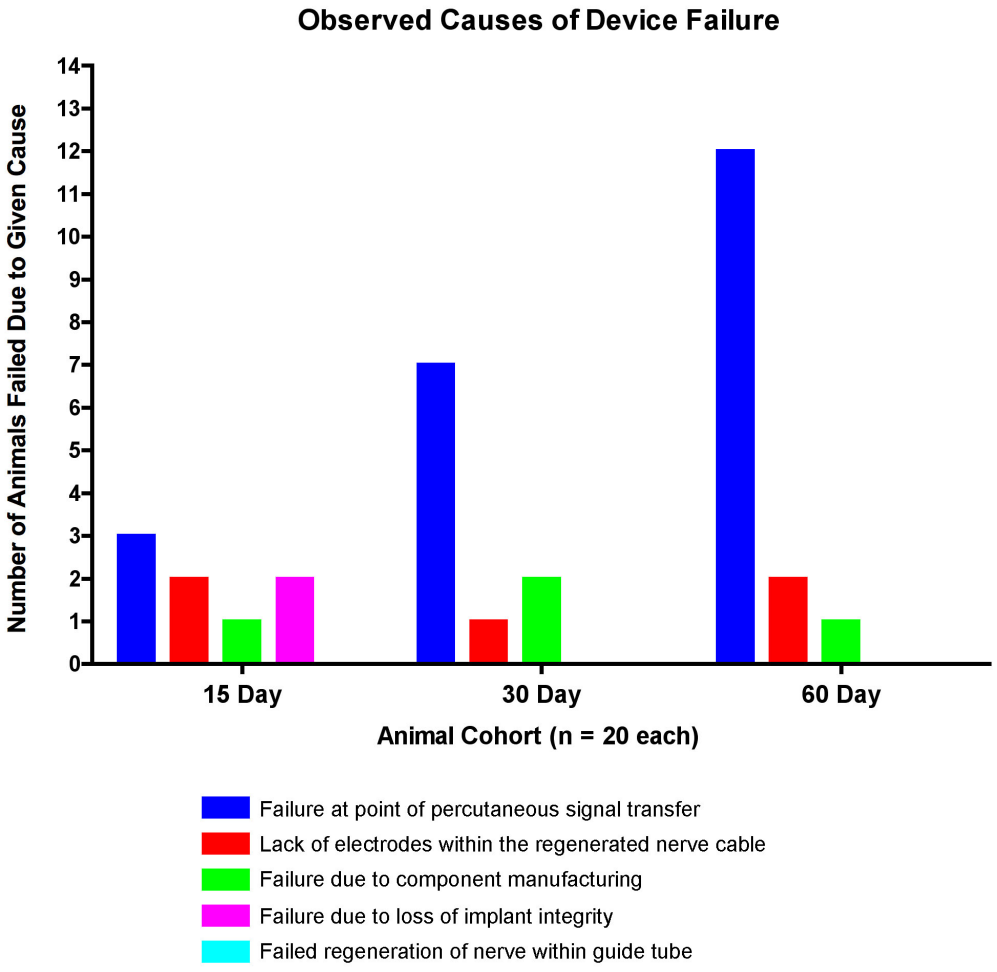

Figure 5.10 A summary of causes of physical device failure observed in the REMI.

Issues relating to the integrity of hardware transferring the detected signal from the internal environment of the animal to the external environment through the skin, such as breakage of the ribbon cable or expulsion of the percutaneous pedestal, represented the major cause of failure, progressing to over 50% of implanted animals by 60 days. Such issues could presumably be alleviated by incorporation of implanted wireless power and transmission technology. Other observed causes of failure each represented 10% or less of implanted animals over 60 days and tended to reflect variability within REMI construction and surgical implantation more so than an intrinsic property of the interface design.

A comparison of these observed causes of failure to other reported causes of failure within regenerative PNIs (Figure 5.11) shows that issues relating to the percutaneous transfer of the signal is the most prominently reported cause of failure across many publication. Failure of successful nerve regeneration through the device appears to be the second most prominent cause of device failure, though this is limited to sieve device architectures.

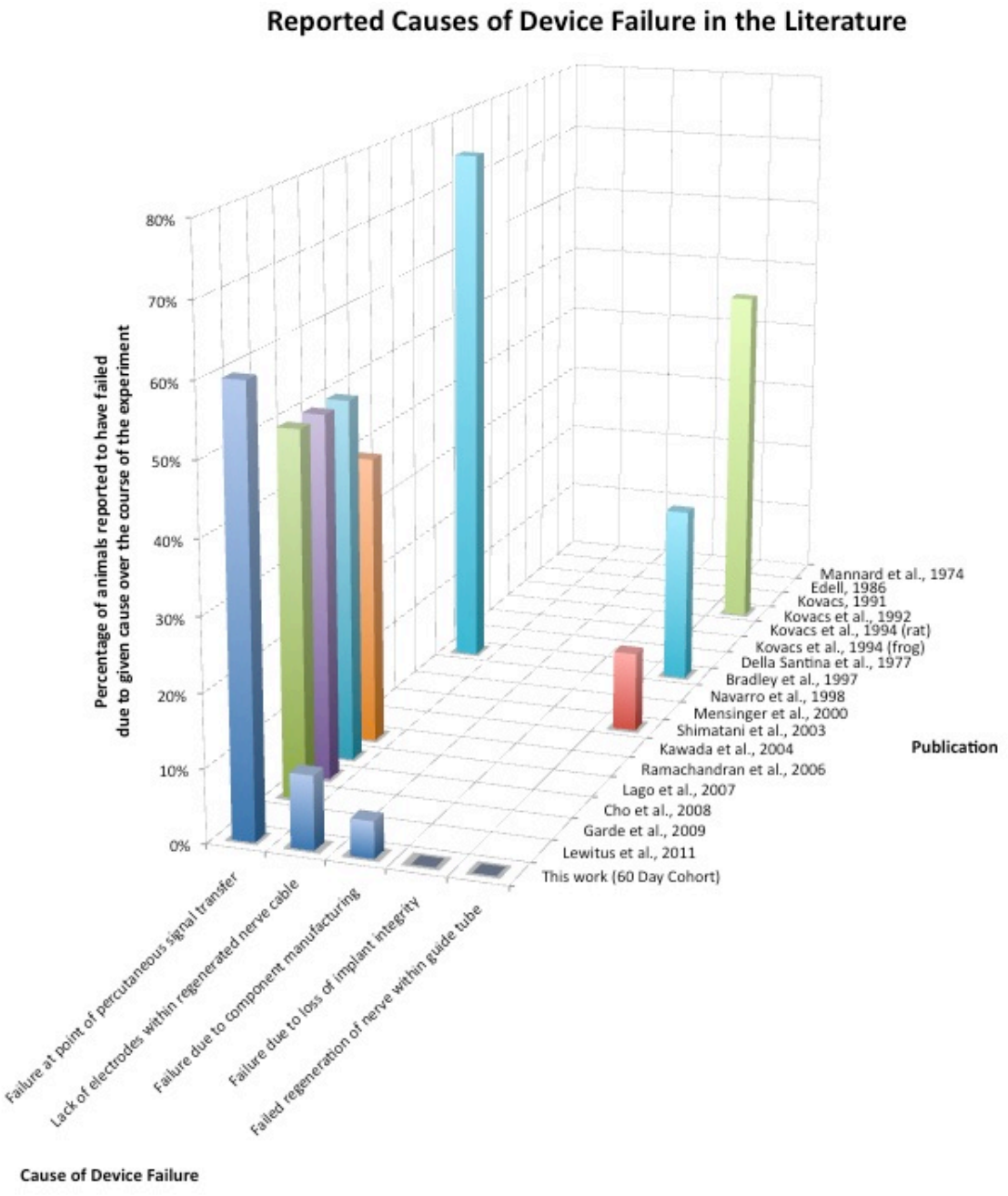

Figure 5.11 A summary of reported causes of RPNI device failure present in the literature. Note: Lago *et al.*, 2007, Cho *et al.*, 2008, and Garde *et al.*, 2009 reported failures associated with percutaneous signal transfer to account for "most" or a "majority" of animals. As such, they are represented here at 50%, though the actual value is implied to be higher. Many of these publications did identify one or more of these causes of failure as present but did not quantify them. See Table 2.10 for additional details. Publications present in this figure were selected from Table 2.1.

5.2.3 Robustness of the REMI with respect to applied stress

After characterization of the common failure modes within the REMI, our laboratory and DARPA were interested in characterizing the robustness of the device by investigating the degree to which applied stress could accelerate device failure or signal loss. We designed an experiment in which, in addition to our weekly electrophysiological monitoring sessions, a subset of animals (three groups, n = 6 each) were subjected to weekly limb stretching sessions to simulate the effects of applied stress due to limb movement. One group was subjected to weekly sessions of cyclic limb stretching at 100% of the physiological range of motion of the hind limb to simulate exaggerated limb motion. Another group was subjected to weekly sessions of cyclic limb stretching at 70% of the physiological range of motion of the hind limb to simulate more natural limb motion. The third group served as an unstretched control.

We were interested in answering three questions with respect to the stress simulated by cyclic limb stretching: Did it result in increased device failure? Did it result in more rapid signal loss due to cumulative effects of stretching? Did it result in larger scar formation or decreased axonal regeneration within the guide tube? The answer to all three questions was no, implying a high degree of robustness and stability with respect to normal and exaggerated limb movements.

Rates of device failure, rates of signal loss, scar sizes, and regenerated axon counts are presented in Figures 5.3, 3.12, 3.30, and 3.31, respectively. The latter three are described in greater detail in Section 3.3.

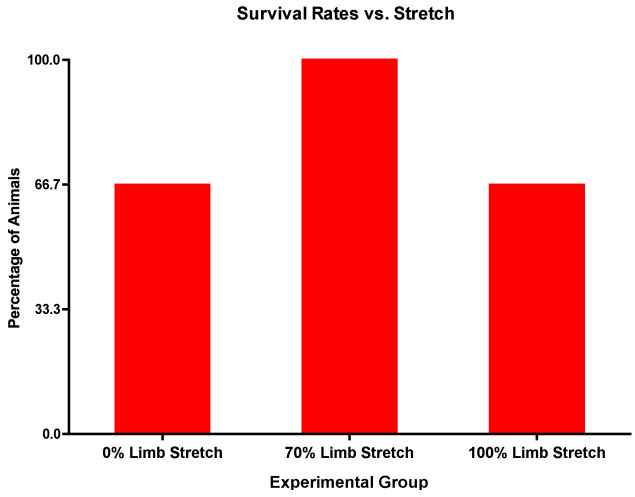

Figure 5.12 Percentage of animals that survived until scheduled termination at 30 days post-implantation without observable device failure relative to limb stretch intensity. Values represent the original 18 animals (n = 6 animals per group) within the limb stretching experiments presented in Chapter 3.

5.2.4 Signal Stability and Presence Over Time

Finally, we were interested in characterizing the REMI with respect to signal quality over time. How stable are observed signals over short periods of time? For how long do we tend to observe individual spiking units? How do our observations of the REMI compare to reports of other RPNIs?

Section 5.1 reveals a high variability in the stability of signals observed over the course of 23 hours at 21 days post-implantation. We observed 2 spiking units with fairly high waveshape stability (fluctuations in peak-to-peak amplitude of less than 25% over the course of 23 hours). While four of the six observed spiking units displayed a relatively low degree of stability over the course of 23 hours, it is unknown whether recorded signals from the REMI would exhibit greater stability if measured at a later time point relative to implantation after nerve regeneration had matured.

Of the 18 animals used within the limb stretching experiments, a total of 69 distinct spiking units were observed among 11 animals over 22 individual recording sessions. Among

these 69 spiking units, there were 7 pairs of units present on the same electrode within the same animal on two consecutive weekly recording sessions. Three of these pairs exhibited similar waveshapes and peak-to-peak amplitude ratios of less than 1 : 1.31 (mean = 1 : 1.16), implying a strong likelihood that the signals represent a continuity of recording from a single axon. Four of these pairs exhibited dissimilar waveshapes and peak-to-peak amplitude ratios of greater than 1 : 3.25 (mean = 1 : 4.18), implying a low likelihood that the signals represent a continuity of recording from an individual axon (ratios taken as smaller amplitude to greater amplitude). While it is not possible to confirm this interpretation of the data, the results imply that we observed 3 distinct spiking units that maintained presence for at least one week and 63 distinct spiking units that were not present one week after initial observation.

Again, it is unknown if the REMI would provide greater signal stability several months post-implantation. A review of the literature reveals very few examples of signal stability within other RPNI architectures with which to compare the REMI. Shimatani et al. (2003), report observing a single unit present for 21 consecutive days, starting at 77 days post-implantation with less than approximately 20% fluctuation in amplitude over the 21 days as measured using a 4-channel silicon-based sieve electrode implanted into a rat cranial nerve (Figure 5.2). It is unknown if this result is typical or anomalous.

Early reports on penetrative needle electrode arrays in peripheral nerves of cats reveal the capacity of these electrodes to record a single spiking unit with a high degree of stability over the course of 36 hours, but most spiking units were lost within days and all within a month (Branner and Normann, 2000; Branner et al., 2004). A subsequent report using an improved containment system to stabilize and electrically shield the implanted 100-channel arrays report observing between approximately 20 to approximately 40 spiking units continually from day of implantation up to 4 months when the study was terminated (Clark et al., 2011). Information on the stability of individual units over time was not reported.

5.3 The Future of Regenerative Interfacing

Many types of regenerative peripheral nerve interface architectures have been proposed in publication, including those reviewed in Section 1.3.6 such as sieve architectures, multiluminal biodegradable architectures, rolled architectures, microchannel-based architectures, and the REMI. Architectures that rely on transplanted muscle tissue as a signal transducer have also been proposed in various forms in publication (Wells *et al.*, 2001), in abstract form (Frost *et al.,* 2009), and in the recent doctoral dissertation of Christopher Langhammer (Rutgers University, 2010). In a conference proceeding (Clements *et al.*, 2007), researchers at the Georgia Institute of Technology introduced the idea of incorporating electrodes onto thin-film sheets of aligned nanofibers that have been shown to improve nerve regeneration through a guidance tube (see Kim *et al.*, 2008; Clements *et al.,* 2009). Such a device architecture could serve as a platform for the development of tissue engineering techniques in two dimensions to improve nerve guidance and investigate strategies to mediate nerve-electrode interactions.

While the experimental successes and associated technology surrounding penetrative PNIs, such as those based upon the Utah Electrode Array (Branner and Normann, 2000; Branner *et al.*, 2004; Clark *et al.*, 2011), implanted into a peripheral nerve are more advanced to-date than those of regenerative PNIs (see Table 1.1, Section 1.3.5), the great advantage of regenerative PNIs in the years to come will be in the potential to incorporate tissue engineering techniques into architecture designs. While penetrative PNIs would likely be more desirable for a patient with an intact limb, regenerative PNIs will likely offer many advantages desirable to amputees.

Tissue engineering techniques may, in the years to come, provide the capacity for RPNIs to guide axons both for the purposes of segregating axons of different types and for producing a divergent growth pattern that would allow for an increased number of electrodes within a device to interface with a greater percentage of axons and provide greater selectivity of

recordings. Researchers at the University of Tuente have recently proposed several schemes to produce divergent growth patterns in a regenerative device; Figure 5.10 (A) provides a visualization of an expansive architecture that would allow for increased volume for the incorporation of more electrodes into a device; Figure 5.10 (B and C) illustrate a progressively bifurcating channel concept which would, hopefully, allow for isolation of individual axons (Wieringa *et al.*, 2010a; Wieringa *et al.*, 2010b; Wieringa *et al.*, 2010c).

Tissue engineering techniques involving cell-seeded scaffolds may also provide opportunities for neural interfacing. Several groups have proposed growing neuronal or neuronal-like cells onto an electrode-embedded scaffold *in vitro* for future implantation into a host with hopes of functional innervation of the device (Stieglitz *et al*., 2001; Kameswaran *et al*., 2008). Such a technique would presumably allow for greater manipulation and consistency of neuron-electrode contacts, could allow for the use of genetically modified or manipulated cells, and could possibly allow for functional synaptic connectivity between myelinated cells (from the host) and unmyelinated cells (within the implant).

Work from our own laboratory has demonstrated the capacity for neurotrophic factors to induce divergent growth patterns of axonal subtypes in a large bifurcating channel (Lotfi *et al*., 2011). It would be the eventual goal of tissue engineering and axonal guidance schemes to be able to segregate and isolate motor axons for recordings and sensory axon subtypes (proprioceptive, temperature, touch, nociceptive etc.) for stimulation.

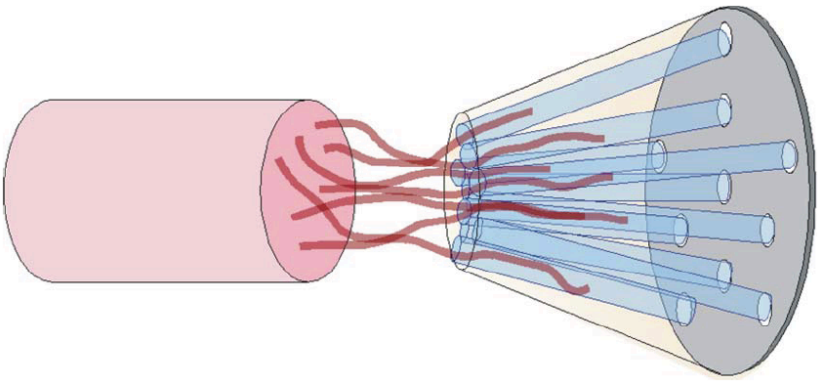

(A)

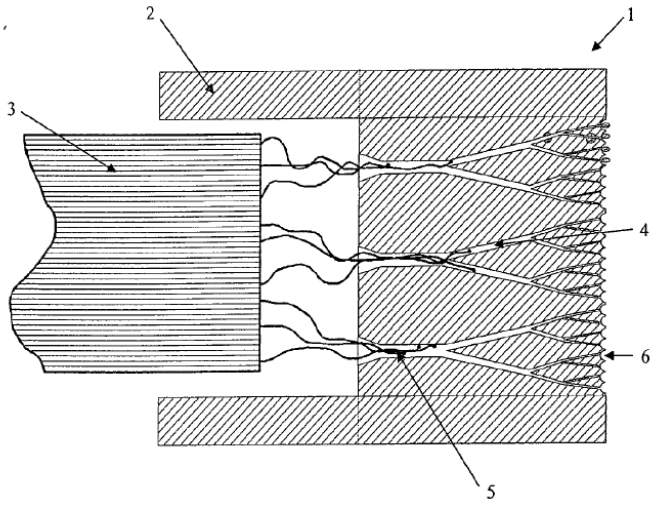

(B)

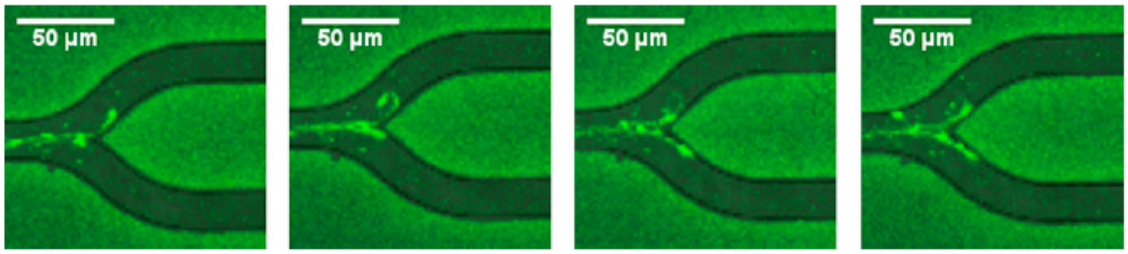

(C)

Figure 5.13 Examples of axonal expansion and bifurcation for the potential improvements of RPNIs. Adapted from Wieringa *et al.*, 2010a; Wieringa *et al.*, 2010b; Wieringa *et al.*, 2010c.

5.4 Conclusions

Three distinct limitations within the current state of regenerative peripheral nerve interfacing technology were identified, leading to the three specific aims of this dissertation. RPNIs tend to fail due to a variety of mechanical and physical causes. RPNIs tend to lose acquired signals over time due to biologically mediated mechanisms of rejection. RPNIs currently lack sufficient sensitivity for clinical use.

The rate of physical failure of implanted devices in animal models, as reported in the literature and as observed here, severely limits the capacity to test biologically oriented hypotheses regarding proposed devices. In a review of the literature and in a large-cohort experiment presented here, failure associated with the percutaneous transfer of the detected signal was observed to be the dominant cause of physical device failure inherent in current experimental designs.

The propensity for nerve deformation or stretch, as a result of natural or excessive limb movement, to aggravate the electrode-tissue interface and promote signal loss within a typical, guide-tube based RPNI has not been investigated. In a small rodent nerve model, it has been shown that nerve strains in excess of approximately 15% result in signal conduction deficits; nerve strains in excess of approximately 38% can result in partial rupture of nerve tissues. Here, we provide evidence that periodic limb stretching resulting in nerve strains of approximately 18% (representing moderate limb stretch) and approximately 35% (representing excessive limb stretch) do not result in decreased axonal regeneration through the guide tube, do not increase the size of the axon-depleted scar surrounding individual electrodes, and do not promote signal loss. These results imply that the nerve guide tube structure provides adequate mechanical support and isolation from stretch to internal nerve components to protect the integrity of the device from any deleterious effects of natural limb movement.

The use of microchannel encapsulation has been proposed as a means to improve the sensitivity of RPNIs with the hopes of providing an increased number of detectable signals per

device as well as mitigating signal loss over time. Here we show strong evidence in support of microchannel amplification of unmyelinated axons.

APPENDIX A

AXON COUNTS

This appendix contains graphical information related to the quantification of histological findings relevant to Chapter 3. Methods of quantification are described in Section 3.2.7.3. The data present in this appendix is summarized in Section 3.3.3.

The counted number of axons per histological slice, grouped by animal, are displayed relative to limb stretch group for both 30 day and 60 day animal cohorts on pages X and X. The counted number of myelinated axons per histological slice, grouped by animal, are displayed relative to limb stretch group for both 30 day and 60 day animal cohorts on pages X and X.

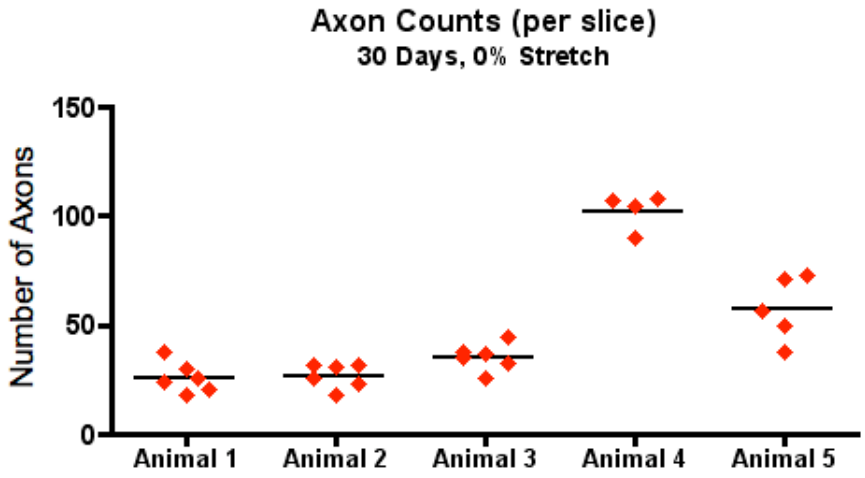
Axon Counts (per slice)
30 Days, 0% Stretch
Number of Axons
150
100
50
0
Animal 1
Animal 2
Animal 3
Animal 4
Animal 5

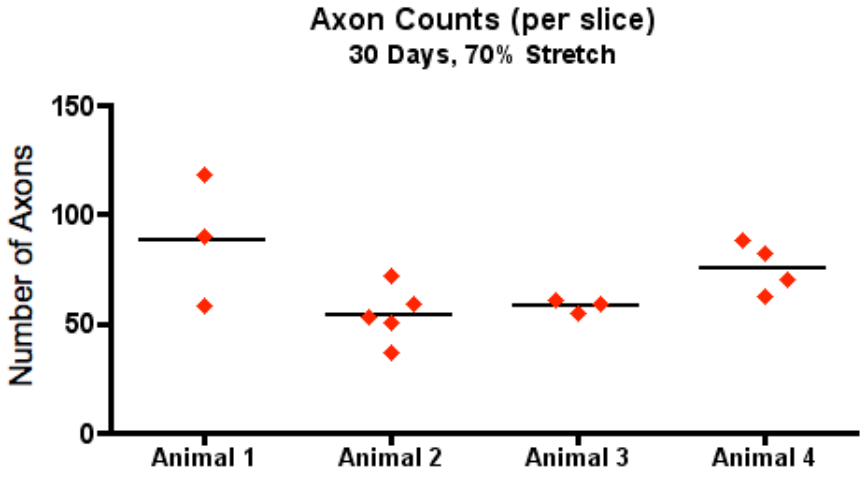
Axon Counts (per slice)
30 Days, 70% Stretch
Number of Axons
150
100
50
0
Animal 1
Animal 2
Animal 3
Animal 4

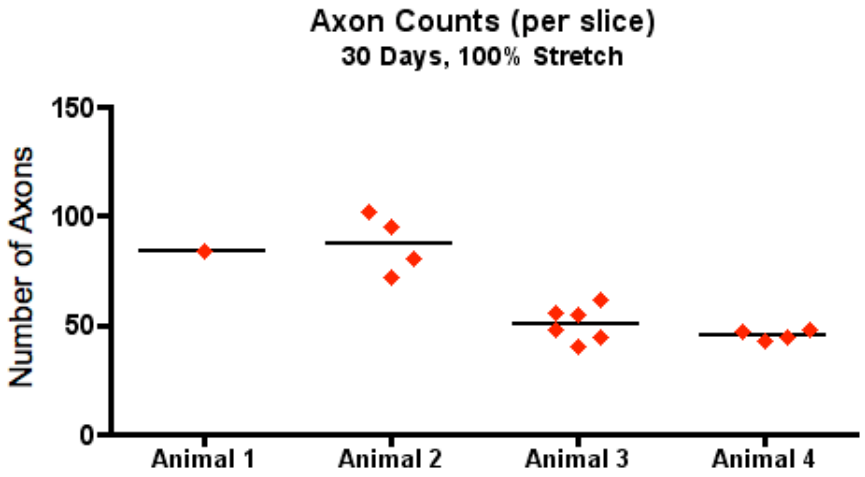
Axon Counts (per slice)
30 Days, 100% Stretch
Number of Axons
150
100
50
0
Animal 1
Animal 2
Animal 3
Animal 4

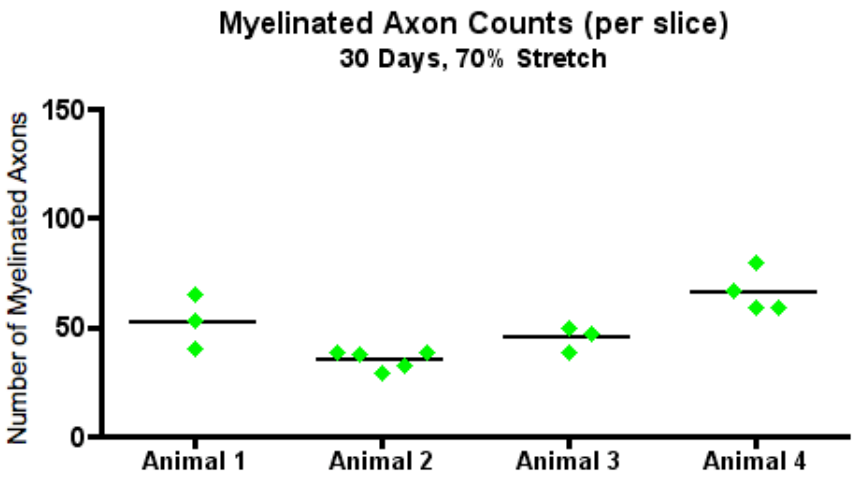
Myelinated Axon Counts (per slice)
30 Days, 70% Stretch
Number of Myelinated Axons
150
100
50
0
Animal 1
Animal 2
Animal 3
Animal 4

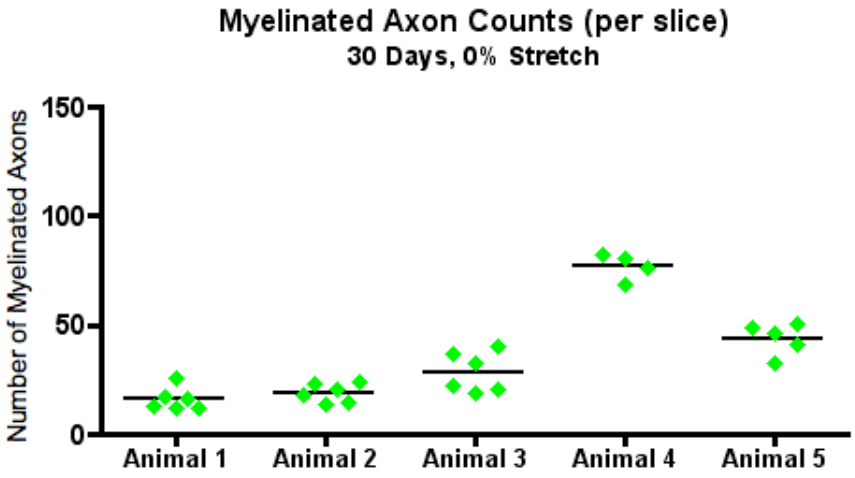
Myelinated Axon Counts (per slice)
30 Days, 0% Stretch
Number of Myelinated Axons
150
100
50
0
Animal 1
Animal 2
Animal 3
Animal 4
Animal 5

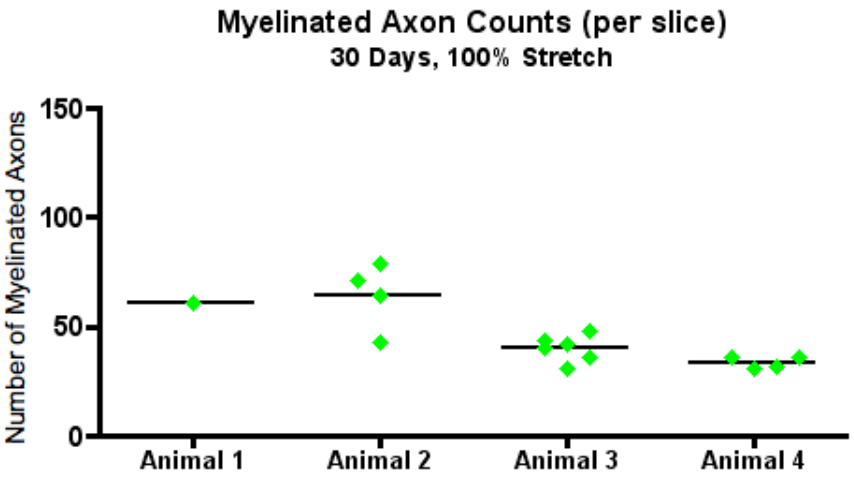
Myelinated Axon Counts (per slice)
30 Days, 100% Stretch
Number of Myelinated Axons
150
100
50
0
Animal 1
Animal 2
Animal 3
Animal 4

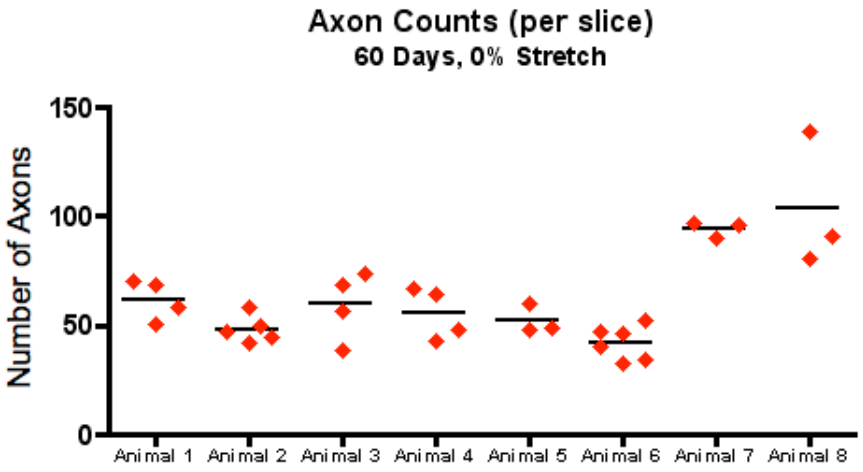
Axon Counts (per slice)
60 Days, 0% Stretch
Number of Axons
150
100
50
0
Animal 1
Animal 2
Animal 3
Animal 4
Animal 5
Animal 6
Animal 7
Animal 8

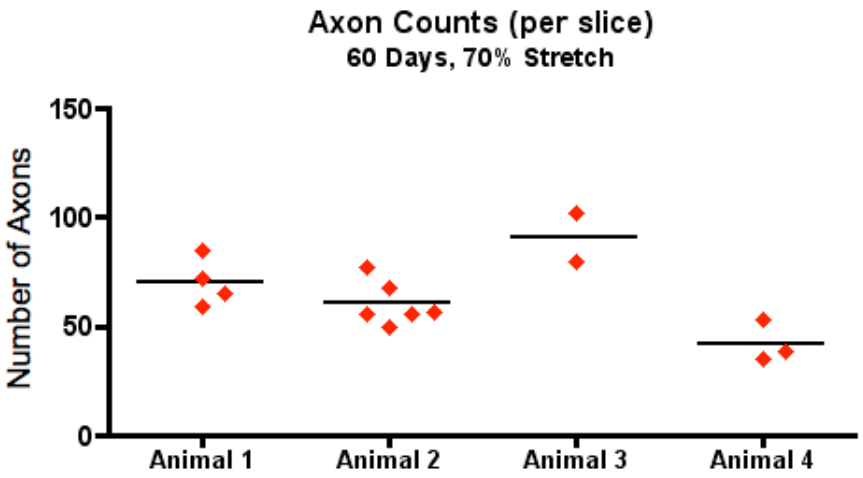
Axon Counts (per slice)
60 Days, 70% Stretch
Number of Axons
150
100
50
0
Animal 1
Animal 2
Animal 3
Animal 4

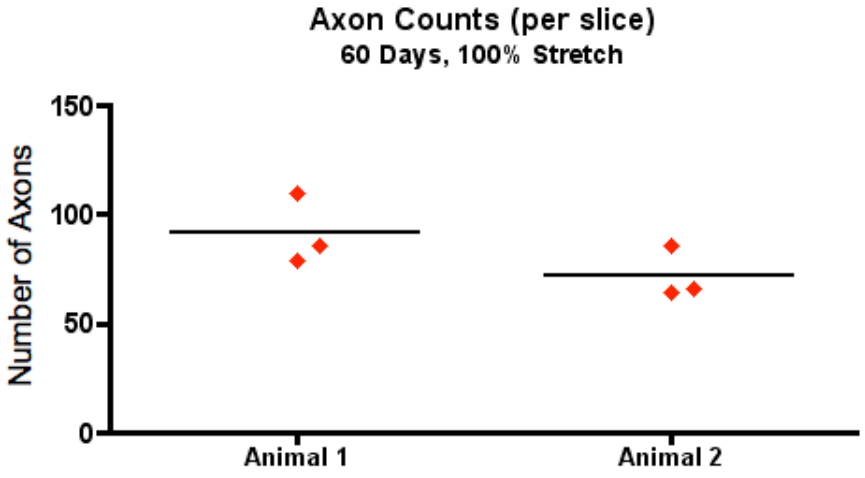
Axon Counts (per slice)
60 Days, 100% Stretch
Number of Axons
150
100
50
0
Animal 1
Animal 2

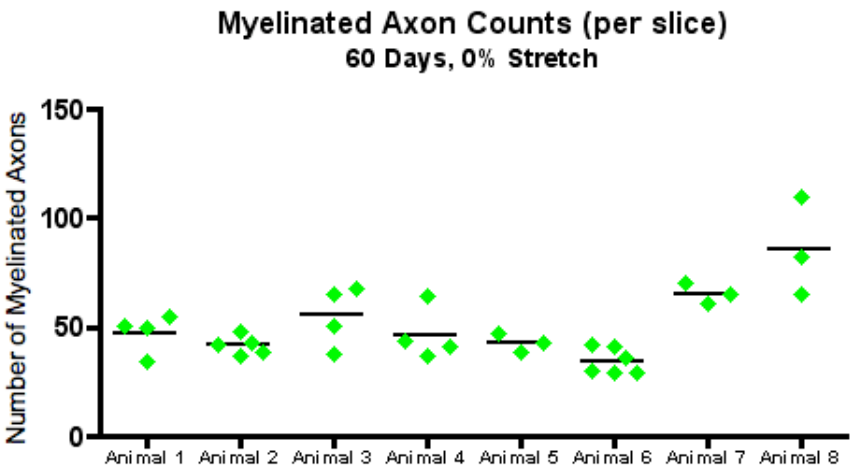
Myelinated Axon Counts (per slice)
60 Days, 0% Stretch
Number of Myelinated Axons
150
100
50
0
Animal 1
Animal 2
Animal 3
Animal 4
Animal 5
Animal 6
Animal 7
Animal 8

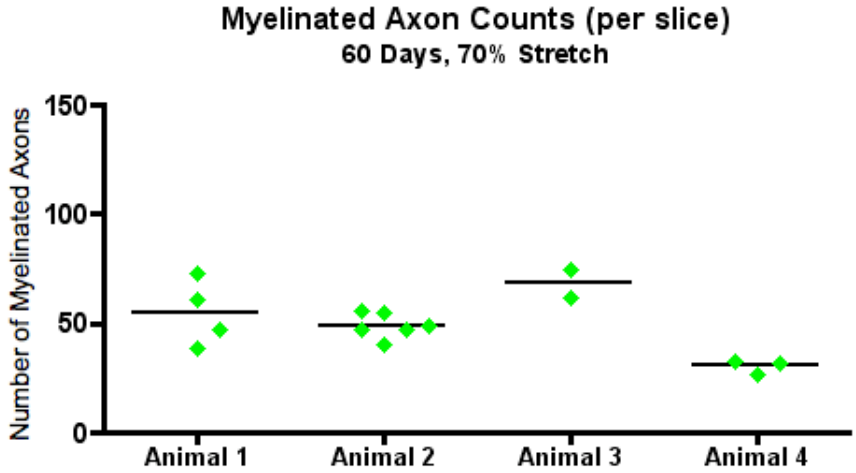
Myelinated Axon Counts (per slice)
60 Days, 70% Stretch
Number of Myelinated Axons
150
100
50
0
Animal 1
Animal 2
Animal 3
Animal 4

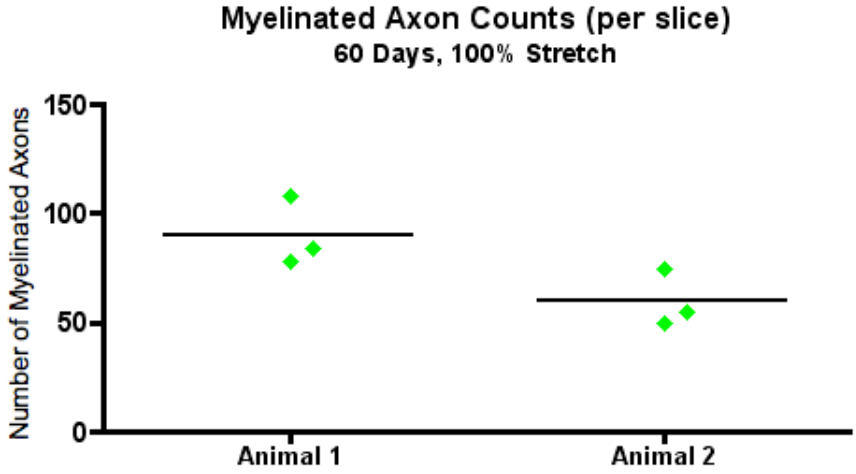
Myelinated Axon Counts (per slice)
60 Days, 100% Stretch
Number of Myelinated Axons
150
100
50
0
Animal 1
Animal 2

APPENDIX B

AXON DEPLETED SCAR SIZES

This appendix contains graphical information related to the quantification of histological findings relevant to Chapter 3. Methods of quantification are described in Section 3.2.7.3. The data present in this appendix is summarized in Section 3.3.4.

The measured size of the axon-depleted scar surrounding each electrode shaft, arranged by histological slice on a given animal, is presented across all three limb stretch groups for both the 30 day and 60 day animal cohorts on pages XX. The average sizes of the axon-depleted scars per histological slice, grouped by respective animal, are presented across all limb stretch groups and time point cohorts on page X.

Axon-Depleted Areas
30 Day, 0% Stretch

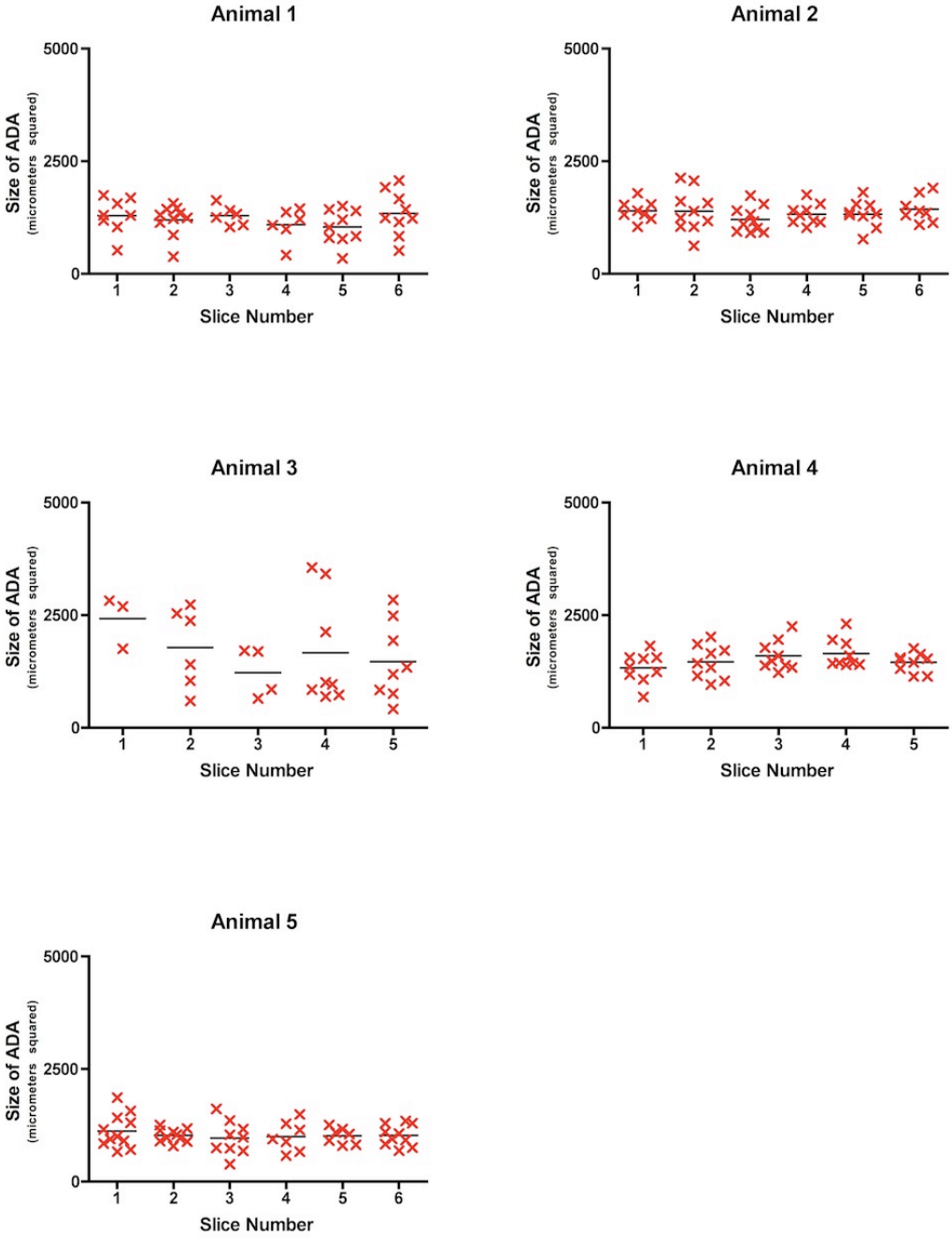

Axon-Depleted Areas
30 Day, 70% Stretch

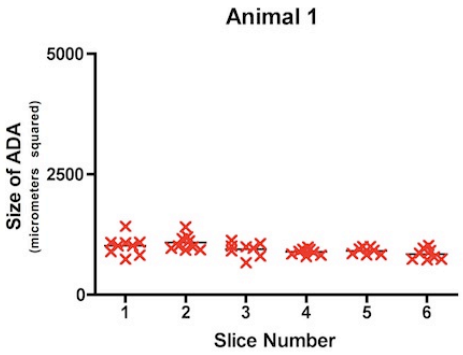

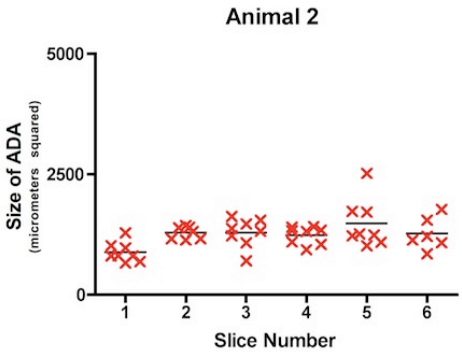

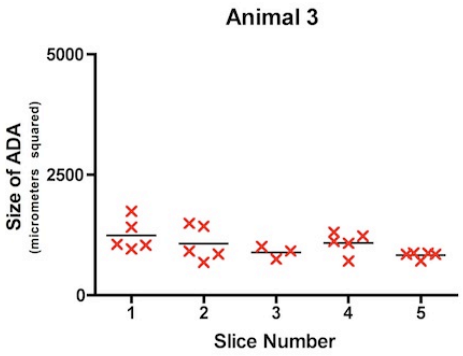

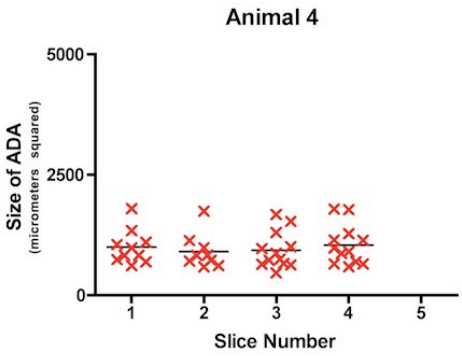

Axon-Depleted Areas
30 Day, 100% Stretch

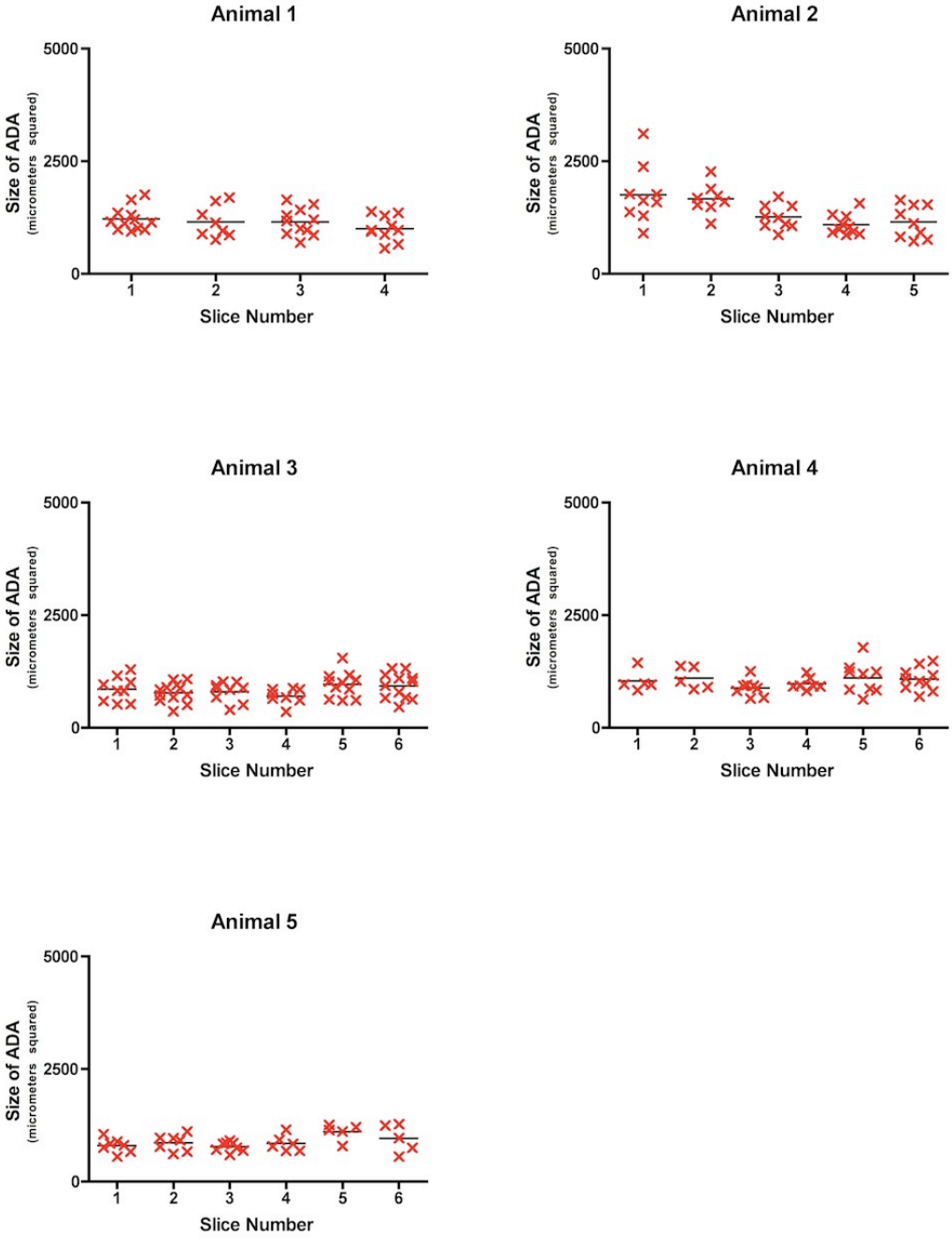

Axon-Depleted Areas
60 Day, 0% Stretch
(page 1 of 2)

Animal 1

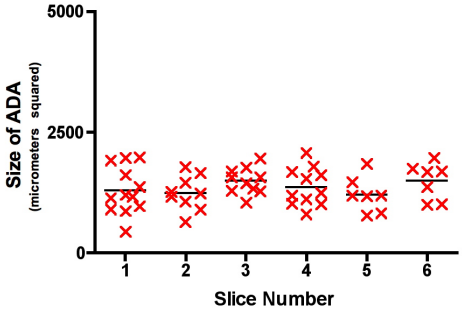

Animal 2

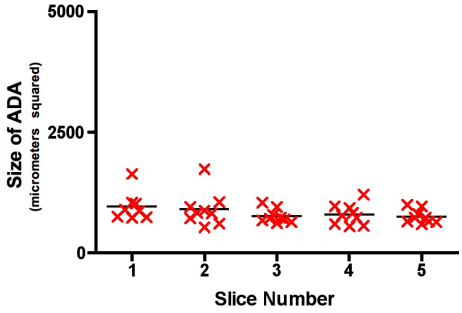

Animal 3

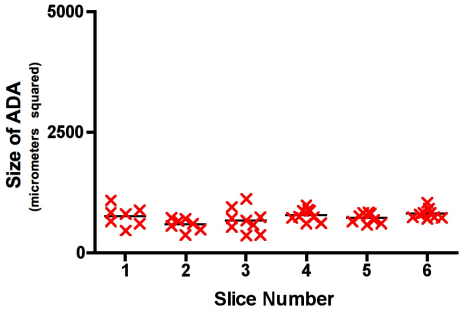

Animal 4

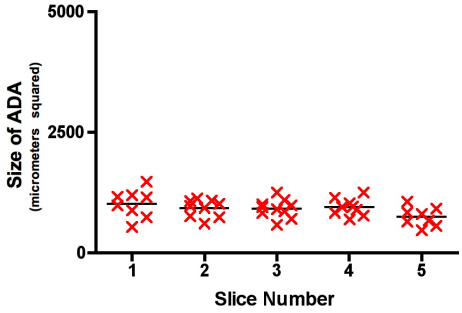

Animal 5

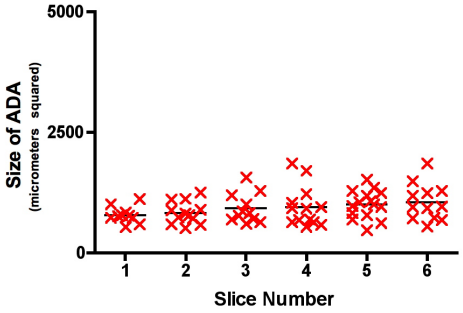

Animal 6

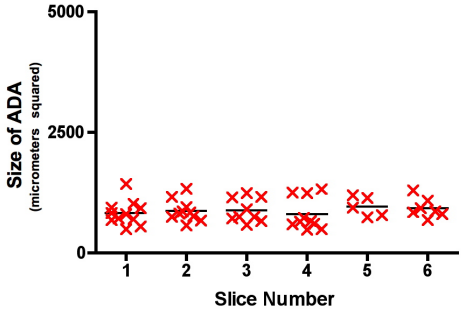

Axon-Depleted Areas
60 Day, 0% Stretch
(page 2 of 2)

Animal 7

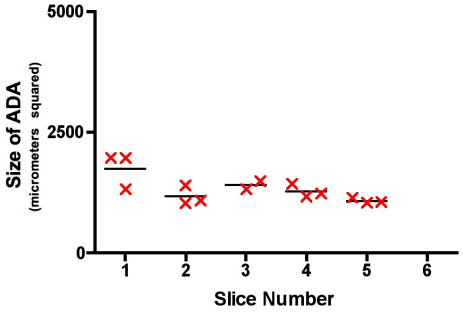

Animal 8

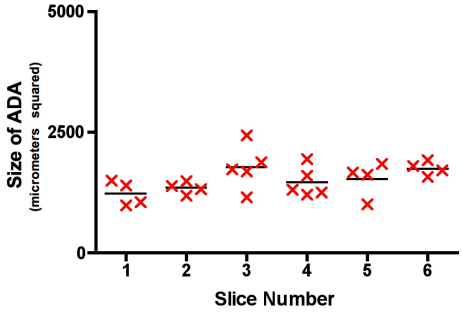

Animal 9

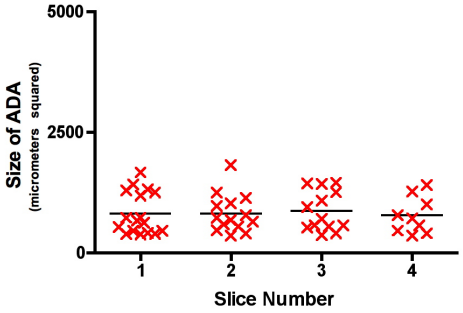

Axon-Depleted Areas
60 Day, 70% Stretch

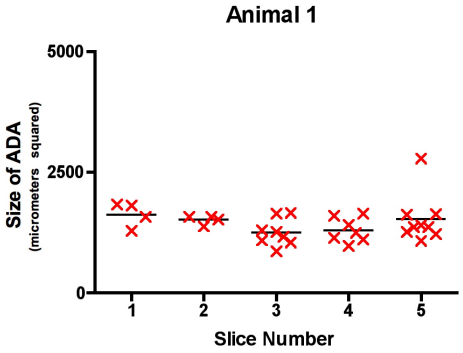

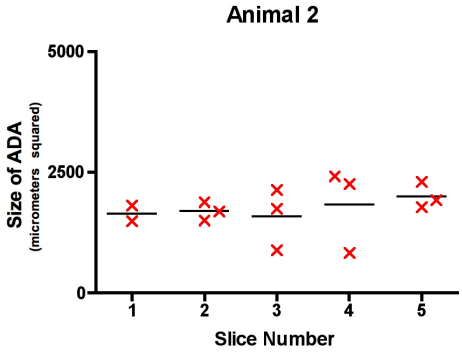

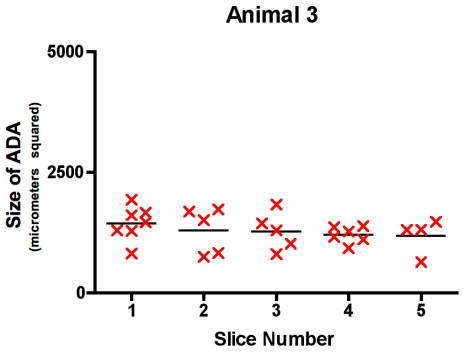

Axon-Depleted Areas
60 Day, 100% Stretch

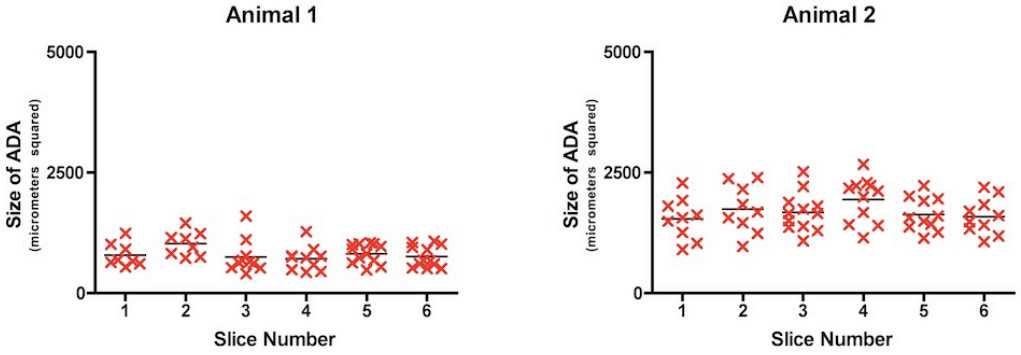

REFERENCES

1 Abe, I., Ochiai, N., Ichimura, H., Tsujino, A., Sun, J. & Hara, Y. Internodes can nearly double in length with gradual elongation of the adult rat sciatic nerve. *Journal of orthopaedic research* 22, 571-577 (2004).

2 Adrian, E. D. & Bronk, D. The discharge of impulses in motor nerve fibres: Part I. Impulses in single fibres of the phrenic nerve. *The Journal of Physiology* 66, 81 (1928).

3 Agnew, S. P., Schultz, A. E., Dumanian, G. A. & Kuiken, T. A. Targeted Reinnervation in the Transfemoral Amputee: A Preliminary Study of Surgical Technique. *Plastic and Reconstructive Surgery* 129, 187 (2012).

4 Ahsan, M. & Ibrahimy, M. I. EMG signal classification for human computer interaction: a review. *European Journal of Scientific Research* 33, 480-501 (2009).

5 Akin, T., Najafi, K. & Bradley, R. M. A wireless implantable multichannel digital neural recording system for a micromachined sieve electrode. *Solid-State Circuits, IEEE Journal of* 33, 109-118 (1998).

6 Akin, T., Najafi, K., Smoke, R. H. & Bradley, R. M. A micromachined silicon sieve electrode for nerve regeneration applications. *Biomedical Engineering, IEEE Transactions on* 41, 305-313 (1994).

7 Aoyagi, Y., Stein, R. B., Branner, A., Pearson, K. G. & Normann, R. A. Capabilities of a penetrating microelectrode array for recording single units in dorsal root ganglia of the cat. *Journal of Neuroscience Methods* 128, 9-20 (2003).

8 Azemi, E., Lagenaur, C. F. & Cui, X. T. The surface immobilization of the neural adhesion molecule L1 on neural probes and its effect on neuronal density and gliosis at the probe/tissue interface. *Biomaterials* 32, 681-692 (2011).

9 Bear, M. F., Connors, B. W. & Paradiso, M. A. *Neuroscience: Exploring the brain*. (Lippincott Williams & Wilkins, 2007).

10 Benmerah, S., Lacour, S. P. & Tarte, E. in *Engineering in Medicine and Biology Society, 2009. EMBC 2009. Annual International Conference of the IEEE.* 6400-6403 (IEEE).

11 Biran, R., Martin, D. C. & Tresco, P. A. Neuronal cell loss accompanies the brain tissue response to chronically implanted silicon microelectrode arrays. *Experimental neurology* 195, 115-126 (2005).

12 Biran, R., Martin, D. C. & Tresco, P. A. The brain tissue response to implanted silicon microelectrode arrays is increased when the device is tethered to the skull. *Journal of Biomedical Materials Research Part A* 82, 169-178 (2007).

13 Blau, A., Ziegler, C., Heyer, M., Endres, F., Schwitzgebel, G., Matthies, T., Stieglitz, T., Meyer, J. U. & Gopel, W. Characterization and optimization of microelectrode arrays for in vivo nerve signal recording and stimulation1. *Biosensors and Bioelectronics* 12, 883-892 (1997).

14 Boretius, T., Badia, J., Pascual-Font, A., Schuettler, M., Navarro, X., Yoshida, K. & Stieglitz, T. A transverse intrafascicular multichannel electrode (TIME) to interface with the peripheral nerve. *Biosensors and Bioelectronics* 26, 62-69 (2010).

15 Bradley, R. M., Cao, X., Akin, T. & Najafi, K. Long term chronic recordings from peripheral sensory fibers using a sieve electrode array. *Journal of Neuroscience Methods* 73, 177-186 (1997).

16 Bradley, R. M., Smoke, R. H., Akin, T. & Najafi, K. Functional regeneration of glossopharyngeal nerve through micromachined sieve electrode arrays. *Brain Research* 594, 84-90 (1992).

17 Branner, A. & Normann, R. A. A multielectrode array for intrafascicular recording and stimulation in sciatic nerve of cats. *Brain research bulletin* 51, 293-306 (2000).

18 Branner, A., Stein, R. B., Fernandez, E., Aoyagi, Y. & Normann, R. A. Long-term stimulation and recording with a penetrating microelectrode array in cat sciatic nerve. *Biomedical Engineering, IEEE Transactions on* 51, 146-157 (2004).

19 Branner, A., Stein, R. B. & Normann, R. A. Selective stimulation of cat sciatic nerve using an array of varying-length microelectrodes. *Journal of Neurophysiology* 85, 1585-1594 (2001).

20 Britt, R. & Rossi, G. Quantitative analysis of methods for reducing physiological brain pulsations. *Journal of Neuroscience Methods* 6, 219-229 (1982).

21 Brown, R., Pedowitz, R., Rydevik, B., Woo, S., Hargens, A., Massie, J., Kwan, M. & Garfin, S. R. Effects of acute graded strain on efferent conduction properties in the rabbit tibial nerve. *Clinical orthopaedics and related research* 296, 288 (1993).

22 Campenot, R. Local control of neurite development by nerve growth factor. *Proceedings of the National Academy of Sciences of the United States of America* 74, 4516 (1977).

23 Campenot, R., Lund, K. & Mok, S. Production of compartmented cultures of rat sympathetic neurons. *Nature Protocols* 4, 1869-1887 (2009).

24 Capadona, J. R., Shanmuganathan, K., Tyler, D. J., Rowan, S. J. & Weder, C. Stimuli-responsive polymer nanocomposites inspired by the sea cucumber dermis. *Science* 319, 1370-1374 (2008).

25 Carmena, J. M., Lebedev, M. A., Crist, R. E., O'Doherty, J. E., Santucci, D. M., Dimitrov, D. F., Patil, P. G., Henriquez, C. S. & Nicolelis, M. A. L. Learning to control a brain,Äìmachine interface for reaching and grasping by primates. *PLoS biology* 1, e42 (2003).

26 Castro, J., Negredo, P. & Avenda√±o, C. Fiber composition of the rat sciatic nerve and its modification during regeneration through a sieve electrode. *Brain Research* 1190, 65-77 (2008).

27 Ceballos, D., Valero CabrÈ, A., Valderrama, E., Sch¸ttler, M., Stieglitz, T. & Navarro, X. Morphologic and functional evaluation of peripheral nerve fibers regenerated through polyimide sieve electrodes over long term implantation. *Journal of biomedical materials research* 60, 517-528 (2002).

28 Chao, Z. C., Nagasaka, Y. & Fujii, N. Long-term asynchronous decoding of arm motion using electrocorticographic signals in monkeys. *Frontiers in Neuroengineering* 3 (2010).

29 Chapin, J. K., Moxon, K. A., Markowitz, R. S. & Nicolelis, M. A. L. Real-time control of a robot arm using simultaneously recorded neurons in the motor cortex. *Nature neuroscience* 2, 664-670 (1999).

30 Chestek, C. A., Gilja, V., Nuyujukian, P., Foster, J. D., Fan, J. M., Kaufman, M. T., Churchland, M. M., Rivera-Alvidrez, Z., Cunningham, J. P. & Ryu, S. I. Long-term stability of neural prosthetic control signals from silicon cortical arrays in rhesus macaque motor cortex. *Journal of Neural Engineering* 8, 045005 (2011).

31 Cho, S. H., Lu, H. M., Cauller, L., Romero-Ortega, M. I., Lee, J. B. & Hughes, G. A. Biocompatible SU-8-based microprobes for recording neural spike signals from regenerated peripheral nerve fibers. *Sensors Journal, IEEE* 8, 1830-1836 (2008).

32 Cho, S. H., Son, S. H., Chung, H. J. & Lee, J. B. A wireless powered fully integrated SU-8-based implantable LC transponder. *Microsystem Technologies* 16, 1657-1663 (2010).

33 Cipriani, C., D'Alonzo, M. & Carrozza, M. C. A Miniature Vibrotactile Sensory Substitution Device for Multi-fingered Hand Prosthetics. *Biomedical Engineering, IEEE Transactions on*, 1-1 (2012).

34 Citi, L., Carpaneto, J., Yoshida, K., Hoffmann, K. P., Koch, K. P., Dario, P. & Micera, S. On the use of wavelet denoising and spike sorting techniques to process electroneurographic signals recorded using intraneural electrodes. *Journal of Neuroscience Methods* 172, 294-302 (2008).

35 Clark, D. Muscle counts of motor units: a study in innervation ratios. *American Journal of Physiology--Legacy Content* 96, 296-304 (1931).

36 Clark, G. A., Ledbetter, N. M., Warren, D. J. & Harrison, R. R. in *Engineering in Medicine and Biology Society,EMBC, 2011 Annual International Conference of the IEEE.* 4641-4644 (IEEE).

37 Clements, I. P. Topographic guidance scaffolds for peripheral nerve interfacing. (2010).

38 Clements, I. P., Kim, Y., English, A. W., Lu, X., Chung, A. & Bellamkonda, R. V. Thin-film enhanced nerve guidance channels for peripheral nerve repair. *Biomaterials* 30, 3834-3846 (2009).

39 Coates, J., T.D. Neural Interfacing: Forging the Human-Machine Connection. *Synthesis Lectures on Biomedical Engineering* 3, 1-112 (2008).

40 Cooper, S. & Eccles, J. The isometric responses of mammalian muscles. *The Journal of Physiology* 69, 377-385 (1930).

41 Dahiya, R. S., Metta, G., Valle, M. & Sandini, G. Tactile sensing,Äîfrom humans to humanoids. *Robotics, IEEE Transactions on* 26, 1-20 (2010).

42 Dalgleish, T. The emotional brain. *Nature Reviews Neuroscience* 5, 583-589 (2004).

43 Damoiseaux, J., D√∂pp, E., Calame, W., Chao, D., MacPherson, G. & Dijkstra, C. Rat macrophage lysosomal membrane antigen recognized by monoclonal antibody ED1. *Immunology* 83, 140 (1994).

44 Dario, P., Garzella, P., Toro, M., Micera, S., Alavi, M., Meyer, U., Valderrama, E., Sebatiani, L., Ghelarducci, B. & Mazzoni, C. Neural interfaces for regenerated nerve stimulation and recording. *Rehabilitation Engineering, IEEE Transactions on* 6, 353-363 (1998).

45 de Luca, C. J., Foley, P. J. & Erim, Z. Motor unit control properties in constant-force isometric contractions. *Journal of Neurophysiology* 76, 1503-1516 (1996).

46 De Luca, C. J. & Gilmore, L. D. Voluntary nerve signals from severed mammalian nerves: long-term recordings. *Science* 191, 193-195 (1976).

47 Della Santina, C. C., Kovacs, G. T. A. & Lewis, E. R. Multi-unit recording from regenerated bullfrog eighth nerve using implantable silicon-substrate microelectrodes. *Journal of Neuroscience Methods* 72, 71-86 (1997).

48 Denny-Brown, D., ADAMS, R. D., Brenner, C. & Doherty, M. M. The Pathology of Injury To Nerve Induced By Cold 1. *Journal of Neuropathology & Experimental Neurology* 4, 305 (1945).

49 Desmedt, J. & Godaux, E. Ballistic contractions in man: characteristic recruitment pattern of single motor units of the tibialis anterior muscle. *The Journal of Physiology* 264, 673-693 (1977).

50 Dhillon, G., Kr√∞ger, T., Sandhu, J. & Horch, K. Effects of short-term training on sensory and motor function in severed nerves of long-term human amputees. *Journal of Neurophysiology* 93, 2625-2633 (2005).

51 Dhillon, G. S. & Horch, K. W. Direct neural sensory feedback and control of a prosthetic arm. *Neural Systems and Rehabilitation Engineering, IEEE Transactions on* 13, 468-472 (2005).

52 Dhillon, G. S., Lawrence, S. M., Hutchinson, D. T. & Horch, K. W. Residual function in peripheral nerve stumps of amputees: implications for neural control of artificial limbs1. *The Journal of hand surgery* 29, 605-615 (2004).

53 Di Pino, G., Guglielmelli, E. & Rossini, P. Neuroplasticity in amputees: main implications on bidirectional interfacing of cybernetic hand prostheses. *Progress in neurobiology* 88, 114-126 (2009).

54 Dickey, A. S., Suminski, A., Amit, Y. & Hatsopoulos, N. G. Single-unit stability using chronically implanted multielectrode arrays. *Journal of Neurophysiology* 102, 1331-1339 (2009).

55 Dijkstra, C., Dopp, E., van den Berg, T. & Damoiseaux, J. Monoclonal antibodies against rat macrophages. *Journal of Immunological Methods* 174, 21 (1994).

56 DiLorenzo, D. J. & Bronzino, J. *Neuroengineering*. (CRC Press, 2007).

57 Donoghue, J. P., Nurmikko, A., Black, M. & Hochberg, L. R. Assistive technology and robotic control using motor cortex ensemble‚Äêbased neural interface systems in humans with tetraplegia. *The Journal of Physiology* 579, 603-611 (2007).

58 Dowden, B. R., Wark, H. A. C. & Normann, R. A. Muscle‚Äêselective block using intrafascicular high‚Äêfrequency alternating current. *Muscle & nerve* 42, 339-347 (2010).

59 Dowden, B. R., Wilder, A. M., Hiatt, S. D., Normann, R. A., Brown, N. & Clark, G. A. Selective and graded recruitment of cat hamstring muscles with intrafascicular stimulation. *Neural Systems and Rehabilitation Engineering, IEEE Transactions on* 17, 545-552 (2009).

60 Driscoll, P. J., Glasby, M. A. & Lawson, G. M. An in vivo study of peripheral nerves in continuity: biomechanical and physiological responses to elongation. *Journal of orthopaedic research* 20, 370-375 (2002).

61 Dworak, B. & Wheeler, B. Novel MEA platform with PDMS microtunnels enables the detection of action potential propagation from isolated axons in culture. *Lab on a Chip* 9, 404-410 (2009).

62 Edell, D. *Development of a chronic neuroelectronic interface*, Doctoral Dissertation UC Davis, (1980).

63 Edell, D. J. A peripheral nerve information transducer for amputees: long-term multichannel recordings from rabbit peripheral nerves. *Biomedical Engineering, IEEE Transactions on*, 203-214 (1986).

64 Edell, D. J., Churchill, J. N. & Gourley, I. M. Biocompatibility of a silicon based peripheral nerve electrode. *Artificial Cells, Blood Substitutes and Biotechnology* 10, 103-122 (1982).

65 Egeland, B. M., Urbanchek, M. G., Peramo, A., Richardson-Burns, S. M., Martin, D. C., Kipke, D. R., Kuzon Jr, W. M. & Cederna, P. S. In Vivo Electrical Conductivity across Critical Nerve Gaps Using Poly (3, 4-ethylenedioxythiophene)-Coated Neural Interfaces. *Plastic and Reconstructive Surgery* 126, 1865 (2010).

66 Ehrlich, H. P., Desmouliere, A., Diegelmann, R. F., Cohen, I., Compton, C. C., Garner, W. L., Kapanci, Y. & Gabbiani, G. Morphological and immunochemical differences between keloid and hypertrophic scar. *The American journal of pathology* 145, 105 (1994).

67 Erlanger, J. & Gasser, H. The action potential in fibers of slow conduction in spinal roots and somatic nerves. *American Journal of Physiology--Legacy Content* 92, 43-82 (1930).

68 Erlanger, J. & Gasser, H. S. The compound nature of the action current of nerve as disclosed by the cathode ray oscillograph. *American Journal of Physiology--Legacy Content* 70, 624-666 (1924).

69 Evarts, E. V. Pyramidal tract activity associated with a conditioned hand movement in the monkey. *J Neurophysiol* 29, 1011-1027 (1966).

70 Evarts, E. V. Relation of pyramidal tract activity to force exerted during voluntary movement. *J Neurophysiol* 31, 14-27 (1968).

71 Feinberg, J. H. & Spielholz, N. I. *Peripheral nerve injuries in the athlete*. (Human Kinetics Publishers, 2003).

72 Fetz, E. & Finocchio, D. Correlations between activity of motor cortex cells and arm muscles during operantly conditioned response patterns. *Experimental Brain Research* 23, 217-240 (1975).

73 Fetz, E. E. Operant conditioning of cortical unit activity. *Science* 163, 955-958 (1969).

74 Fetz, E. E. & Baker, M. A. Operantly Conditioned Patterns of Activity and Correlated Responses Cells and Contralateral Muscles. (1973).

75 Fetz, E. E. & Finocchio, D. V. Operant conditioning of specific patterns of neural and muscular activity. *Science* 174, 431-435 (1971).

76 FitzGerald, J., Lacour, S., McMahon, S. & Fawcett, J. Microchannels as axonal amplifiers. *Biomedical Engineering, IEEE Transactions on* 55, 1136-1146 (2008).

77 FitzGerald, J., Lacour, S., McMahon, S. & Fawcett, J. Microchannel electrodes for recording and stimulation: in vitro evaluation. *IEEE transactions on bio-medical engineering* 56, 1524 (2009).

78 FitzGerald, J. J., Lago, N., Benmerah, S., Serra, J., Watling, C. P., Cameron, R. E., Tarte, E., Lacour, S. P., McMahon, S. B. & Fawcett, J. W. A regenerative microchannel neural interface for recording from and stimulating peripheral axons in vivo. *Journal of Neural Engineering* 9, 016010 (2012).

79 Foley, C. P., Nishimura, N., Neeves, K. B., Schaffer, C. B. & Olbricht, W. L. Flexible microfluidic devices supported by biodegradable insertion scaffolds for convection-enhanced neural drug delivery. *Biomedical microdevices* 11, 915-924 (2009).

80 Frankel, M., Dowden, B., Mathews, V., Normann, R., Clark, G. & Meek, S. Multiple-input single-output closed-loop isometric force control using asynchronous intrafascicular multi-electrode stimulation. *Neural Systems and Rehabilitation Engineering, IEEE Transactions on*, 1-1 (2011).

81 Freund, H., Budingen, H. & Dietz, V. Activity of single motor units from human forearm muscles during voluntary isometric contractions. *Journal of Neurophysiology* 38, 933-946 (1975).

82 Frost, C. M., Urbanchek, M. G., Egeland, B. M., Larkin, L. M., Kuzon Jr, W. M., Martin, D. C. & Cederna, P. S. Innervation of a Biosynthetic" Living Interface" by Severed Peripheral Nerve. *Plastic and Reconstructive Surgery* 124, 14 (2009).

83 Frost, C. M., Wei, B., Baghmanli, Z., Cederna, P. S. & Urbanchek, M. G. PEDOT Electrochemical Polymerization Improves Electrode Fidelity and Sensitivity. *Plastic and Reconstructive Surgery* 129, 933 (2012).

84 Gandevia, S. & Hales, J. The methodology and scope of human microneurography. *Journal of Neuroscience Methods* 74, 123-136 (1997).

85 Garde, K., Keefer, E., Botterman, B., Galvan, P. & Romero, M. I. Early interfaced neural activity from chronic amputated nerves. *Frontiers in Neuroengineering* 2 (2009).

86 Gasser, H. & Grundfest, H. Axon diameters in relation to the spike dimensions and the conduction velocity in mammalian A fibers. *American Journal of Physiology--Legacy Content* 127, 393-414 (1939).

87 Gasser, H. S. The classification of nerve fibers. *Ohio Journal of Science; Ohio Journal of Science* (1941).

88 Gasser, H. S. & Erlanger, J. A study of the action currents of nerve with the cathode ray oscillograph. *Am J Physiol* 62, 496-524 (1922).

89 Gasson, M., Hutt, B., Goodhew, I., Kyberd, P. & Warwick, K. Invasive neural prosthesis for neural signal detection and nerve stimulation. *International journal of adaptive control and signal processing* 19, 365-375 (2005).

90 Gilja, V., Chestek, C., Diester, I., Henderson, J., Deisseroth, K. & Shenoy, K. Challenges and opportunities for next-generation intra-cortically based neural prostheses. *Biomedical Engineering, IEEE Transactions on*, 1-1 (2011).

91 Gilja, V., Chestek, C. A., Nuyujukian, P., Foster, J. & Shenoy, K. V. Autonomous head-mounted electrophysiology systems for freely behaving primates. *Current opinion in neurobiology* 20, 676-686 (2010).

92 Gilletti, A. & Muthuswamy, J. Brain micromotion around implants in the rodent somatosensory cortex. *Journal of Neural Engineering* 3, 189 (2006).

93 Gojo, R., Kotake, N., Suzuki, T., Mabuchi, K. & Takeuchi, S. in *Micro Electro Mechanical Systems, 2009. MEMS 2009. IEEE 22nd International Conference on.* 256-259 (IEEE).

94 Gojo, R., Saito, H., Suzuki, T. & Mabuchi, K. in *Engineering in Medicine and Biology Society (EMBC), 2010 Annual International Conference of the IEEE* 1531-1534 (IEEE).

95 Gonenli, I., Celik-Butler, Z. & Butler, D. Surface Micromachined MEMS Accelerometers on Flexible Polyimide Substrate. *Sensors Journal, IEEE*, 1-1 (2011).

96 Goodall, E. V. & Horch, K. Separation of action potentials in multiunit intrafascicular recordings. *Biomedical Engineering, IEEE Transactions on* 39, 289-295 (1992).

97 Goodall, E. V., Lefurge, T. & Horch, K. Information contained in sensory nerve recordings made with intrafascicular electrodes. *Biomedical Engineering, IEEE Transactions on* 38, 846-850 (1991).

98 Grill, W. M., Norman, S. E. & Bellamkonda, R. V. Implanted neural interfaces: biochallenges and engineered solutions. *Annual Review of Biomedical Engineering* 11, 1-24 (2009).

99 Grinnell, F. Fibroblasts, myofibroblasts, and wound contraction. *The Journal of Cell Biology* 124, 401-404 (1994).

100 Gross, G., Williams, A. & Lucas, J. Recording of spontaneous activity with photoetched microelectrode surfaces from mouse spinal neurons in culture. *Journal of Neuroscience Methods* 5, 13-22 (1982).

101 Guo, L., Clements, I. P., Li, D., Bellamkonda, R. V. & DeWeerth, S. P. 194-197 (IEEE).

102 Gustafson, K. J., Pinault, G. C. J., Neville, J. J., Syed, I., Davis Jr, J. A., Jean-Claude, J. & Triolo, R. J. Fascicular anatomy of human femoral nerve: Implications for neural prostheses using nerve cuff electrodes. *Journal of rehabilitation research and development* 46, 973 (2009).

103 Haftek, J. Stretch injury of peripheral nerve. *The Journal of Bone and Joint Surgery* 52, 354-365 (1970).

104 Harris, J., Capadona, J., Miller, R., Healy, B., Shanmuganathan, K., Rowan, S., Weder, C. & Tyler, D. Mechanically adaptive intracortical implants improve the proximity of neuronal cell bodies. *Journal of Neural Engineering* 8, 066011 (2011).

105 Harrison, R. R., Watkins, P. T., Kier, R. J., Lovejoy, R. O., Black, D. J., Greger, B. & Solzbacher, F. A low-power integrated circuit for a wireless 100-electrode neural recording system. *Solid-State Circuits, IEEE Journal of* 42, 123-133 (2007).

106 Hassler, C., Boretius, T. & Stieglitz, T. Polymers for neural implants. *Journal of Polymer Science Part B: Polymer Physics* 49, 18-33 (2011).

107 Hassler, C., Guy, J., Nietzschmann, M., Staiger, J. F. & Stieglitz, T. in *Engineering in Medicine and Biology Society,EMBC, 2011 Annual International Conference of the IEEE.* 644-647 (IEEE).

108 He, W., McConnell, G. C., Schneider, T. M. & Bellamkonda, R. V. A Novel Anti‚Äêinflammatory Surface for Neural Electrodes. *Advanced Materials* 19, 3529-3533 (2007).

109 Heiduschka, P., Romann, I., Stieglitz, T. & Thanos, S. Perforated microelectrode arrays implanted in the regenerating adult central nervous system. *Experimental neurology* 171, 1-10 (2001).

110 Higgins, T. M., Moulton, S. E., Gilmore, K. J. & Wallace, G. G. Gellan gum doped polypyrrole neural prosthetic electrode coatings. *Soft Matter* 7, 4690-4695 (2011).

111 Hochberg, L. R., Serruya, M. D., Friehs, G. M., Mukand, J. A., Saleh, M., Caplan, A. H., Branner, A., Chen, D., Penn, R. D. & Donoghue, J. P. Neuronal ensemble control of prosthetic devices by a human with tetraplegia. *Nature* 442, 164-171 (2006).

112 Hodgkin, A. & Huxley, A. A quantitative description of membrane current and its application to conduction and excitation in nerve. *The Journal of Physiology* 117, 500-544 (1952).

113 Hodgkin, A. L. & Huxley, A. F. Action potentials recorded from inside a nerve fibre. *Nature* 144, 710-711 (1939).

114 Hoogerwerf, A. C. & Wise, K. A three-dimensional microelectrode array for chronic neural recording. *Biomedical Engineering, IEEE Transactions on* 41, 1136-1146 (1994).

115 Hopcroft, M. A., Nix, W. D. & Kenny, T. W. What is the Young's Modulus of Silicon? *Microelectromechanical Systems, Journal of* 19, 229-238 (2010).

116 Horch, K. & Dhillon, G. in *Biomedical Robotics and Biomechatronics, 2006. BioRob 2006. The First IEEE/RAS-EMBS International Conference on.* 1125-1128 (IEEE).

117 Horch, K. W. & Dhillon, G. S. *Neuroprosthetics theory and practice*. (World Scientific Pub Co Inc, 2004).

118 Huang, H., Zhou, P., Li, G. & Kuiken, T. A. An analysis of EMG electrode configuration for targeted muscle reinnervation based neural machine interface. *Neural Systems and Rehabilitation Engineering, IEEE Transactions on* 16, 37-45 (2008).

119 James, S. E. F. M. Contractures in orthopaedic and neurological conditions: a review of causes and treatment. *Disability & Rehabilitation* 23, 549-558 (2001).

120 Jang, T. & Davis, B. J. The chorda tympani and glossopharyngeal nerves in the adult hamster. *Chemical Senses* 12, 381-395 (1987).

121 Jaroch, D. B., Ward, M. P., Chow, E. Y., Rickus, J. L. & Irazoqui, P. P. Magnetic insertion system for flexible electrode implantation. *Journal of Neuroscience Methods* 183, 213-222 (2009).

122 Jia, X., Koenig, M. A., Zhang, X., Zhang, J., Chen, T. & Chen, Z. Residual motor signal in long-term human severed peripheral nerves and feasibility of neural signal-controlled artificial limb. *The Journal of hand surgery* 32, 657-666 (2007).

123 Kameswaran, N., Cullen, D. K., Pfister, B., Ranalli, N., Huang, J., Zager, E. & Smith, D. A novel neuroprosthetic interface with the peripheral nervous system using artificially engineered axonal tracts. *Neurological Research* 30, 1063-1067 (2008).

124 Kawada, T., Zheng, C., Tanabe, S., Uemura, T., Sunagawa, K. & Sugimachi, M. in *Engineering in Medicine and Biology Society, 2004. IEMBS '04. 26th Annual International Conference of the IEEE* 4318-4321 (IEEE).

125 Kim, S., Bhandari, R., Klein, M., Negi, S., Rieth, L., Tathireddy, P., Toepper, M., Oppermann, H. & Solzbacher, F. Integrated wireless neural interface based on the Utah electrode array. *Biomedical microdevices* 11, 453-466 (2009).

126 Kim, Y., Haftel, V. K., Kumar, S. & Bellamkonda, R. V. The role of aligned polymer fiber-based constructs in the bridging of long peripheral nerve gaps. *Biomaterials* 29, 3117-3127 (2008).

127 Kim, Y. H., Kim, Y. J., Ami, K. M., Lee, C., Lee, M. & Lee, J. H. in *IEEE Sensors 2007 Conference.* 1140-1143 (IEEE).

128 Kim, Y. H., Lee, C., Ahn, K. M., Kim, Y. J. & Lee, M. Function-inspection scheme for an injured peripheral nerve using a polymer based microelectrode array. *Sensors and Actuators A: Physical* 139, 58-65 (2007).

129 Kim, Y. H., Lee, C., Ahn, K. M., Lee, M. & Kim, Y. J. Robust and real-time monitoring of nerve regeneration using implantable flexible microelectrode array. *Biosensors and Bioelectronics* 24, 1883-1887 (2009).

130 Kim, Y. T., Hitchcock, R. W., Bridge, M. J. & Tresco, P. A. Chronic response of adult rat brain tissue to implants anchored to the skull. *Biomaterials* 25, 2229-2237 (2004).

131 Kim, Y. & Romero-Ortega, M. I. Material considerations for peripheral nerve interfacing. *MRS Bulletin* 37, 573-580 (2012).

132 Klinge, P. M., Vafa, M. A., Brinker, T., Brandis, A., Walter, G. F., Stieglitz, T., Samii, M. & Wewetzer, K. Immunohistochemical characterization of axonal sprouting and reactive tissue changes after long-term implantation of a polyimide sieve electrode to the transected adult rat sciatic nerve. *Biomaterials* 22, 2333-2343 (2001).

133 Kotov, N. A., Winter, J. O., Clements, I. P., Jan, E., Timko, B. P., Campidelli, S., Pathak, S., Mazzatenta, A., Lieber, C. M. & Prato, M. Nanomaterials for neural interfaces. *Advanced Materials* 21, 3970-4004 (2009).

134 Kovacs, G. T. A. in *Solid-State Sensors and Actuators, 1991. Digest of Technical Papers, TRANSDUCERS '91., 1991 International Conference on* 116-119 (IEEE).

135 Kovacs, G. T. A., Storment, C. W., Halks-Miller, M., Belczynski Jr, C., Santina, C. C. D., Lewis, E. & Maluf, N. Silicon-substrate microelectrode arrays for parallel recording of neural activity in peripheral and cranial nerves. *Biomedical Engineering, IEEE Transactions on* 41, 567-577 (1994).

136 Kovacs, G. T. A., Storment, C. W. & Rosen, J. M. Regeneration microelectrode array for peripheral nerve recording and stimulation. *Biomedical Engineering, IEEE Transactions on* 39, 893-902 (1992).

137 Kozai, T. D. Y. & Kipke, D. R. Insertion shuttle with carboxyl terminated self-assembled monolayer coatings for implanting flexible polymer neural probes in the brain. *Journal of Neuroscience Methods* 184, 199-205 (2009).

138 Kuiken, T., Dumanian, G., Lipschutz, R., Miller, L. & Stubblefield, K. The use of targeted muscle reinnervation for improved myoelectric prosthesis control in a bilateral shoulder disarticulation amputee. *Prosthetics and orthotics international* 28, 245-253 (2004).

139 Kuiken, T. A., Li, G., Lock, B. A., Lipschutz, R. D., Miller, L. A., Stubblefield, K. A. & Englehart, K. B. Targeted muscle reinnervation for real-time myoelectric control of multifunction artificial arms. *JAMA: the journal of the American Medical Association* 301, 619-628 (2009).

140 Kuiken, T. A., Miller, L. A., Lipschutz, R. D., Lock, B. A., Stubblefield, K., Marasco, P. D., Zhou, P. & Dumanian, G. A. Targeted reinnervation for enhanced prosthetic arm function in a woman with a proximal amputation: a case study. *The Lancet* 369, 371-380 (2007).

141 Kwan, M. K., Wall, E. J., Massie, J. & Garfin, S. R. Strain, stress and stretch of peripheral nerve Rabbit experiments in vitro and in vivo. *Acta Orthopaedica* 63, 267-272 (1992).

142 Lacour, S., Atta, R., FitzGerald, J., Blamire, M., Tarte, E. & Fawcett, J. Polyimide micro-channel arrays for peripheral nerve regenerative implants. *Sensors and Actuators A: Physical* 147, 456-463 (2008).

143 Lacour, S., Fitzgerald, J., Lago, N., Tarte, E., McMahon, S. & Fawcett, J. Long micro-channel electrode arrays: a novel type of regenerative peripheral nerve interface. *Neural Systems and Rehabilitation Engineering, IEEE Transactions on* 17, 454-460 (2009).

144 Lacour, S. P., Benmerah, S., Tarte, E., FitzGerald, J., Serra, J., McMahon, S., Fawcett, J., Graudejus, O., Yu, Z. & Morrison, B. Flexible and stretchable micro-electrodes for in vitro and in vivo neural interfaces. *Medical and Biological Engineering and Computing* 48, 945-954 (2010).

145 Lago, N. & Ceballos, D. Long term assessment of axonal regeneration through polyimide regenerative electrodes to interface the peripheral nerve. *Biomaterials* 26, 2021-2031 (2005).

146 Lago, N., Udina, E., Ramachandran, A. & Navarro, X. Neurobiological assessment of regenerative electrodes for bidirectional interfacing injured peripheral nerves. *Biomedical Engineering, IEEE Transactions on* 54, 1129-1137 (2007).

147 Langhammer, C. G. *A neuromuscular junction-based neural interface: the myotube-integrated microelectrode array*, Rutgers University-Graduate School-New Brunswick, (2010).

148 Leach, J., Achyuta, A. & Murthy, S. Bridging the Divide between Neuroprosthetic Design, Tissue Engineering and Neurobiology. *Frontiers in Neuroengineering* 2, 18 (2010).

149 Leach, J. B., Achyuta, A. K. H. & Murthy, S. K. Bridging the divide between neuroprosthetic design, tissue engineering and neurobiology. *Frontiers in Neuroengineering* 2 (2009).

150 Lebedev, M. A. & Nicolelis, M. A. L. Brain-machine interfaces: past, present and future. *TRENDS in Neurosciences* 29, 536-546 (2006).

151 Lee, C., Kim, Y., Shin, H. & Lee, M. in *Engineering in Medicine and Biology Society, 2006. EMBS '06. 28th Annual International Conference of the IEEE* 3002-3004 (IEEE).

152 Lee, H., Bellamkonda, R. V., Sun, W. & Levenston, M. E. Biomechanical analysis of silicon microelectrode-induced strain in the brain. *Journal of Neural Engineering* 2, 81 (2005).

153 Lefurge, T., Goodall, E., Horch, K., Stensaas, L. & Schoenberg, A. Chronically implanted intrafascicular recording electrodes. *Annals of biomedical engineering* 19, 197-207 (1991).

154 Leventhal, D. K. & Durand, D. M. Chronic measurement of the stimulation selectivity of the flat interface nerve electrode. *Biomedical Engineering, IEEE Transactions on* 51, 1649-1658 (2004).

155 Lewitus, D., Vogelstein, R. J., Zhen, G., Choi, Y. S., Kohn, J., Harshbarger, S. & Jia, X. Designing Tyrosine-Derived Polycarbonate Polymers for Biodegradable Regenerative Type Neural Interface Capable of Neural Recording. *Neural Systems and Rehabilitation Engineering, IEEE Transactions on*, 1-1 (2011).

156 Li, J. & Shi, R. A device for the electrophysiological recording of peripheral nerves in response to stretch. *Journal of Neuroscience Methods* 154, 102-108 (2006).

157 Li, J. & Shi, R. Stretch-induced nerve conduction deficits in guinea pig ex vivo nerve. *Journal of Biomechanics* 40, 569-578 (2007).

158 Lind, G., Linsmeier, C. E., Thelin, J. & Schouenborg, J. Gelatine-embedded electrodes,Äîa novel biocompatible vehicle allowing implantation of highly flexible microelectrodes. *Journal of Neural Engineering* 7, 046005 (2010).

159 Ling, G. S. F., Rhee, P. & Ecklund, J. M. Surgical innovations arising from the Iraq and Afghanistan wars. *Annual review of medicine* 61, 457-468 (2010).

160 Liu, X., McCreery, D. B., Bullara, L. A. & Agnew, W. F. Evaluation of the stability of intracortical microelectrode arrays. *Neural Systems and Rehabilitation Engineering, IEEE Transactions on* 14, 91-100 (2006).

161 Liu, X., McCreery, D. B., Carter, R. R., Bullara, L. A., Yuen, T. G. H. & Agnew, W. F. Stability of the interface between neural tissue and chronically implanted intracortical microelectrodes. *Rehabilitation Engineering, IEEE Transactions on* 7, 315-326 (1999).

162 Llinás, R., Nicholson, C. & Johnson, K. Implantable monolithic wafer recording electrodes for neurophysiology. *Brain Unit Activity During Behaviour*, 105-111 (1973).

163 Loeb, G., Marks, W. & Beatty, P. Analysis and microelectronic design of tubular electrode arrays intended for chronic, multiple singleunit recording from captured nerve fibres. *Medical and Biological Engineering and Computing* 15, 195-201 (1977).

164 Loeb, G. E. & Ghez, C. The motor unit and muscle action. *Principles of neural science*, 674-694 (2000).

165 Loeb, G. E., Tsianos, G. A., Fishel, J. A., Wettels, N. & Schaal, S. 9 Understanding haptics by evolving mechatronic systems. *Progress in Brain Research* 192, 129 (2011).

166 Lotfi, P., Garde, K., Chouhan, A. K., Bengali, E. & Romero-Ortega, M. I. Modality-specific axonal regeneration: toward selective regenerative neural interfaces. *Frontiers in Neuroengineering* 4 (2011).

167 Lotfi, P. & Romero-Ortega, M. in *Engineering in Medicine and Biology Society,EMBC, 2011 Annual International Conference of the IEEE* 4633-4636 (IEEE).

168 Lundborg, G. *Nerve injury and repair*. (Churchill Livingstone Edinburg, 1988).

169 Lundborg, G. & Rydevik, B. Effects of stretching the tibial nerve of the rabbit. A preliminary study of the intraneural circulation and the barrier function of the perineurium. *The Journal of bone and joint surgery British volume* 55, 390-401 (1973).

170 MacInnis, B. L. & Campenot, R. B. Retrograde support of neuronal survival without retrograde transport of nerve growth factor. *Science* 295, 1536 (2002).

171 Malagodi, M. S., Horch, K. W. & Schoenberg, A. A. An intrafascicular electrode for recording of action potentials in peripheral nerves. *Annals of biomedical engineering* 17, 397-410 (1989).

172 Mannard, A., Stein, R. B. & Charles, D. Regeneration electrode units: implants for recording from single peripheral nerve fibers in freely moving animals. *Science* 183, 547 (1974).

173 Marin, C. & Fernandez, E. Biocompatibility of intracortical microelectrodes: current status and future prospects. *Frontiers in Neuroengineering* 3 (2010).

174 Marks, A. Bullfrog nerve regeneration into porous implants. *Anat. Rec* 163, 226 (1969).

175 Masuda, T. & De Luca, C. J. Recruitment threshold and muscle fiber conduction velocity of single motor units. *Journal of Electromyography and Kinesiology* 1, 116-123 (1991).

176 Matsuo, T., Yamaguchi, A. & Esashi, M. Fabrication of multiholeactive electrode for nerve bundle. *Jpn. J. Med. Electron. Biological Eng* 16, 261 (1978).

177 McConnell, G. C., Rees, H. D., Levey, A. I., Gutekunst, C. A., Gross, R. E. & Bellamkonda, R. V. Implanted neural electrodes cause chronic, local inflammation that is correlated with local neurodegeneration. *Journal of Neural Engineering* 6, 056003 (2009).

178 McDonnall, D., Clark, G. A. & Normann, R. A. Selective motor unit recruitment via intrafascicular multielectrode stimulation. *Canadian Journal of Physiology and Pharmacology, 82* 8, 599-609 (2004).

179 McFarland, D. J., Sarnacki, W. A. & Wolpaw, J. R. IOPscience-Electroencephalographic (EEG) control of three-dimensional movement. *Journal of Neural Engineering* 7, 036007 (2010).

180 McLoughlin, M. P. DARPA Revolutionizing Prosthetics 2009. (DTIC Document, 2009).

181 McNaughton, T. & Horch, K. Action potential classification with dual channel intrafascicular electrodes. *Biomedical Engineering, IEEE Transactions on* 41, 609-616 (1994).

182 McNaughton, T. G. & Horch, K. W. Metallized polymer fibers as leadwires and intrafascicular microelectrodes. *Journal of Neuroscience Methods* 70, 103-107 (1996).

183 Mensinger, A. F., Anderson, D. J., Buchko, C. J., Johnson, M. A., Martin, D. C., Tresco, P. A., Silver, R. B. & Highstein, S. M. Chronic recording of regenerating VIIIth nerve axons with a sieve electrode. *Journal of Neurophysiology* 83, 611 (2000).

184 Mercanzini, A., Cheung, K., Buhl, D. L., Boers, M., Maillard, A., Colin, P., Bensadoun, J. C., Bertsch, A. & Renaud, P. Demonstration of cortical recording using novel flexible polymer neural probes. *Sensors and Actuators A: Physical* 143, 90-96 (2008).

185 Micera, S., Carpaneto, J. & Raspopovic, S. Control of hand prostheses using peripheral information. *Biomedical Engineering, IEEE Reviews in* 3, 48-68 (2010).

186 Micera, S., Citi, L., Rigosa, J., Carpaneto, J., Raspopovic, S., Di Pino, G., Rossini, L., Yoshida, K., Denaro, L. & Dario, P. Decoding information from neural signals recorded using intraneural electrodes: Toward the development of a neurocontrolled hand prosthesis. *Proceedings of the IEEE* 98, 407-417 (2010).

187 Micera, S., Navarro, X., Carpaneto, J., Citi, L., Tonet, O., Rossini, P. M., Carrozza, M. C., Hoffmann, K. P., Viv√≥, M. & Yoshida, K. On the use of longitudinal intrafascicular peripheral interfaces for the control of cybernetic hand prostheses in amputees. *Neural Systems and Rehabilitation Engineering, IEEE Transactions on* 16, 453-472 (2008).

188 Miller, L. A., Stubblefield, K. A., Lipschutz, R. D., Lock, B. A. & Kuiken, T. A. Improved myoelectric prosthesis control using targeted reinnervation surgery: a case series. *Neural Systems and Rehabilitation Engineering, IEEE Transactions on* 16, 46-50 (2008).

189 Minev, I. R., Chew, D. J., Delivopoulos, E., Fawcett, J. W. & Lacour, S. P. in *Neural Engineering (NER), 2011 5th International IEEE/EMBS Conference on* 482-485 (IEEE).

190 Minev, I. R., Chew, D. J., Delivopoulos, E., Fawcett, J. W. & Lacour, S. P. High sensitivity recording of afferent nerve activity using ultra-compliant microchannel electrodes: an acute in vivo validation. *Journal of Neural Engineering* 9, 026005 (2012).

191 Moritz, C. T. & Fetz, E. E. Volitional control of single cortical neurons in a brain machine interface. *Journal of Neural Engineering* 8, 025017 (2011).

192 Moritz, C. T., Perlmutter, S. I. & Fetz, E. E. Direct control of paralysed muscles by cortical neurons. *Nature* 456, 639-642 (2008).

193 Najafi, K. Solid-state microsensors for cortical nerve recordings. *Engineering in Medicine and Biology Magazine, IEEE* 13, 375-387 (1994).

194 Nannini, N. & Horch, K. Muscle recruitment with intrafascicular electrodes. *Biomedical Engineering, IEEE Transactions on* 38, 769-776 (1991).

195 Navarro, X., Calvet, S., But√≠, M., G√≥mez, N., Cabruja, E., Garrido, P., Villa, R. & Valderrama, E. Peripheral nerve regeneration through microelectrode arrays based on silicon technology. *Restorative Neurology and Neuroscience* 9, 151-160 (1996).

196 Navarro, X., Calvet, S., Rodriguez, F., Stieglitz, T., Blau, C., Buti, M., Valderrama, E. & Meyer, J. Stimulation and recording from regenerated peripheral nerves through polyimide sieve electrodes. *Journal of the peripheral nervous system: JPNS* 3, 91 (1998).

197 Navarro, X., Krueger, T. B., Lago, N., Micera, S., Stieglitz, T. & Dario, P. A critical review of interfaces with the peripheral nervous system for the control of neuroprostheses and hybrid bionic systems. *Journal of the Peripheral Nervous System* 10, 229-258 (2005).

198 Negredo, P., Castro, J., Lago, N., Navarro, X. & Avenda√±o, C. Differential growth of axons from sensory and motor neurons through a regenerative electrode: A stereological, retrograde tracer, and functional study in the rat. *Neuroscience* 128, 605-615 (2004).

199 Nicolas-Alonso, L. F. & Gomez-Gil, J. Brain Computer Interfaces, a Review. *Sensors* 12, 1211-1279 (2012).

200 Nicolelis, M. A., Baccala, L. A., Lin, R. & Chapin, J. K. Sensorimotor encoding by synchronous neural ensemble activity at multiple levels of the somatosensory system. *Science* 268, 1353-1358 (1995).

201 Nicolelis, M. A. L., Ghazanfar, A. A., Faggin, B. M., Votaw, S. & Oliveira, L. M. O. Reconstructing the engram: simultaneous, multisite, many single neuron recordings. *Neuron* 18, 529-537 (1997).

202 Nordhausen, C. T., Maynard, E. M. & Normann, R. A. Single unit recording capabilities of a 100 microelectrode array. *Brain Research* 726, 129-140 (1996).

203 O'Doherty, J., Lebedev, M., Ifft, P., Zhuang, K., Shokur, S., Bleuler, H. & Nicolelis, M. Active tactile exploration using a brain-machine-brain interface. *Nature* (2011).

204 O'Doherty, J. E., Lebedev, M., Hanson, T. L., Fitzsimmons, N. & Nicolelis, M. A. L. Frontiers: A brain-machine interface instructed by direct intracortical microstimulation. *Frontiers in Integrative Neuroscience* 3 (2009).

205 Oakley, B. Trophic competence in mammalian gustation. *Taste, olfaction and the central nervous system. New York: Rockefeller University Press. p*, 92-103 (1985).

206 Ochoa, J. & Torebj√∂rk, E. Sensations evoked by intraneural microstimulation of single mechanoreceptor units innervating the human hand. *The Journal of Physiology* 342, 633-654 (1983).

207 Ochs, S., Pourmand, R., Si, K. & Friedman, R. N. Stretch of mammalian nerve in vitro: Effect on compound action potentials. *Journal of the Peripheral Nervous System* 5, 227-235 (2000).

208 Ogata, K. & Naito, M. Blood flow of peripheral nerve effects of dissection stretching and compression. *The Journal of Hand Surgery: Journal of the British Society for Surgery of the Hand* 11, 10-14 (1986).

209 Ohnishi, K., Weir, R. F. & Kuiken, T. A. Neural machine interfaces for controlling multifunctional powered upper-limb prostheses. *Expert review of medical devices* 4, 43-53 (2007).

210 Ommaya, A. K. Mechanical properties of tissues of the nervous system. *Journal of Biomechanics* 1, 127-136, IN123, 137-138 (1968).

211 Onose, G., Grozea, C., Anghelescu, A., Daia, C., Sinescu, C., Ciurea, A., Spircu, T., Mirea, A., Andone, I. & Sp√¢nu, A. On the feasibility of using motor imagery EEG-based brain,Äìcomputer interface in chronic tetraplegics for assistive robotic arm control: a clinical test and long-term post-trial follow-up. *Spinal Cord* (2012).

212 Panetsos, F., Avenda√±o, C., Negredo, P., Castro, J. & Bonacasa, V. Neural prostheses: electrophysiological and histological evaluation of central nervous system alterations due to long-term implants of sieve electrodes to peripheral nerves in cats. *Neural Systems and Rehabilitation Engineering, IEEE Transactions on* 16, 223-232 (2008).

213 Perez-Orive, J. & Durund, D. Modeling study of peripheral nerve recording selectivity. *Rehabilitation Engineering, IEEE Transactions on* 8, 320-329 (2000).

214 Piccolino, M. Animal electricity and the birth of electrophysiology: the legacy of Luigi Galvani. *Brain research bulletin* 46, 381-407 (1998).

215 Pistohl, T., Ball, T., Schulze-Bonhage, A., Aertsen, A. & Mehring, C. Prediction of arm movement trajectories from ECoG-recordings in humans. *Journal of Neuroscience Methods* 167, 105-114 (2008).

216 Polikov, V. S., Tresco, P. A. & Reichert, W. M. Response of brain tissue to chronically implanted neural electrodes. *Journal of Neuroscience Methods* 148, 1-18 (2005).

217 Purcell, E., Seymour, J., Yandamuri, S. & Kipke, D. In vivo evaluation of a neural stem cell-seeded prosthesis. *Journal of Neural Engineering* 6, 026005 (2009).

218 Raffe, M. R. Principles of peripheral nerve repair. *Newton CD and Nunam* (1985).

219 Ramachandran, A., Schuettler, M., Lago, N., Doerge, T., Koch, K. P., Navarro, X., Hoffmann, K. P. & Stieglitz, T. Design, in vitro and in vivo assessment of a multi-channel sieve electrode with integrated multiplexer. *Journal of Neural Engineering* 3, 114 (2006).

220 Ransom, B., Neale, E., Henkart, M., Bullock, P. & Nelson, P. Mouse spinal cord in cell culture. I. Morphology and intrinsic neuronal electrophysiologic properties. *Journal of Neurophysiology* 40, 1132 (1977).

221 Raspopovic, S., Carpaneto, J., Udina, E., Navarro, X. & Micera, S. Research On the identification of sensory information from mixed nerves by using single-channel cuff electrodes. (2010).

222 Ravula, S., McClain, M., Wang, M., Glass, J. & Frazier, A. A multielectrode microcompartment culture platform for studying signal transduction in the nervous system. *Lab on a Chip* 6, 1530-1536 (2006).

223 Ravula, S., Wang, M., Asress, S., Glass, J. & Bruno Frazier, A. A compartmented neuronal culture system in microdevice format. *Journal of Neuroscience Methods* 159, 78-85 (2007).

224 Rhee, S., Taylor, A., Tu, C., Cribbs, D., Cotman, C. & Jeon, N. Patterned cell culture inside microfluidic devices. *Lab on a Chip* 5, 102-107 (2005).

225 Rickett, T., Connell, S., Bastijanic, J., Hegde, S. & Shi, R. Functional and Mechanical Evaluation of Nerve Stretch Injury. *Journal of medical systems* 35, 787 (2011).

226 Rosen, J. M., Grosser, M. & Hentz, V. R. Preliminary experiments in nerve regeneration through laser-drilled holes in silicon chips. *Restorative Neurology and Neuroscience* 2, 89-102 (1990).

227 Rossini, P., Rigosa, J., Micera, S., Assenza, G., Rossini, L. & Ferreri, F. Stump nerve signals during transcranial magnetic motor cortex stimulation recorded in an amputee via longitudinal intrafascicular electrodes. *Experimental Brain Research* 210, 1-11 (2011).

228 Rossini, P. M., Micera, S., Benvenuto, A., Carpaneto, J., Cavallo, G., Citi, L., Cipriani, C., Denaro, L., Denaro, V. & Di Pino, G. Double nerve intraneural interface implant on a human amputee for robotic hand control. *Clinical neurophysiology* 121, 777-783 (2010).

229 Rothschild, R. M. Neuroengineering tools/applications for bidirectional interfaces, brain‚Äìcomputer interfaces, and neuroprosthetic implants‚Äìa review of recent progress. *Frontiers in Neuroengineering* 3 (2010).

230 Rousche, P. J. & Normann, R. A. Chronic recording capability of the Utah Intracortical Electrode Array in cat sensory cortex. *Journal of Neuroscience Methods* 82, 1-15 (1998).

231 Rutten, W. L. C., Smit, J. P. A., Frieswijk, T. A., Bielen, J. A., Brouwer, A. L. H., Buitenweg, J. R. & Heida, C. Neuro-electronic interfacing with multielectrode arrays. *Engineering in Medicine and Biology Magazine, IEEE* 18, 47-55 (1999).

232 Sahin, M., Haxhiu, M. A., Durand, D. M. & Dreshaj, I. A. Spiral nerve cuff electrode for recordings of respiratory output. *Journal of Applied Physiology* 83, 317-322 (1997).

233 Schalk, G. & Leuthardt, E. Brain-Computer Interfaces Using Electrocorticographic (ECoG) Signals. *Biomedical Engineering, IEEE Reviews in*, 1-1 (2011).

234 Schalk, G., Miller, K., Anderson, N., Wilson, J., Smyth, M., Ojemann, J., Moran, D., Wolpaw, J. R. & Leuthardt, E. Two-dimensional movement control using electrocorticographic signals in humans. *Journal of Neural Engineering* 5, 75 (2008).

235 Schiefer, M. A., Triolo, R. J., Durand, D. M. & Tyler, D. J. 356-359 (IEEE).

236 Schmalbruch, H. Fiber composition of the rat sciatic nerve. *The anatomical record* 215, 71-81 (1986).

237 Schmidt, E., Bak, M. & McIntosh, J. Long-term chronic recording from cortical neurons. *Experimental neurology* 52, 496-506 (1976).

238 Schmidt, E. M. Single neuron recording from motor cortex as a possible source of signals for control of external devices. *Annals of biomedical engineering* 8, 339-349 (1980).

239 Schmidt, E. M. Electrodes for many single neuron recordings. *Methods for Neural Ensemble Recordings*, 1-23 (1999).

240 Schuetze, S. M. The discovery of the action potential. *TRENDS in Neurosciences* 6, 164-168 (1983).

241 Schwartz, A. B. Cortical neural prosthetics. *Annu. Rev. Neurosci.* 27, 487-507 (2004).

242 Seddon, H. Volkmann's ischaemia. *British Medical Journal* 1, 1587-1592 (1964).

243 Seifert, J., Desai, V., Watson, R., Musa, T., Kim, Y., Keefer, E. & Romero-Ortega, M. Normal Molecular Repair Mechanisms in Regenerative Peripheral Nerve Interfaces Allow Recording of Early Spike Activity Despite Immature Myelination. *IEEE transactions on neural systems and rehabilitation engineering: a publication of the IEEE Engineering in Medicine and Biology Society* 20 (2012).

244 Serruya, M. D., Hatsopoulos, N. G., Paninski, L., Fellows, M. R. & Donoghue, J. P. Brain-machine interface: Instant neural control of a movement signal. *Nature* 416, 141-142 (2002).

245 Seymour, J. P., Elkasabi, Y. M., Chen, H. Y., Lahann, J. & Kipke, D. R. The insulation performance of reactive parylene films in implantable electronic devices. *Biomaterials* 30, 6158-6167 (2009).

246 Seymour, J. P. & Kipke, D. R. Neural probe design for reduced tissue encapsulation in CNS. *Biomaterials* 28, 3594-3607 (2007).

247 Shimatani, Y., Nikles, S. A., Najafi, K. & Bradley, R. M. Long-term recordings from afferent taste fibers. *Physiology & behavior* 80, 309-315 (2003).

248 Simeral, J., Kim, S., Black, M., Donoghue, J. & Hochberg, L. Neural control of cursor trajectory and click by a human with tetraplegia 1000 days after implant of an intracortical microelectrode array. *Journal of Neural Engineering* 8, 025027 (2011).

249 Smit, J. P. A., Rutten, W. L. C. & Boom, H. B. K. Endoneural selective stimulating using wire-microelectrode arrays. *Rehabilitation Engineering, IEEE Transactions on* 7, 399-412 (1999).

250 Smith, K. L., Herron, B., Dowell-Mesfin, N., Wu, H., Kim, S. J., Shain, W. & Hynd, M. R. Knockdown of cortical transthyretin expression around implanted neural prosthetic devices using intraventricular siRNA injection in the brain. *Journal of Neuroscience Methods*, 398-406 (2012).

251 Spataro, L., Dilgen, J., Retterer, S., Spence, A., Isaacson, M., Turner, J. & Shain, W. Dexamethasone treatment reduces astroglia responses to inserted neuroprosthetic devices in rat neocortex. *Experimental neurology* 194, 289-300 (2005).

252 Srinivasan, A., Guo, L. & Bellamkonda, R. V. 253-256 (IEEE).

253 Stein, R. & Pearson, K. Predicted amplitude and form of action potentials recorded from unmyelinated nerve fibres. *Journal of theoretical biology* 32, 539-558 (1971).

254 Stein, R. B., Charles, D., Davis, L., Jhamandas, J., Mannard, A. & Nichols, T. Principles underlying new methods for chronic neural recording. *The Canadian journal of neurological sciences. Le journal canadien des sciences neurologiques* 2, 235 (1975).

255 Stein, R. B., Nichols, T., Jhamandas, J., Davis, L. & Charles, D. Stable long-term recordings from cat peripheral nerves. *Brain Research* 128, 21-38 (1977).

256 Stevanovic, M. & Sharpe, F. Management of established Volkmann's contracture of the forearm in children. *Hand Clin* 22, 99-111 (2006).

257 Stice, P. & Muthuswamy, J. Assessment of gliosis around moveable implants in the brain. *Journal of Neural Engineering* 6, 046004 (2009).

258 Stieglitz, T., Navarro, X., Calvet, S., Blau, C. & Meyer, J. U. in *Engineering in Medicine and Biology Society, 1996. Bridging Disciplines for Biomedicine. Proceedings of the 18th Annual International Conference of the IEEE* 365-366 vol. 361 (IEEE).

259 Struijk, J. J., Thomsen, M., Larsen, J. O. & Sinkjaer, T. Cuff electrodes for long-term recording of natural sensory information. *Engineering in Medicine and Biology Magazine, IEEE* 18, 91-98 (1999).

260 Subbaroyan, J., Martin, D. C. & Kipke, D. R. A finite-element model of the mechanical effects of implantable microelectrodes in the cerebral cortex. *Journal of Neural Engineering* 2, 103 (2005).

261 Sunderland, S. Nerves and Nerve injuries E & S Livingstone Ltd. *Edinburgh and Londan: p* 895 (1968).

262 Sunderland, S. & Bradley, K. Stress-strain phenomena in human peripheral nerve trunks. *Brain* 84, 102-119 (1961).

263 Sunderland, S. & SMITH, J. W. Nerves and Nerve Injuries. *Plastic and Reconstructive Surgery* 44, 601 (1969).

264 Suner, S., Fellows, M. R., Vargas-Irwin, C., Nakata, G. K. & Donoghue, J. P. Reliability of signals from a chronically implanted, silicon-based electrode array in non-human primate primary motor cortex. *Neural Systems and Rehabilitation Engineering, IEEE Transactions on* 13, 524-541 (2005).

265 Suzuki, T., Kotake, N., Mabuchi, K. & Takeuchi, S. in *Microtechnologies in Medicine and Biology, 2006 International Conference on* 303-305 (IEEE).

266 Suzuki, T., Kotake, N., Mabuchi, K. & Takeuchi, S. Regeneration-Type Nerve Electrode Using Bundled Microfluidic Channels. *IEEJ Transactions on Electronics, Information and Systems* 127, 1544-1548 (2007).

267 Suzuki, T., Kotake, N., Mabuchi, K. & Takeuchi, S. in *Neural Engineering, 2007. CNE '07. 3rd International IEEE/EMBS Conference on* 17-18 (IEEE).

268 Suzuki, T., Maeda, T., Chinzei, T., Mabuchi, K., Imachi, K. & Tachi, S. in *Engineering in Medicine and Biology Society, 1997. Proceedings of the 19th Annual International Conference of the IEEE* 2270-2272 vol. 2275 (IEEE).

269 Takai, S., Dohno, H., Watanabe, Y., Yoshino, N., Ogura, T. & Hirasawa, Y. In situ strain and stress of nerve conduction blocking in the brachial plexus. *Journal of orthopaedic research* 20, 1311-1314 (2002).

270 Tansey, K., Seifert, J., Botterman, B., Delgado, M. & Romero, M. Peripheral nerve repair through multi-luminal biosynthetic implants. *Annals of biomedical engineering* 39, 1815-1828 (2011).

271 Taylor, A., Blurton-Jones, M., Rhee, S., Cribbs, D., Cotman, C. & Jeon, N. A microfluidic culture platform for CNS axonal injury, regeneration and transport. *Nature methods* 2, 599-605 (2005).

272 Taylor, D. M., Tillery, S. I. H. & Schwartz, A. B. Direct cortical control of 3D neuroprosthetic devices. *Science* 296, 1829 (2002).

273 Terzis, J., Faibisoff, B. & Williams, B. The nerve gap: suture under tension vs. graft. *Plast Reconstr Surg* 56, 166-170 (1975).

274 Thomas, P. Recent advances in the clinical electrophysiology of muscle and nerve. *Postgraduate medical journal* 37, 377-384 (1961).

275 Torab, K., Davis, T., Warren, D., House, P., Normann, R. & Greger, B. Multiple factors may influence the performance of a visual prosthesis based on intracortical microstimulation: nonhuman primate behavioural experimentation. *Journal of Neural Engineering* 8, 035001 (2011).

276 Tyler, D. J. & Durand, D. in *Engineering in Medicine and Biology Society, 1993. Proceedings of the 15th Annual International Conference of the IEEE* 1247-1248 (IEEE).

277 Tyler, D. J. & Durand, D. M. in *Engineering in Medicine and Biology Society, 1996. Bridging Disciplines for Biomedicine. Proceedings of the 18th Annual International Conference of the IEEE* 351-352 vol. 351 (IEEE).

278 Tyler, D. J. & Durand, D. M. A slowly penetrating interfascicular nerve electrode for selective activation of peripheral nerves. *Rehabilitation Engineering, IEEE Transactions on* 5, 51-61 (1997).

279 Tyler, D. J. & Durand, D. M. Functionally selective peripheral nerve stimulation with a flat interface nerve electrode. *Neural Systems and Rehabilitation Engineering, IEEE Transactions on* 10, 294-303 (2002).

280 Tyler, D. J., Peterson, E. J., Brill, N. & White, K. in *Neural Engineering (NER), 2011 5th International IEEE/EMBS Conference on* 257-260 (IEEE).

281 Urbanchek, M. G., Wei, B., Egeland, B. M., Abidian, M. R., Kipke, D. R. & Cederna, P. S. Microscale Electrode Implantation during Nerve Repair: Effects on Nerve Morphology, Electromyography, and Recovery of Muscle Contractile Function. *Plastic and Reconstructive Surgery* 128, 270e (2011).

282 Vallbo, Ö. B., Hagbarth, K. E. & Wallin, B. G. Microneurography: how the technique developed and its role in the investigation of the sympathetic nervous system. *Journal of Applied Physiology* 96, 1262-1269 (2004).

283 Velliste, M., Perel, S., Spalding, M. C., Whitford, A. S. & Schwartz, A. B. Cortical control of a prosthetic arm for self-feeding. *Nature* 453, 1098-1101 (2008).

284 Wall, E. J., Kwan, M. K., Rydevik, B. L., Woo, S. L. Y. & Garfin, S. R. Stress relaxation of a peripheral nerve. *The Journal of hand surgery* 16, 859-863 (1991).

285 Wallman, L., Levinsson, A., Schouenborg, J., Holmberg, H., Danielsen, N. & Laurell, T. Perforated silicon nerve chips with doped registration electrodes: in vitro performance and in vivo operation. *Biomedical Engineering, IEEE Transactions on* 46, 1065-1073 (1999).

286 Wallman, L., Zhang, Y., Laurell, T. & Danielsen, N. The geometric design of micromachined silicon sieve electrodes influences functional nerve regeneration. *Biomaterials* 22, 1187-1193 (2001).

287 Wan, E. A., Kovacs, G. T. A., Rosen, J. M. & Widrow, B. in *Proc. Intl. Joint Conf. on Neural Networks, Wash., DC, Lawrence Erlbaum Associates, pp. II-3 - II-21, January 1990.*

288 Warwick, K., Gasson, M., Hutt, B., Goodhew, I., Kyberd, P., Andrews, B., Teddy, P. & Shad, A. The application of implant technology for cybernetic systems. *Archives of Neurology* 60, 1369 (2003).

289 Waters, D. Brain control headset for gamers. *BBC News* 20 (2008).

290 Wells, M. R., Vaidya, U., Ricci, J. L. & Christie, C. A neuromuscular platform to extract electrophysiological signals from lesioned nerves: a technical note. *Journal of rehabilitation research and development* 38, 385-390 (2001).

291 Wester, B., Lee, R. & LaPlaca, M. Development and characterization of in vivo flexible electrodes compatible with large tissue displacements. *Journal of Neural Engineering* 6, 024002 (2009).

292 Whitney, N. P., Eidem, T. M., Peng, H., Huang, Y. & Zheng, J. C. Inflammation mediates varying effects in neurogenesis: relevance to the pathogenesis of brain injury and neurodegenerative disorders. *Journal of neurochemistry* 108, 1343-1359 (2009).

293 Wieringa, P. & Rutten, W. L. C. A three-dimensional bifurcating micro-channel construct for regenerative bidirectional neuro-electric interfacing. (2010).

294 Wieringa, P., Wiertz, R., De Weerd, E. & Rutten, W. In vitro verification of a 3-D regenerative neural interface design: examination of neurite growth and electrical properties within a bifurcating microchannel structure. *Proceedings of the IEEE* 98, 389-397 (2010).

295 Wieringa, P., R. Wiertz, et al. (2010). "Bifurcating microchannels as a scaffold to induce separation of regenerating neurites." Journal of Neural Engineering 7: 016001.

296 Williams, J. C., Rennaker, R. L. & Kipke, D. R. Long-term neural recording characteristics of wire microelectrode arrays implanted in cerebral cortex. *Brain Research Protocols* 4, 303-313 (1999).

297 Williams, J. C., Rennaker, R. L. & Kipke, D. R. Stability of chronic multichannel neural recordings: implications for a long-term neural interface. *Neurocomputing* 26, 1069-1076 (1999).

298 Wise, K. D., Sodagar, A. M., Yao, Y., Gulari, M. N., Perlin, G. E. & Najafi, K. Microelectrodes, microelectronics, and implantable neural microsystems. *Proceedings of the IEEE* 96, 1184-1202 (2008).

299 Wolpaw, J. R. & McFarland, D. J. Control of a two-dimensional movement signal by a noninvasive brain-computer interface in humans. *Proceedings of the National Academy of Sciences of the United States of America* 101, 17849 (2004).

300 Yoshida, K. & Horch, K. Closed-loop control of ankle position using muscle afferent feedback with functional neuromuscular stimulation. *Biomedical Engineering, IEEE Transactions on* 43, 167-176 (1996).

301 Zhang, B., Wang, J. & Fuhlbrigge, T. in *Automation and Logistics (ICAL), 2010 IEEE International Conference on* 379-384 (IEEE).

302 Zhao, Q., Drott, J., Laurell, T., Wallman, L., Bjursten, L. M., Lundborg, G., Montelius, L. & Danielsen, N. Rat sciatic nerve regeneration through a micromachined silicon chip. *Biomaterials* 18, 75-80 (1997).

303 Ziegler-Graham, K., MacKenzie, E. J., Ephraim, P. L., Travison, T. G. & Brookmeyer, R. Estimating the prevalence of limb loss in the United States: 2005 to 2050. *Archives of physical medicine and rehabilitation* 89, 422-429 (2008).

BIOGRAPHICAL INFORMATION

Collins Watson earned a B.S. in Engineering from Texas Christian University in 2003 and a Ph.D. in Biomedical Engineering from the University of Texas Arlington in 2012.